NDOR Research Project Number P568

FINAL REPORT

Steel Box System Monitoring of N-2 over I-80 Bridge

Nima Ala
Saeed Javidi Niroumand
Luke Glaser
Kyle Burner
Aaron Yakel, Ph.D.
Atorod Azizinamini, Ph.D., P.E.

National Bridge Research Organization (NaBRO)
(http://www.NaBRO.unl.edu)
Department of Civil Engineering
College of Engineering and Technology

W150 Nebraska Hall
Lincoln, Nebraska 68588-0528
Telephone (402) 472-5106
Fax (402) 472-6658

Sponsored By
Nebraska Department of Roads

June, 2009

Table of Contents

Abstract

"Simple for dead, continuous for live load" is a new method of bridge construction aiming at eliminating bolted field splices by developing a new connection at the pier. This will result in a reduction in steel girder construction expenses and in essence enhancing the steel girders' competitiveness in the short to medium span length bridges over other materials such as concrete. This connection detail allows the girders to be set as simply supported spans, and then once the deck is cast, the structure acts as a continuous one for any further applied loads, such as live loads or superimposed dead loads, due to the continuity provided by the bars in the concrete slab. The N-2 over I-80 Bridge, Nebraska, was constructed using the simple for dead, continuous for live load technology. The bridge was instrumented and then monitored during and after its construction. During construction behavior was monitored in order to verify the simple connection behavior and also determine the amount of possible continuity before the concrete is cast. A live load testing using dump trucks was also carried out prior to opening the bridge to the traffic. A Finite Element study was then carried out in order to assess the live load testing results and check whether or not the bridge behavior can be well predicted using conventional finite element packages commonly used in the design firms. The long-term monitoring of the structure shows the structure behavior to be satisfactory and stable over time with no significant bias from the predicted bridge behavior. The results obtained from this extensive monitoring along with other case studies and numerical modeling provided insight into the potential problems associated with this method of construction as well as the possible remedies for the problems.

Acknowledgement

Funding for this investigation was provided by the Nebraska Department of Roads. The authors would like to express their appreciation for this support. The authors would also like to express their thanks to Mr. Lyman Freemon, Fouad Jaber, and Sam Fallaha of the Bridge Division at the Nebraska Department of Roads (NDOR), and Curtis Smith of Capital Contractors for their assistance.

The views and opinions of the authors [or agency] expressed herein do not necessarily state or reflect those of the U. S. Department of Transportation.

Executive Summary

The previously performed market analysis of bridge material in the range of short to medium span length indicates a declining trend for steel girders during the last two decades. The "simple for dead, continuous for live load" is a new method of bridge construction aiming at reducing the steel girder construction expenses and in essence enhancing the steel girders' competitiveness in the short to medium span length bridges. This method of construction takes the advantage of the simple span construction as well as reduction of the forces in the bridge elements due to the continuous span behavior. The continuity of girders is provided by reinforcements in deck and concrete diaphragm after the concrete is hardened. In this case therefore, the field splices are eliminated and there is no need for temporary shoring.

Due to the novelty of the idea and the fact that not many bridges have been constructed using this idea, there was a need to monitor the behavior of a bridge constructed using the "simple for dead, continuous for live load" method. The main objective of this project was to closely monitor the behavior of a bridge constructed using simple for dead, continuous for live load idea during the construction, right after the construction before opening to traffic, and in long-term under traffic load. Extensive instrumentation was installed on the bridge. The results of this project provides a better understanding of the behavior of the new system, further utilizing the system in future practices, and potential problems associated with the new system and their possible remedies.

Chapter 1
Introduction

1.1 Project Description and Objective

Over the past several years, steel has become less competitive in bridge construction. Several reasons exist, including limited research and innovation with regards to steel bridges. Additionally, fabricators have become accustomed to the use of outdated, complicated, and costly details and standards of practice. Bolted field splices are one very expensive item in steel bridge construction, with each bolt costing as much as $20.00 between the cost of material, installation, and inspection. (Lampe 2001) As a result, research was performed at the University of Nebraska focused on trying to eliminate bolted field splices by developing a new connection at the pier. This connection detail, called the "Simple for Dead, Continuous for Live Load" connection, allows the girders to be set as simply supported spans, and then once the deck is cast, the structure acts as a continuous one for any further applied loads, such as live loads or superimposed dead loads. Laboratory testing was performed on three different specimens in order to develop an economical detail that has adequate strength and fatigue resistance.

Replacement of the N-2 over I-80 overpass near Grand Island, Nebraska provided an opportunity to construct a bridge using the Simple for Dead, Continuous for Live Load detail. The first bridge to use this detail, it was also the first to utilize HPS-100W High Performance Weathering Steel. The bridge utilized a box girder configuration. Since it was the first bridge to use the Simple for Dead, Continuous for Live Load connection detail, it was beneficial to monitor both short and long-term behavior of the new bridge. Various types of instrumentation were used to monitor steel and concrete strains, bridge deflections, and weather characteristics. With the instrumentation, data could be collected during construction and beyond.

1.2 Organization of the report

This report consists of six chapters plus an appendix.

Chapter 1 introduces the reader a background to the “Simple for Dead, Continuous for Live” construction method.

Chapter 2 provides a description of the bridge system and its design.

Chapter 3 addresses the construction sequence and the girder fabrication sequence of the bridge.

Chapter 4 provides the information on the instruments installed on the bridge to determine the behavior of the structure and their locations.

Chapter 5 presents the analysis of the data collected from the instrumentation during the construction phases of the bridge and its conclusions.

Chapter 6 is devoted to the analysis and results obtained from the diagnostic Live Load Test carried out on the N-2 over I-80 Bridge.

Chapter 7 focuses on the long-term monitoring of N-2 over I-80 bridge.

Chapter 8 provides the summary and conclusions of the N-2 over I-80 instrumentation and monitoring.

Chapter 9 is the references used in various chapters of the report.

Appendix A demonstrates the graphs associated with the.

Chapter 2
Box Girder System

This chapter provides a description of the system and its design

2.1 Structure Geometry

The N-2 over I-80 overpass is a two-span structure, each span being 139' in length. It replaces a four-span prestressed concrete girder bridge. There are three lines of girders, spaced at 16'-1" on center. The girders are steel box girders fabricated from HPS-100W High Performance Weathering Steel. The system utilizes the Simple for Dead, Continuous for Live load connection detail at the pier. The deck is 46'-4" wide and is 7-1/2" thick which includes a ½" wearing surface. Figure 2-1 shows a cross section of the structure.

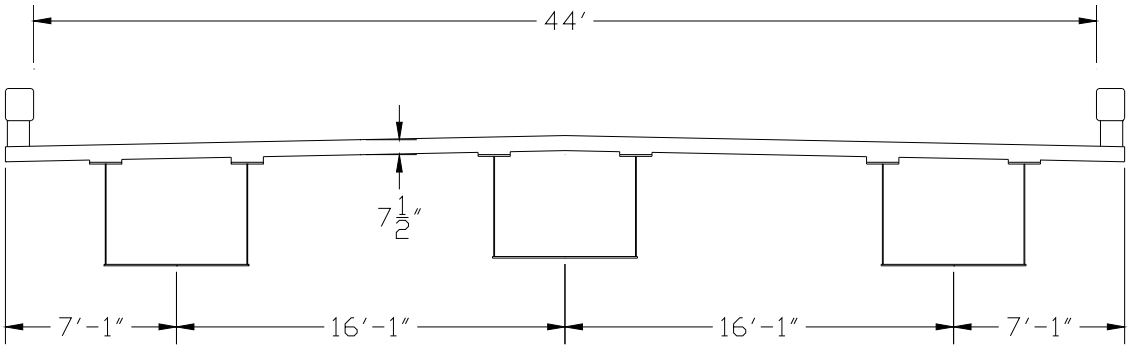

Figure 2-1. Bridge cross section

2.2 Girder Geometry

As previously mentioned, the girders were fabricated using HPS-100W High Performance Weathering Steel. Figure 2-2 shows a cross section of the steel girders. The top flanges are made from 7/8" by 1'-4" plate. The webs are made from 3/8" by 4'-2" plate. The bottom flange is made from ¾" by 6' plate. These plate thicknesses remain constant throughout the entire bridge length. Near the pier, there is a concrete slab cast onto and made composite with the bottom flange that helps prevent the bottom flange from buckling in compression. The stiffening of the bottom flange allows the bottom flange to be of constant thickness throughout the entire length of the girder. The bottom flange slab can be seen in Figure 2-3. Cross frames were located inside of each girder at the spacing shown in Figure 2-4. The layout is symmetric about the pier. Figure 2-5 shows the typical cross frame detail.

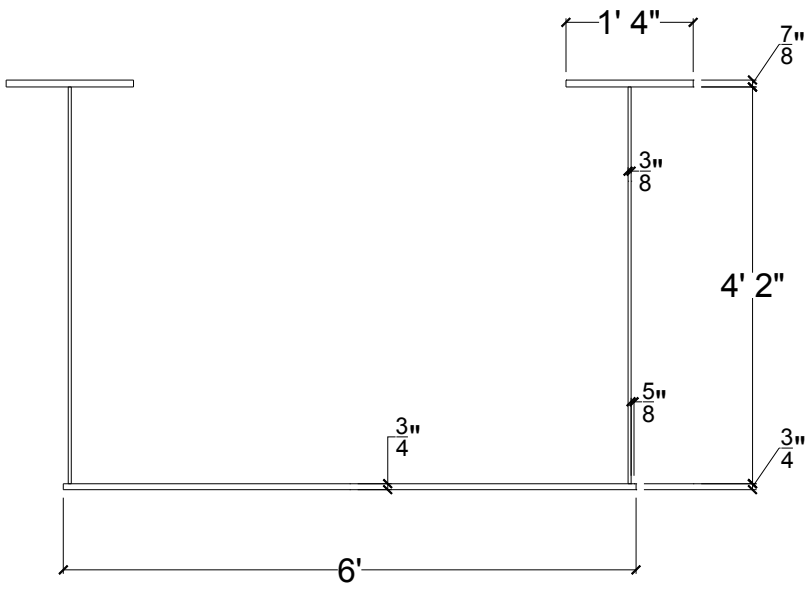

Figure 2-2. Girder cross section

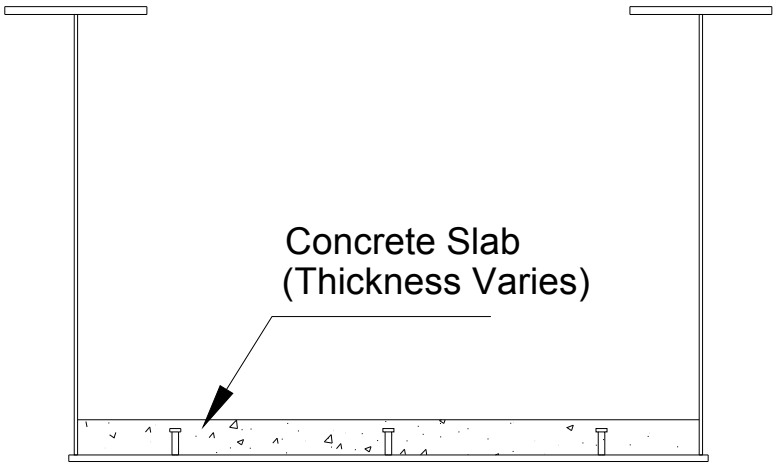

Figure 2-3. Girder cross section showing concrete slab at bottom flange

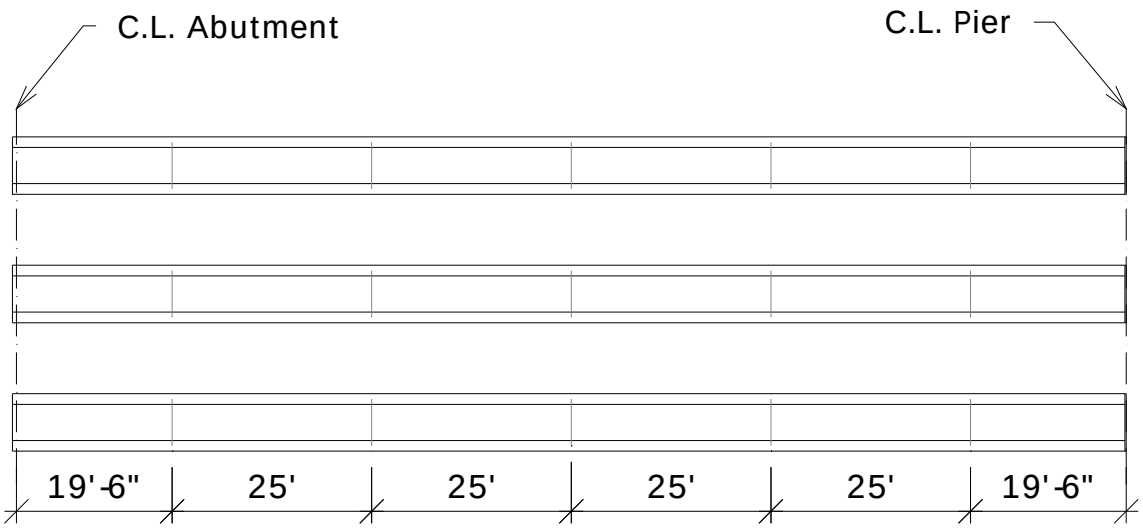

Figure 2-4. Cross-frame layout

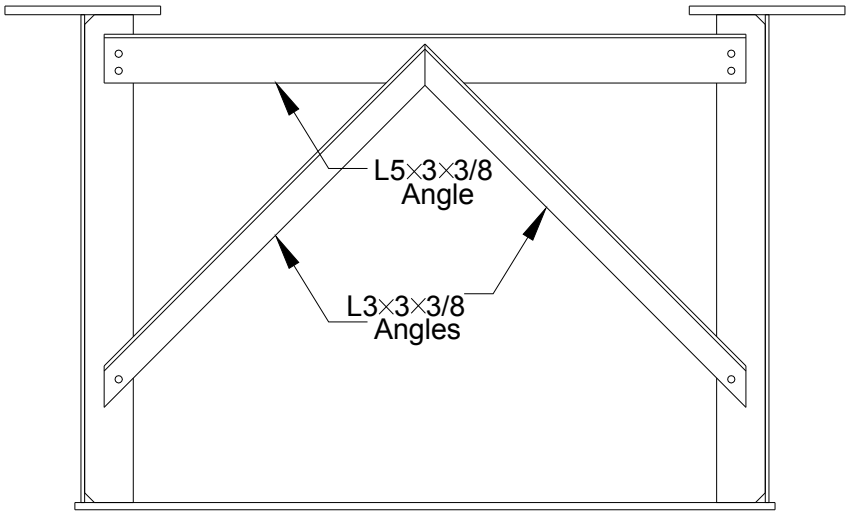

Figure 2-5. Cross-frame detail

2.3 Pier Connection Detail

The pier connection detail is shown in Figure 2-6. Each girder was set on 2 - 12 inch long steel tubes that were filled with epoxy grout. To prevent interruption to the diaphragm face steel, #4 bars were placed through the holes in the girder webs and tied with #4 stirrups. (Figure 2-7) The bulkheads served as formwork for when the diaphragm was poured. The bulkheads were also designed to transfer the compressive force through the bottom flanges. In addition to this, bearing plates were welded to the bottom flanges so that they would touch in their final condition. Since the spans are of equal length, the bottom flanges at the pier will never experience tensile forces, so no connection was required between the bearing plates. (Figure 2-7)

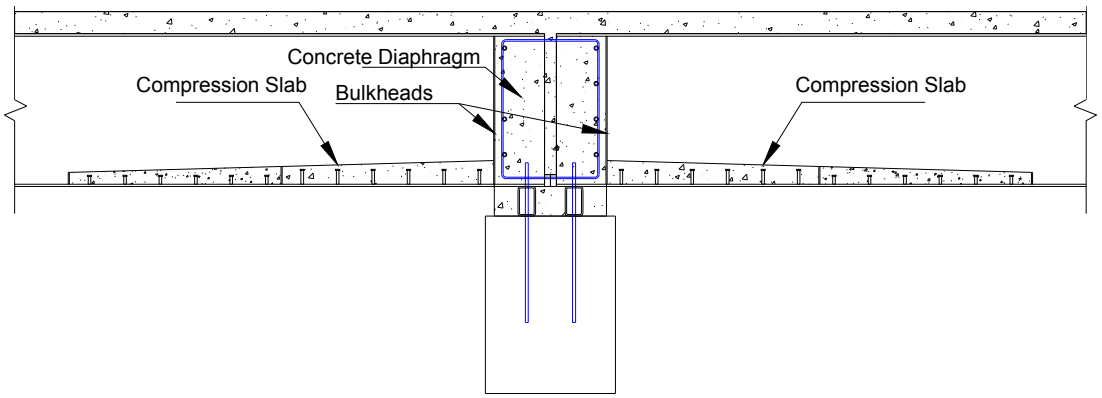

Figure 2-6. Pier connection detail

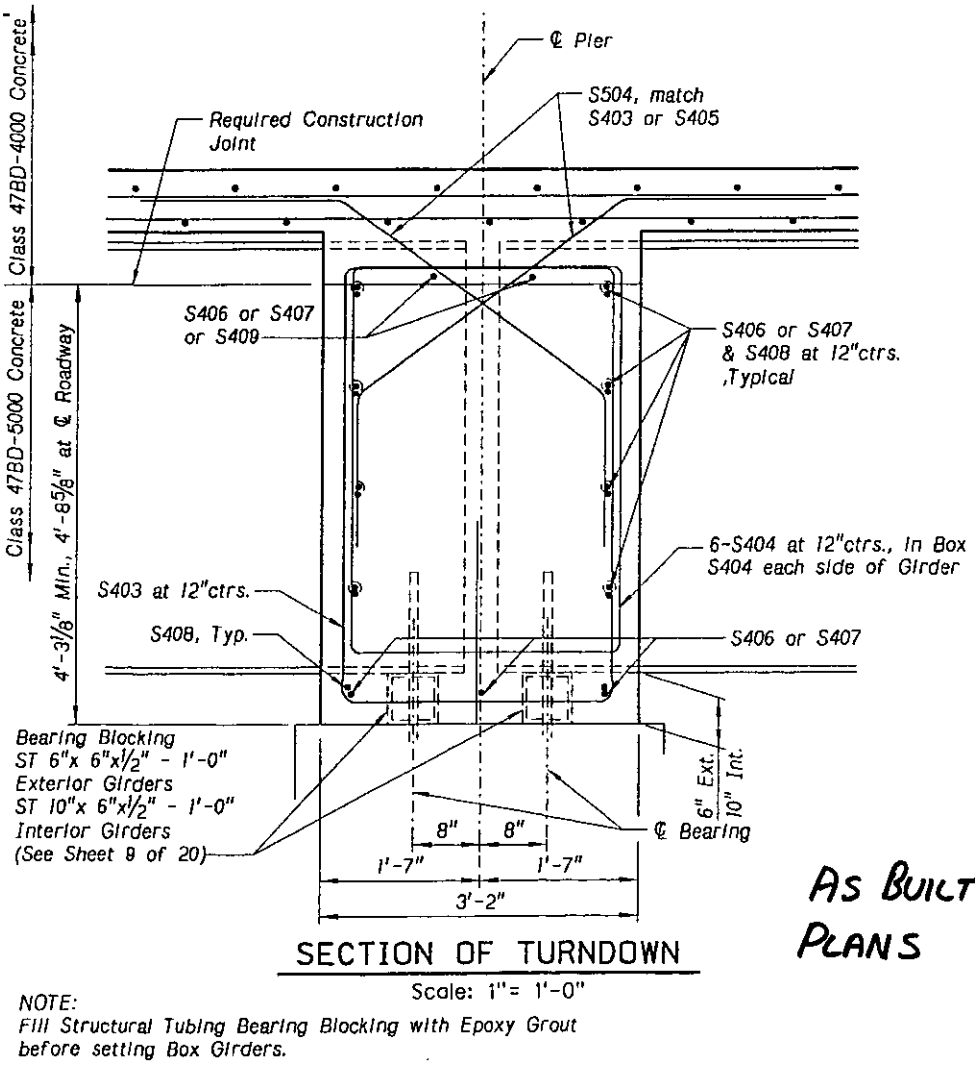

Figure 2-7. Bar detail at the connection over the pier

2.4 Deck

The deck is a 7-1/2" thick which includes a ½" integral wearing surface. The width of the deck is 46'-4". Longitudinal reinforcement consisted of #4 bars at 12" on center in the top layer, and #5 bars at 12" on center in the bottom layer. Transverse reinforcement consisted of #5 bars at 12" on center in both the top and bottom layers. Additionally, over the pier, two #7 bars were placed between each #4 bar in the top layer, and a #7 bar was placed between each #5 bar in the bottom layer. A detail showing this deck reinforcement over the pier can be seen in Figure 2-8.

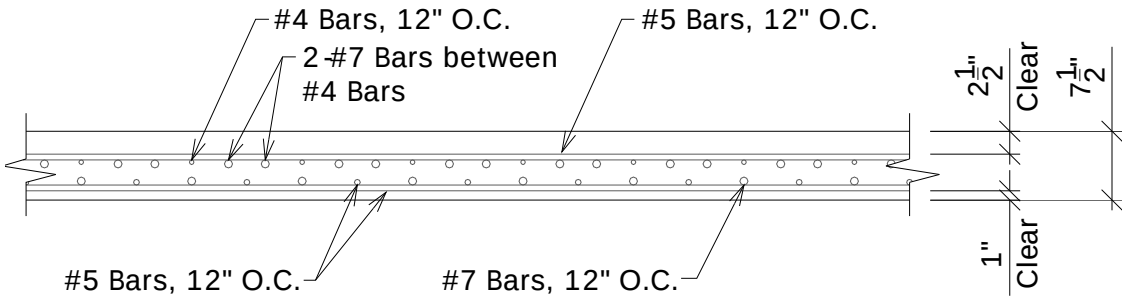

Figure 2-8. Longitudinal Deck reinforcement near pier

2.5 Guardrails

The guardrails on this bridge were standard NDOR closed guardrails, 2'-5" in height by 1'-2" in width. (Figure 2-9)

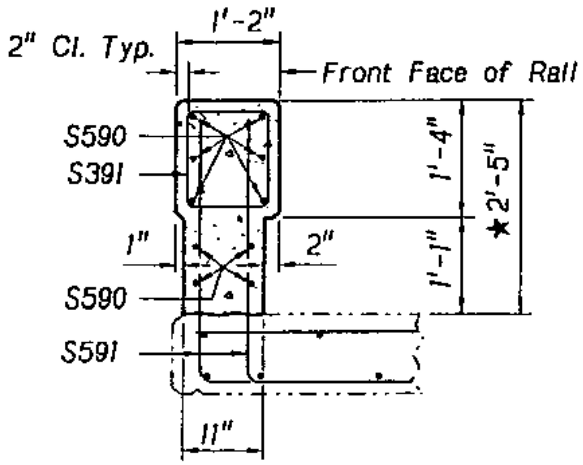

Figure 2-9. Guardrail detail

Chapter 3
Construction Overview

Construction of the N-2 over I-80 overpass began in May 2003. Girder fabrication began in June 2003. The construction sequence and the girder fabrication sequence are outlined in the following sections.

3.1 Substructure Construction

Upon completion of demolition of the old structure, which lasted from May 6, 2003 to June 12, 2003, construction of the new substructure began. The first thing built was the pier. Piling for the pier was driven between June 3 and June 10, 2003. The footing was poured on June 11, 2003. After that, the rebar cage was tied and forms were built. Concrete was poured for the pier on June 26, 2003. Forms were removed on June 30 and July 1, 2003.

Next, the pilings for the south abutment were driven. These piles were driven between July 7 and July 10, 2003. Twelve pipe piles were driven at each abutment, to a depth of approximately 66 feet. Three sets of four piles were connected at the top with a steel channel, which the girders would bear on. This can be seen in Figure 3-1.

Figure 3-1. Girder bearing on channel across piles

After the pilings were driven, the abutment was formed and poured. This occurred between July 14 and July 17, 2003. Then wing walls for the south abutment were next formed on July 23, and poured on July 25 and July 29, 2003. The slope protection at the south abutment was poured on August 12 and 14, 2003.

At this point, the south span girders could be set. These were set on August 21, 2003. This will be discussed in further detail in a later section. Once the south girders were set, work began on the north abutment. Piles were driven on August 20 and 21, 2003. Concrete for the abutment was poured on August 28, 2003. Concrete was poured for the north wing walls on September 5. The slope protection was poured on September 12 and September 15, 2003.

3.2 Girder Fabrication

Fabrication of the girders began in June, 2003. The south span girders were fabricated first. Several trips were made to Capital Contractors throughout the fabrication process, for observation and instrumentation. The typical fabrication sequence for each girder is as follows. The flange material was sent through the bead blaster for cleanup before the fabrication. Next, full width plates were spliced together to form a long slab. Each joint was magnetic particle tested to highlight any possible problem area, which were then fixed. After the welding was finished, X-ray testing was performed. Once complete, the long slab was stripped to the proper flange width.

For the webs, a similar procedure was followed. Welding of the web can be seen in Figure 3-2. After welding, the webs were cut to their proper width and camber, as shown in Figure 3-3.

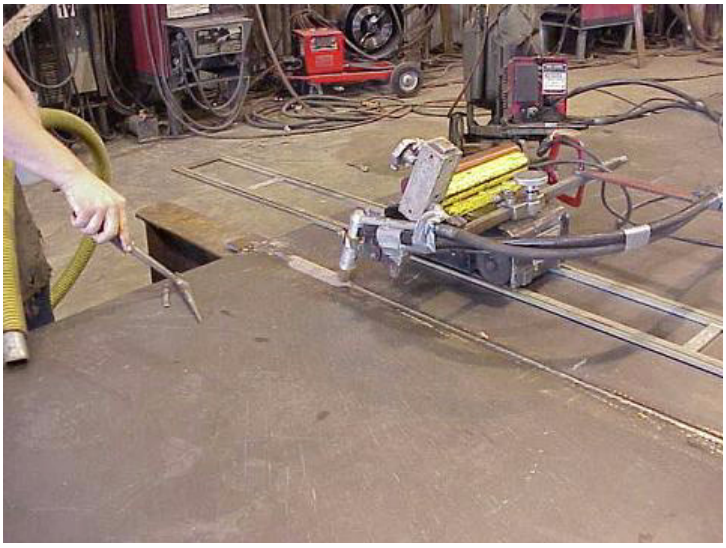

Figure 3-2. Web weld

Figure 3-3. Web being torch cut to proper height and camber

Once all the plates were welded up for the first girder, the webs and top flanges were tacked together, as shown in Figure 3-4. Once the flange and web were tacked together, they were flipped over and wire-fed welded together, as shown in Figure 3-5. They were flipped back over, and the tack welds were ground out. Then the other side was wire-fed welded.

Figure 3-4. Top flange tack-welded to web

Figure 3-5. Top flange being wire welded to web

After the top flange and web were welded together as one unit, they were then attached to the bottom flange. The bottom flange was placed on several saw horses and shimmed as required to match the camber of the web. Using a combination of jacks, hammers, clamps, the crane, and angles, as shown in Figure 3-6, the web was set into position onto the bottom flange and tacked to it. Welds were about 6 inches long and alternated from one side of the web to the other. Once both webs were in place, a similar process to what was used for the top flange-web weld was used to weld them to the bottom flange.

Figure 3-6. Positioning web on bottom flange

Once the box was completed, stiffeners and cross frames were installed, as well as the bulkhead at the pier end. Fabrication of the first girder, A1, took approximately 5 weeks to complete.

Fabrication of girder B1 began on July 29. It was completed August 13. Girder C1 was completed August 21, and all three were shipped that day. They were set that night. Fabrication of A2, B2, and C2 began shortly thereafter. Girder A2 was completed on September 9. Girder B2 was completed on September 16. Girder C2 was completed on September 17. The north girders were shipped on September 17 and 18, and set on the night of September 18.

Chapter 4
Instrumentation

Various types of instruments were used to determine the behavior of the structure. These instruments monitored strains, deflections, and various climatic effects both during construction events such as the deck pour and rail casting, and after construction was completed to evaluate the long-term behavior.

4.1 Data Acquisition System

The data acquisition system (DAS) used consists of several different components that work together to collect data for analysis. The system is capable of collecting data at appropriate intervals, record the data for later retrieval, and protect the data in case of power failure so that it is not lost. The system used is produced by Slope Indicator Co., of Mukilteo, Washington.

The primary component of the system is the CR10X Measurement and Control System. The CR10X controls all of the other devices in the system and stores the system's program.

The CR10X also provides storage for the data and keeps it in non-volatile memory so that the data is not lost should power loss occur.

The next component in the system is the AM16/32 Relay Multiplexer. The AM16/32, shown in Figure 4-1, is the wiring hub for the gages. These act as switches allowing each gage to be individually sampled. The AVW100 modules are used for reading the vibrating wire type gages.

Figure 4-1. AM 16/32 Relay Multiplexer

Other components in the system include a PS12LA battery/charger. This provides the system with power. A solar panel, produced by Solarex of Frederick, MD, is connected to the PS12LA to run the system and charge the battery during the day so that the system can run on battery power at night. The solar panel can be seen in Figure 4-2. An SC32B Optically Isolated RS232 serial interface allows the system to be linked to a PC so that data can be retrieved or a new program can be uploaded to the CR10X locally. To do this remotely from the office, a COM 100 Cellular Phone Package and a COM 210 Telephone Modem can be installed. An ASP-962 yagi antenna, produced by Allen Telecom Inc., of Dallas, TX, is used with the COM100 to improve cellular signal strength.

Except for those noted, the components of the system were manufactured by Campbell Scientific of Logan, Utah. The system is assembled by Slope Indicator Co. to fit the needs of the project. Figure 4-3 shows a schematic of the DAS system used on the N-2 over I-80 project.

Figure 4-2. Solar Panel

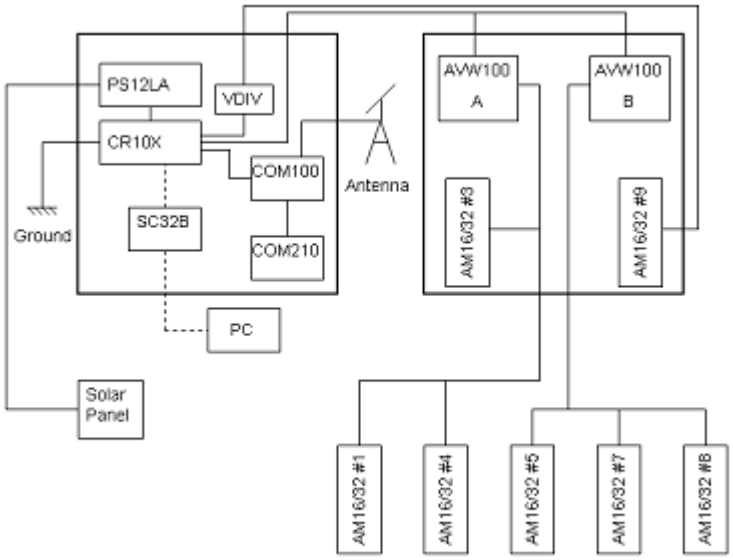

Figure 4-3. Data acquisition system schematic

Figure 4-4 shows a picture of some of the mentioned components. The PS12LA is in the upper left, with the CR10X just below that. Below the CR10X is the SC32B Optically Isolated Serial Interface. The COM100 modem is in the upper right, and the COM210 cellular phone is below that. Figure 4-5 shows a picture of the AVW100 vibrating wire module.

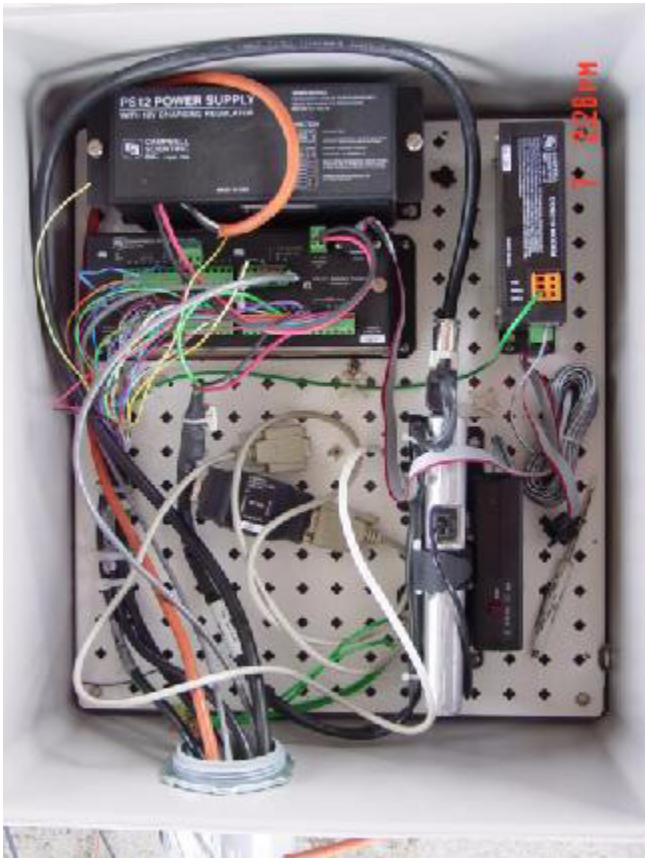

Figure 4-4. Data Acquisition Components

Figure 4-5. AVW100 Vibrating wire module

4.2 Gages and Instrumentation

Several different kinds of gages and instrumentation can be used with the DAS. There are gages that read strains in concrete and steel, gages to measure deflection of the girders, and gages to monitor movements in the pier and abutments. The gages selected must be capable of withstanding several years of use while exposed to the elements.

4.2.1 Steel Strain Gages

To monitor steel strains, spot weldable vibrating wire strain gauges made by Slope Indicator Co. are used. The gage, shown in Figure 4-6, consists of a small wire held in tension inside a small tube that has a flange on it so that it can be spot welded to the girder. After the gage is attached to the girder, a reader, shown in Figure 4-7, is attached

to the top of it. The reader "plucks" the tensioned wire and causes it to vibrate. The frequency is read and recorded by the DAS. The frequency can then be converted to strain. Control and frequency measurement are provided by the AVW100 modules.

Figure 4-6. Spot welded vibrating wire strain gage

Figure 4-7. Strain gage reader

4.2.2 Concrete Strain Gages

To monitor concrete strains, two different things are done. To monitor compressive strains, vibrating wire embedment gauges made by Slope Indicator Co. are used. This gage, shown in Figure 4-8, works similarly to the spot weldable gage by reading the frequency of a vibrating wire held in tension. To monitor the tensile strains in the concrete, spot weldable gages are attached to pieces of reinforcing steel to create "sister bars". These bars are placed in the concrete deck along side the longitudinal reinforcement. See Figure 4-9 and Figure 4-10.

Figure 4-8. Vibrating wire embedment gage

Figure 4-9. Sister bar prior to completion

Figure 4-10. Completed sister bar

4.2.3 Tiltmeters

To monitor movements of the abutments and pier, Monopod EL Tiltmeters made by Slope Indicator Co. were used. As indicated in the name, this gage measures change in tilt. This gauge has a rebar stud on it that is epoxied into a hole in concrete. Once the epoxy has set up, the gage is then leveled using the bubble level on top. The gage is capable of detecting rotations in two planes. See Figure 4-11.

Figure 4-11. Tiltmeter

4.2.4 Deflection Monitoring

To measure deflections in the girders, linearly variable displacement transformers (LVDTs) made by Trans-Tek, Inc., of Ellington, Connecticut were used. These LVDTs, similar to what is shown in Figure 4-12, detect movement of a rod that slides through the middle of the device. Voltage is applied to the device, and depending on the position of the rod in the middle, the output voltage varies. Knowing the input and output voltages, and a gage calibration factor, the change in displacement can be found.

Figure 4-12. Linearly Variable Displacement Transducer (LVDT)

A water-level system was built in conjunction with the LVDTs to monitor the deflections. For each span, a PVC tube was placed at the pier, and at midspan. The tube at the pier is considered a reference point. Each mid-span tube was connected to its corresponding reference tube at the pier with plastic hose. Bobbers with the LVDT rods inserted into them were placed in the PVC tubes. The system was then filled with water and antifreeze so that the bobbers would float. The LVDTs were placed over the rods, and then the pipes were adjusted so that the bobbers were at approximately the middle of their strokes. Since the device at the pier is the reference, the water levels of the other gages are assumed to change with respect to that one, while the pier device is assumed to not move. The change in water level represents the deflection of the girder at the point where the instrument is located. One of these units can be seen in Figure 4-13.

Figure 4-13. Water Level

4.2.5 Weather Instrumentation

Finally, weather instrumentation was installed in order to correlate data with changes in weather. A TE525 Tipping Bucket Rain Gage was installed to measure precipitation. A CS500 Temperature and Relative Humidity Probe were installed to measure temperature and relative humidity. An LI200X Pyranometer was installed to measure solar radiation. These three instruments were provided by Campbell Scientific through Slope Indicator Co.

4.2.6 Gage Locations

Placing gages on all of the girders at identical places is very costly and creates large amounts of unnecessary data. Care was taken to place gages with as little redundancy as possible. This allowed more instrumentation to be placed in the area of interest, which was near the diaphragm at the pier.

The majority of the instrumentation was installed on the interior (B) girder on both spans, while only the north span, east exterior (C) girder had instrumentation installed on it. Gages were placed such that the behavior could be investigated near the abutments, at mid-span, and near the diaphragm.

4.2.7 Vibrating Wire Gages

Vibrating wire strain gages were placed on the flanges and webs at several locations along the girders. Vibrating wire embedment gages were placed in the slabs inside the girders near the pier and inside the diaphragm as well. Figure 4-14 and Figure 4-15 show a schematic plan view of the girders of the bridge. Along the bridge, from north to south, there are sections denoted by the letters A-P. The north abutment is denoted by the letter X, and the south abutment is denoted by the letter Z. Figure 4-16 to Figure 4-19 show gage configurations for all sections, if gages are present. For instance, section C on girder B can be found in Figure 4-16. At this location, there are 3 types of gages. All of the gages are labeled "B-Cx", where "B" indicates the gage is on girder B, "C" indicates the section the gage is located at, and "x" indicates where the gage is at on the girder at that section. "T" indicates the gage is on the top flange. "W" indicates that it is on the web. "B" indicates that it is on the bottom flange. "D" indicates that the gage is in the concrete slab in the box girder near the pier, which means that it is an embedment gage.

"S" means that the gage is a sister bar, and is located in the deck. "P" indicates that the gage is inside the diaphragm at the pier. If there is a number after the last letter, then there is more than one gage of that type at that location. At Section C, girder B, there are 3 sister bars, so they are labeled "S1", "S2", and "S3".

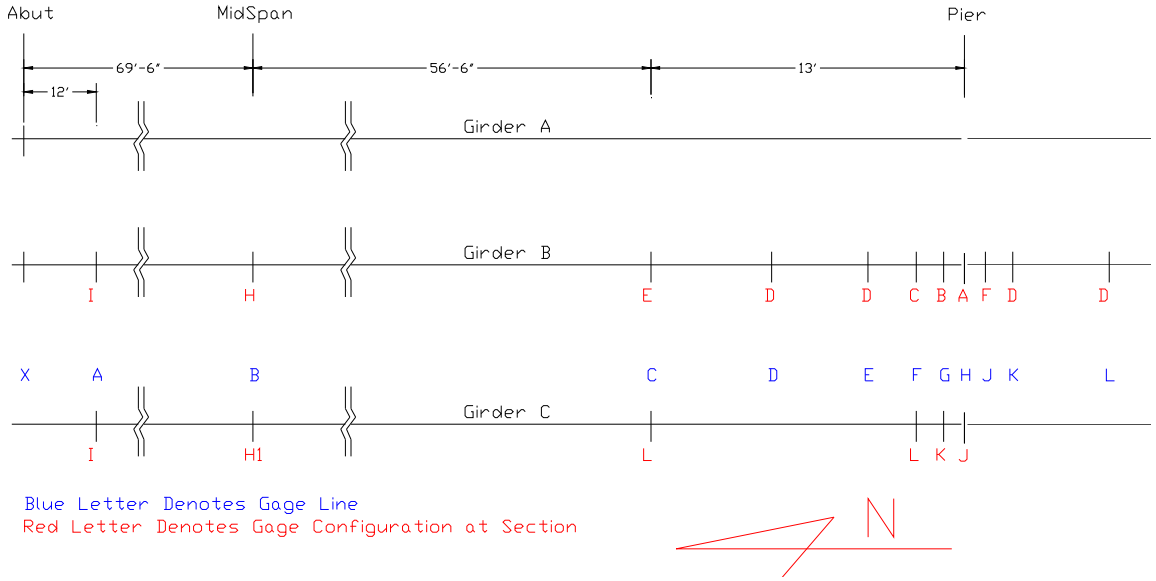

Figure 4-14. Gage layout plan for north span

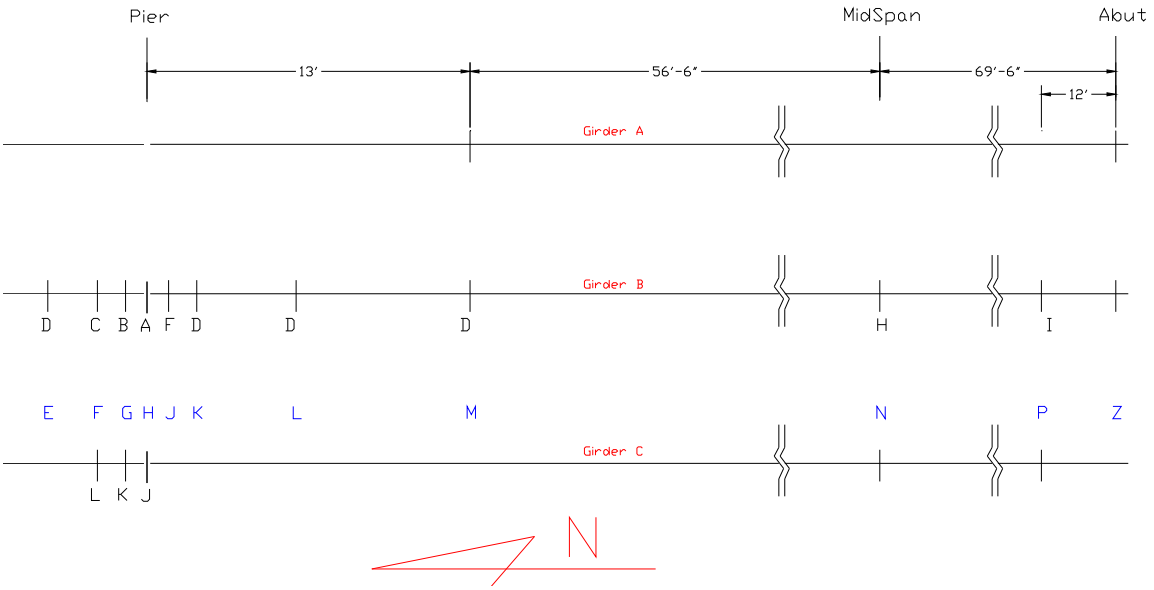

Figure 4-15. Gage layout plan for south span

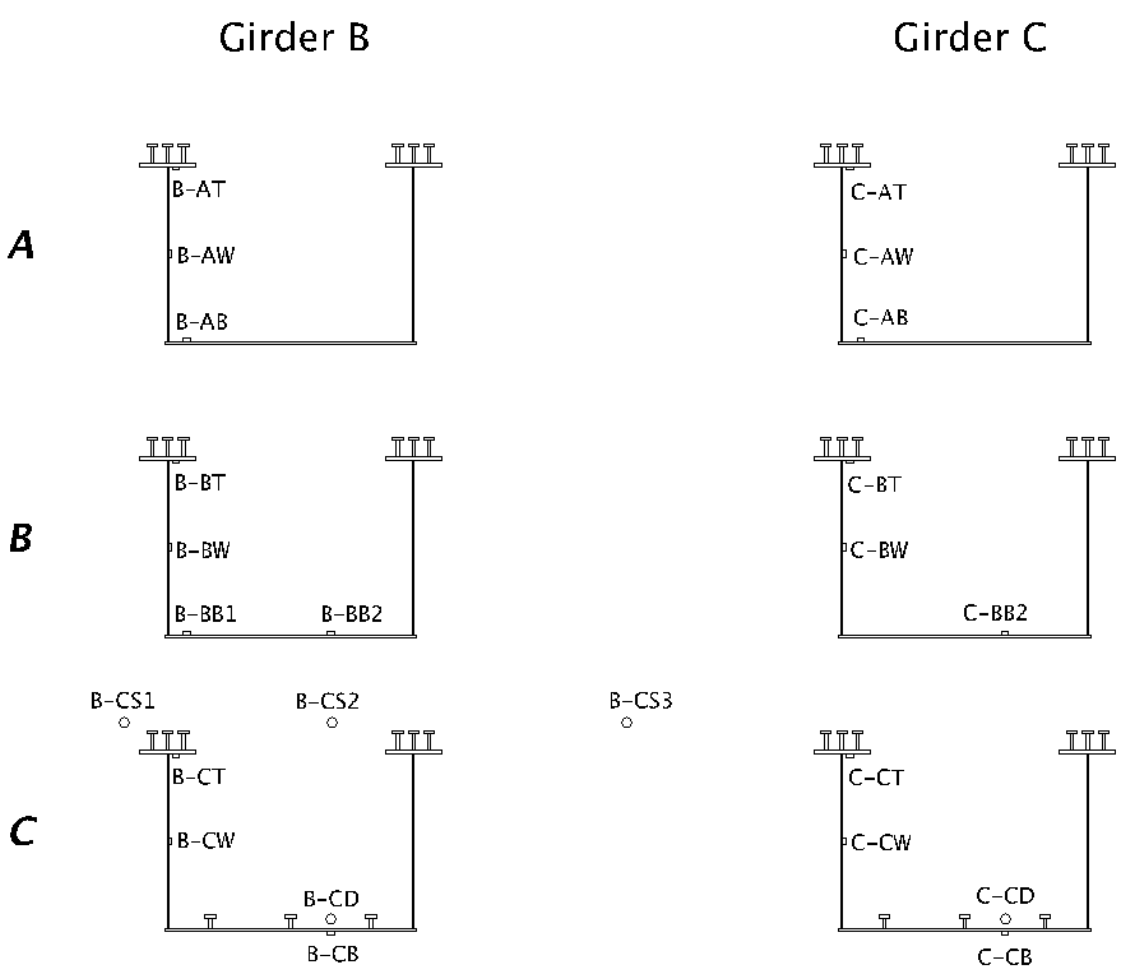

Figure 4-16. Gage sections A through C

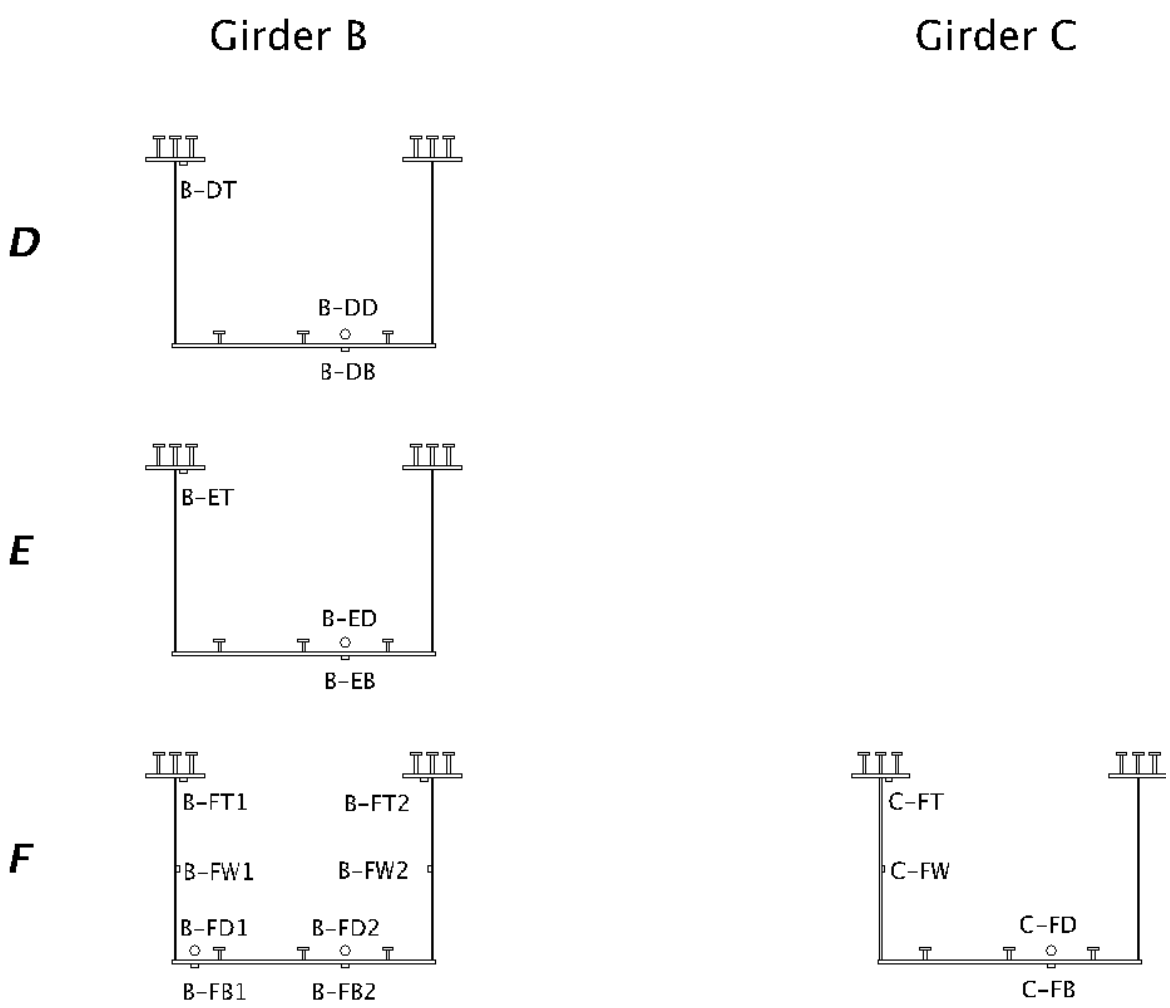

Figure 4-17. Gage sections D through F

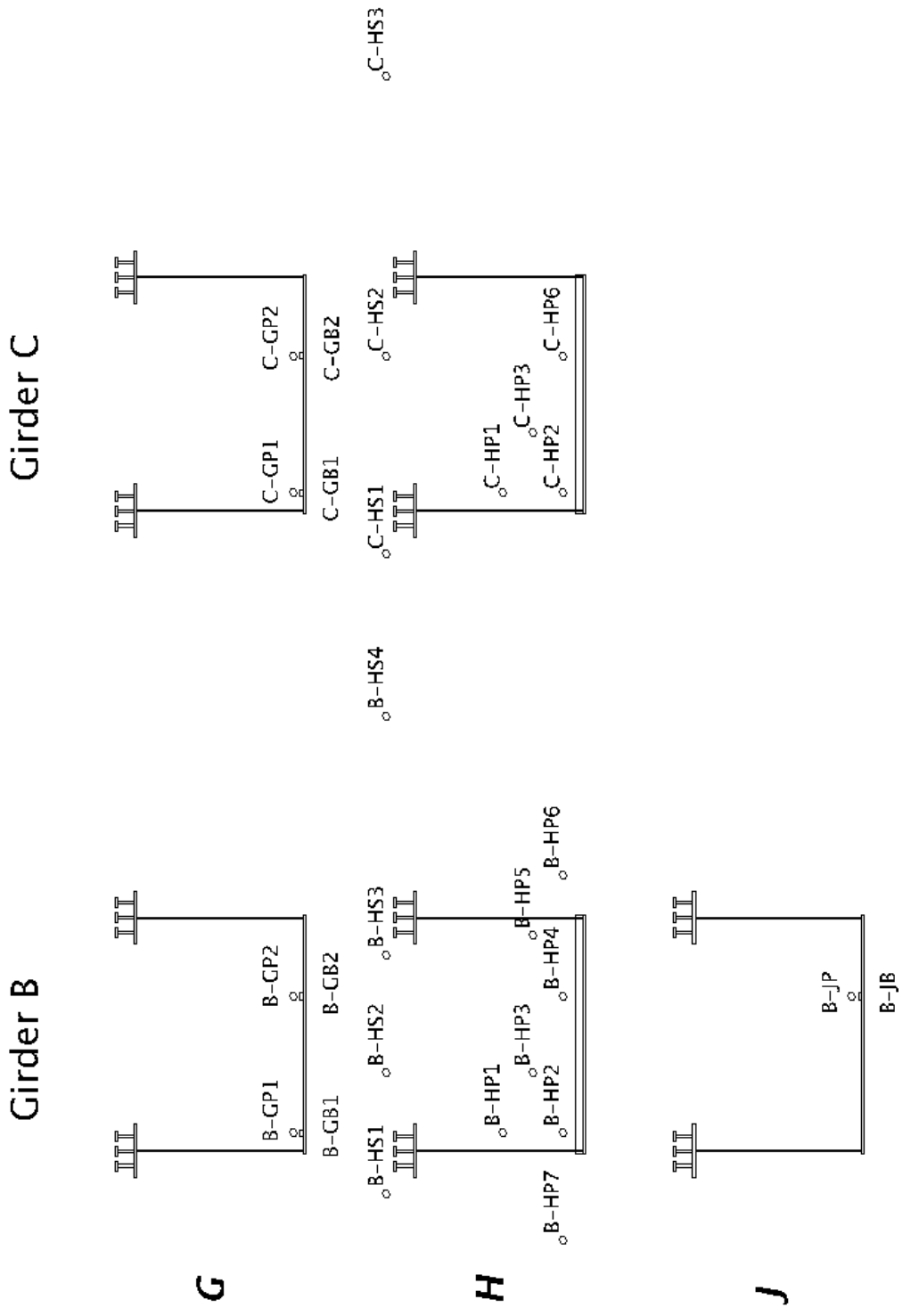

Figure 4-18. Gage sections G through J

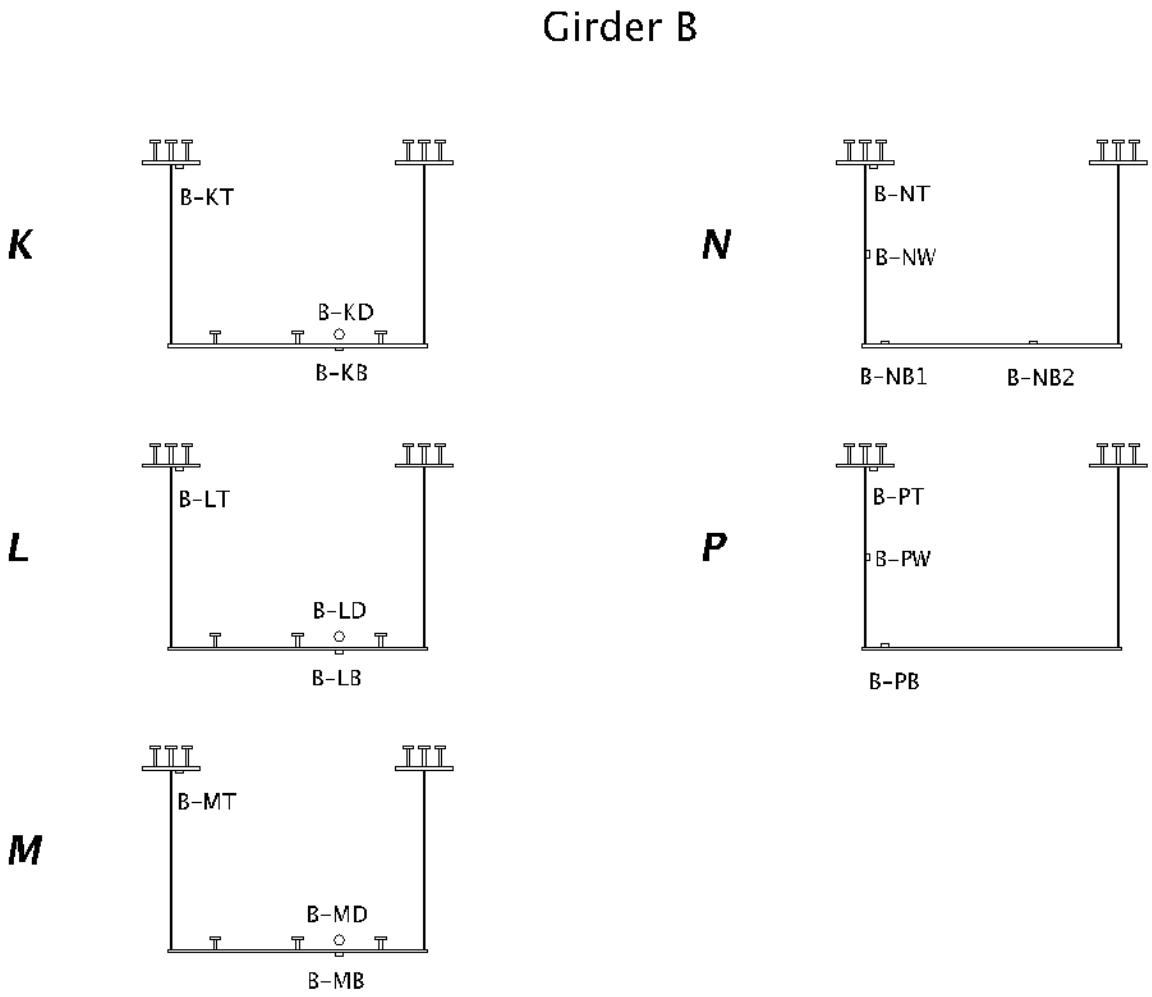

Figure 4-19. Gage sections K through P

4.2.8 Tiltmeters

Several tiltmeters were installed on the north face of the pier at different heights, as shown in Figure 4-20. Two were placed on the pier, and one was placed on the diaphragm. Placing multiple tiltmeters on the pier allowed better assumptions to be made as to how the pier deformed when lateral load from the girders was applied to it. From the data collected from the tiltmeters, a reasonable estimate of how much the top of the pier moved could be calculated.

An additional tiltmeter was placed on each abutment inside the center girder, as shown in Figure 4-21.

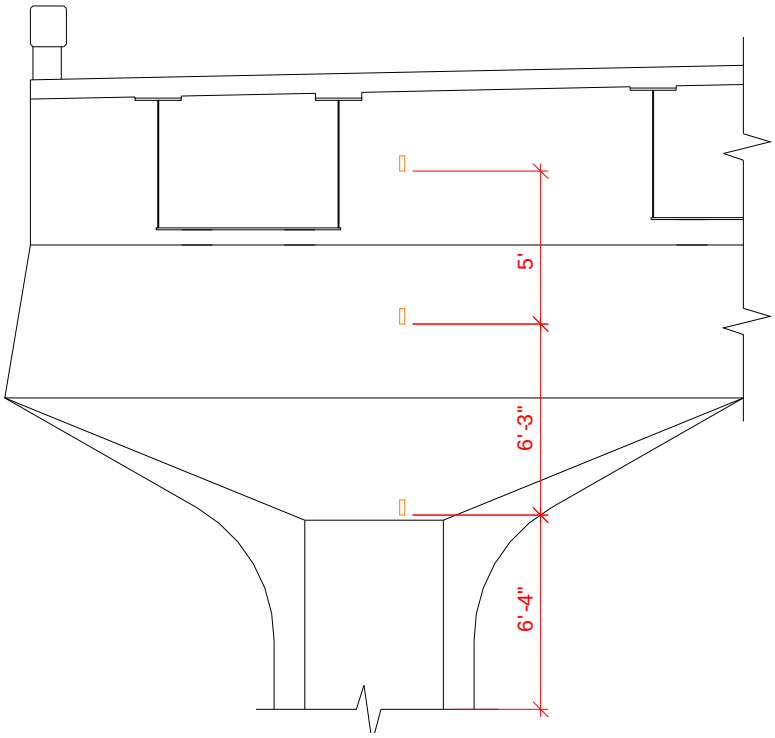

Figure 4-20. Tiltmeter layout at pier

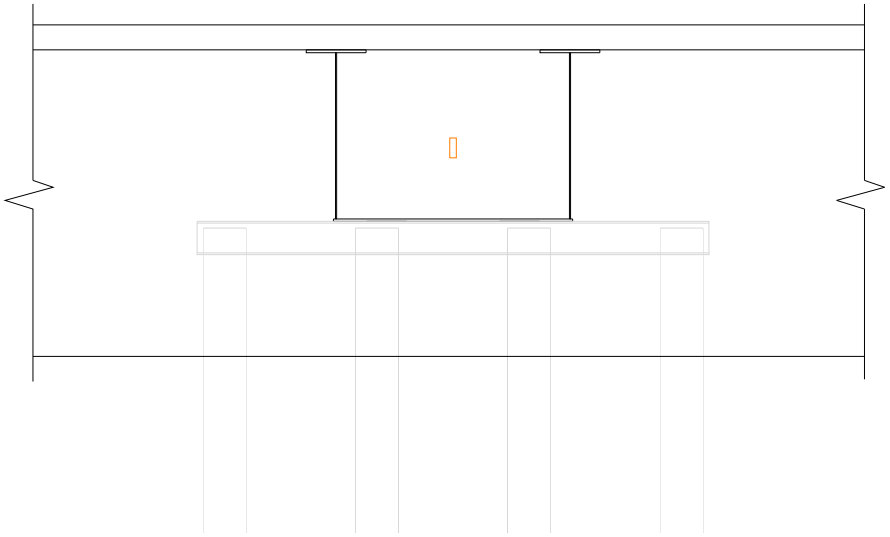

Figure 4-21. Tiltmeter placement at abutments

4.2.9 Deflection Device

As mentioned previously, the deflections were monitored with a water level system using LVDTs. An LVDT was placed at mid-span of each span, inside the interior girder, and another on each side of the diaphragm. The mid-span devices were clamped to the mid-span crossframe. Each span had an independent system.

4.2.10 Weather Instrumentation

The TE525 tipping bucket rain gage and the LI200X pyranometer were attached to a frame that was installed on the west side of the diaphragm (Figure 4-22). The CS500 temperature and humidity probe was installed near the pier underneath the bridge deck in order to shield it from direct sunlight or rain.

Figure 4-22. Weather instrumentation

Chapter 5
Construction Monitoring

The analysis of the data collected from the instrumentation during the construction phases of the bridge and its conclusions are presented in this chapter.

5.1 Introduction

The majority of the sensors and the data acquisition system were installed and operational shortly after the girders were placed. This meant data could be collected during significant construction events such as the deck pour and the rail pours. The time intervals at which readings were taken were shortened in order to pinpoint any significant occurrences during the construction events. The collected data will then be compared to the expected values from analysis in order to evaluate the difference of the actual system behavior from what was expected.

5.2 Environmental strain variation

Several environmental factors can create strain in the structure. Some of the more important factors are ambient temperature, temperature gradient and wind. Temperature gradient is typically caused by solar radiation (sunshine). Temperature gradient along the depth of the girder can create thermal strains that result in bending of the girder. Wind can create lateral movement in the girder that causes strain. However, since wind is such a transient phenomenon its effects are typically not observed.

5.2.1 Thermal strains

The strain gages installed on the girders measure the total strain including strain due to loading and thermal effects. To determine the strain due to loading, the importance and magnitude of the thermal strains have to be determined. The most important sources that can change the girder's temperature are ambient temperature, heat created by the hydration of concrete, and sunlight.

Thermal strains do not create stresses in statically determinate structures. However, in statically indeterminate structures, thermal strains cause stress in the structure. The thermal strains in statically indeterminate structures may not be measured via strain gages because they can be canceled out via the elastic stresses formed in the structure. For example, in Figure 5-1, the strain gage cannot measure any strain although there is a stress in the bar because the strains from load and the ones from thermal effects cancel each other out. Figure 5-2 shows free end bar. In this case, the strain gage measures a strain while there is no stress in the bar to cancel the effect of the thermal strain out. Consequently, it means that strain gages always measure the total strain while the stress is just due to elastic (or plastic) strain.

$$\varepsilon_\theta + \varepsilon_e + \varepsilon_p = 0$$

$$\varepsilon_e = - \varepsilon_\theta$$

Figure 5-1. A bar with two end fix under a uniform temperature variation

$$\varepsilon_\theta + \varepsilon_e + \varepsilon_p \neq 0$$

$$\varepsilon_\theta \neq 0 \qquad \varepsilon_e = 0 \qquad \varepsilon_p = 0$$

Figure 5-2. A free end bar under a uniform temperature variation

5.2.2 Temperature variation in girder

Changes in the ambient temperature can change the temperature of the girder significantly. Table 5-1 shows the average ambient temperature at the closest weather station to the bridge from Record of Climatological observations.

Table 5-1. Average ambient temperature at the month of concrete pouring

Station: GRAND ISLAND AP
State: NE **County:** HALL **Standard Time:** CENTRAL
Observation Time (LST) **Temperature:** **Precipitation:** 2400
Evaporation: **Soil:**

Preliminary	Year	Month	Day	Temperature (°F)			Precipitation (see **)				
				24 hrs. ending at observation time		at Observation	24 Hour Amounts ending at observation time				At Observation Time
				Max.	Min.		Rain, melted snow, etc. (Inches & hundredths)	Flag	Snow, ice pellets, (Inches & tenths)	Flag	Snow, ice pellets, hail, ice on ground (Inches)
	2003	10	1	67	39		0		0		0
	2003	10	2	66	37		0		0		0
	2003	10	3	74	44		0		0		0
	2003	10	4	80	40		0		0		0
	2003	10	5	82	44		0		0		0
	2003	10	6	82	50		0		0		0
	2003	10	7	80	51		0		0		0
	2003	10	8	77	57		0		0		0
	2003	10	9	78	54		0		0		0
	2003	10	10	71	58		0		0		0
	2003	10	11	66	41		0.53		0		0
	2003	10	12	71	38		0		0		0
	2003	10	13	60	40		0.11		0		0
	2003	10	14	66	40		0		0		0
	2003	10	15	65	37		0		0		0
	2003	10	16	53	33		T		0		0
	2003	10	17	69	33		0		0		0
	2003	10	18	89	44		0		0		0
	2003	10	19	90	46		0		0		0
	2003	10	20	84	49		0		0		0
	2003	10	21	86	46		0		0		0
	2003	10	22	88	50		0		0		0
	2003	10	23	72	44		0		0		0
	2003	10	24	62	42		0		0		0
	2003	10	25	53	26		T		0		0
	2003	10	26	58	22		T		0		0
	2003	10	27	67	33		T		0		0
	2003	10	28	56	41		T		0		0
	2003	10	29	76	41		0		0		0
	2003	10	30	45	36		0		0		0
	2003	10	31	43	34		0		0		0
			Summary	70.2	41.6		0.64		0		

In addition to strain, all vibrating gages on the girders can measure the temperature too. Figure 5-3 shows the temperature changes at the top, bottom, and web of the internal girders for few days before the construction. As can be seen in the figure, the temperature fluctuations during all days follow a similar pattern. Temperature of the top flange during the day is higher than the web and the bottom flange due to sun shine while temperature of the girder is very similar during the night.

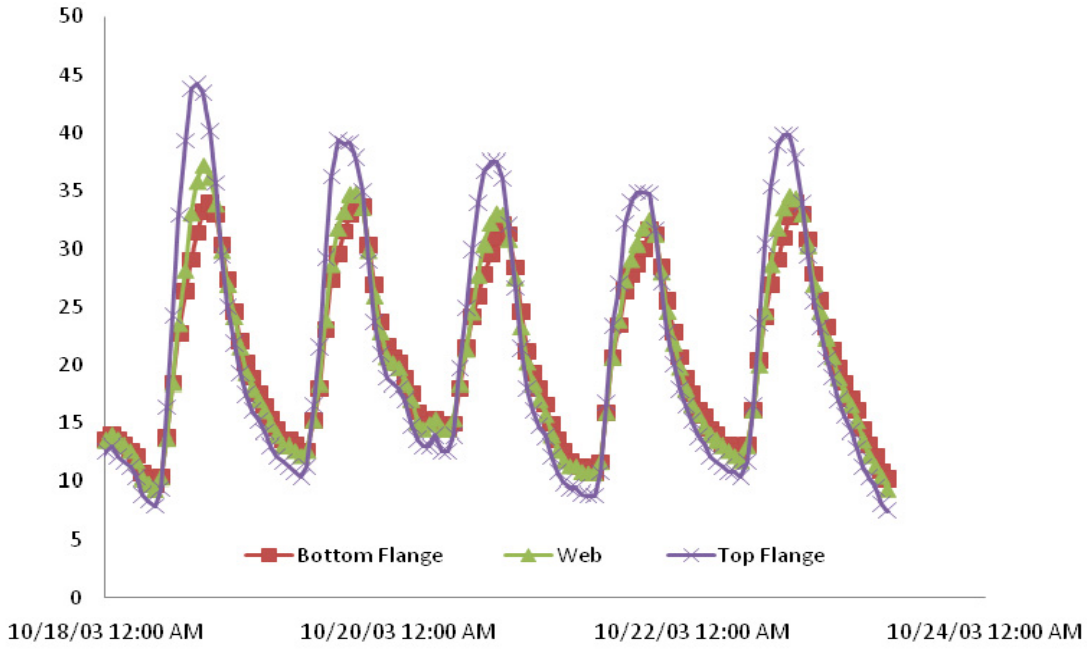

Figure 5-3. Temperature variation of an internal girder for a few days before the concrete casting of the deck

Figure 5-4 shows the temperature variations of the girder during the concrete casting. Note how the heat of the hydrating concrete in contact with the top flange causes the temperature in the flange to remain high while the remainder of the girder experiences the usual overnight reduction in temperature.

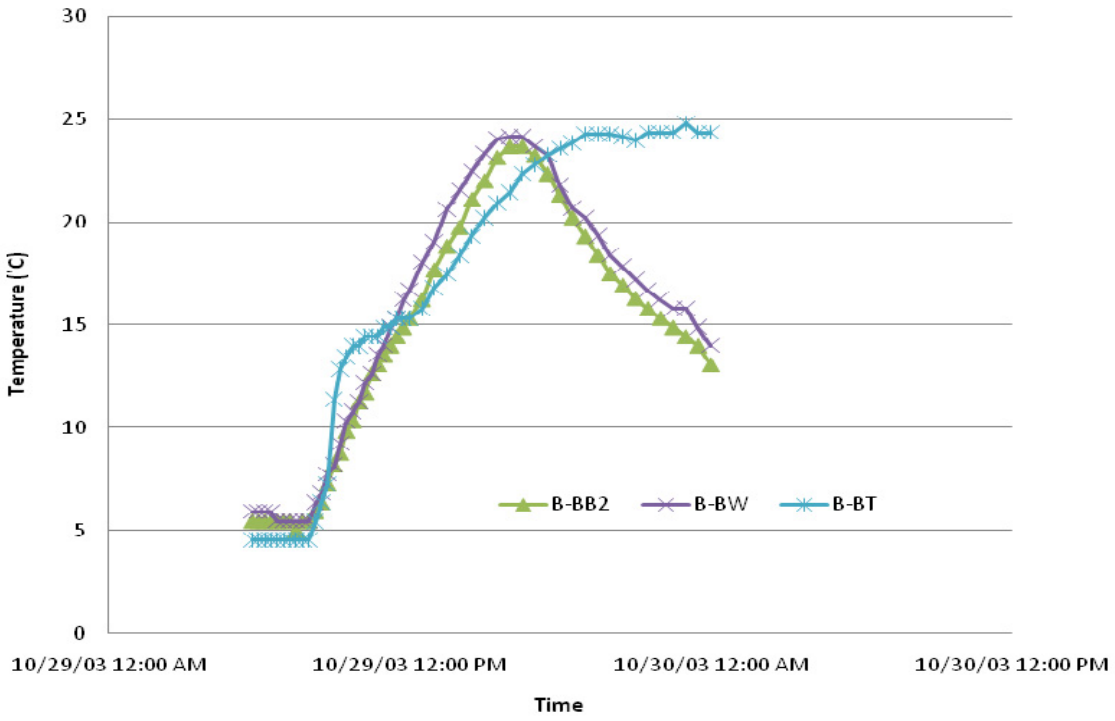

Figure 5-4. Temperature variation of an internal girder during the concrete casting of the deck

Since all top flange gages are located on the bottom side of the top flange, there is no direct contact between these gages and concrete.

By comparing the temperature variation on the pouring day and the days before the pouring, the following can be concluded:

1. Temperature has been raised in the girder mostly due to the ambient temperature.
2. The lower maximum recorded temperature at the pouring day is due to the lower maximum recorded ambient temperature.
3. Temperature variation is almost linear between 8 AM and noon.
4. There are time periods that no significant temperature gradient can be seen along the height of the girder.
5. On the normal days, the temperature of top flange is higher than the web and bottom flange due to sun shine.
6. During the concrete pouring day, the temperature of the top flange has not been dropped due to the concrete which has covered the top flange and keeps it warm due to its temperature.
7. The strains created in the girder due to temperature and thermal gradient are between 10 and 50 (microstrains), which is very small in comparison with the strains due to the dead loads during construction.

5.2.3 Thermal strain compensation

To minimize the effects of ambient temperature and sunlight, this study is carried out on the data collected between 7:00 PM and 7:00 AM while the temperature gradient along the depth of the girder is minimal. As can be seen in Figure 5-5, the average temperature difference between the bottom flange and the web is 0.35 (°C) and this difference between the bottom flange and the top flange is 1.33 (°C). Figure 5-6 shows the strain variation corresponding to the shown temperature variation in Figure 5-5. As it can be seen in the figures, the strain variation follows the same pattern during all nights. Therefore, this strain has to be mostly caused by temperature variations rather than wind. Usually the wind velocity and direction vary every night so they cannot create this kind of pattern for strain variation. There is an average of 20 με strain variation during night at the mid-point of the central girder.

Figure 5-7 and Figure 5-8 show the temperature and strain variation during few days before construction phase at a section 13 (ft) away from the pier. Again, there is a similar pattern in temperature and strain variation that shows that the temperature variation was the main reason of the strains variation.

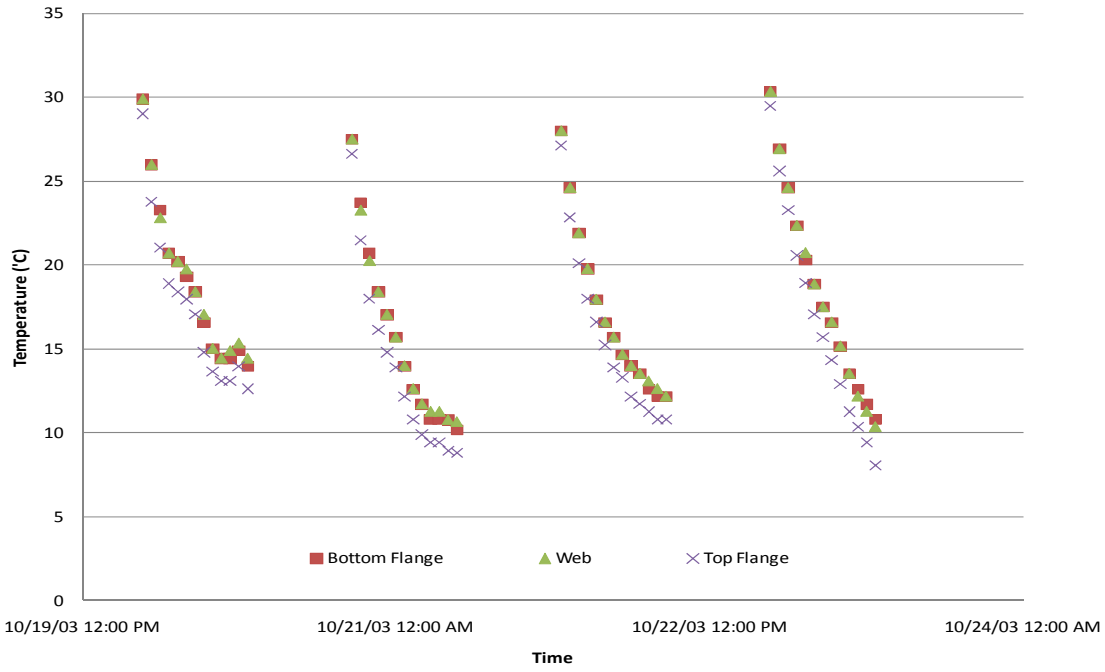

Figure 5-5. Temperature variation during night (7:00 PM – 7:00 AM) at the mid-span section

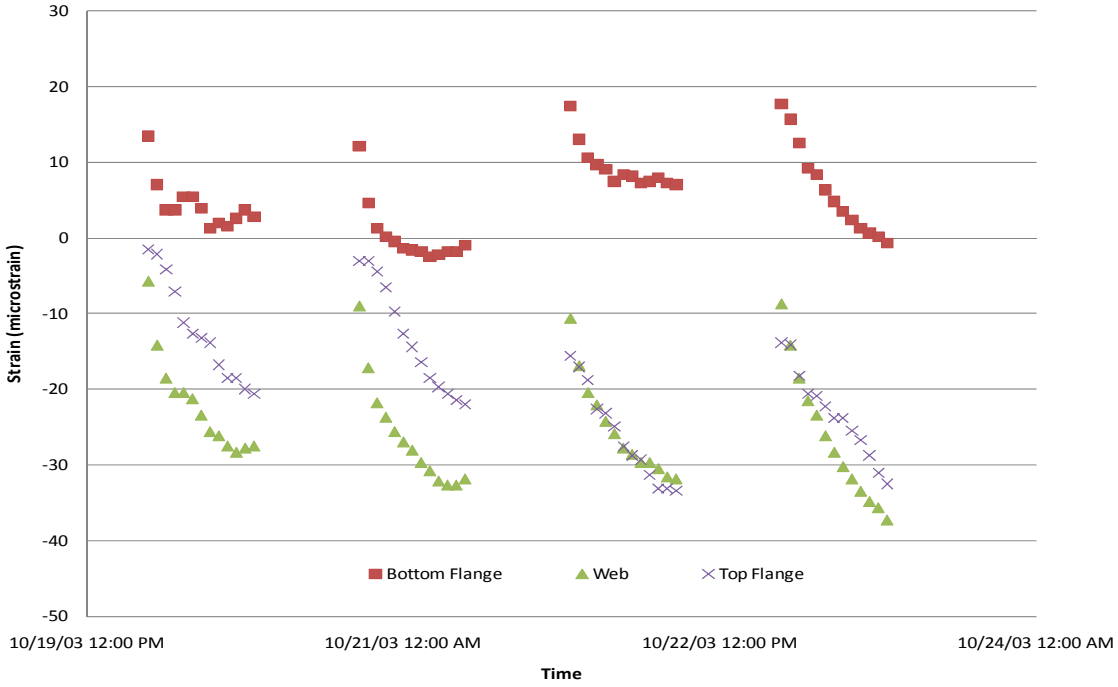

Figure 5-6. Strain variation during night (7:00 PM – 7:00 AM) at the mid-span section

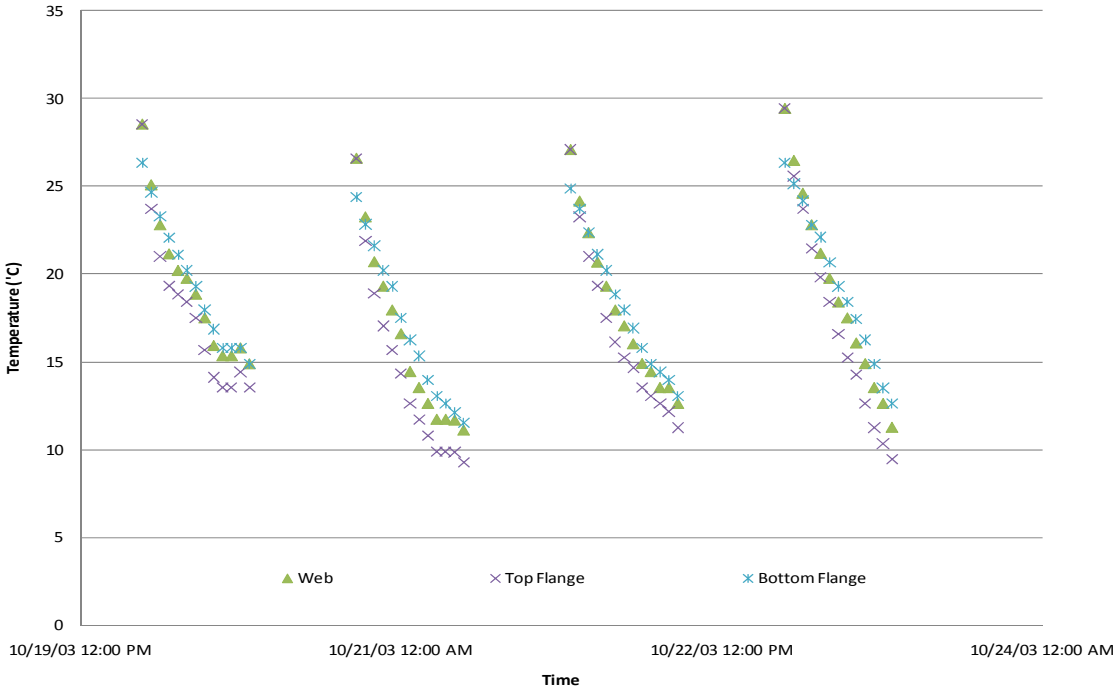

Figure 5-7. Temperature variation during night (7:00PM–7:00AM) at a section close to the pier

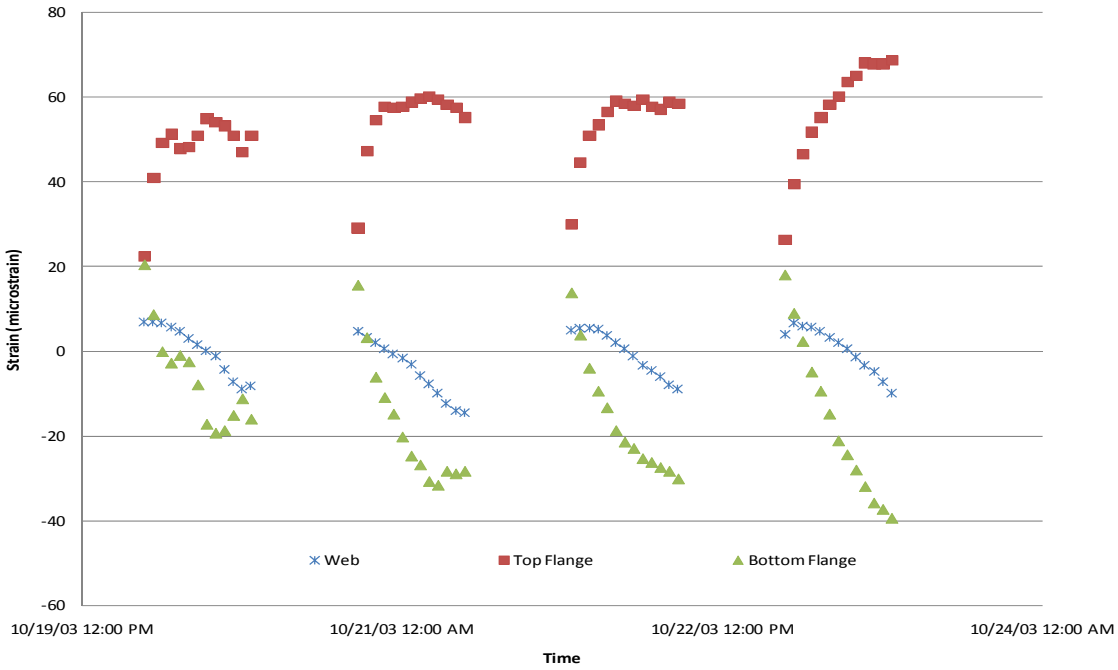

Figure 5-8. Strain variation during night (7:00 PM – 7:00 AM) at a section close to the pier

5.3 Casting Operations

The data obtained during two separate casting operations was collected and analyzed. The following sections provide an overview of these operations and the flange strains obtained along the length of the girders. Additional, in-depth analysis was also performed looking at the degree of continuity. This analysis is presented in later sections.

5.3.1 Deck pour

The deck pour provided an opportunity to monitor the behavior of the bridge girders during application of non-composite dead loads. This will help to determine whether or not the system behaves as two simply-supported spans.

5.3.1.1 Strain at Midspan

The times corresponding to the beginning and ending of the concrete casting of the north and south spans are available in the daily construction report. These times can also be determined based on the changes of the girder strains resulted from the concrete casting. Therefore, the times of concrete casting sequences are determined based on the strain variations and were verified by the daily construction report. Figure 5-9 shows the strain at the mid-span of both spans at the top flange, bottom flange, and web.

In this chart, the first letter (B) represents the girder B that is the internal girder, the second letter (B or N) represents the strain gage location, and the third letter B, W, or T refers to the bottom flange, web, and top flange, respectively.

Based on the strains variations, it was observed that:

1. Concrete pouring was started at 8:00 AM from the north span when all strains are zero before that time
2. It was continued until 9:30 AM on the south Span
3. Pouring ended at 11:45 AM where the strains become stationary.

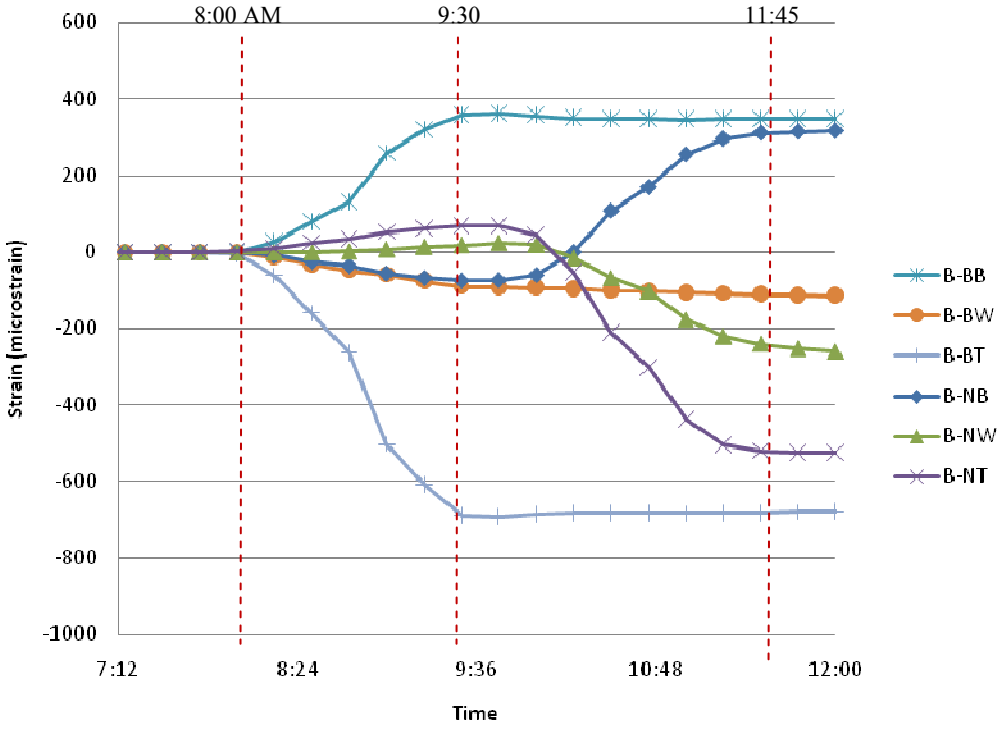

Figure 5-9. Strain changes at the mid-span on both internal girders during pouring the north and south spans

5.3.1.2 Deflection

During the deck pour, the deflections at the mid-spans of the east exterior girders were recorded along the bridge length in order to determine the girder deflections versus time. The north mid-span deflection was 5.22 inches at the end of the pour. The final recorded south mid-span deflection was 4.66 inches. Figure 5-10 show the observed deflection during concrete casting on the deck. The casting progressed from north to south. Observe that the north began deflecting downwards until the casting reached the pier at which point the deflection remained relatively constant. The south span did not begin to deflect until the casting operation entered the south span. In fact, the south span initially deflected upwards as casting was occurring in the north span, as would be expected of a continuous girder.

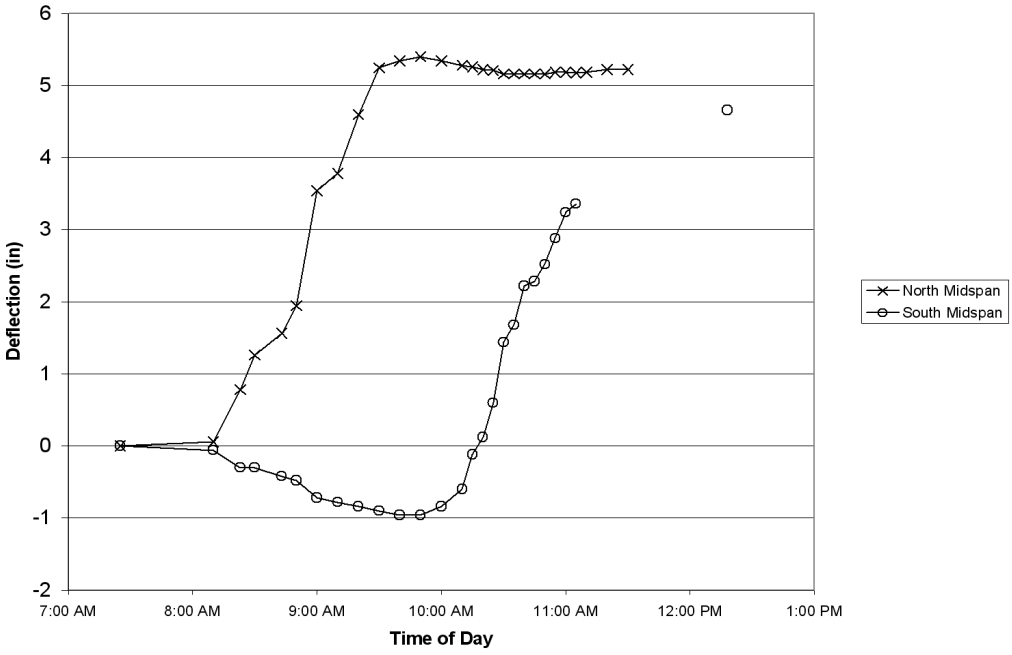

Figure 5-10. Observed girder deflections during the deck pour

5.3.1.3 Top Flange Strain along Girder

Figure 5-11 shows the interior girder top flange strains due to the weight of the concrete from gages located at various locations along the length of the bridge, from north to south. The initial strains at the beginning of the pour were subtracted from the final strains at the conclusion of the deck pour in order to determine strain changes due to the deck pour. These values will later be compared to the expected values obtained from analysis.

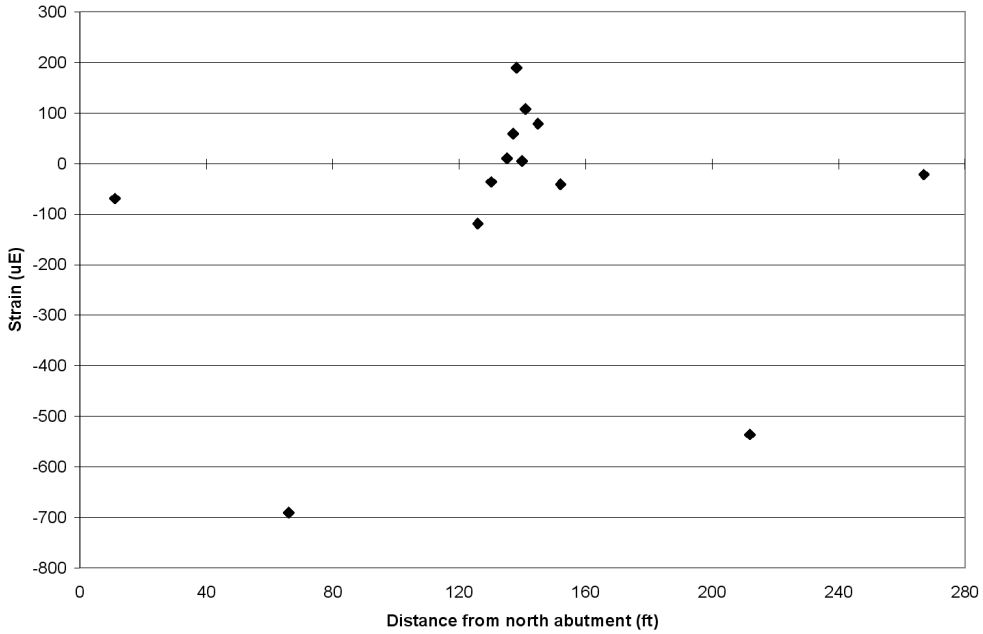

Figure 5-11. Top flange strains obtained from the deck pour (various locations)

5.3.1.4 Bottom flange strain along girder

Figure 5-12 shows the interior girder bottom flange strains due to the weight of the wet concrete determined in a similar fashion as Figure 5-11. Again, the initial strains were subtracted from the final strains in order to calculate the changes in strains resulted from the deck pour.

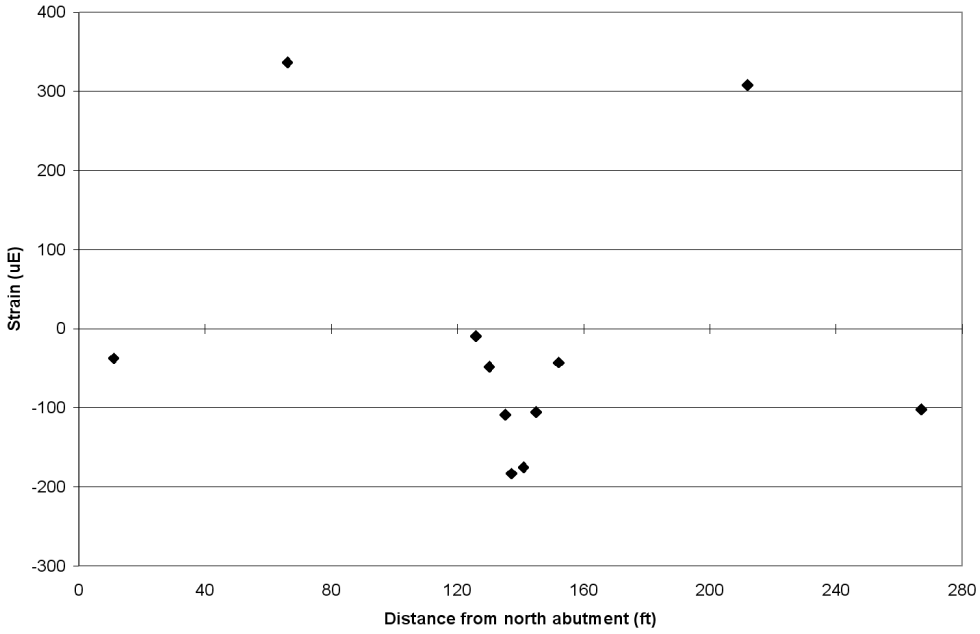

Figure 5-12. Bottom flange strains resulting from the deck pour

5.3.2 Rail Pours

Data was collected at small time intervals during the rail pours similar to the deck pour. The rails could be cast once the deck concrete strength was at least 3/4 the design strength. Figure 5-13 shows the interior girder's top and bottom flange strains resulted from the west rail pour, while Figure 5-14 shows the interior girder's top and bottom flange strains resulting from the east rail pour. Although in the design process it is assumed that the weight of the rails is equally distributed to all of the girders, data analyses from the exterior girders may indicate otherwise. Please note that the magnitudes of strains developed as a result of the rail pour are quite small.

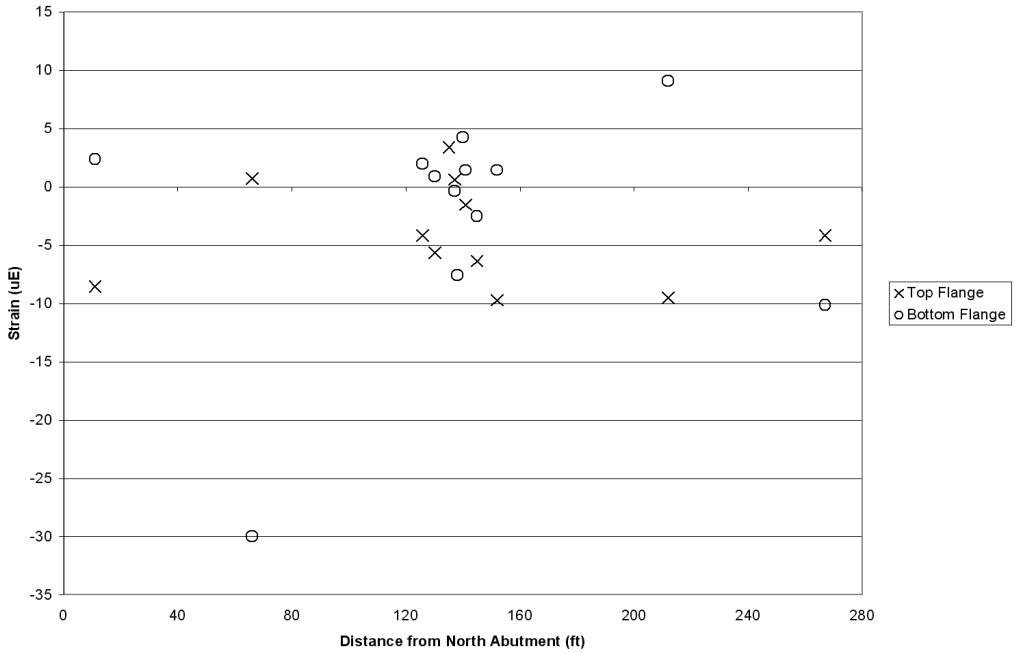

Figure 5-13. Interior girder strains due to the west rail pour

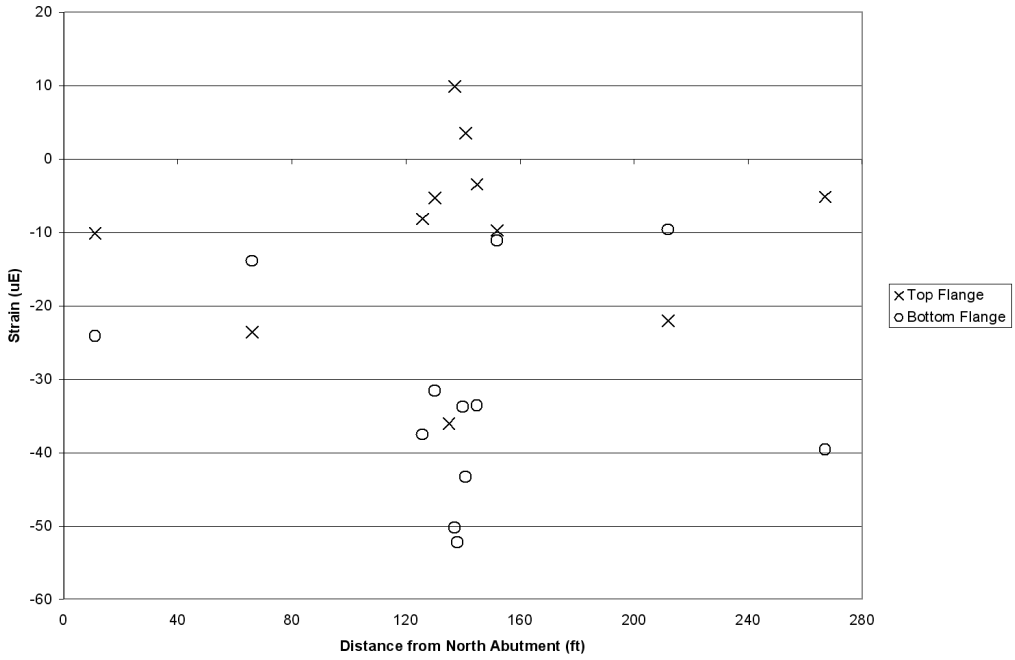

Figure 5-14. Interior girder strains due to the east rail pour

5.4 Data analysis and discussion of casting operations

Analysis of the data collected during the bridge construction and the data collected since the bridge was opened to traffic provides a comparison of the actual results and the results expected from the design. The following sections provide an in-depth overview of the events during the construction and beyond, comparing the data acquired during the monitoring and what was expected from the design.

As explained earlier in this report, two of the three girders were instrumented for short and long term monitoring. The strains will be individually studied for each girder and then a comparison between both girders will be carried out. Deck pouring data can be used for studying the continuity of the connection over the pier. Although the connection over the pier is considered as a simple connection before the concrete hardening it could have a partial continuity over the pier. In this case, a portion of the moment from the wet concrete weight will be transferred to the other span during casting of the first span.

5.4.1 Strain distribution

Figure 5-15 shows the cross section and section properties of the girders. There are three strain gages over the depth of the girders located on the top flange, on the middle of the web, and on the bottom flange. The neutral axis location can be calculated based on the strains recorded during loading. These strain gages record the total strain including elastic strain due to construction loads and thermal strain. There is no plastic strain during construction.

Neutral axis from bottom flange = 20.4 (in)

Moment of inertia = 55377 (in^4)

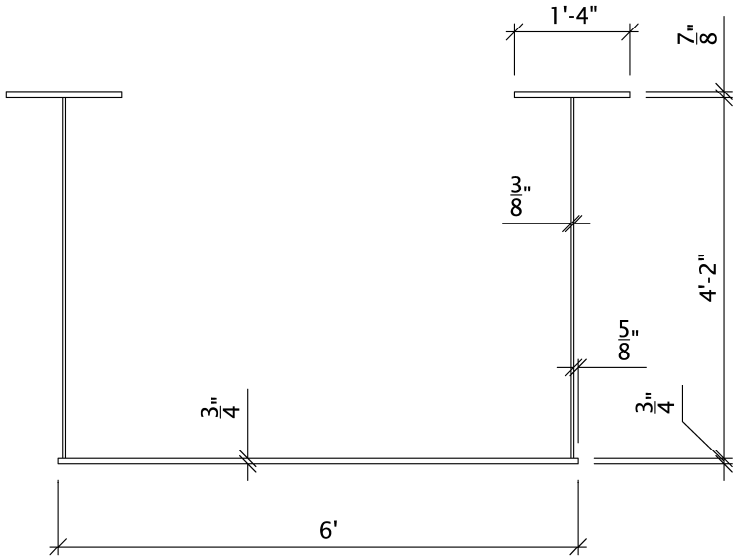

Figure 5-15. Cross section of the box girders

By connecting the three measured strains, the location of neutral axis can be found and can be compared to the theoretical neutral axis. The following sections look at the neutral axis location for several conditions.

5.4.1.2 Strain at mid-span of the north girder during construction

Figures 5-16 through 5-18 show the strain distribution at a section located at the mid-span of the north central girder (girder B) and its variations over time.

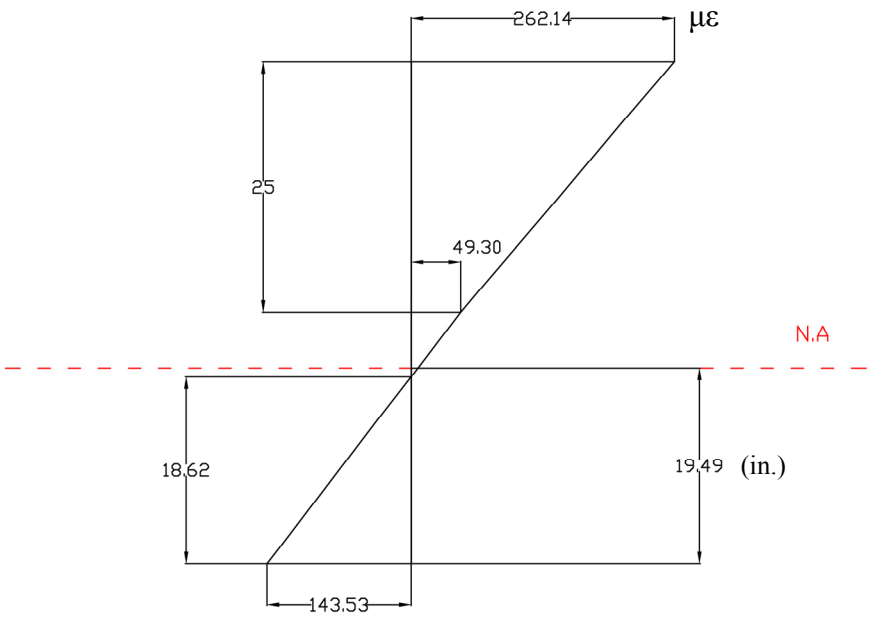

Figure 5-16. Strain distribution at 8:45 AM (mid-span girder B)

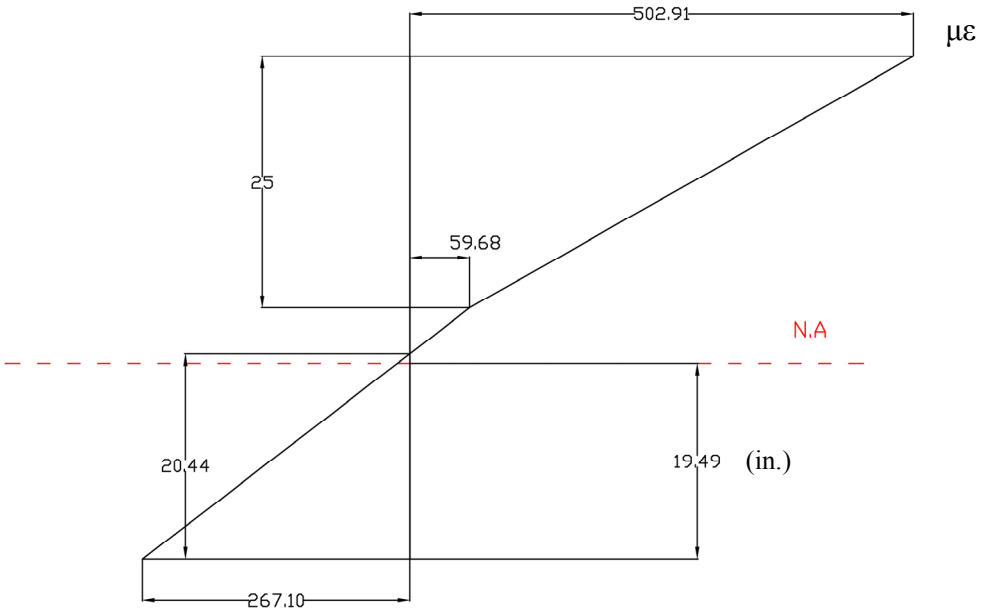

Figure 5-17. Strain distribution at 9:00 AM (mid-span girder B)

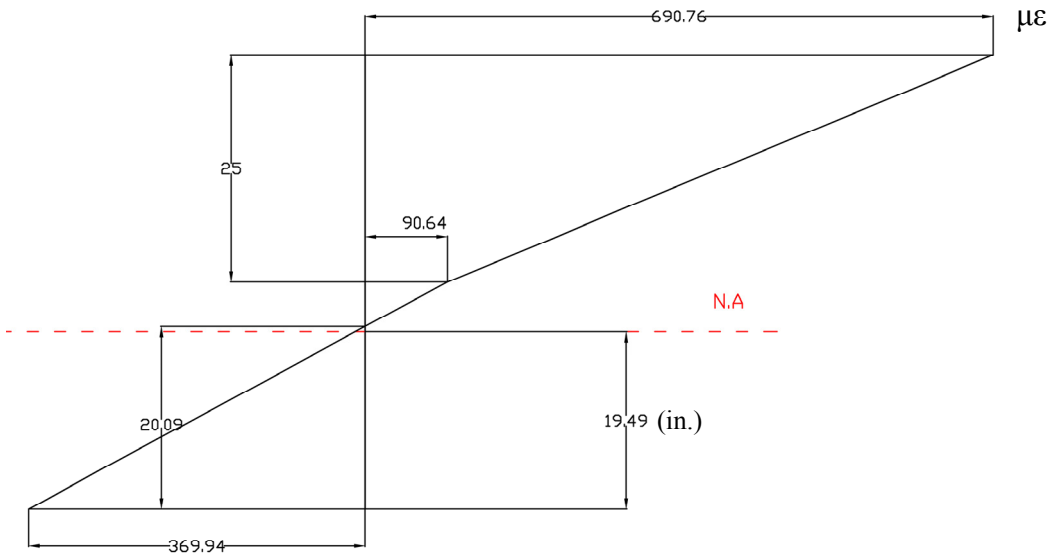

Figure 5-18. Strain distribution at 9:30 AM (mid-span girder B)

The neutral axis depth found based on the experimental data is about 4% off of the theoretical neutral axis depth. This discrepancy could be due to a number of reasons including thermal strains and geometric tolerances. As can be seen in the figures, the three strain points within a section cannot be connected together by a straight line. Of particular note is that during casting the hydrating concrete, which was warmer than the ambient temperature, was in contact with the top flange. The resulting thermal strains could likely account for the observed non-linearity seen in Figure 5-18.

5.4.1.3 Strain at the mid-span of the south girder during construction

Figure 5-19 through Figure 5-21 show the strain distribution along the cross section at the mid-span section (south). In this span, the strain from the gage located on the web shows a high strain during and after the concrete pouring. The location of the neutral axis can be found by connecting the strain from the bottom flange and the web or by connecting the strain from the top flange and the bottom flange. Due to the web's large strain, determination of the neutral axis depth based on this strain may result in an incorrect location of the neutral axis. Rather, using the strain data from the top flange would result in a more accurate neutral axis depth calculation with the minimal offset from the theoretical location. The strain distribution shows that the strain at bottom flange is more reliable to consider for calculating the moment at the section.

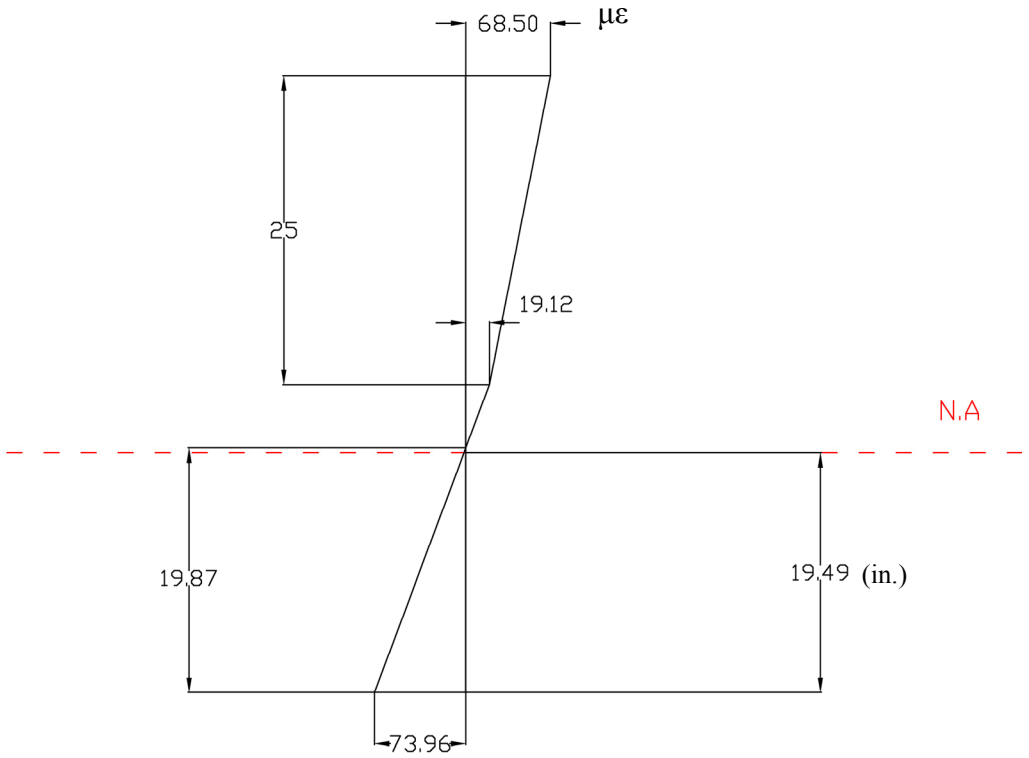

Figure 5-19. Strain distribution at mid-south span at 9:30 AM

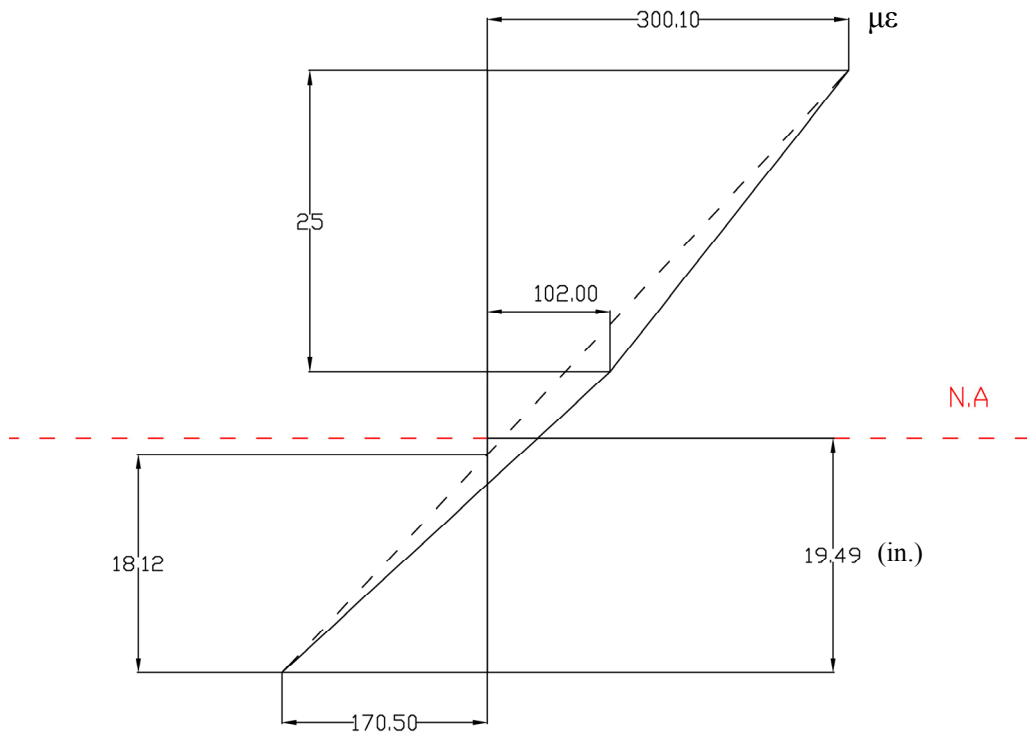

Figure 5-20. Strain distribution at mid-south span at 10:45 AM

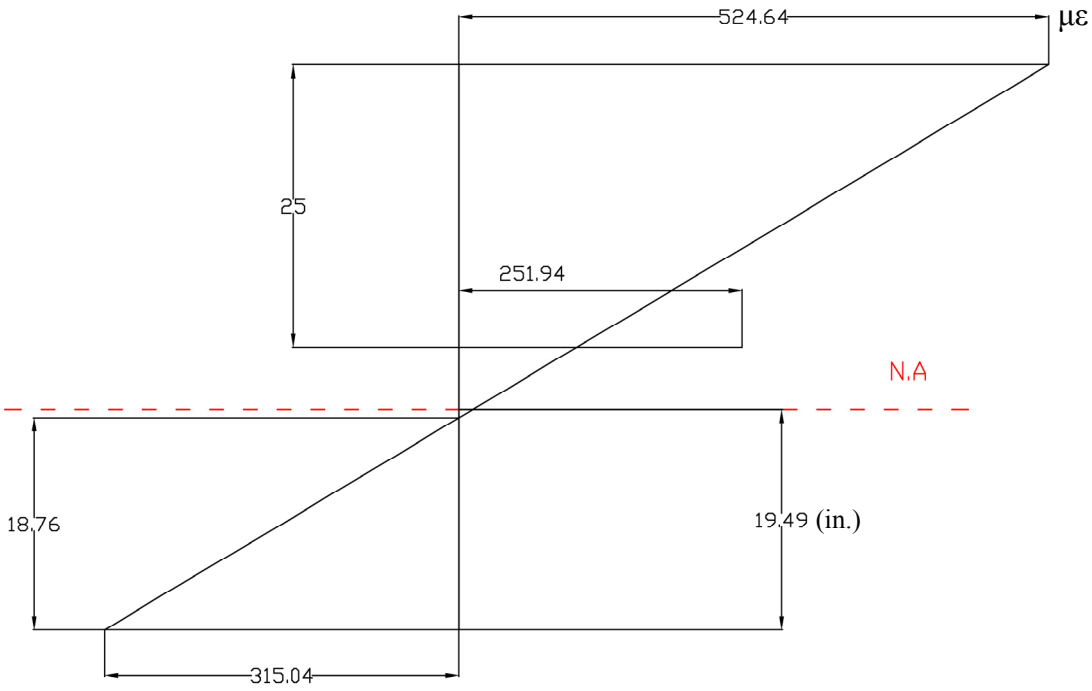

Figure 5-21. Strain distribution at mid-south span at 11:45 AM

Similar to the north span, the location of the neutral axis calculated based on the experimental data is about 4% different from the location of theoretical neutral axis. Again, this difference could be due to the thermal strains or geometry tolerances.

5.5 Determination of continuity percentage over the pier

The connection of the girders over the pier has been assumed to not transfer any moment from one span to the other during the construction phase (simple span behavior), but it could have a partial continuity due to the concrete diaphragm and hoop shaped bars and dowels passed through the web. To determine the amount (percentage of moment transferred from one side of the connection to the other) of this possible continuity studies were carried out on the data obtained through instrumentation. This partial continuity over the pier transfers some of the forces from the north span to the south span during the pouring of the concrete on the north span so the strains can be measured and from that, the amount of the continuity over the pier can be determined. (Table 5-22)

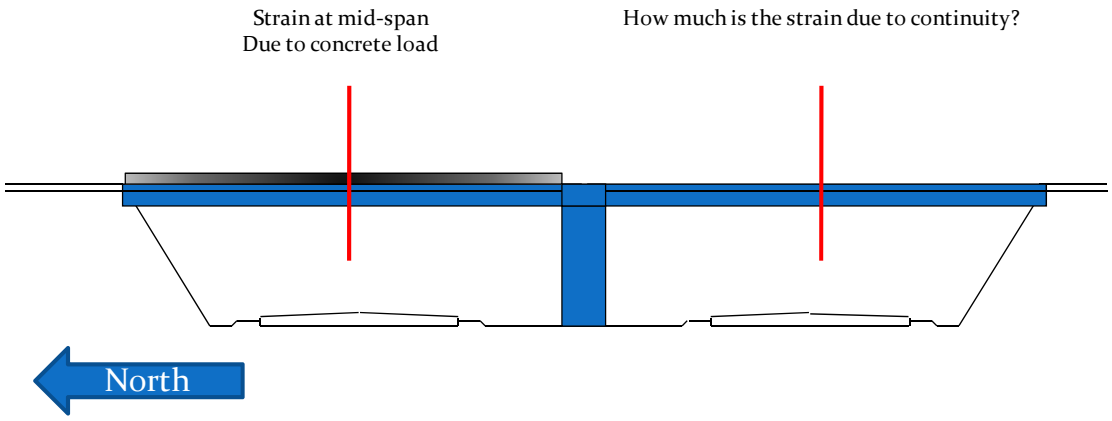

Table 5-22. Strain at South span due to dead load on North span

Furthermore, the magnitude of the strains when pouring is finished in both spans can be used to study the continuity. On the other hand, the amount of the continuity can be different on internal and external girders. Also the amount of this partial continuity may vary during pouring the concrete.

5.5.2 Moment

The objective of the study on the data during construction is to determine the continuity percentage over the pier. This way, the designer can calculate the positive moment, negative moment, and deflection based on the amount of partial continuity over the pier. A study on the strains from the bottom flange, web, and top flange of the girders showed that the strains from the bottom flange are affected from the temperature variations to a lesser amount. Therefore, the moment diagram along the bridge is calculated based on the strains from the bottom flange. Three strain gages are used for predicting the moment diagram along the bridge. These strain gages are located at sections 12 (ft) from the abutment, 12 (ft) from the mid-span, and 13 (ft) from the pier.

Because the dead load due to the deck concrete casting is a uniformly distributed load over the span, the moment diagram is a second order polynomial curve. Therefore, knowing three points of the polynomial curve, the equation of the curve can be determined. Girder B was instrumented in both spans while girder C has strain gages in the north span only.

Figure 5-23 and Figure 5-24 show the moment diagrams along girder B of the bridge at the end of the concrete casting on the north and south spans, respectively. Figure 5-24 moment diagram shows the moment along the bridge when construction phase (only deck concrete casting) was ended.

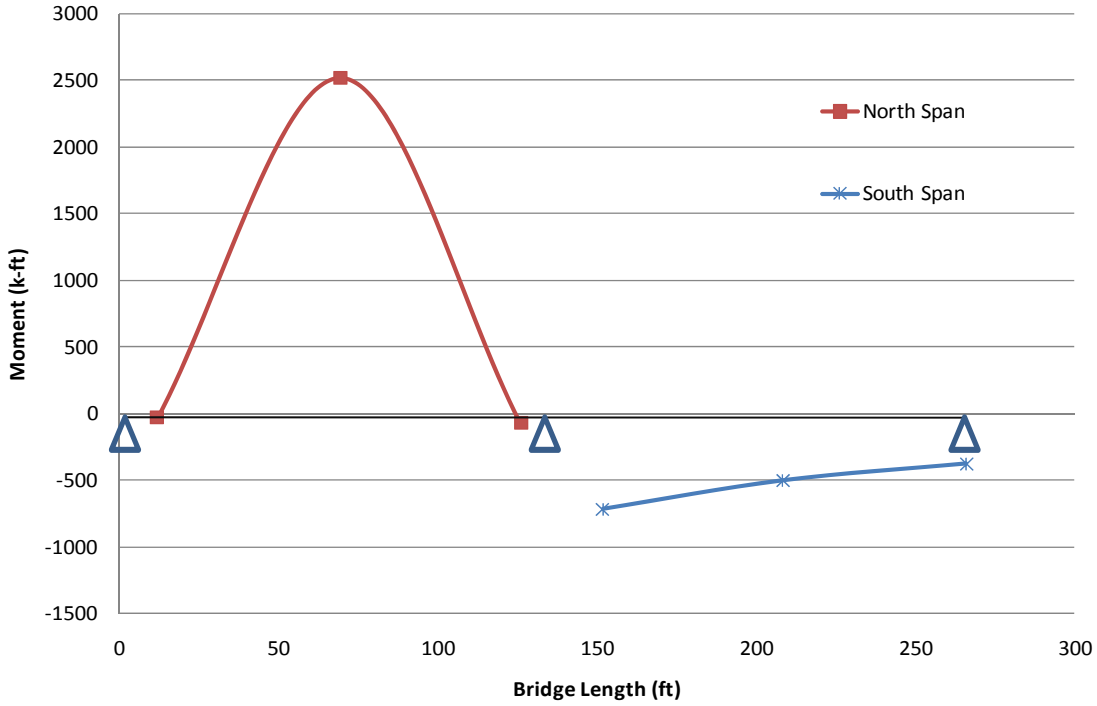

Figure 5-23. Moment diagram along the bridge (girder B) after north span deck concrete casting

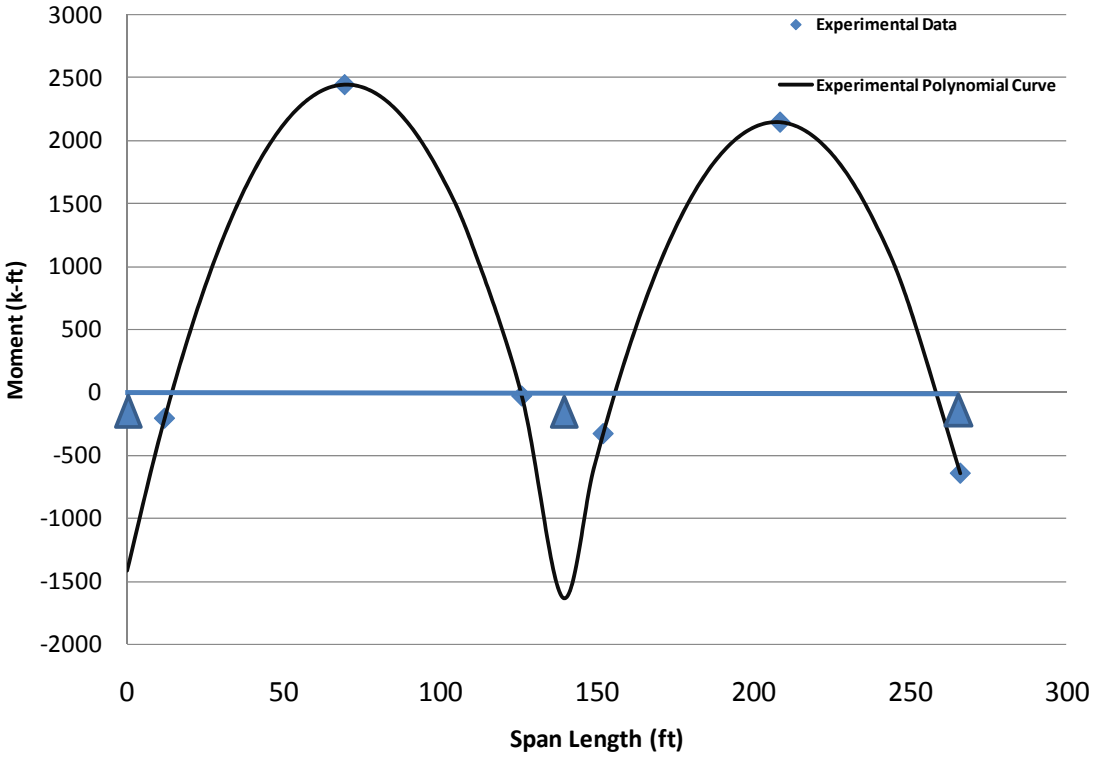

Figure 5-24. Moment diagram along the bridge (girder B) after both spans deck concrete casting

Although the bridge is assumed to have simple support at the abutments, in reality there are rotational restraints due to the field and practical details. Many parameters are involved in the amount of this rotational stiffness. As is shown in the Figure 5-24, although the details of both of the abutments are the same, the north abutment has higher rotation stiffness than the south abutment. In order to determine the amount of this rotational stiffness, SAP2000, a design and analysis commercial software, was used. The geometry of the bridge, the load, and the amount of moment are given. The moment over the pier can be predicted by fitting a second order polynomial curve to the moment diagram curve. Then, the calculated moment over the pier is applied to the girder as a concentrated moment. A rotational spring is defined in the model at the girder ends at the abutment to simulate the rotational stiffness of the abutment. A trial error method over the amount of spring stiffness was used in order to find the needed spring stiffness that makes the moment diagram of the girder the same as the moment diagram found based on the strain gage results.

Figure 5-25 and Figure 5-26 show a comparison of the experimental moment diagram versus analysis of a girder with a proposed rotational spring for the north and south spans, respectively.

The analysis shows that rotational stiffness is 1.55E+5 and 4E+5 (k-ft/rad) for the north abutment and south abutment, respectively. Since the rotational stiffness is

constant during construction, it will be also used for further analysis to determine the continuity percentage over pier.

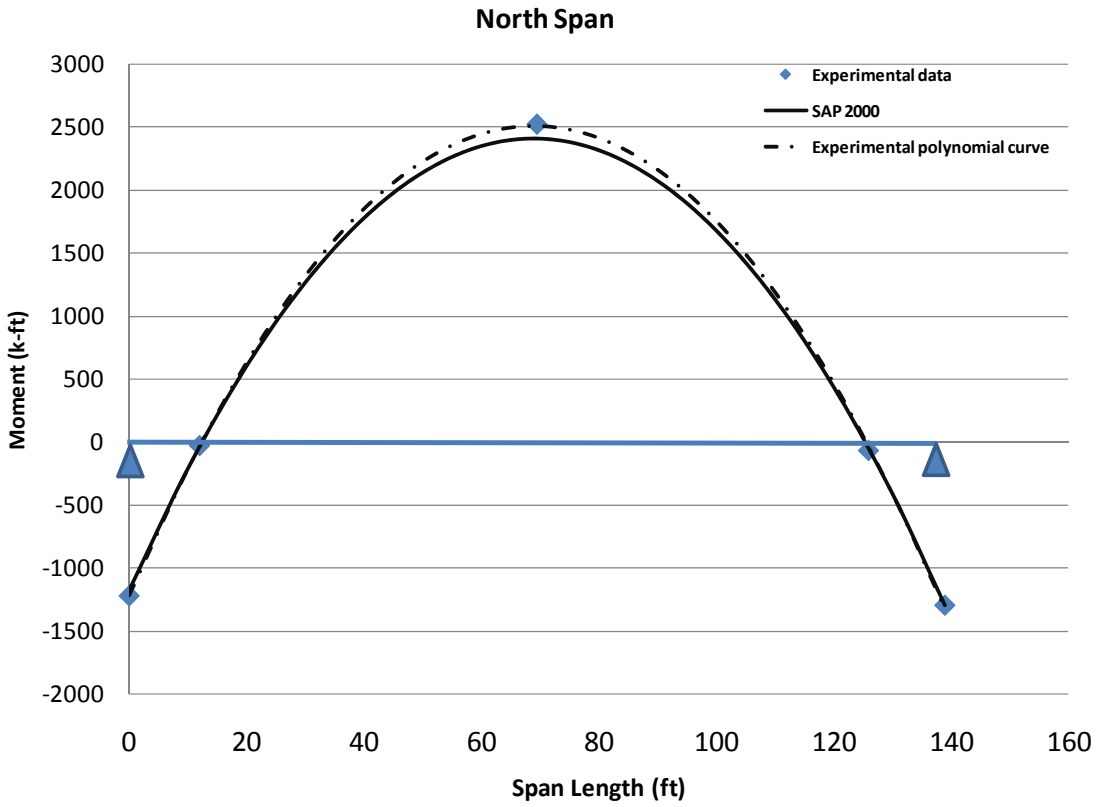

Figure 5-25. Comparison between the moment diagram from experimental results and SAP2000 results based on the k = 1.55e5 (k-ft/rad) (North Span)

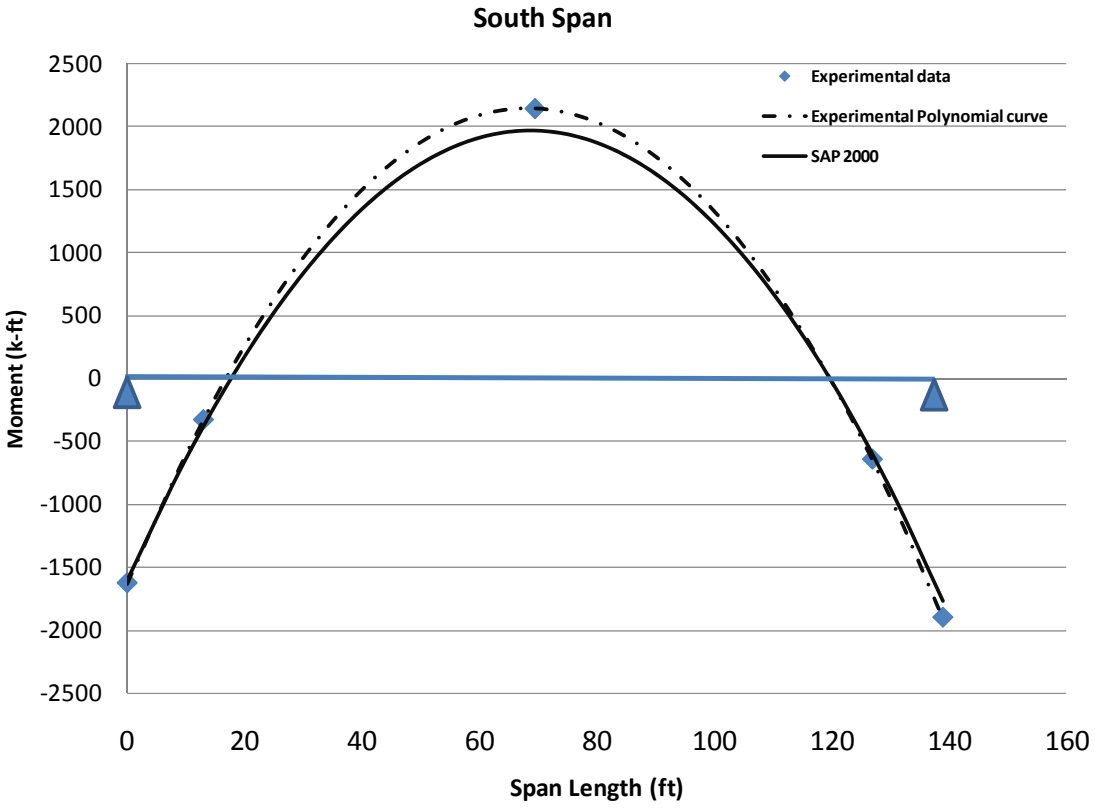

Figure 5-26. Comparison between the moment diagram from experimental results and SAP2000 results based on the k = 4e5 (k-ft/rad) (South Span)

In order to determine the amount of continuity over the pier, two separate analysis are carried out, one with a simple connection assumption over the pier and the other with a full continuity assumption over the pier. The results of these two analyses are then compared to the experimental results in order to determine the continuity percentage over the pier in the real life.

Figure 5-27 shows a comparison of the moment diagrams for a two span bridge with a simple connection assumption, full continuity over pier assumption, and experimental observation in the practice.

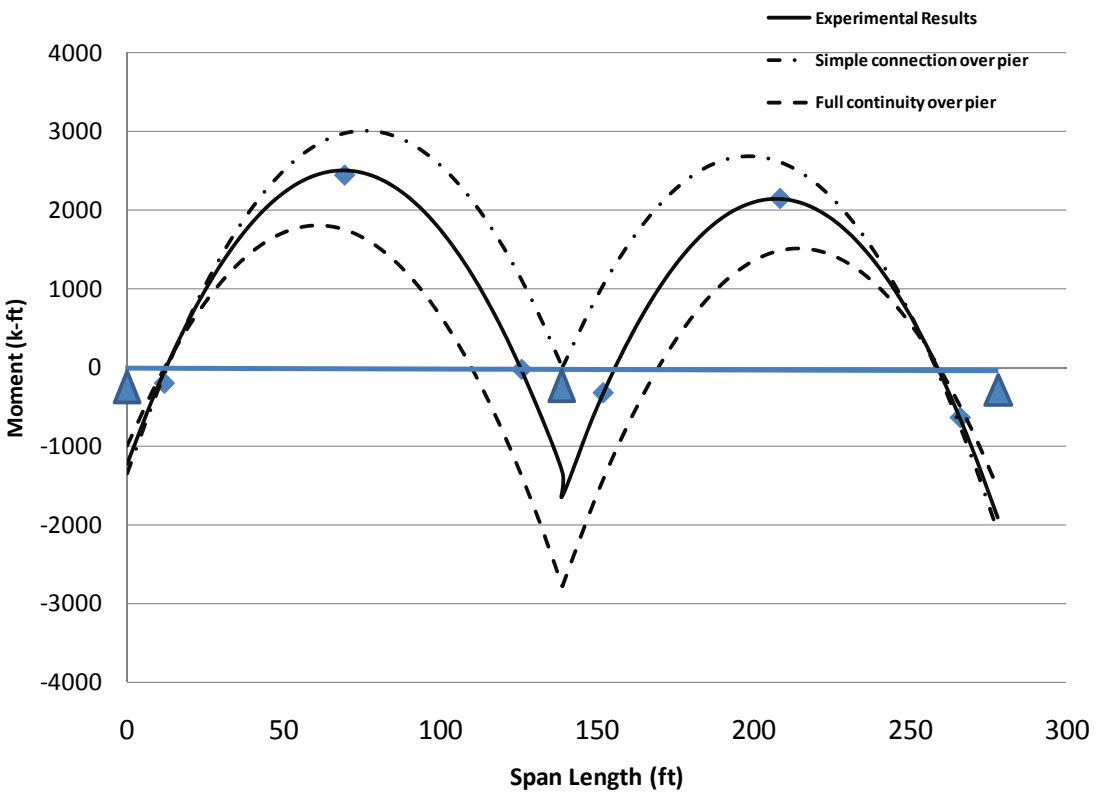

Figure 5-27. Comparison among simple connection, full continuous, and experimental observation

As was expected, the behavior of the connection should be a partially continuous one. If the transition from a simple connection to a full continuous connection is assumed to be linear, for the positive moment at mid-span, it can be written that:

At North span:

$$\frac{Full\ \ Continuous - Simple\ \ Connection}{Moment\ \ for\ \ Full\ \ Continuous - Moment\ \ for\ Simple\ \ Connection} =$$

$$\frac{Simple\ \ Connection - Continuity\ \ Percentage\ \ of\ \ Designed\ \ Connection}{Moment\ \ for\ \ Simple\ \ Continuous - Moment\ \ for\ Designed\ \ Connection}$$

$$\frac{100\% - 0\%}{1760 - 2974(k - ft)} = \frac{0 - Designed\ \ Connection\%}{2974 - 2445(k - ft)}$$

From the above equations the continuity percentage for designed connection = 44%

That is, 44 percent of continuity has to be considered over the pier to calculate the positive moment at the north span.

Table 5-2 shows the summary of the continuity percentage for positive and negative moment at both spans.

Table 5-2. Continuity percentage for positive and negative moment at both spans

	North Span (%)	South Span (%)
Positive moment at mid-span	44	42
Negative moment over pier	46	55

5.5.3 Deflection

The amount of continuity over the pier affects the deflection too. Determination of the deflection during construction is very important, because it will be used for determining the amount of camber needed during the girders' fabrication.

Table 5-3 lists the deflections corresponding to a two span bridge with simple connection , fully continuous connection, and the field observation for the designed connection.

Table 5-3. Deflection at three conditions for the bridge

	Deflection at mid-north span (in)	Deflection at mid-south span (in)
Simple connection over pier	6.15	5.2
Full continuity over pier	3	2.3
Designed connection	5.22	4.66

Based on the comparisons carried out for deflections from the field measurements and the analytically calculated deflections for a simple connection and a fully continuous connection, there was 29.5% and 19% continuity for the constructed connection for the deflection at the north and south spans, respectively.

5.6 Data analysis using least-square regression method

As an alternative method to analyze the data for during construction, the least-squares method can be used. In this analysis all data collected from the gages regardless of location of the gage are used for finding an equation predicts the deflection of the bridge during the construction. The process for the least-squares regression involved several steps. First, assuming simply supported girders for each span, moments due to the deck weight were calculated to develop the moment diagram, M_o, such as what is shown in Figure 5-28. Of particular interest are the moments at the locations of the strain gages.

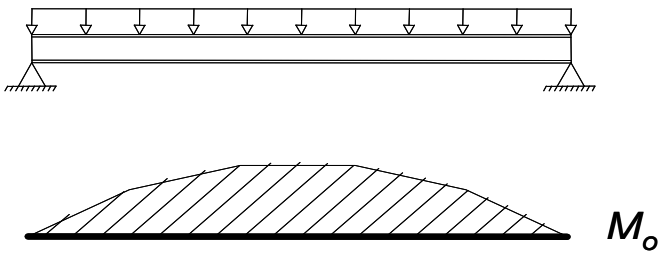

Figure 5-28. Moment due to weight of concrete

Next, restraining moments, M_1 and M_2, were assumed for each end of the span. This will create a moment diagram, M_r, similar to what is shown in Figure 5-29.

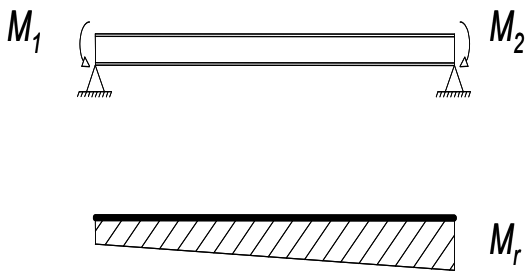

Figure 5-29. Moment due to end restraints

The M_o and M_r diagrams are added together resulting in the moment diagram shown in Figure 5-30. Using the moment diagram in Figure 5-30 , strains at each gage location can be calculated from the moments at those locations.

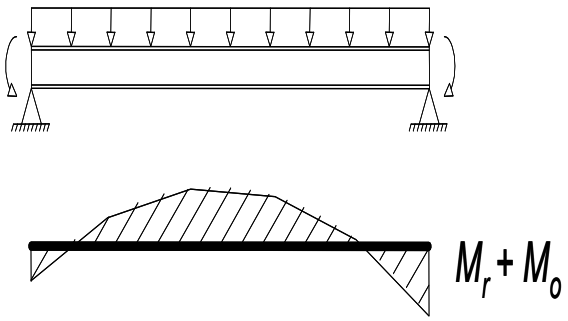

Figure 5-30. Moment due to concrete weight and end restrain

5.6.2 Moment

By developing a table such as what is shown in Table 5-4, the least-squares regression can be performed. The gages locations are listed in the first column sorted with respect to their distance from the end of the bridge are placed in the first column. Data from the strain gages are listed in columns A and B. The strains calculated from the moment diagram in Figure 5-30 are listed in columns C and D. A is subtracted from C, and the result is placed in column E. Likewise, B is subtracted from D, and the result is placed in column F. Columns E and F are squared and added then placed in column G. Finally the sum of all of the values in column G is calculated. This is the value that is to be minimized by varying the end restraining moments. This can be done using a tool such as Microsoft Excel's solver function.

Table 5-4. Example table for performing least-squares regression analysis

Gage Loc.	Experimental		Calculated				
	Top Fl. (A)	Bot. Fl. (B)	Top Fl. (C)	Bot. Fl. (D)	(C-A) (E)	(D-B) (F)	(E^2+F^2) (G)
						Σ	

Additionally, another step was taken to improve the accuracy of the analysis; that is the strain values at mid-span were weighted in order to pull the strain curve closer to the real values. This was done because the number of strain points close to the pier was too large making the curve fitting process somewhat awkward, plus the fact that the values at the mid-span are significantly larger than the other sections hence they have a lower percentage of error. The final results of the least-squares regression analyses are shown in Figure 5-31 and Figure 5-32. The top flange strains are shown in Figure 5-31 and the bottom flange strains are shown in Figure 5-32. The corresponding moment diagram is shown in Figure 5-33. As can be seen, the restraining moments at the abutments were determined to be 1125.31 kip-ft, and the restraining moment at the pier was determined to be 986.14 kip-ft. These values are significantly large because in the design zero moment was assumed for these sections.

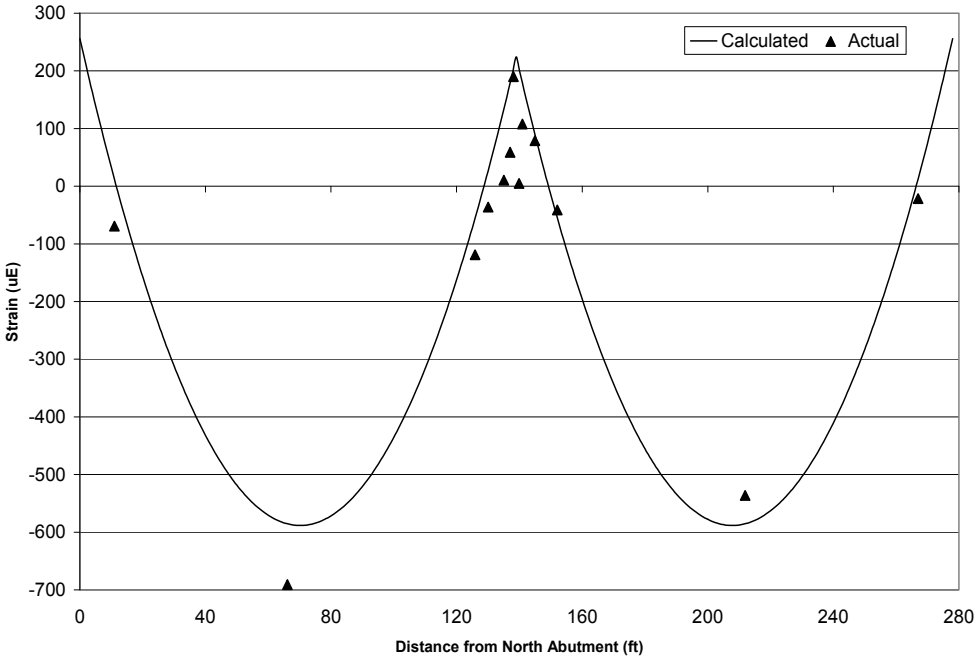

Figure 5-31. Results of least-squares regression for top flange

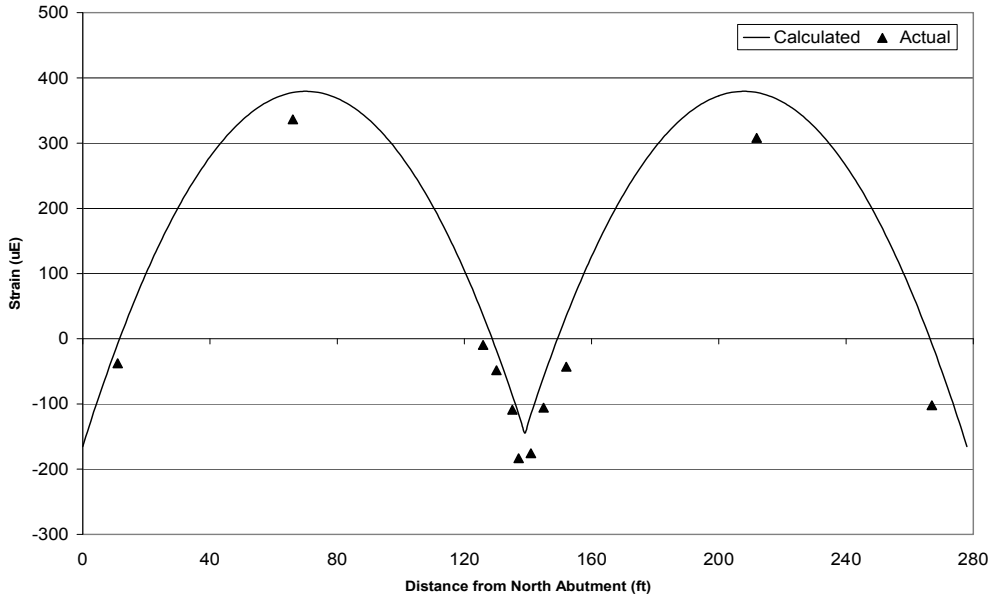

Figure 5-32. Results of the least-squares regression analysis for the bottom flange

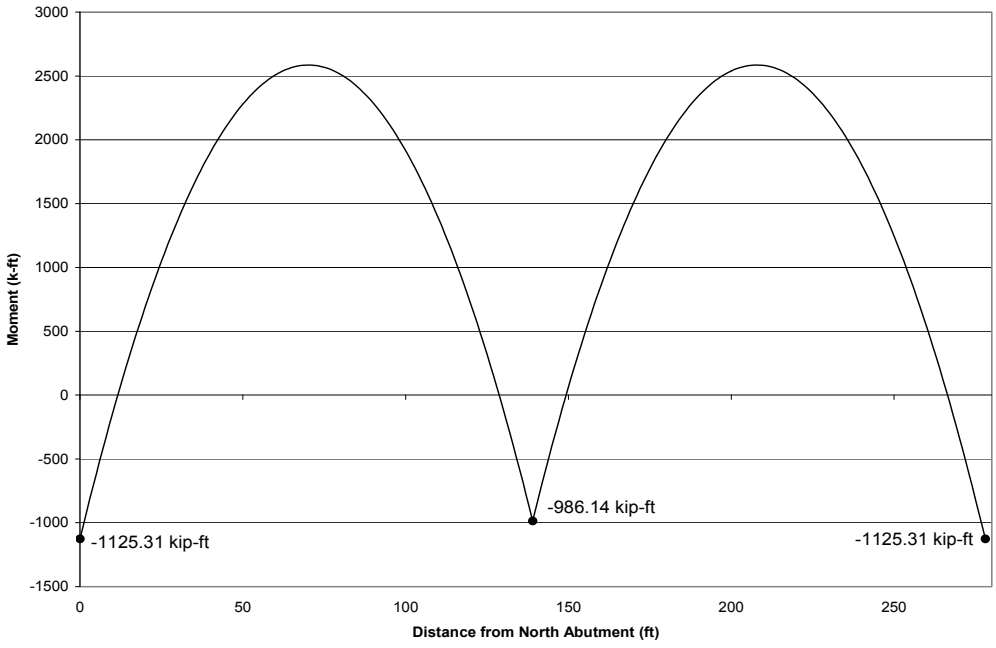

Figure 5-33. Moment diagram using calculated restraining moments

5.6.3 Deflection

During the deck pour, the elevations of the mid-spans of the east exterior girders were measured as the concrete was placed along the length of the bridge in order to determine

girder deflections. The actual deflection was compared to the calculated value in order to evaluate their difference. The calculated deflection from the design at the mid-span section was 7.65 inches. Figure 5-10 shows the mid-span deflections plotted against time during the deck casting. The final north mid-span deflection was 5.22 inches. The final recorded south mid-span deflection was 4.66 inches.

The significant difference in deflections was likely due to the restraints from the supports. Plugging the calculated restraining moments in Equation 5-1, which is the deflection equation for a beam with a uniform load and dissimilar end moments:

$$\Delta_x = \frac{wx}{EI}\left[x^3 - \left(2l + \frac{4M_1}{wl} - \frac{4M_2}{wl} \right) x^2 + \frac{12M_1}{w} x + l^3 - \frac{8M_1 l}{w} - \frac{4M_2 l}{w} \right] \quad 5\text{-}1$$

Where

Δ_x	=	Deflection at distance x from the end of the beam
w	=	Uniform load on beam, kips/inch
x	=	Distance from end of beam, inches
E	=	Module of elasticity of material, ksi
I	=	Moment of inertia of beam, in^4
M_1	=	Higher of end restraining moments, kip-in
M_2	=	Lower of end restraining moments, kip-in
l	=	Length of beam, in

and

M_1	=	1125.31 kip-ft
M_2	=	986.14 kip-ft

The calculated mid-span deflection is 4.99 inches. There is a 4.4% difference from the actual north mid-span deflection of 5.22 inches, and a 7.1% difference from the actual south mid-span deflection of 4.66 inches.

In Figure 5-10, a positive deflection denotes downward movement. As the pour progressed from north to south, the north span deflection increased downward. However, until concrete was cast on the south span, the south span deflected upward. This behavior is also indicative of continuity existing prior to the deck being composite with the girders.

Chapter 6
Live Load Testing

The analysis and results obtained from the diagnostic Live Load Test carried out on the N-2 over I 80 Bridge are presented in this chapter.

6.1 Introduction

Due to the complicated nature of an integrated bridge system, design procedures are authored to produce reliable, yet conservative results. It is obvious that the actual behavior of a structure is best determined through load testing. Conducting an ultimate load test and testing the structure to failure will give the most accurate behavior of the structure. However, for structures already in service this is not possible. A diagnostic live-load test must be performed at load levels in the elastic range of the structure. Through live-load testing, behavior beyond the test load can be predicted and a load rating can be determined. Assumptions made during design can also be checked. Depending on the type of data collected, many different aspects of the structure can be characterized.

A live-load test was performed on the N-2 over I-80 bridge near Grand Island on July 20, 2005 (The temperature was 105 degrees.) Three trucks filled with gravel were obtained from NDOR to conduct the test. The behavior under the live-load was recorded through instrumentation placed throughout the structure. The bridge also contained instrumentation installed for a previous monitoring project. The location of the instrumentation and configuration of test vehicles was based on the objectives of the live-load test. Several objectives were considered for testing.

1. Compare distribution factors to AASHTO values.
2. Determine load rating according to AASHTO standards.
3. Confirm the assumption of superposition.
4. Develop a finite element model and compare to test results.
5. Investigate bottom flange slab behavior near pier.
6. Determine neutral axis locations.
7. Investigate continuity over the pier.

The configuration of tests trucks and instrumentation was based on these objectives and constraints of the test equipment. The following chapter discusses the instrumentation setup and truck configuration of each load test.

6.2 Test Setup and Procedures

In this section the instrument locations on the bridge are explained as well as the test truck configurations.

6.2.1 Instrumentation

Before and during construction of the bridge, instrumentation was installed to monitor the behavior of the structure while in service. Nearly all of the strain gages were still operational at the time of the live-load test. The locations of these gages can be found in the previous sections. The previously installed instrumentation was supplied by slope indicator and is referred to as SI.

Additional testing equipment was supplied by Bridge Diagnostics Inc. and is referred to as BDI. The strain transducers contain a full wheatstone bridge with 4 active 350 foil gages. The range of these 3" gages is approximately ±1000 με for steel. Extensions to increase the gage length were used for the concrete tension gages on the bridge deck. These transducers, shown in Figure 6-1, were attached to the steel and concrete using loctite adhesive. The steel surface in contact with the metal tabs was smoothed using a wire grinding wheel. Similar preparation was done to the concrete surfaces using a concrete grinding disc. The gages were connected to the STS control box in series with military-style connections allowing quick assembly and relocation.

Figure 6-1. Intelliducer

During the load testing sequence, two different gage configurations were used to monitor strain at various locations. The locations of each section with instrumentation are shown in Figure 6-2. Additional gages were only placed on the south span because the north span contained previously installed instrumentation.

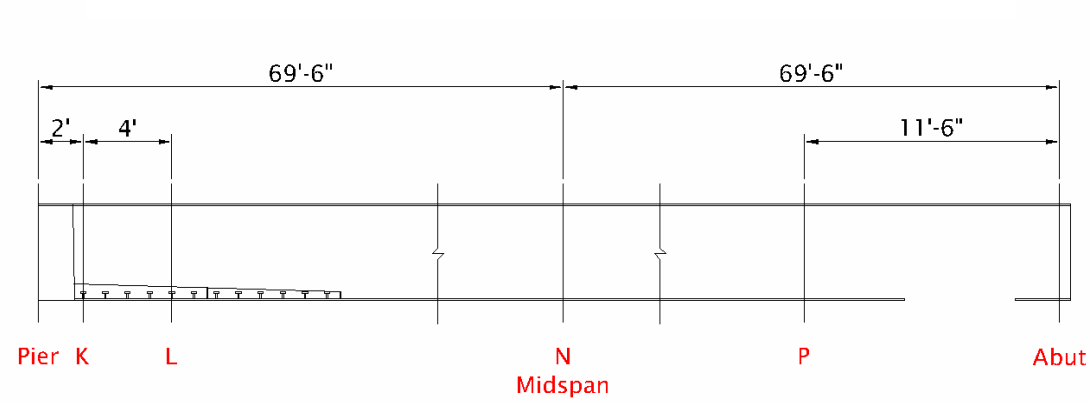

Figure 6-2. Gage Sections

The main objective for the first gage configuration was to monitor the top and bottom flanges of each girder at identical transverse locations. For each girder, gages were placed on the top and bottom flanges at mid-span (Section N) and the top flanges and bottom of the webs near the pier (Section K). Near the abutment (Section P), a gage was placed on the top flange and bottom flange of Girders A and C.

The main objective for the second gage configuration was to monitor the bottom flange compression slab near the pier. For girders A and B, gages were placed on the top flanges, bottom of the webs and top of the bottom flange slab at two sections near the pier (Sections K and L). Three gages were also placed over the centerline of the pier on top of the bridge deck. Extensions were used for these gages to increase the gage length for measuring tensile strain in the concrete. The gage configurations are shown in Figure 6-3.

Gage Configuration No. 1

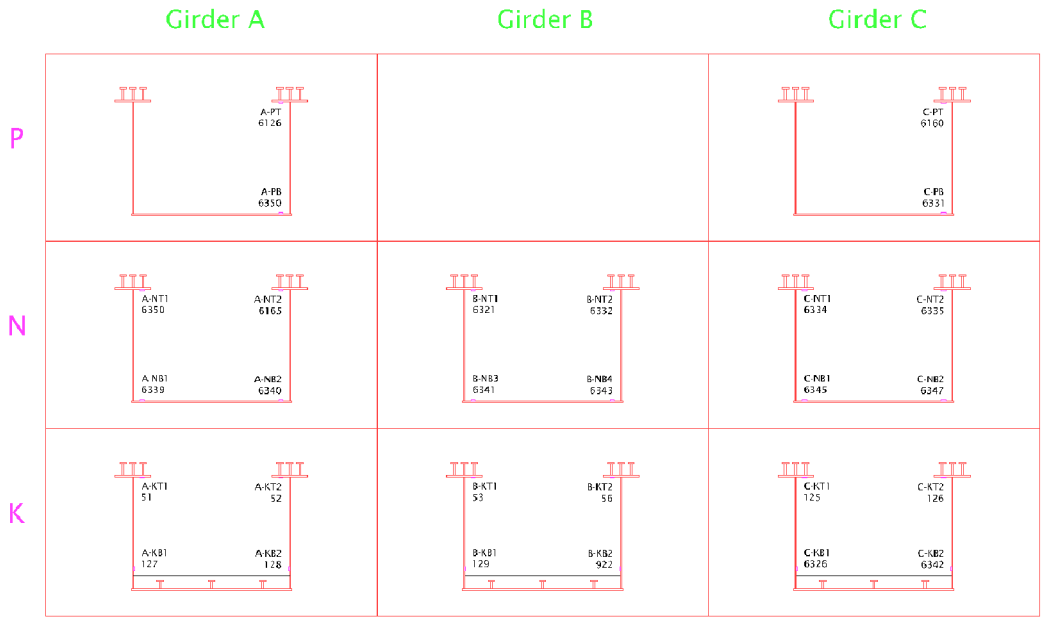

Sections P, N, K
* Sections orientated looking north

Gage Configuration No. 2

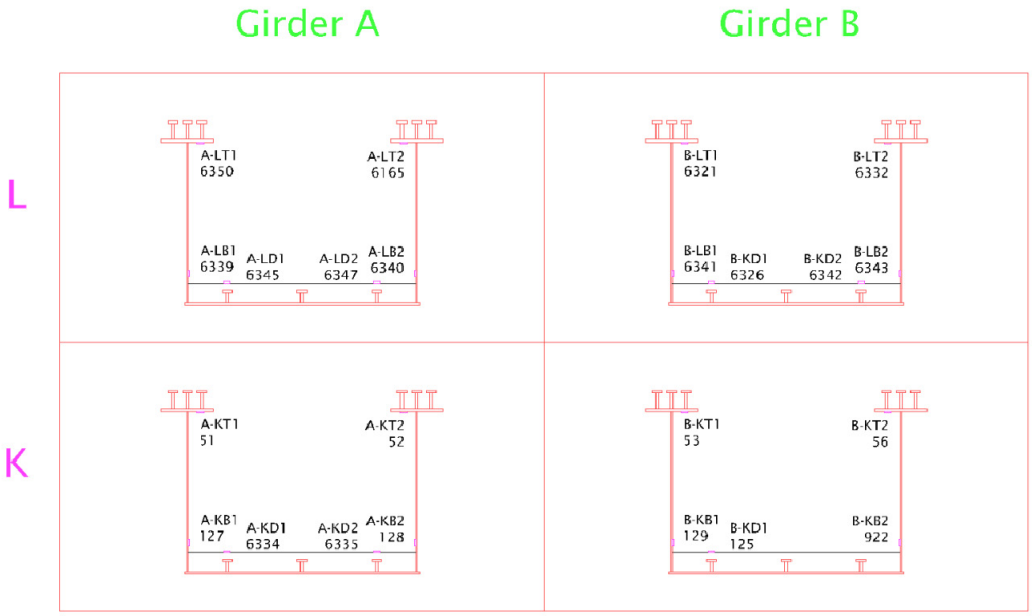

Figure 6-3. Gage Locations

The gages were labeled to describe their location. The first letter of the gage label stands for the girder name (A, B, or C). The second letter stands for the cross section label (P, N, K, or L). The last letter describes the location of the gage (T= Top flange, B= Bottom flange or web, D= Compression slab near the pier).

The number at the end represents the East or West side of the girder (1= West, 2= East). The gage number is shown along with the gage label for each. For example, a gage with the label A-KT1 51 is located on Girder A at Section K on the West top flange and the gage number is 51.

Wire potentiometers (pots) were also added at several locations to measure displacement of the girders. Pots were located on each girder, 60 ft from each abutment at the center of the bottom flange, for a total of six pots. The pots were c-clamped to a small platform which was staked into the ground. A picture of the pot setup is shown in Figure 6-4. The pots are labeled with the first letter representing the span location (N= North, S= South), and the second letter stands for the girder label (A, B, or C). For example, a pot labeled NC is on the North span of Girder C.

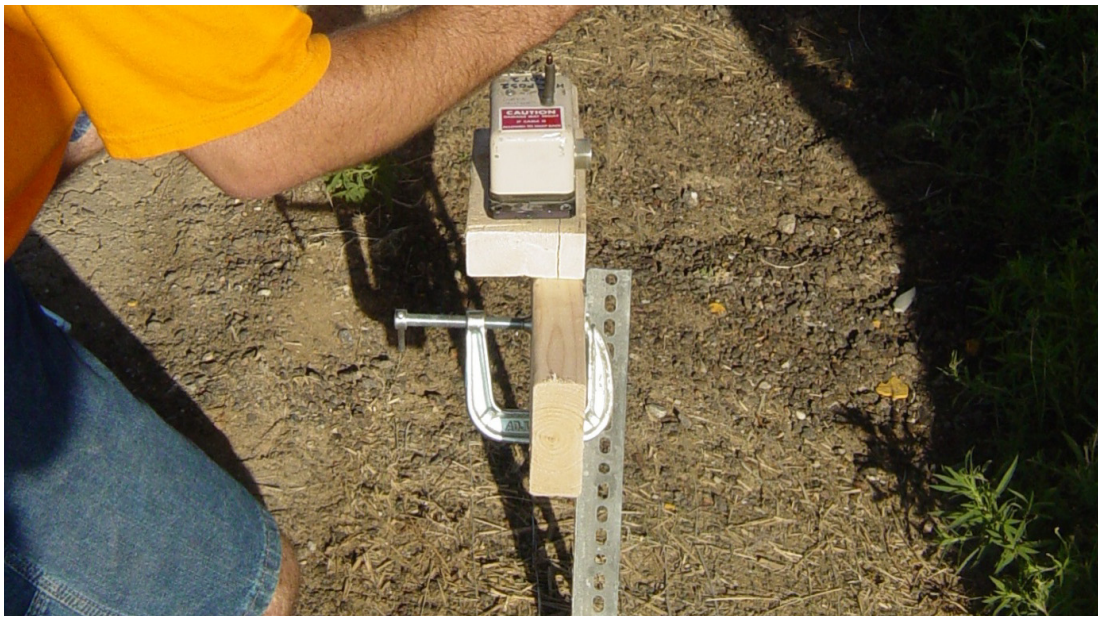

Figure 6-4. Pot Setup

6.2.2 Truck Configuration

The truck configurations, their locations on the bridge during the live load tests, and the combinations used are explained in this section.

6.2.2.1 Truck weight and dimensions

The test load vehicles were provided by the Nebraska Department of Roads (NDOR). The trucks were filled with gravel and weighed prior to the load test. Each axle was weighed using portable scales. The distance of each front wheel revolution was measured to be the same for each truck. One wheel revolution was measured to be 129.4". The dimensions and total weights of each vehicle are shown in Figure 6-5.

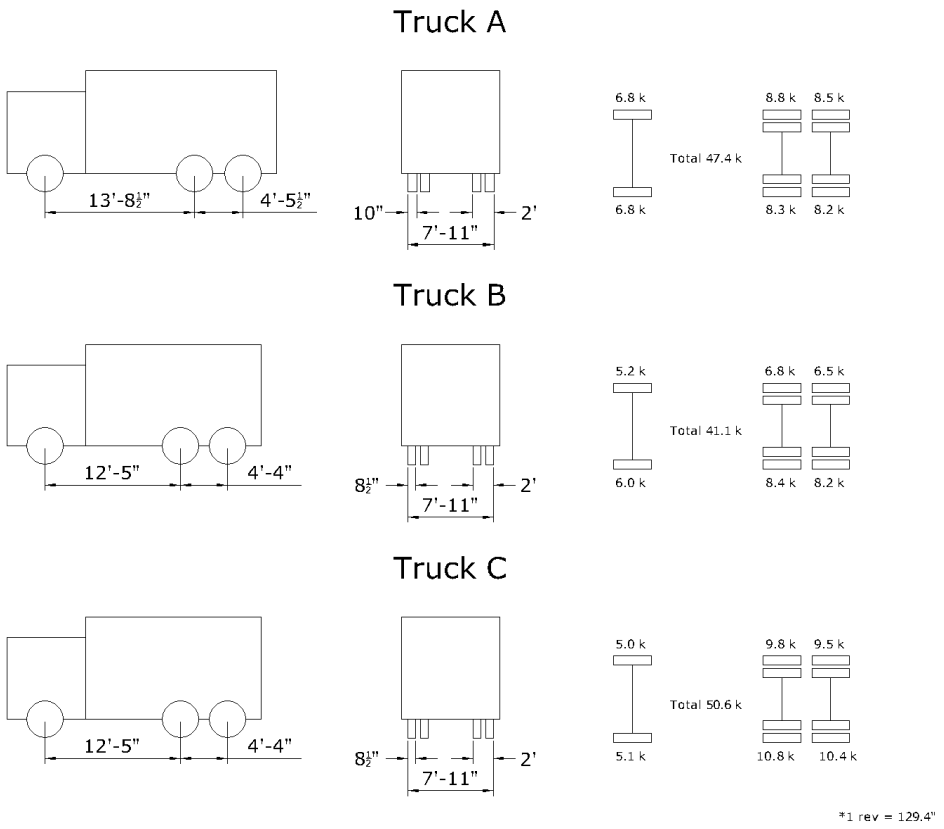

Figure 6-5. Truck Specifications

6.2.2.2 Truck Locations

The clear roadway width of the bridge is 44'-0" which corresponds to 3 design lanes. The two outside trucks were spaced 5'-0" from the edge of the concrete barrier while the middle truck followed the centerline of the bridge. The test was in accordance with the AASTHO Load Rating Manual requirement for the minimum distance from the truck wheel to the edge of the barrier of 2'-0". Due to constraints of the data acquisition system, the deflection and strain could not be measured at the same time. For most of the tests, a first run was made to measure strain with the BDI system followed by a second run to measure the deflection and strain of the existing gages at certain truck locations. For the tests designated BDI, the strain data was recorded continuously throughout duration. For the tests designated positions on the bridge. Tests 1- 16 were run with gage configuration No. l while Tests 17-20 were run with gage configuration No. 2. The various truck positions and type of test are shown in Figure 6-6 and Figure 6-7.

The longitudinal position of the truck on the bridge was measured using the BDI Autoclicker. The time of each revolution is recorded using this contraption. A picture of the Autoclicker is shown in Figure 6-8.

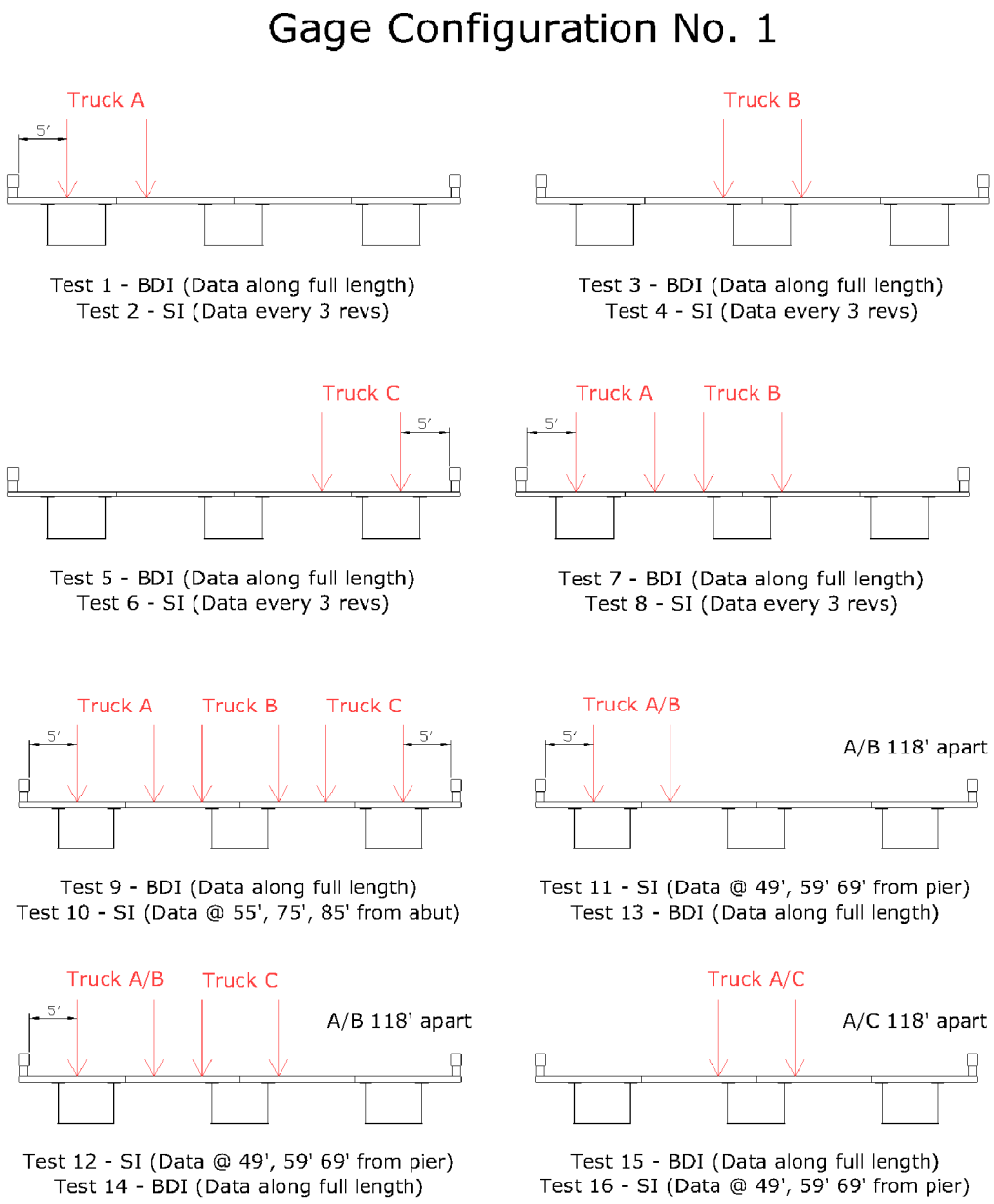

Figure 6-6. Truck Locations for Gage Configuration No. 1

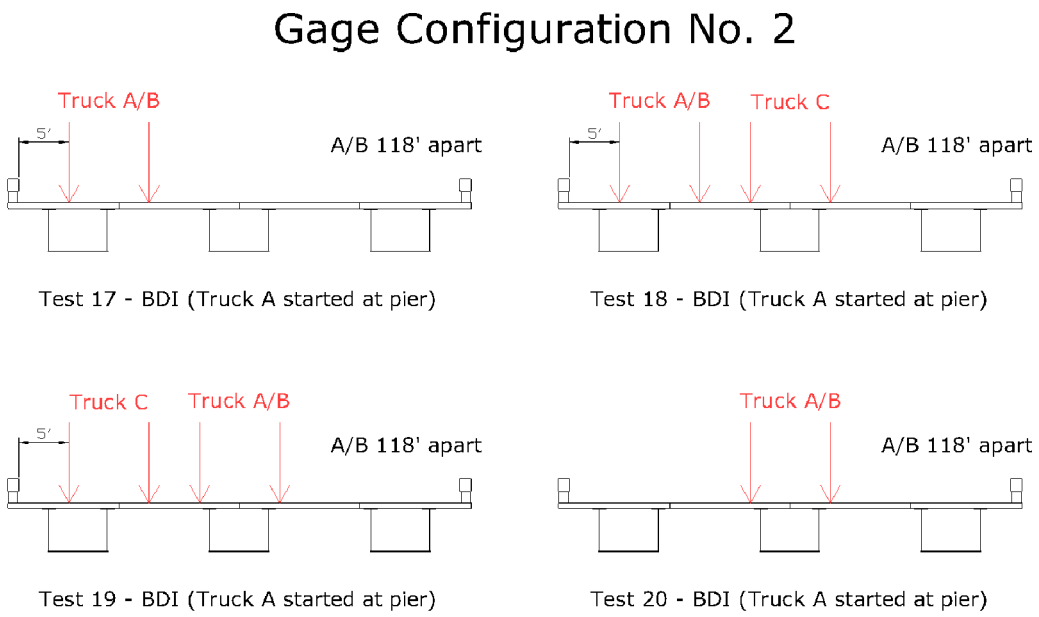

Figure 6-7. Truck Locations for Gage Configuration No. 2

Figure 6-8. Autoclicker

Figure 6-9. Gravel in Trucks

Figure 6-10. Three Trucks on Bridge

6.3 Distribution Factors

Live load distribution factors are specified by AASHTO to account for increased load effect due to multiple loaded lanes of a bridge. Through analytical and model studies Equation 6-1 is specified in AASHTO Table 4.6.2.2.2b-1 for a concrete deck on multiple steel beams:

$$DF = 0.05 + 0.85\frac{N_L}{N_b} + \frac{0.425}{N_L} \quad for \quad 0.5 \le \frac{N_L}{N_b} \le 1.5 \qquad \text{6-1}$$

Where

DF = distribution factor
N_L = number of lanes loaded
N_b = number of box girders

This equation takes into account the multiple presence of live load on the structure, thus additional factors need not be applied. This equation was developed for simple spans but it is considered applicable to continuous span bridges as well. The distribution factor is used for both interior and exterior girders as well as for moment and shear.

One of the objectives of the live load test was to determine the live load distribution factors for test data for comparison to code values. To determine distribution factors, strain data is needed for each girder at a particular cross section. The bottom flange tensile strains are commonly used because they have the largest magnitude and smallest error. A small error in strain is magnified if the total magnitude of the strain is small. The strains used to calculate the distribution factors were taken from the bottom flange gages at the midspan section. Equation 6-2 gives the formula to calculate distribution factors from strain data (Stallings and Yoo 1993):

$$DF_i = \frac{mn\varepsilon_i}{\sum_{j=1}^{k} \varepsilon_j w_j} \qquad \textbf{6-2}$$

Where

DF_i = distribution factor for the i^{th} girder
m = multiple presence factor
n = number of lanes loaded
k = number of girders
ε_j = bottom flange strain of j^{th} girder
w_j = ratio of moment of inertia of j^{th} girder to an interior girder

The weighting factor, w_j, is typically taken equal to one. This means that all girders are assumed to have equal stiffness. The multiple presence factor is included to compare the measured values to AASHTO values. A distribution factor can be calculated for every load position where a reading is taken. The controlling distribution factor is the maximum along the span. The values of interest are those near the point of maximum loading where strains are the highest. The strain values for the two bottom flange gages at midspan were averaged to determine the distribution factor for each individual box girder. Distribution factors were calculated for tests 1, 3, 5, 7, and 9. Tests 1, 3, and 5 have a single lane loaded over Girders A, B and D respectively. Test 7 has two lanes loaded over Girders A and B while Test 9 has all three lanes loaded. Table 6-1 shows the calculated AASHTO distribution factors compare to the measured values for 1, 2, and 3 lanes loaded. For the single lane loaded value, the maximum measured distribution factor from Tests 1, 3, and 5 is reported.

Table 6-1. Distribution Factors

No. Lanes Loaded	Multiple Presence Factor	Distribution Factor		Measured / AASHTO
		AASHTO	Measured	
1	1.20	0.758	0.727	0.96
2	1.00	0.829	0.891	1.07
3	0.85	1.042	0.890	0.85
	Max	1.042	0.891	0.86

The error between measured values and AASHTO values is within 15% for the 3 cases of number of lanes loaded. The AASHTO value compared to the measured value is slightly conservative for one lane loaded and slightly unconservative for two lanes loaded. The AASHTO distribution factor for three lanes loaded is conservative compared to the measured value. The live load test verifies that the distribution factor used for design is accurate to a certain degree. Comparing the maximum distribution factors from AASHTO and measured values indicates that the AASHTO equation slightly overestimates the distribution factor.

The following three figures show how the distribution factor changes as the load moves across the bridge. The average strain for each girder is also plotted on the same graph. As stated earlier, areas with small strain values do not give an accurate representation of the distribution factor. For this reason, the distribution factor is not shown for areas of small strain when the load is near the abutments or pier. On the horizontal axis, zero corresponds to the front axle load at 20’ behind the abutment, at the centerline of the grade beam. The centroid of the truck load is approximately 15’ behind the front axle.

Figure 6-11 shows the distribution factor and midspan, bottom flange strain for each girder during Test 5. Test 1 and 3 were similar but yielded lower distribution factors. Since only one lane is loaded, the distribution factor is simply the percentage of the total strain each girder feels. The maximum distribution factor corresponds to the maximum strain measured at Girder C.

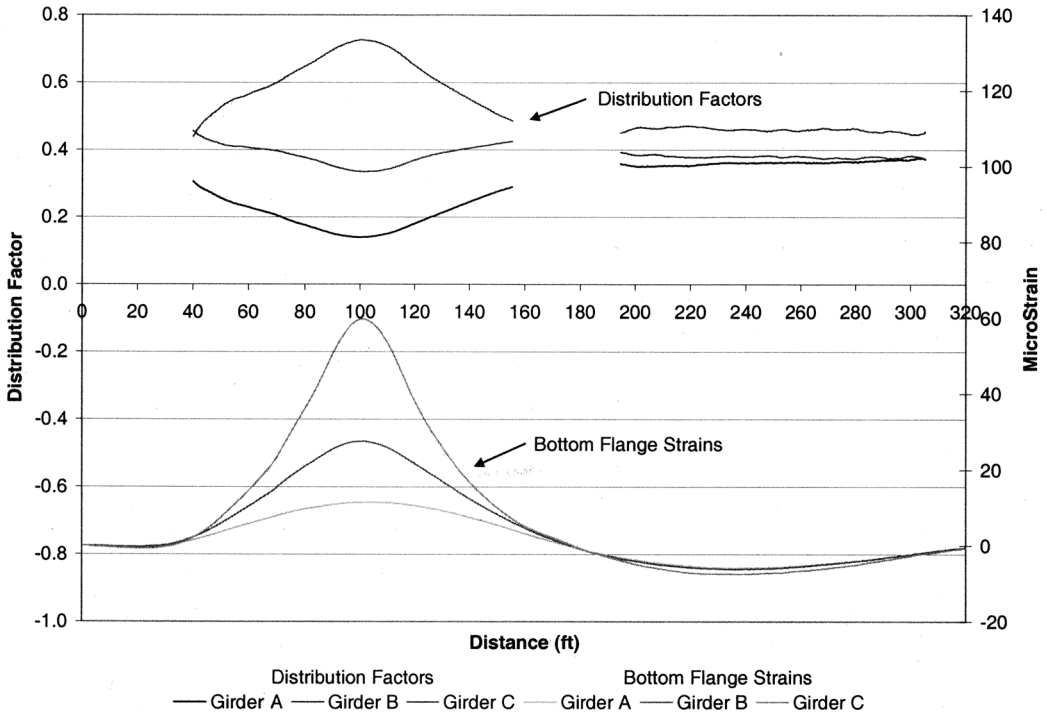

Figure 6-11. Test 5

Figure 6-12 shows how the distribution factor changes as the load moves across the bridge during Test 7. For this test, lanes over Girders A and B were loaded. The maximum distribution factor corresponds to the maximum strain measure at Girder B. The distribution factor varies only slightly for Girder A when the load is over the first span.

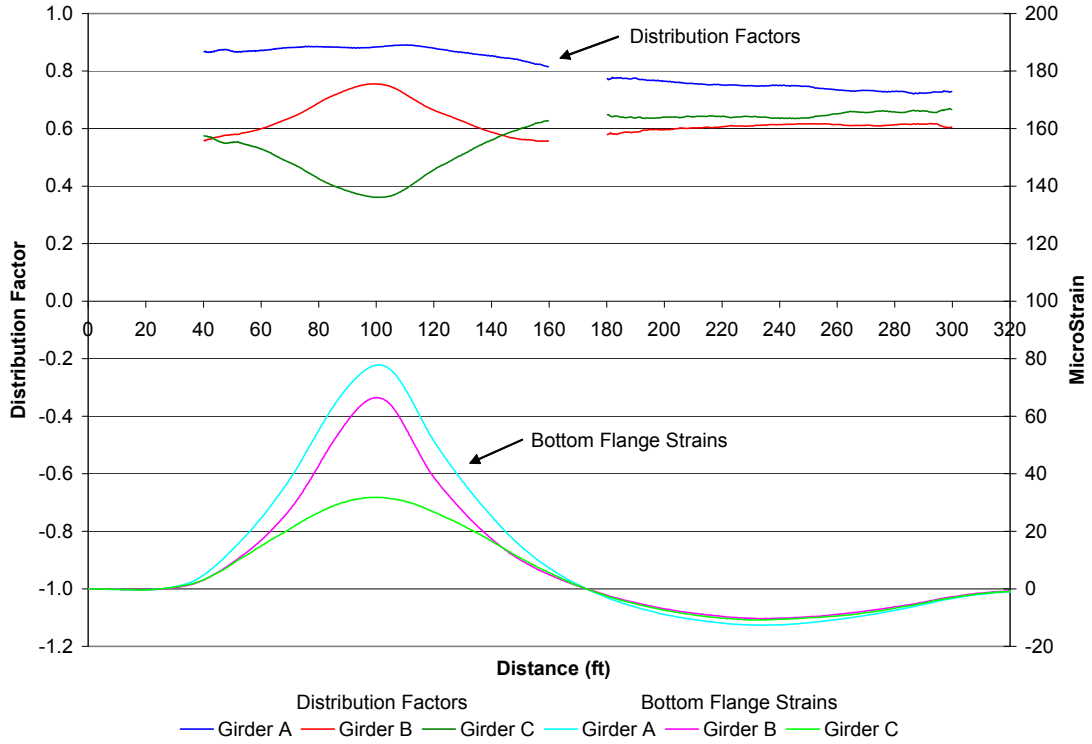

Figure 6-12. Test 7

Figure 6-13 shows how the distribution factor changes as the load moves across the bridge during Test 9. Since all three lanes are loaded, the average strain values are nearly the same for each girder. The maximum distribution factor occurs at Girder C where the strain is the highest. Only the distribution factors near the maximum strain values were considered.

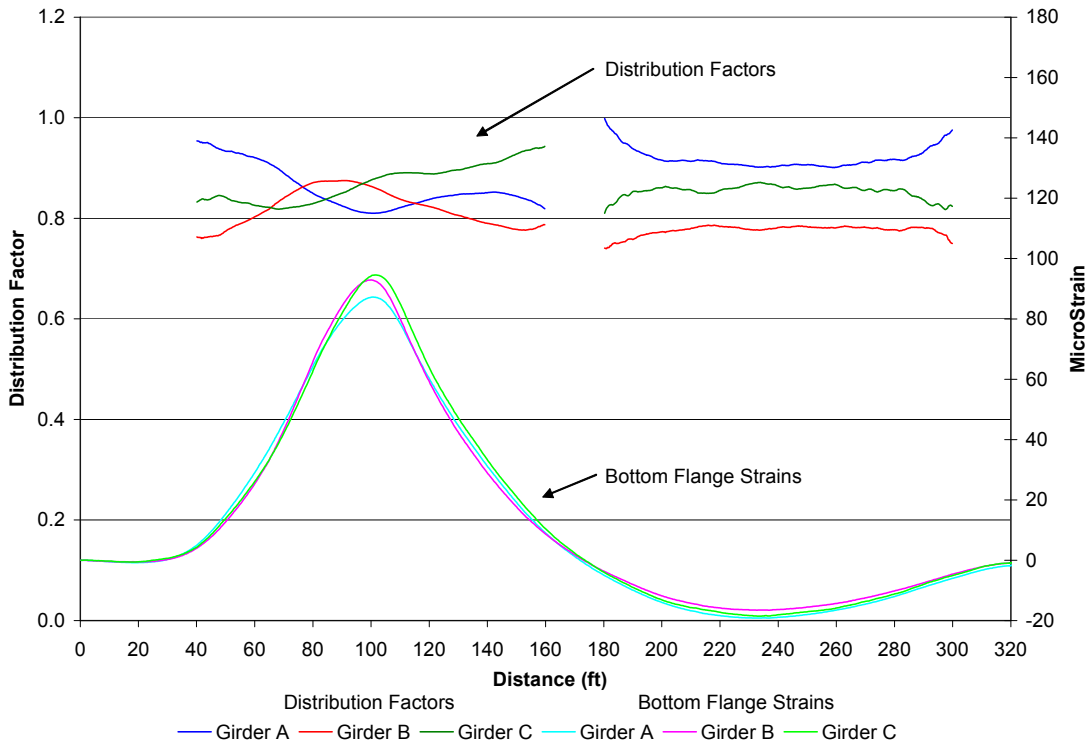

Figure 6-13. Test 9

6.4 Superposition

The theory of superposition is assumed when adding load effects in the elastic range of a structure. To check this assumption, strain history from tests 1, 3 and 5 were added and compared to tests 7 and 9. The truck configuration for each test is described in section 6.2.2.

Figure 6-14 shows the strain history of Gage A-NB1 (Girder A, Midspan, bottom flange) from test 7 compared to that of test 1 and 3 added together. The strain history should be the same which is confirmed. It can be seen for the larger strain values the two curves match closely. The strain history from this location is representative of the other locations not shown. This confirms superposition. In general, the error in superposition decreases as the magnitude of the strain increases.

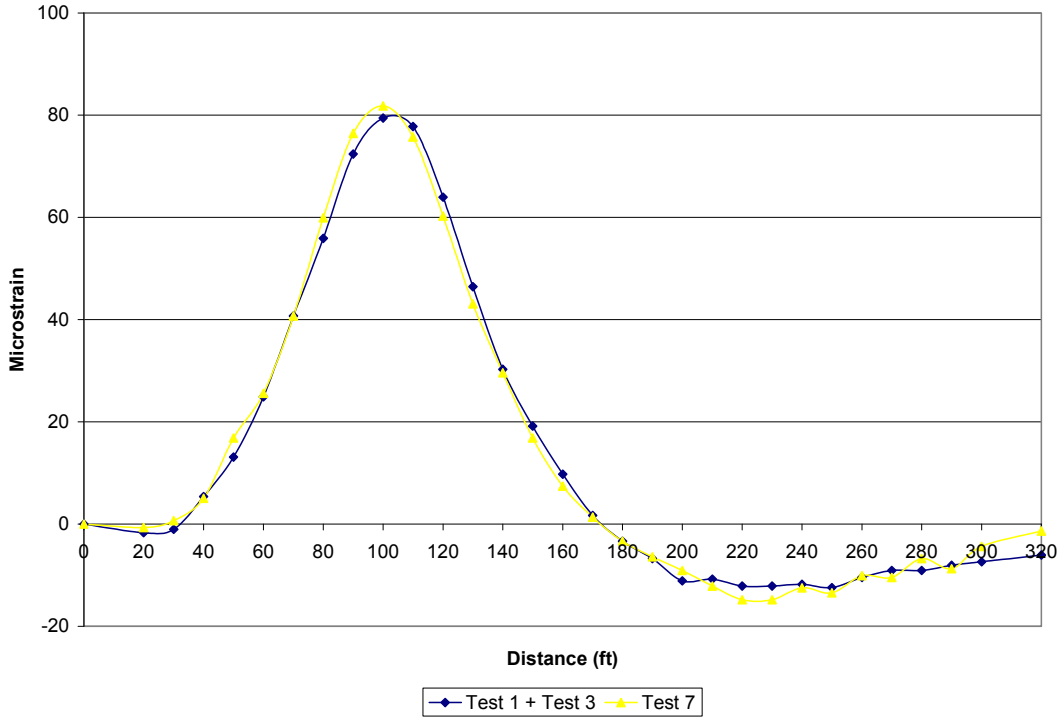

Figure 6-14. Girder A Midspan Bottom Flange- Strain History

Figure 6-15 shows the strain history of Gage B-NB2 (Girder B, Midspan, Bottom flange) from Test 9 compared to that of Test 1, 3 and 5 added together. This plot is similar to the previous showing small error in strains.

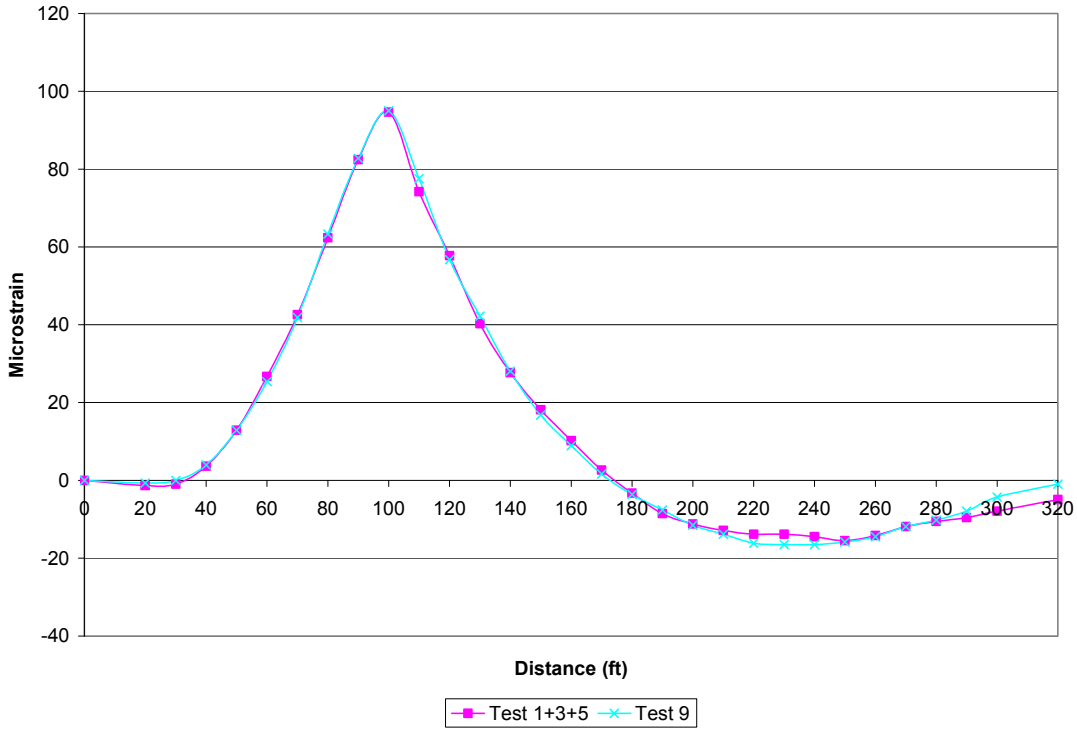

Figure 6-15. Girder B, Midspan, Bottom Flange- Strain History

Figure 6-16 shows the strain history of Gage C-KB2 (Girder C, Pier, Bottom Flange) from Test 9 compared to that of Test 1, 3 and 5 added together. This more error is seen in this plot compared to the previous two ones; however, the error in strain is still relatively small. This figure shows that the relative error increases at lower magnitude of strain, but the total error is still small.

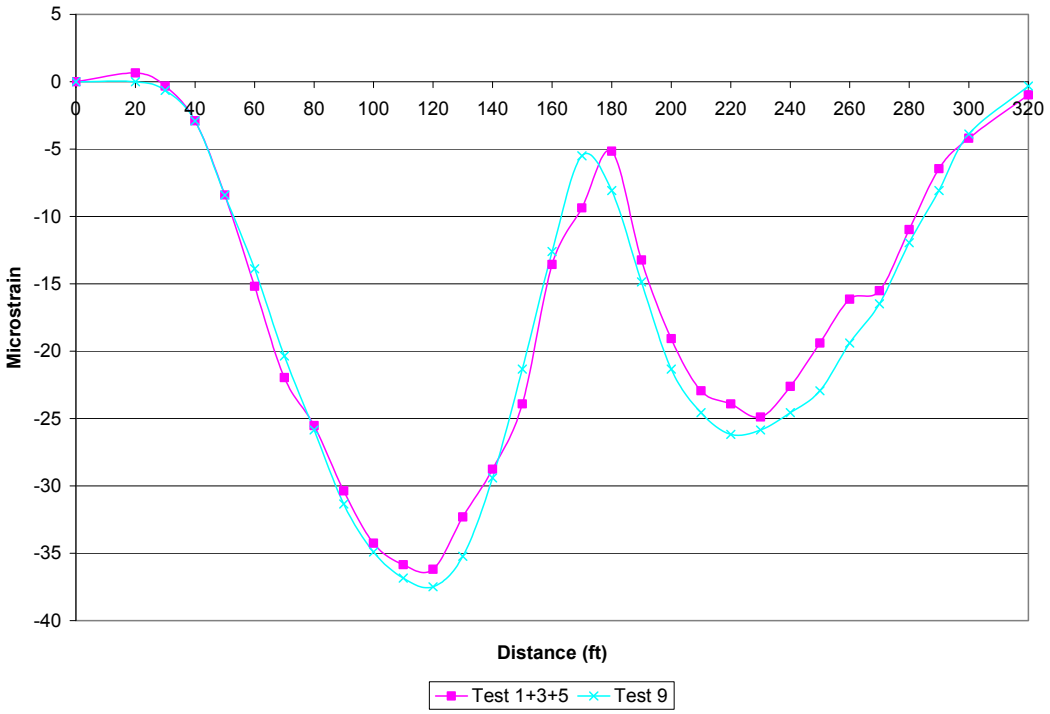

Figure 6-16. Girder C, Pier, Bottom Flange- Strain History

The superposition was examined at the bottom flange gages since the highest magnitude of strain was measured at these locations. The maximum error in strain when comparing Test 7 to Tests 1 and 3 was 8 με. The maximum error in strain when comparing Test 9 to Test 1, 3 and 6 was 9 με. The maximum error occurred at the pier for each comparison.

Another way to check superposition is to compare deflection values from the different tests. The deflection was only measured at certain locations due to equipment constraints. Deflection was recorded at approximately every 3 wheel revolutions or 43' for Tests 2, 4, 6 and 8. For Test 10 deflection was only recorded at five truck locations due to time constraints. Since continuous data was not recorded, comparing deflection does not illustrate superposition as well as comparing strain. The deflection was recorded at different truck locations for Test 2 than for Test 4 and 6. Deflection values from Test 2 at locations measured in Tests 4 and 6 were obtained by curve fitting the data. Figure 6-17 shows the deflection of a section from girder B located above the road's shoulder (where the pots were placed) from Test 10 compared to the sum of Tests 2, 4 and 6. The error is small, approximately 0.05" for this comparison. The maximum error for this girder was 0.053, which represents a 12% error. The error for comparing Girders A and C were typically higher with a maximum error of 34%. When comparing Tests 8 to the sum of Tests 2 and 4, results were similar to the previous comparison, also with a maximum error of 34%. A possible source for error may be from vehicles allowed to cross the bridge during Tests 2, 4, 6 and 8. At times vehicles may have been on the bridge while data was being recorded.

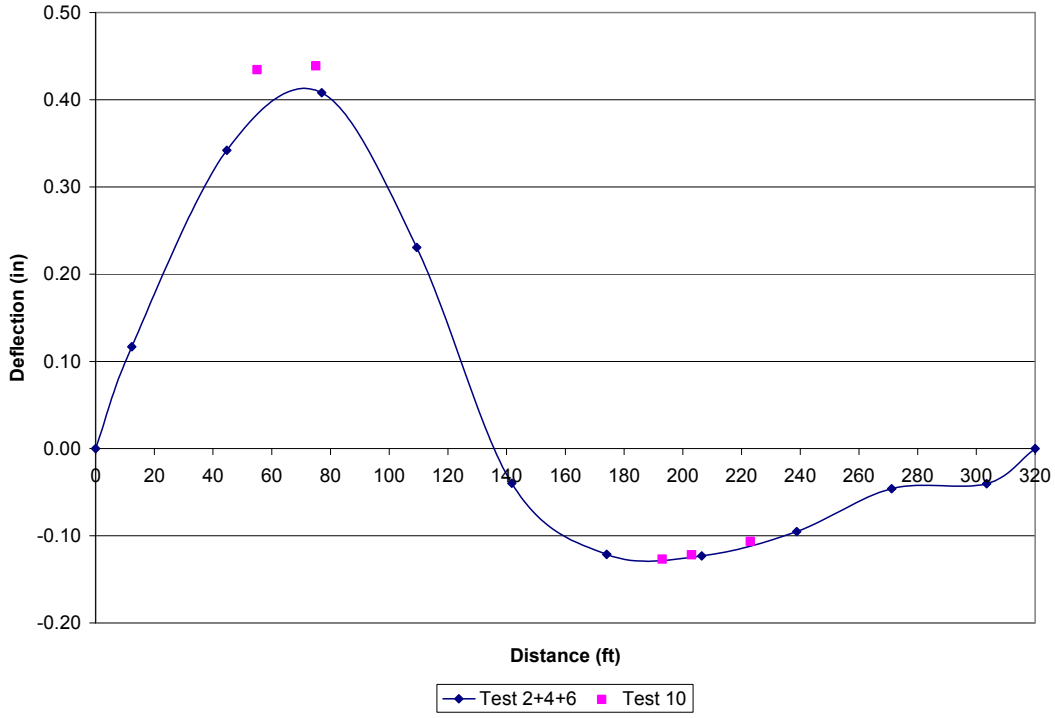

Figure 6-17. Superposition of the deflection of a section from girder B located above the road's shoulder

In conclusion, the theory of superposition is confirmed when comparing measured strain values. Comparing the deflection shows varied results, however at larger deflection values the error tends to decrease.

6.5 Load Rating

The bridge was load rated according to the procedure specified in the Manual for Condition Evaluation and Load and Resistance Factor Rating of Highway Bridges (LRFR) published by AASHTO. This procedure is consistent with the LRFD bridge design philosophy. The purpose of this rating is to recognize any need for the posting of loads or the strengthening of the bridge. It is also a basis for determining the safe loading capacity. The basic load rating equation is as follows

$$RF = \frac{C - (\gamma_{DC})(DC) - (\gamma_{DW})(DW) \pm (\gamma_P)(P)}{(\gamma_L)(LL + IM)} \qquad \textbf{6-3}$$

Where

RF = Rating factor
C = Capacity
DC = Dead-load effect due to structural components and attachments
DW = Dead-load effect due to wearing surface and utilities
P = Permanent loads other than dead loads
LL = Live-load effect

IM = Dynamic load allowance
γ_{DC} = LRFD load factor for structural components and attachments
γ_{DW} = LRFD load factor for wearing surface and utilities
γ_P = LRFD load factor for permanent loads other than dead loads
γ_L = Evaluation live-load factor

The ratings can be completed using load effects such as bending moments, shear, bending stresses or axial stresses to name a few. A preliminary analysis of design rating factors found using bending moments and bending stresses found that bending moments would yield smaller rating factors in the Strength I analysis, so bending moments were the main consideration of this bridge. Also considered, as suggested in the manual, was shear loading effect.

The rating procedures work on an element by element basis. This means that each potentially critical structural element of the bridge is rated using each load effect and the lowest resulting rating factor from those found is taken as the bridge rating factor. In this analysis, the bending moment and shear capacity of and interior and exterior girder was considered. Since the manual requires not only a Strength I analysis, but also a Service II analysis, the top and bottom flange of the girders were rated for bending stresses as well.

The design rating procedures for this bridge resulting in an inventory design rating factor of 1.47, governed by the shear capacity. Because this factor is greater than one, the bridge has sufficient capacity for the HL-93 loading. This also implies that the bridge has adequate capacity for all AASHTO legal loads, so no load posting is required. Completing a legal load rating was therefore not required for this bridge, but was performed anyway, as legal rating is the basis for determining safe load capacity figures.

To examine how the N-2 Bridge over I-80 was performing, a live load test was conducted. This kind of diagnostic test is suggested in the load rating manual as a way to refine the rating factor of a bridge. This procedure is specified in the load rating manual as the following equation:

$$RF_T = RF_C \times K \qquad \textbf{6-4}$$

Where
RF_T = Load-rating factor for the live-load capacity based on the load test result
RF_C = Load-rating factor based on calculations prior to incorporating testing results.
K = Adjustment factor resulting from the comparison of measured test behavior with the analytical model

The K factor is calculated directly from load testing results using the following equation:

$$K = 1 + K_a + K_b \qquad \textbf{6-5}$$

Where

K_a = Accounts for both the benefit derived from the load test, if any, and consideration of the section factor resisting the applied test load

K_b = Accounts for the understanding of the load test results when compared with those predicted by theory

Through the diagnostic load testing the K_a and K_b values were calculated according to LRFR 8.8.2.3 to be 0.63 and 0.8 respectively. From Equation 6-5, the K value is 1.50. The adjusted design load-rating factor is then calculated to be 2.21 using Equation 6-4.

Next, the legal load rating was completed. For this purpose, a rating factor is calculated for each of the AASHTO legal loads, namely Type 3, Type 3S2, and Type 3-3. Once these factors were computed they were multiplied by the previously calculated K factor to come up with the adjusted rating factors. Finally, these factors were multiplied by the total weight of the corresponding truck to come up with values for the safe load capacity of the bridge. The results of this analysis are listed in Table 6-2.

Table 6-2. Load Rating

Loading	Weight (kips)	RF_c	K	RF_t	Capacity (Tons)
HL93	72	1.02	1.5	1.53	**110**
Type 3	50	3.28	1.5	4.93	**123**
Type 3S2	72	2.43	1.5	3.64	**131**
Type 3-3	80	2.25	1.5	3.38	**135**

Two items that have not been considered as of yet are the fatigue limit state or permit rating. To justify the completion of a rating taking into account the fatigue limit state, a fatigue-prone detail must be identified. No such detail was defined. The permit load rating procedure is used to calculate if a certain loading permit should be issued for the passing of a permit truck over the bridge. A certain permit type has not been specified for load-rating, although a general permit rating specified in the manual will be used for rating in the near future.

6.6 Bottom Flange Slab Behavior

The design for this bridge included a 10’ concrete slab with an average thickness of 6” placed on top the bottom flange on either side of the pier diaphragm. Shear studs were provided to develop composite action between the slab and the bottom flange. The slab was designed to supply additional capacity over the pier for moment and shear effects. The design calculations were done with and without the capacity of the slab taken into account. To ensure a better understanding of the behavior and effectiveness of the slab, strain gages were provided at several locations throughout the slab and steel box section. Figure 6-18 shows the bottom flange slab near the pier and the sections where gages were located.

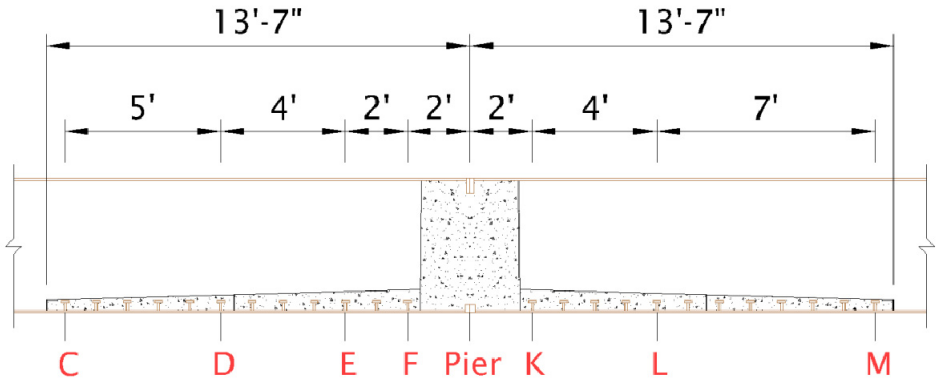

Figure 6-18. Bottom Flange Slab

Figure 6-19 shows strain data for Section K of Girder A for Test 18. During Test 18 Trucks A and C were adjacent to each other while Truck B followed Track A at 118; to produce a large negative moment over the pier. For simplicity the gages are labeled 1-6. In the figure, tension is positive and compression is negative. Gages 5 and 6 were located on the top of the bottom flange slab, as illustrated in the figure. Strain data from these gages indicate that the top of the bottom flange slab is in tension. For composite action to occur, these strains should be in compression with values slightly higher than Gages 3 and 4. The strain data indicates that the bottom flange slab does not act compositely with the steel section.

The same behavior is seen in the other sections monitored near the pier (see gage configuration No. 2 in Figure A-2) for Tests 17-20. Girder B acts similar to Girder A in that local bending of the bottom flange slab occurs indicating non-composite action.

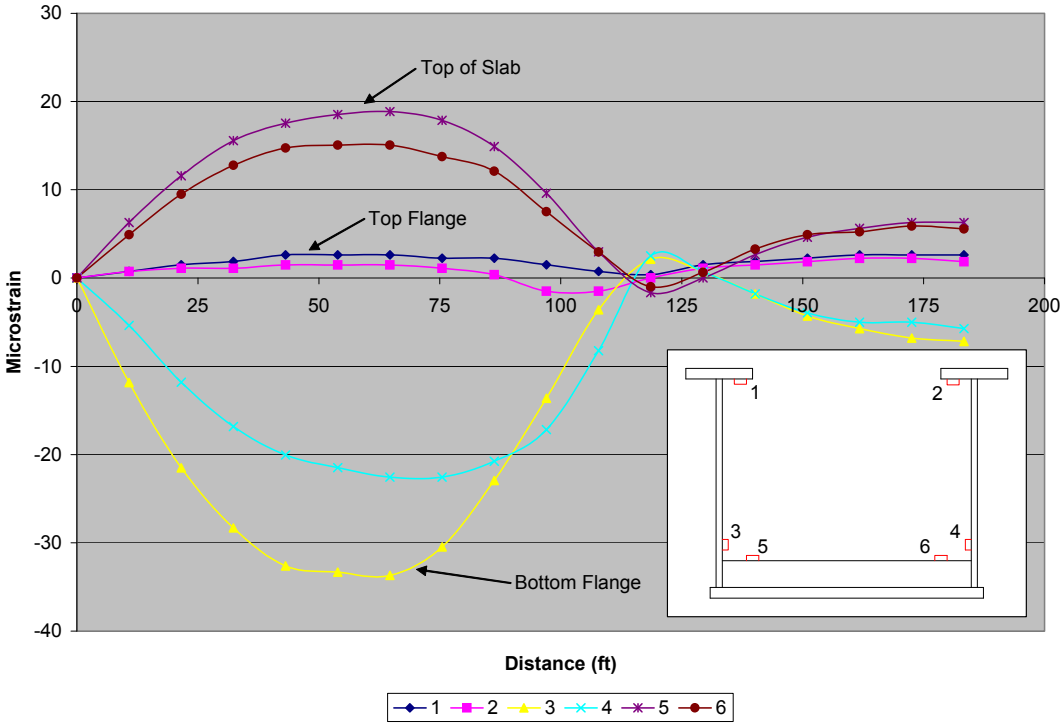

Figure 6-19. Section K, Girder A, Test 18

Sections near the pier were also monitored with existing gages which included concrete embedment gages in the bottom flange slab. Figure 6-20 shows strain data for Section K of Girder B for Test 12. The truck configuration is the same as that in Test 18. Data was taken at only three tuck locations for this test. The strain measured with the concrete embedment gage shows little strain due to the truck loads. This observation is consistent with local bending seen in Figure 6-19. The gage is located in the center of the slab which would experience minimal strain if the slab did not act compositely with the steel section. If the slab acted compositely, the expected strain measured in the embedment gage would be slightly less than that from Gage3. This graph is representatice of the other sections measured near the pier for Tests 11, 12 and 16.

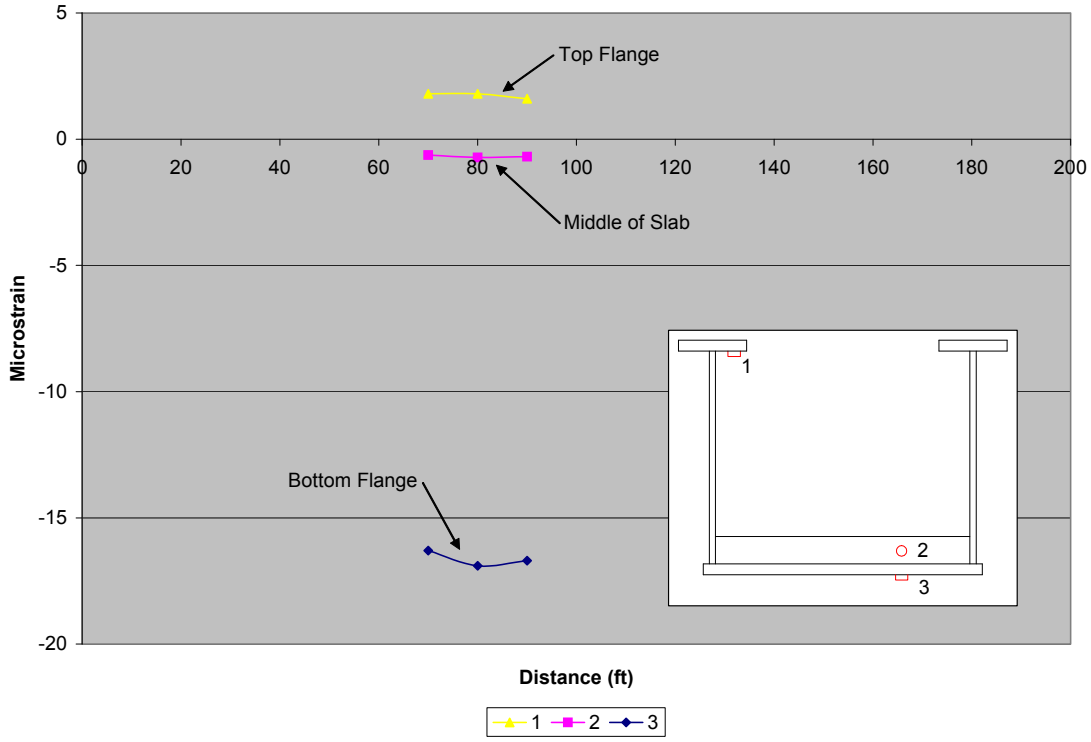

Figure 6-20. Section K, Girder B, Test 12

In conclusion, the strain data measured at the pier sections indicate that the bottom flange slab does not act compositely with the steel section. The steel used was grade 100HPS which created several problems with welding. This may be the reason for the ineffectiveness of the shear studs.

In general, the strains measured with the BDI gages were higher when compared to the strains measured with the SI gages at similar locations for the tests with the same truck configurations.

6.7 Neutral Axis Locations

The following assumptions are made in order to determine the locations of neutral axis in the bridge sections.

- Based on effective slab width
- Ignore shim height
- Short-term and Long-term Properties
- Ignore concrete deck for negative section
- Ignore effects of railing

The effective slab width and the tributary width for the girders used are shown in Figure 6-21.

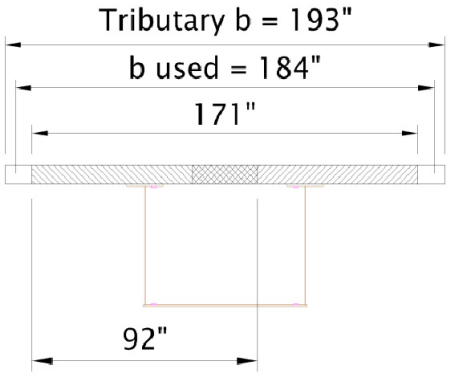

Figure 6-21. Effective slab width and the tributary width for the girders

The neutral axis positions in the mid-span and pier sections over the bridge width are shown in Figure 6-22.

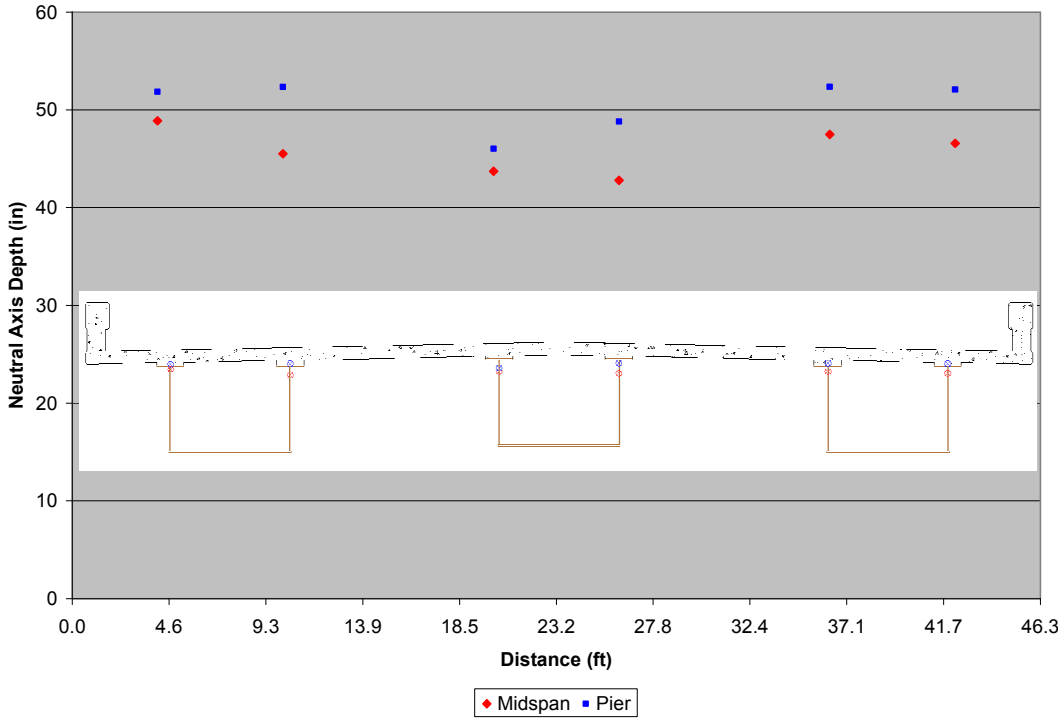

Figure 6-22. The neutral axis positions in the mid-span and pier sections over the bridge width

Table 6-3 summarizes the position of the neutral axis in the positive and negative moment sections of the bridge.

Table 6-3. Position of neutral axis

Neutral Axis Depth (in)						
Beam Location	Positive Section			Negative Section		
	Measured	Calculated Short-Term	Calculated Long-Term	Measured	Calc. w/ Bot. Slab	Calc. w/o Bot. Slab
Interior	43.3	40.1	30.9	47.1	21.9	28.0
Exterior	47.4			52.2		

Followings are some of the conclusions resulted from the neutral axis calculation.

- Calculated values are lower for all cases
- The differences between the calculated values and the measured values are higher in the negative region values
- Max strain values used to calculate the measured values
- Neutral Axis is higher at exterior girders due to the contribution of railing

6.8 Finite Element Model

A finite element model developed using SAP2000 software in order to compare the results obtained from the Live Load Testing to that of the Finite Element Model.

6.8.1 Model Development

Duo to the following reasons it was decided to develop a 2D model and compare the results to that of the live load testing.

- N-2 over I-80 is a straight bridge with no skew
- Bridge deflections duo to the live load testing are very small and they fall well within the elastic range of the bridge behavior which can accurately be predicted using a 2D finite element model
- Most design firms use 2D analysis for a bridge with specifications like the N-2 over I-80 bridge. This 2D analysis will show how the common analyses are comparable to the real life results and whether this type of analysis results in conservative results.

6.8.1.1 Determination of the 2D model elements

This sections provides information on how the different needed SAP2000 model parameters have been determined.

- Girders

$A=119.5$ in.^{2}

$I_x=57081.6$ in.^{4}

- Girders with Composite Bottom Flange

$A_{Converted\ section}$=154.06 in.^{2}

I_x=64478.0 in.^{4}

In order to determine the bridge deflections due to live load testing the total moment of inertia of the whole structure should be determined. In addition, since the whole bridge is a composite section of the concrete deck and the steel girders, the moment of inertia of the converted section needs to be calculated as follows.

The modular ratio can be calculated as follows. This will be used to scale the width of all concrete parts.

$$\begin{aligned} E_S &= 50000\ psi \\ E_C &= 4000\ psi \end{aligned} \qquad \Rightarrow\ n = \frac{50000}{4000} = 12.5$$

Figure 6-23 shows the bridge converted section. As can be seen, the bridge guard rails have also been considered in the converted section's configuration.

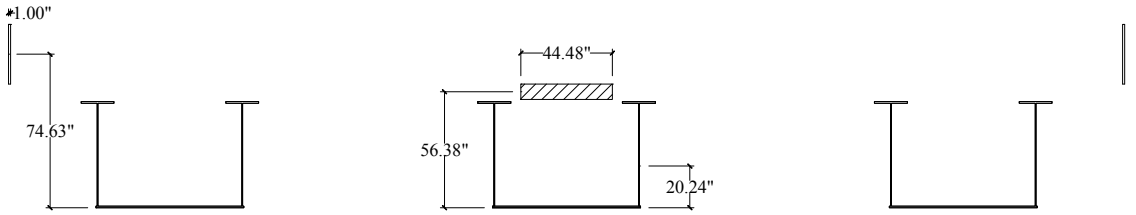

Figure 6-23. The converted section of the entire bridge

Having this converted section, the following section properties can be calculated.

$y_{N.A.} = 39.80 in.$

$I_x^{Total} = 475972.7 in.^4$

$A^{Total} = 727.9 in.^2$

Figure 6-24 shows the bridge converted section in the 14 ft neighborhood of pier where there is an additional concrete slab composited with the girders' bottom flanges. An average thickness of 6" has been considered for this concrete slab.

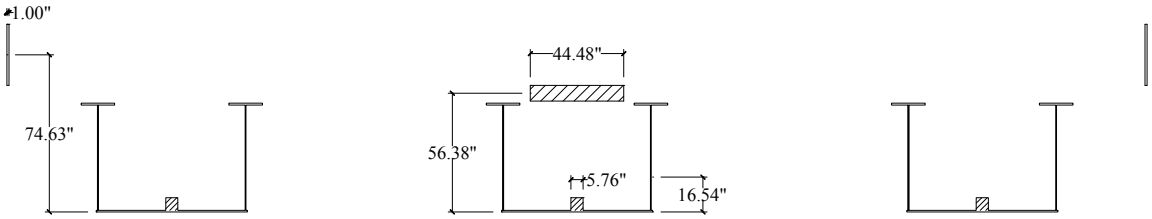

Figure 6-24. The converted section of the entire bridge around the pier

Having this converted section, the following section properties can be calculated.

$y_{N.A.} = 35.48 in.$

$I_x^{Total} = 491496.40 in.^4$

$A^{Total} = 831.62 in.^2$

It should be noted that the bridge detailing at the abutments causes some amount of fixity that has been calculated earlier. This amount is 4.00×10^5 k-ft/rad per girder. Because the total amount of fixity for the bridge is of interest in this section, two rotational springs with 12.00×10^5 k-ft/rad are defined on each side of the model.

6.8.1.2 SAP2000 model of the structure

In order to obtain more accurate results from the finite element model the bridge was modeled using 1 ft long beam elements so there are 139 beam elements modeled in each span of the bridge. Figure 6-25 shows the "Truck A" definition in SAP2000 software. The same method is used for trucks B and C definitions.

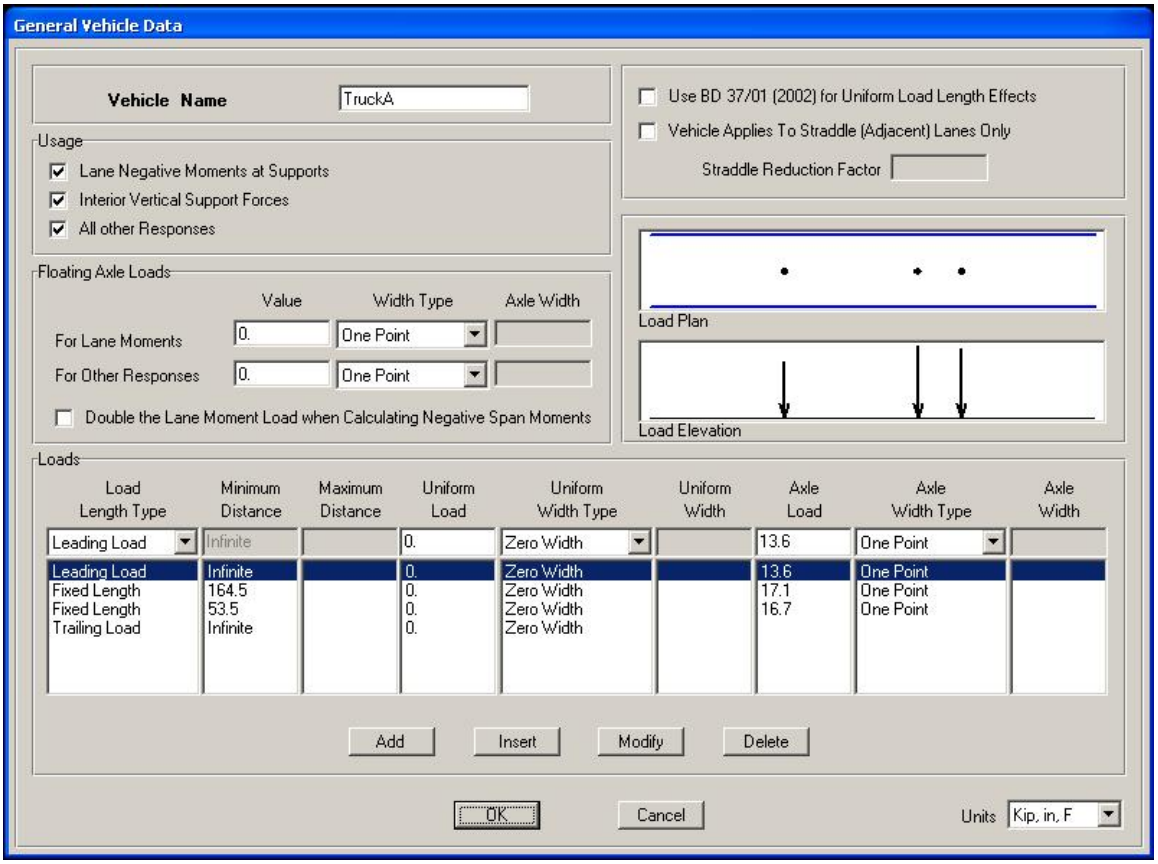

Figure 6-25. Definition of TruckA in SAP2000

As stated earlier, pots were located on each girder, 60 ft from each abutment, at the center of the bottom flange. Therefore, the deflection influence life of the bridge on that location is of interest. Figure 6-26 shows the deflection influence line of the bridge for a location 60 ft from each abutment.

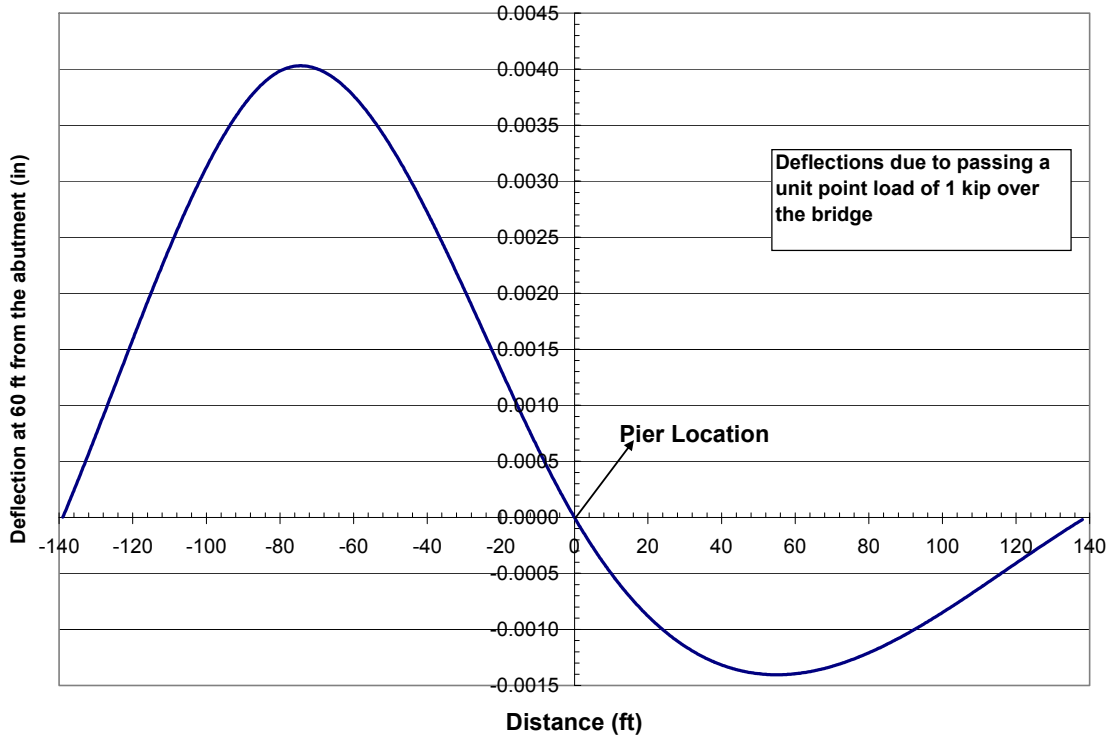

Figure 6-26. Deflection influence line of the bridge for a location 60 ft from each abutment

Now having the deflection influence line in Figure 6-26, the influence lines associated with Test2, Test4, and Test6 corresponding to trucks A, B, and C respectively can be developed which are shown in Figure 6-27 to Figure 6-29.

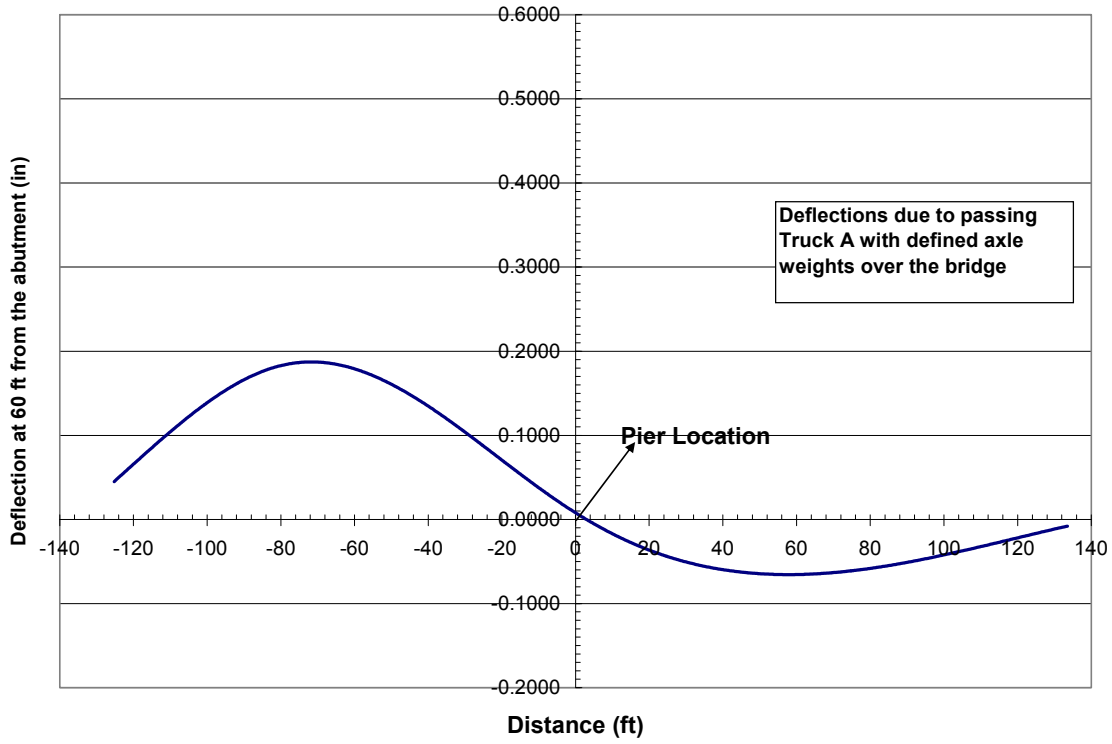

Figure 6-27. Influence line associated with Test2 corresponding to truck A

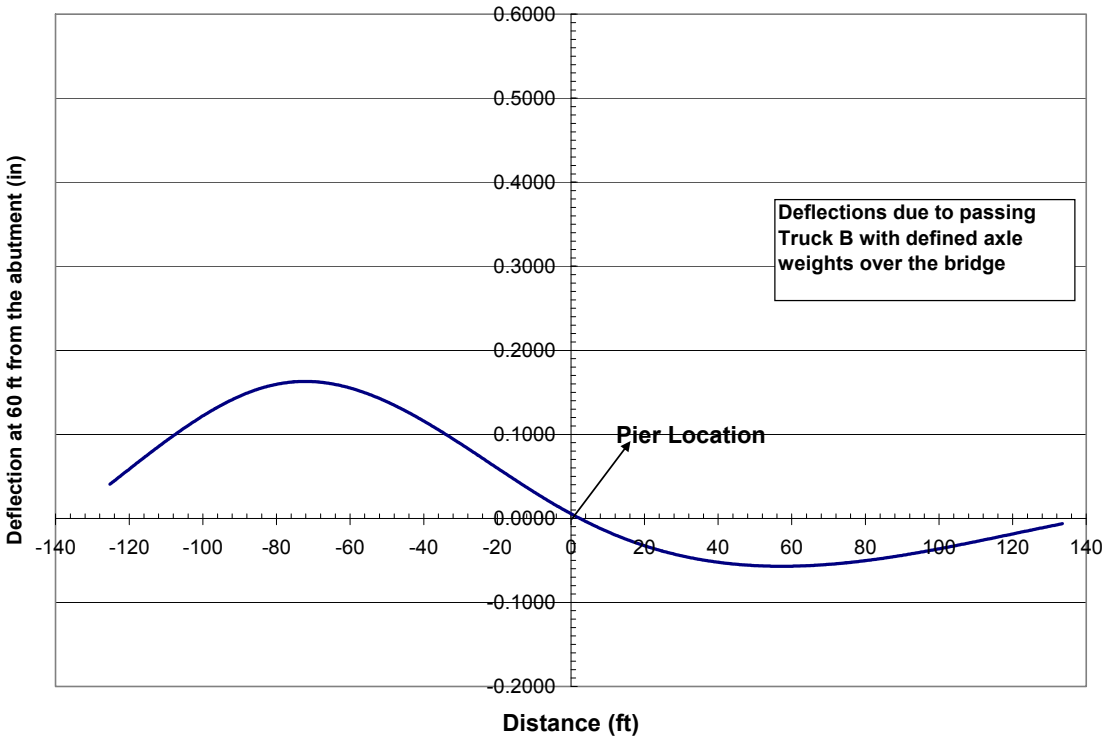

Figure 6-28. Influence line associated with Test4 corresponding to truck B

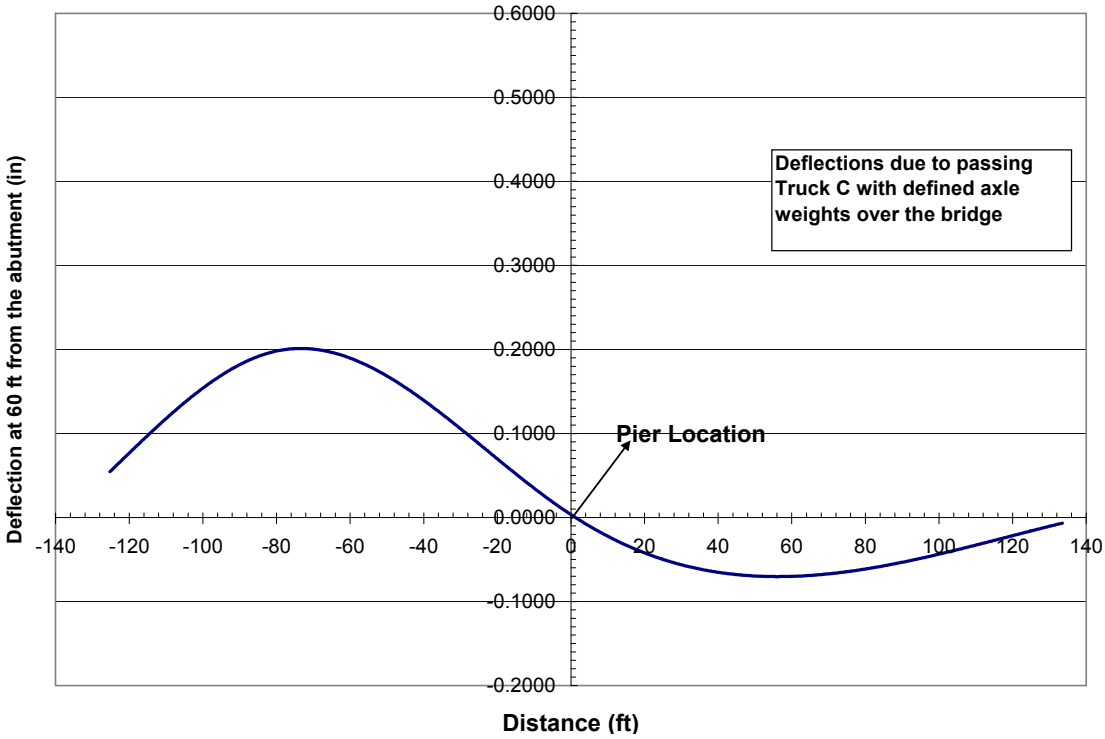

Figure 6-29. Influence line associated with Test6 corresponding to truck C

Figure 6-30 shows test 10 (corresponding to all trucks passing the bridge at the same time) deflection results. The theory of superposition was used to develop this plot.

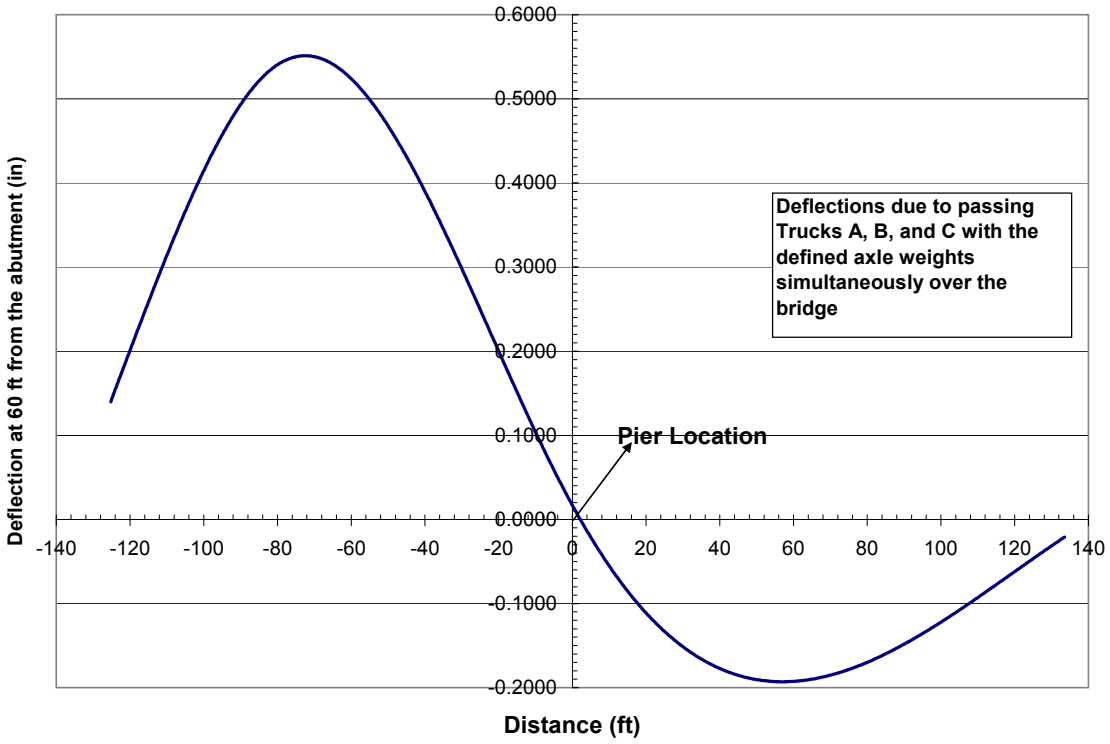

Figure 6-30. Influence line associated with Test10 corresponding to trucks A, B and C

6.8.2 Test Comparison to FEM Results

As described earlier in this report the bridge components remain well in the elastic range of behavior during the live load testing. Therefore, the deflections of the bridge will be of a great interest especially that they control the vibration of the bridge as well.

Figure 6-31 shows a comparison of the deflection results from linear superposition of Test2+4+6, Test10 and SAP2000. As can be seen in this figure, the resulted deflections from the SAP2000 model are slightly larger than that of the live load testing at the sections with maximum deflections. At other sections of the bridge, the deflections resulted from the Live load testing and the SAP2000 model closely follow each other.

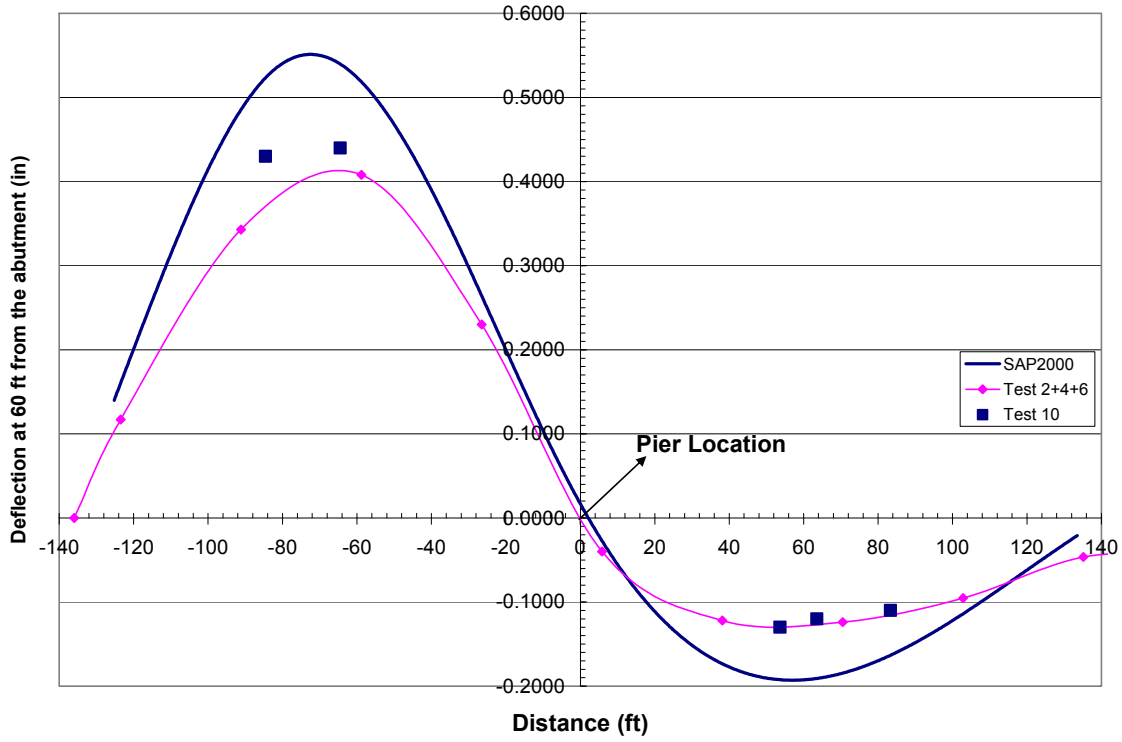

Figure 6-31. Comparison of the deflection results from linear superposition of Test2+4+6, Test10 and SAP2000

Chapter 7
Long Term Monitoring

7.1 Introduction

This chapter focuses on the monitoring of the long-term behavior of N-2 over I-80 bridge. The system was initially activated on October 23, 2003 and continued to collect data until December 14, 2008 and this chapter covers the understandings of the structure behavior during this five years period of time.

7.2 Temperature

Daily and seasonal temperature variations influence the bridge performance as well as the readings from strain gages. Therefore these data were needed to be recorded to modify the readings from other gages. Figure 7-1 shows an example of ambient temperature over time from the temperature and humidity probe that was installed on the bridge. All of the figures showing the temperature data over time are presented in Appendix A.

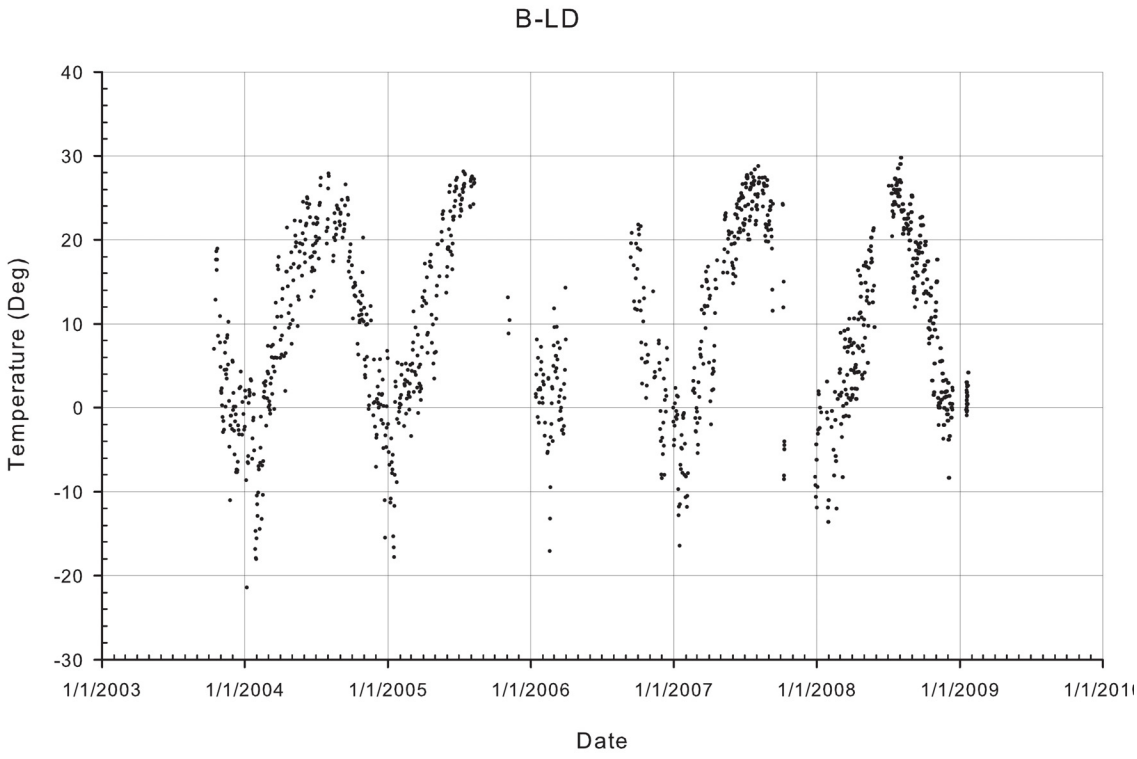

Figure 7-1. Example of ambient temperature over time

7.3 Humidity

Humidity influences the concrete behavior. For example, concrete shrinkage is sensitive to humidity. Therefore, the relative humidity over time was measured in order to determine any correlation between the concrete behavior and the humidity change. Figure 7-2 shows an example of the relative humidity over time. All of the figures showing the temperature data over time are presented in Appendix A.

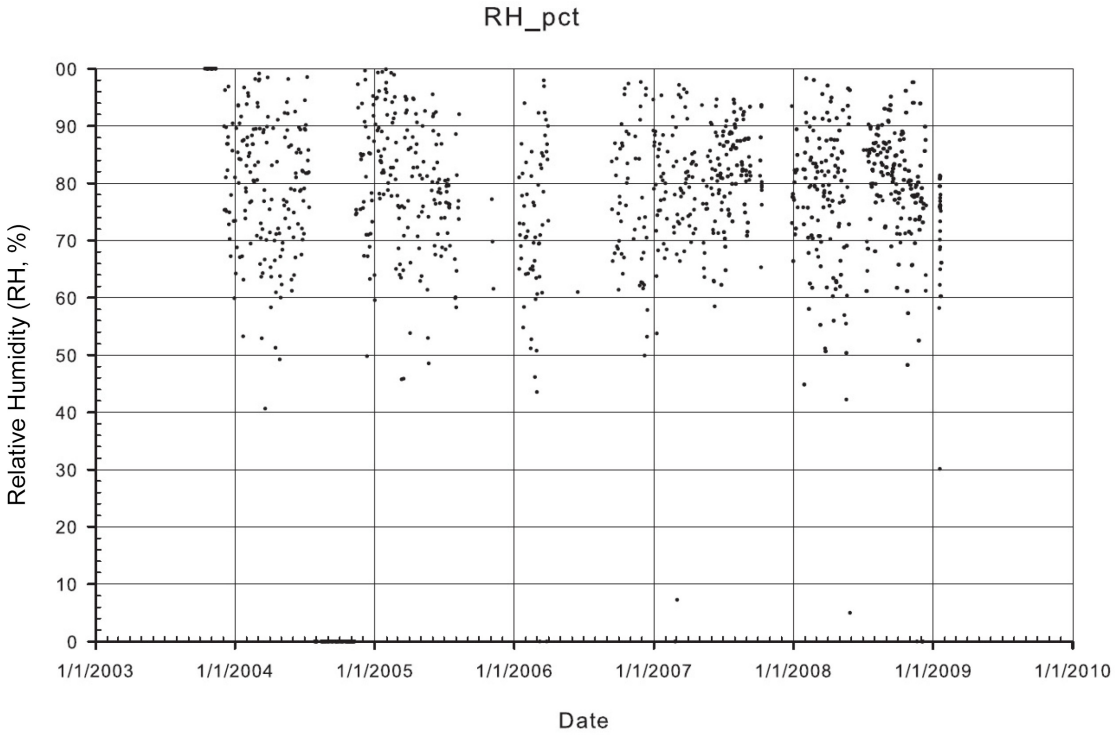

Figure 7-2. Example of the relative humidity over time

7.4 Precipitation

Precipitation influences the concrete behavior because it changes the humidity of the concrete significantly. The bridge was equipped with a tipping bucket rain gage so that the bridge behavior can be investigated during precipitation. Figure 7-3 shows precipitation over time. The system was recording the amount of precipitation in an hour, so the spikes that occur in the graph would be an amount of precipitation that fell during an hour's time.

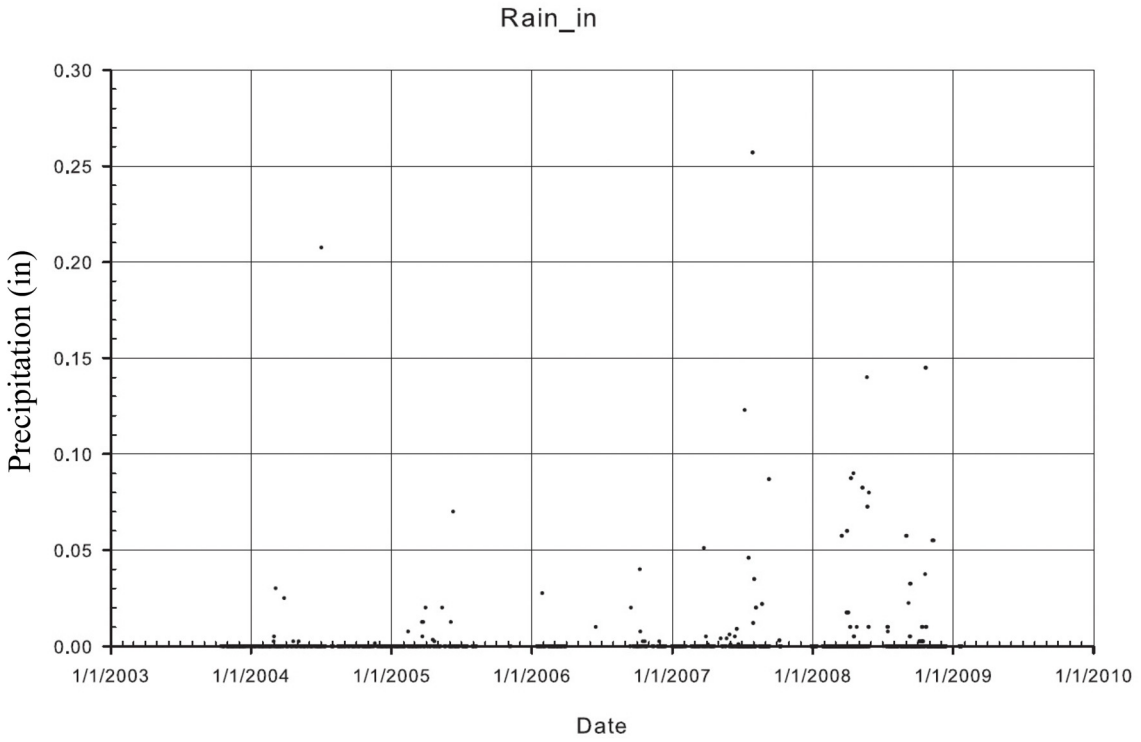

Figure 7-3. Amount of Precipitation in the bridge area over time

7.5 Strain Data from Long-Term Monitoring

Data obtained from the strain gages and concrete embedment gages over time can be used to investigate the long-term behavior of the bridge over time. Data from the temperature and humidity gages can be used to investigate the effects of weather on the bridge behavior. These data may also be useful to justify some of the unexpected bridge behaviors on some circumstances. Moreover, in the case that some certain climate conditions pose dramatic changes to the structure behavior, they can be predicted and taken care of during the design process.

In order to access the long-term bridge behavior from the strain gages data, the general trend of the strain data is of interest. In fact, since the strain data has large fluctuations over time (depending to the temperature, season, etc.), it is rational to access the strain data and the bridge behavior over a long period of time based on the whole trend of the data. Therefore, in the case that the measured strains and its seasonal fluctuations do not significantly change over the data logging period, it can be concluded that the bridge responses to loading remains stationary.

7.5.1 Spot-Weldable Strain Gages

The spot-weldable gages provide data that are useful in determining the behavior of the steel girders. Locations of interest include mid-span and near the diaphragm.

Beginning with the mid-span of the north interior girder, Figure 7-4 shows data from the top and bottom flanges, and the web. Figure 7-5 shows data from the flange and web gages located just outside the north side of the diaphragm. Figure 7-6 shows data from

the flange and web gages located on the interior girder at the south mid-span. Figure 7-7 shows east exterior girder strains at mid-span and near the diaphragm, respectively.

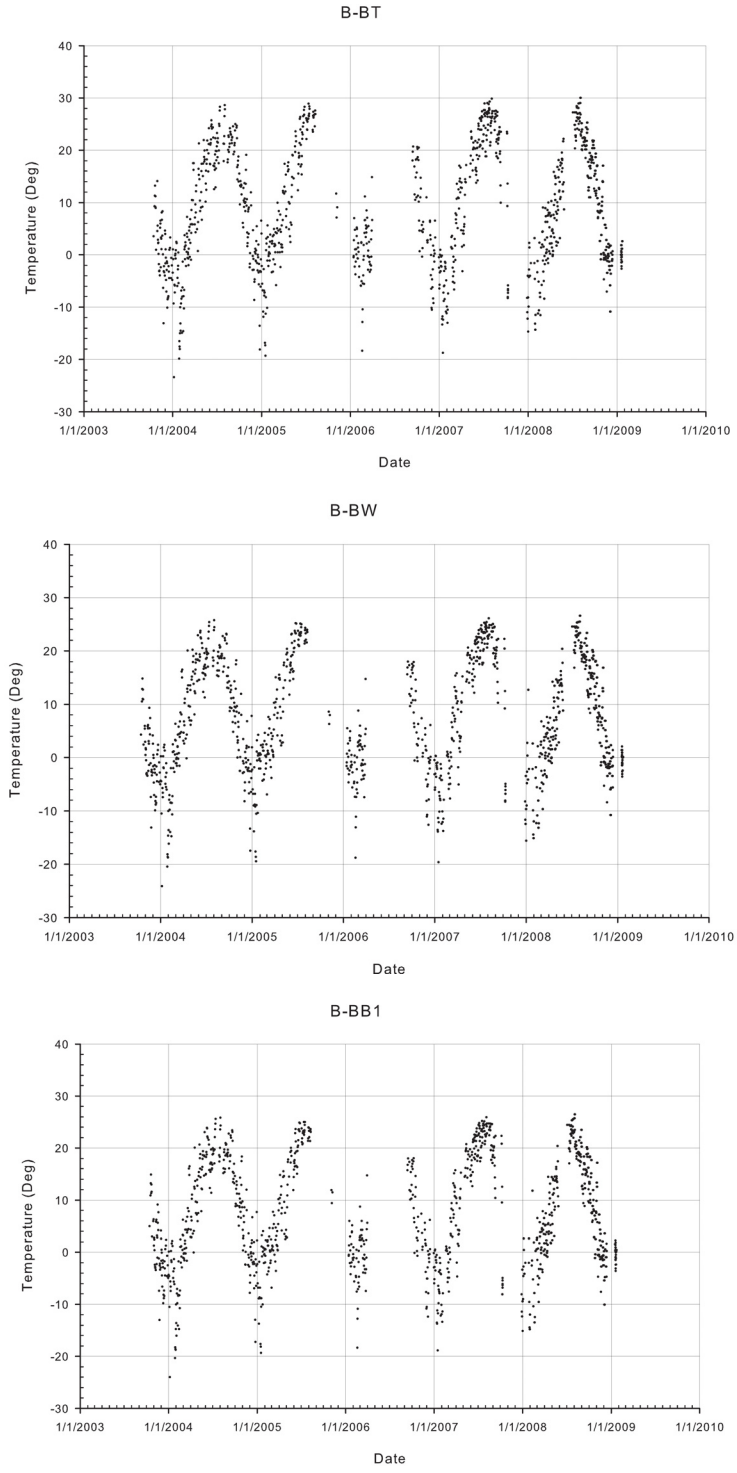

Figure 7-4. Strain data from the top and bottom flanges and the web at mid-span from the north interior girder

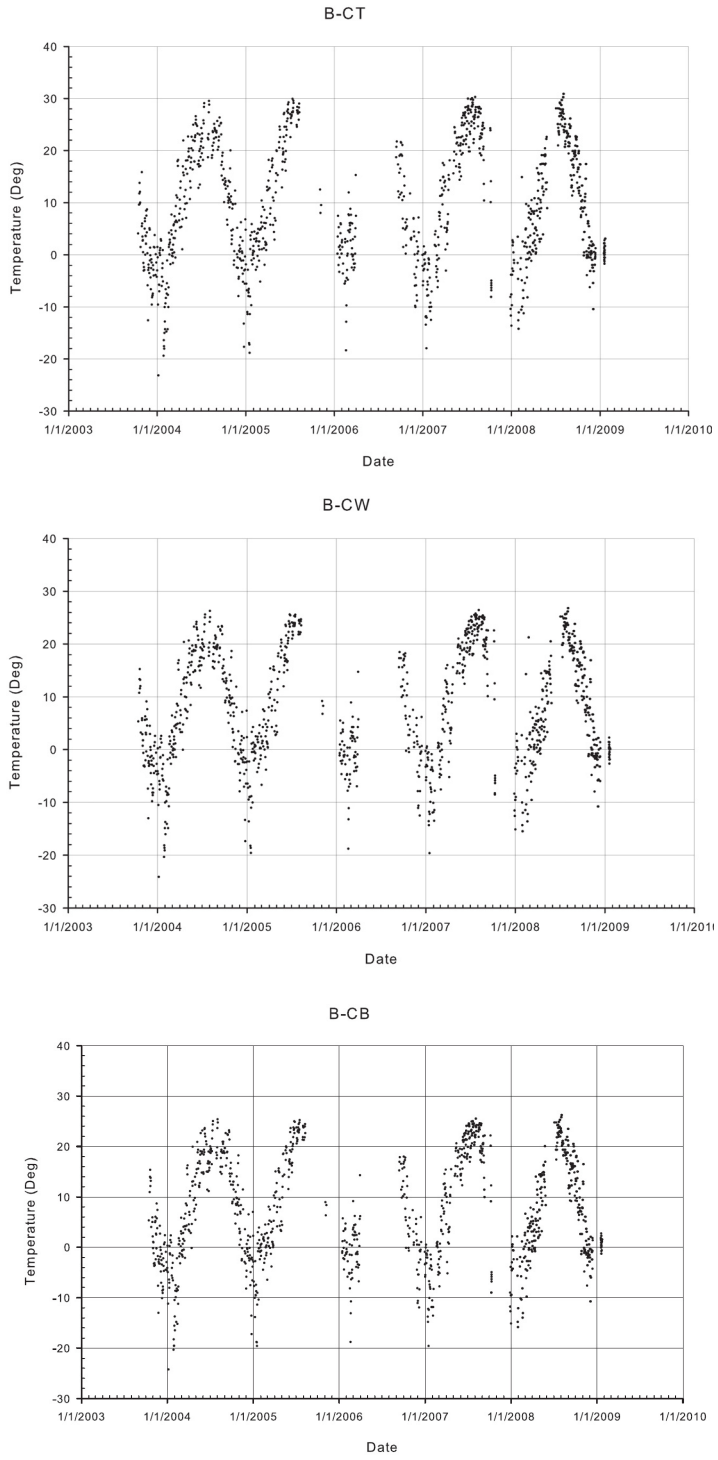

Figure 7-5. Strain data from the flange and the web just outside of the north side of the diaphragm

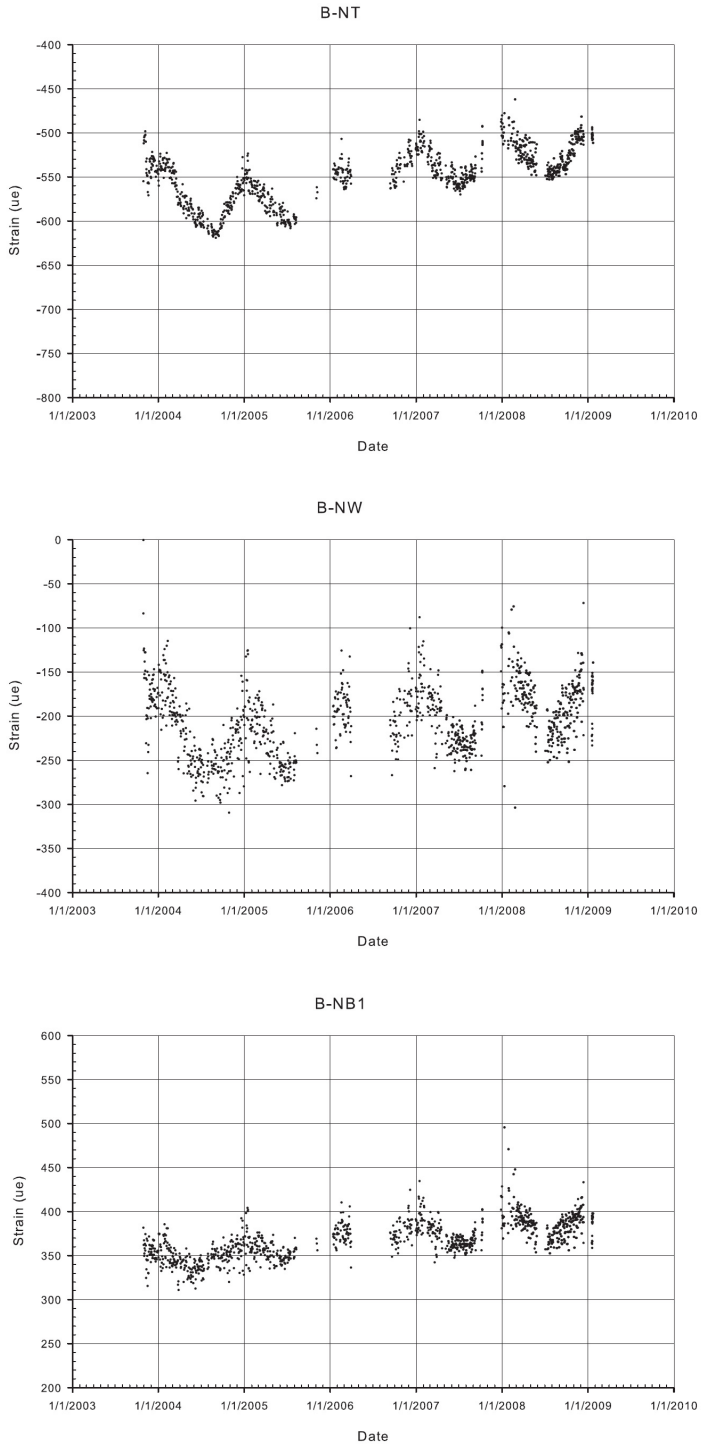

Figure 7-6. Strain data from the flange and the web on the interior girder at the south mid-span

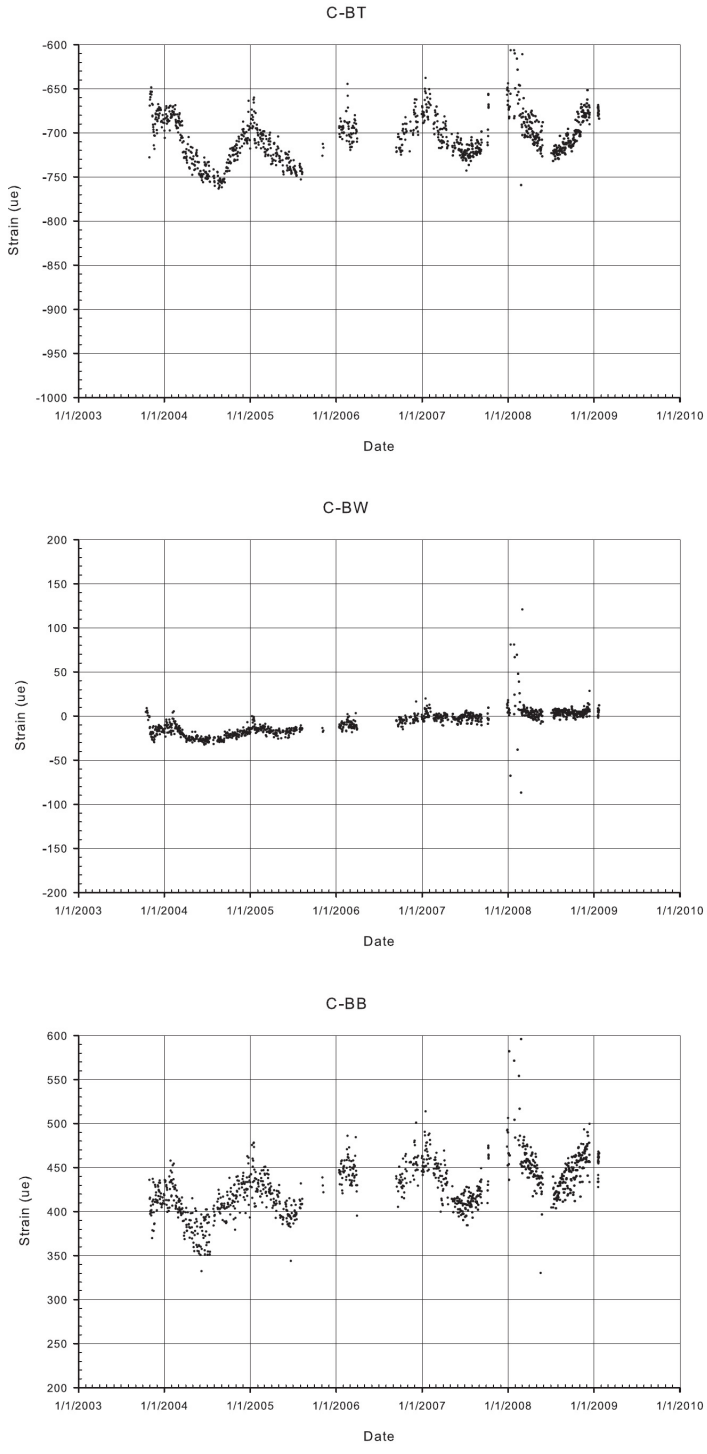

Figure 7-7. Strain data from east exterior girder at mid-span and near the diaphragm

7.5.2 Embedment Gages

Embedment gages were installed inside of the concrete double slab on the girders' bottom flange over the pier in order to monitor the behavior of the concrete diaphragm.

The diaphragm is vital to the performance of the bridge, so it was crucial to have instrumentation in this region of the bridge. Figure 7-8 shows data collected from the embedment gages at the interior girder. As can be seen in the figure, the resulted strains are negative representing the compressive behavior of the doubled slab on the girders' bottom flanges.

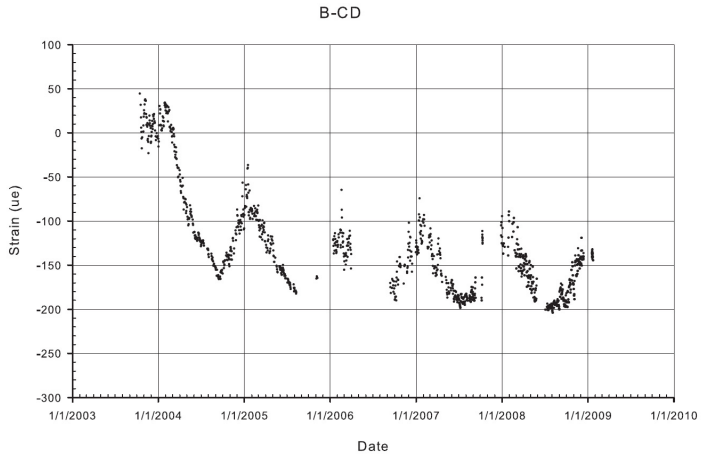
B-CD
100
50
0
-50
-100
-150
-200
-250
-300
Strain (ue)
1/1/2003
1/1/2004
1/1/2005
1/1/2006
1/1/2007
1/1/2008
1/1/2009
1/1/2010
Date

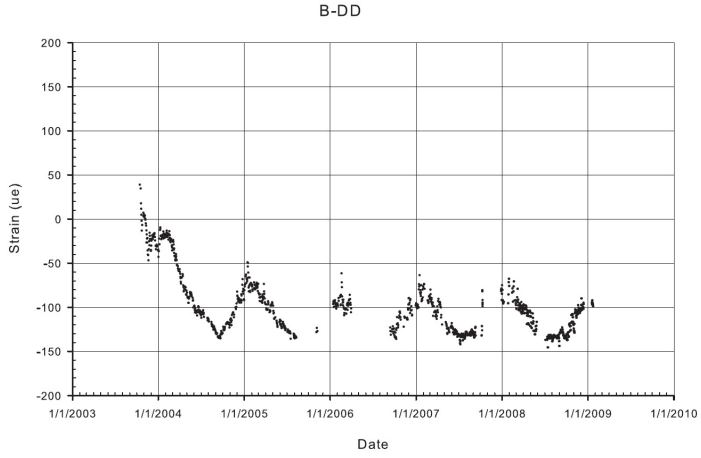
B-DD
200
150
100
50
0
-50
-100
-150
-200
Strain (ue)
1/1/2003
1/1/2004
1/1/2005
1/1/2006
1/1/2007
1/1/2008
1/1/2009
1/1/2010
Date

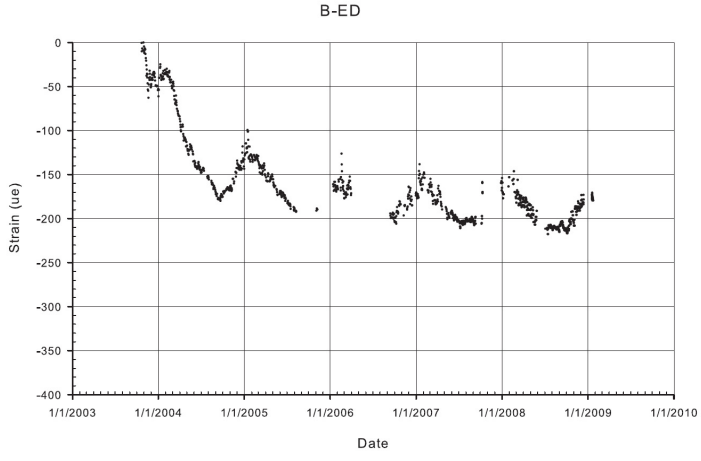
B-ED
0
-50
-100
-150
-200
-250
-300
-350
-400
Strain (ue)
1/1/2003
1/1/2004
1/1/2005
1/1/2006
1/1/2007
1/1/2008
1/1/2009
1/1/2010
Date

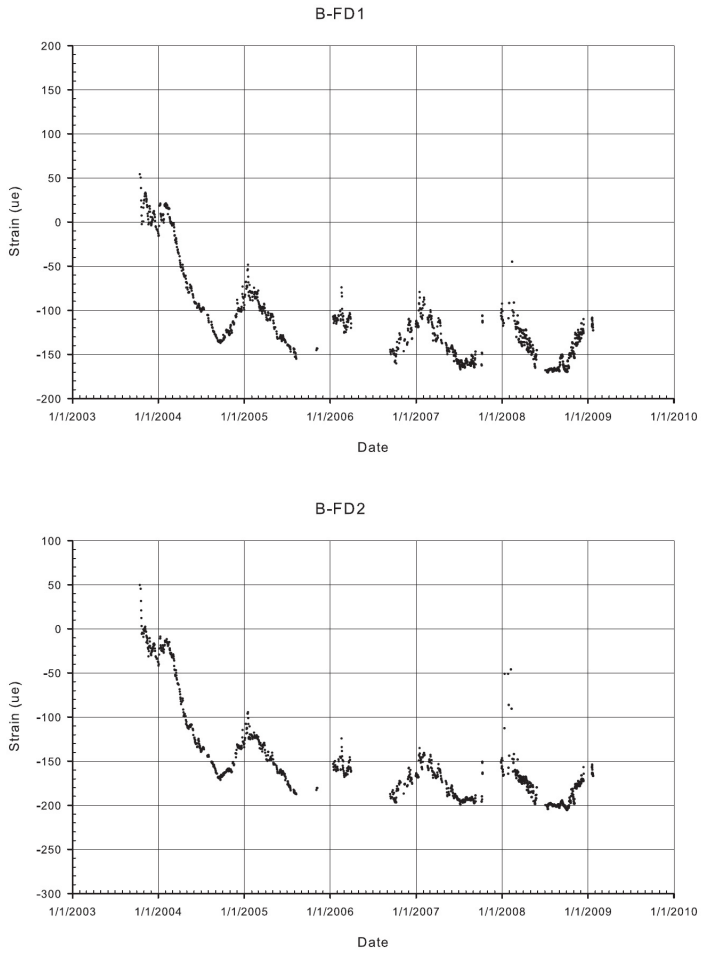

Figure 7-8. Data collected from the embedment gages at the interior girder

7.5.3 Sister Bar Gages

Sister bars were installed in the deck at two places along the length of the bridge. Figure 7-9 shows data from sister bar gages that were installed in the deck over the interior girder at approximately 13 feet from the pier centerline. Figure 7-10 shows data from sister bar gages in the deck at pier centerline, over the interior girder. Figure 7-11 shows data from gages in the deck at the pier centerline, over the east exterior girder.

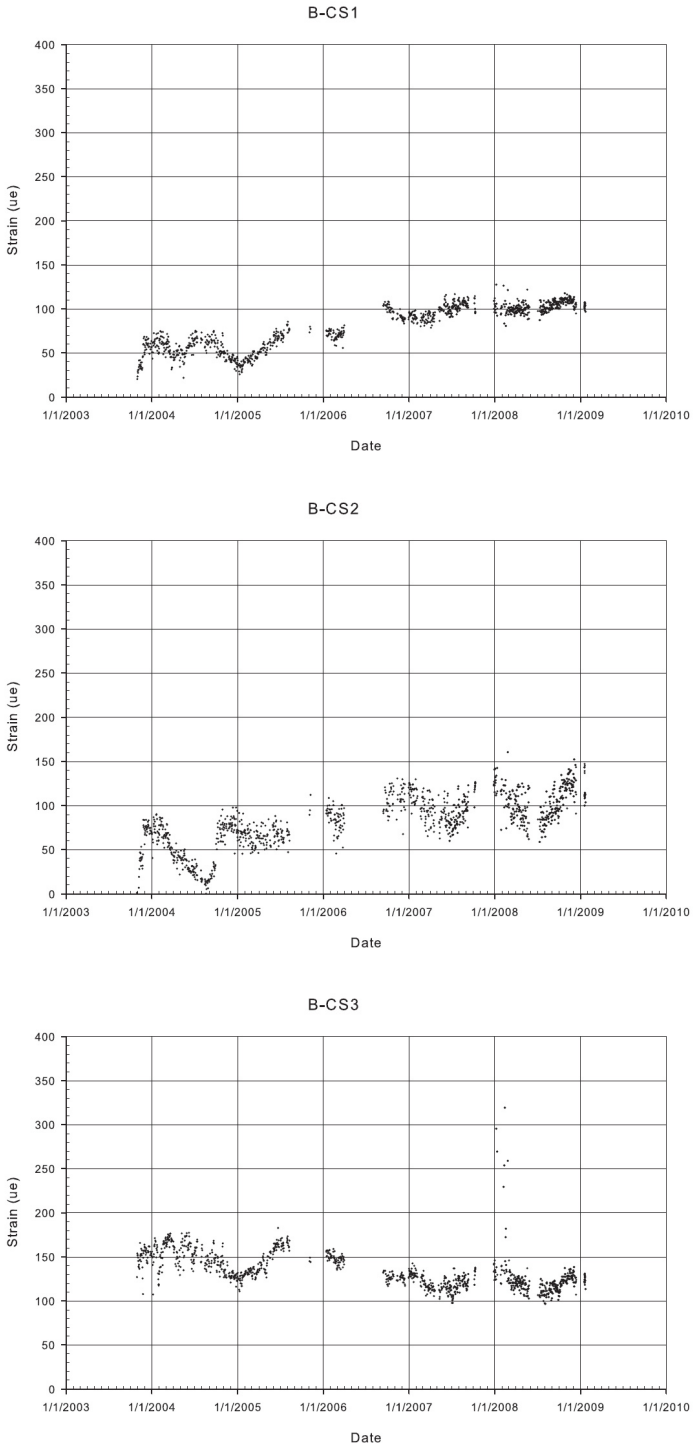

Figure 7-9. Data from sister bar gages installed in the deck over the interior girder at approximately 13 feet from the pier centerline

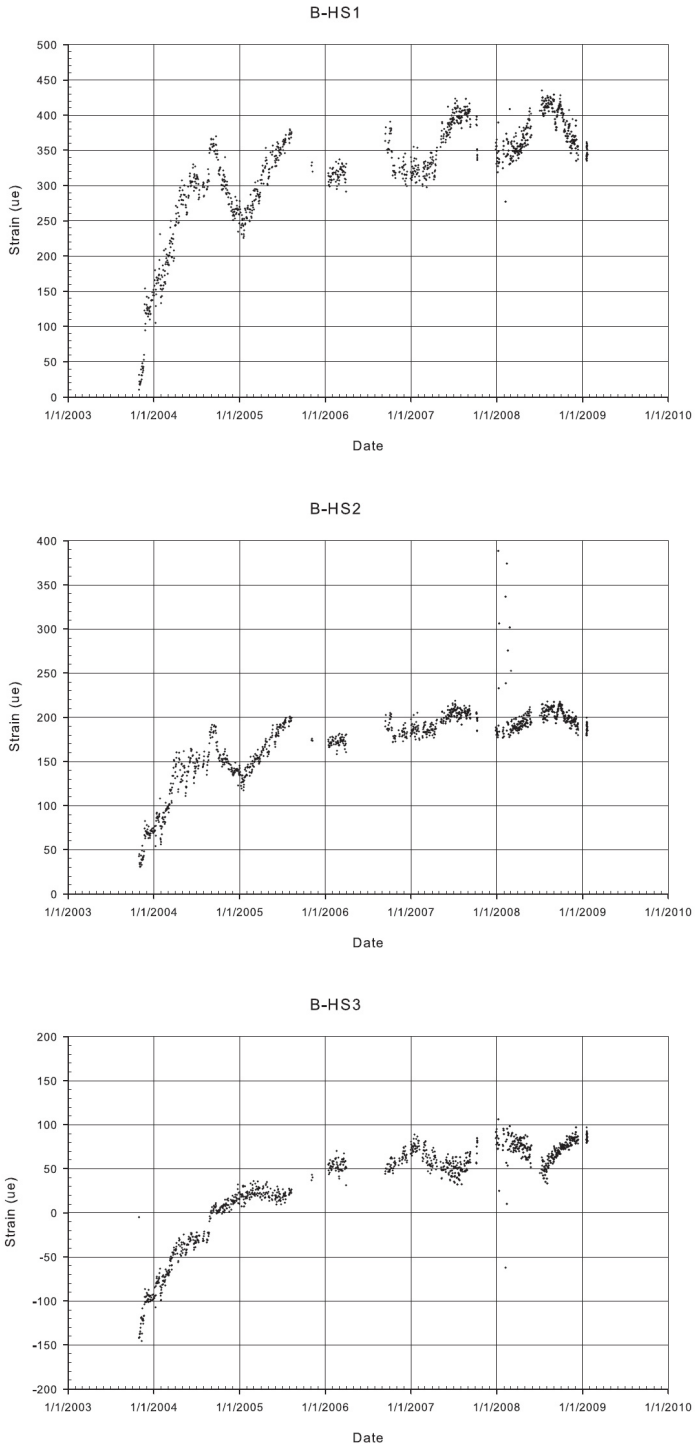

Figure 7-10. Data from sister bar gages installed in the deck at pier centerline, over the interior girder

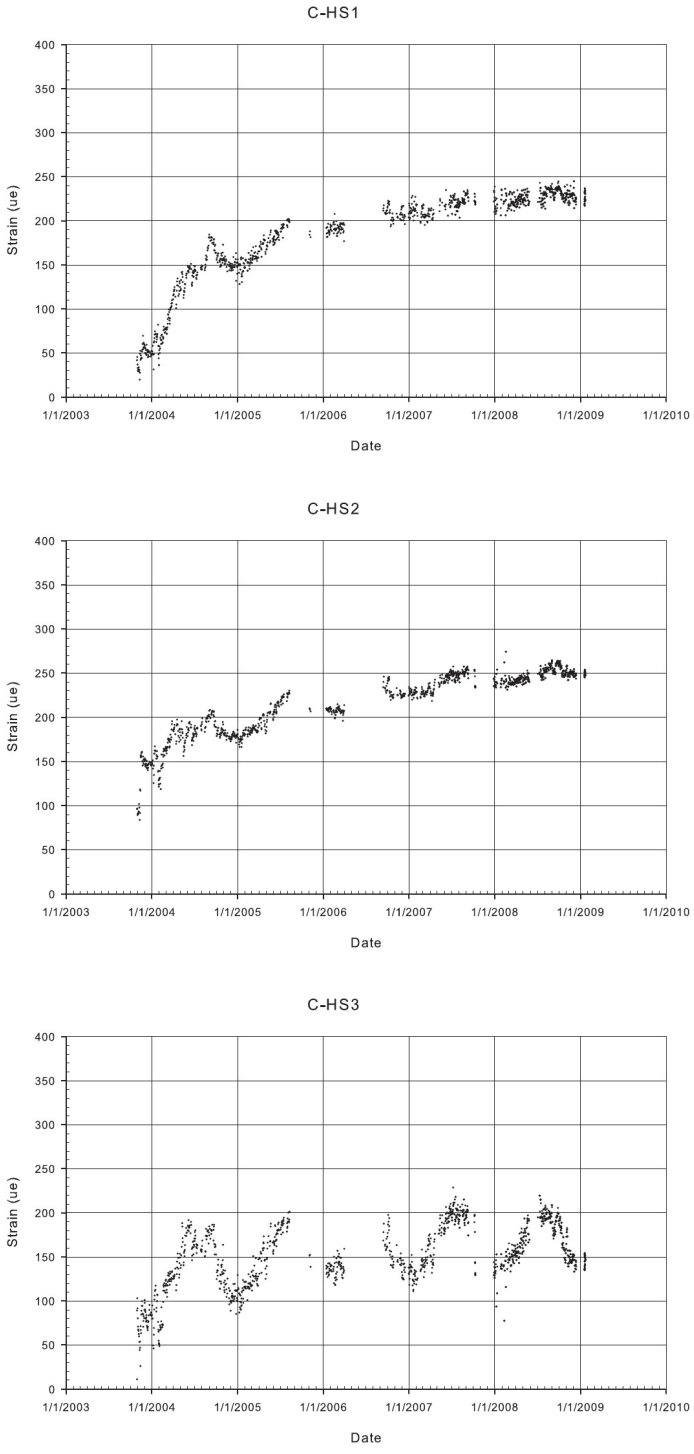

Figure 7-11. Data from gages installed in the deck at the pier centerline, over the east exterior girder

7.5.4 Tiltmeters

Tiltmeters were installed on the pier at three heights. One was located on the diaphragm, and two were located toward the top of the pier. Figure 7-12 shows data from the gages located on the pier. The top gage is the one located on the concrete diaphragm.

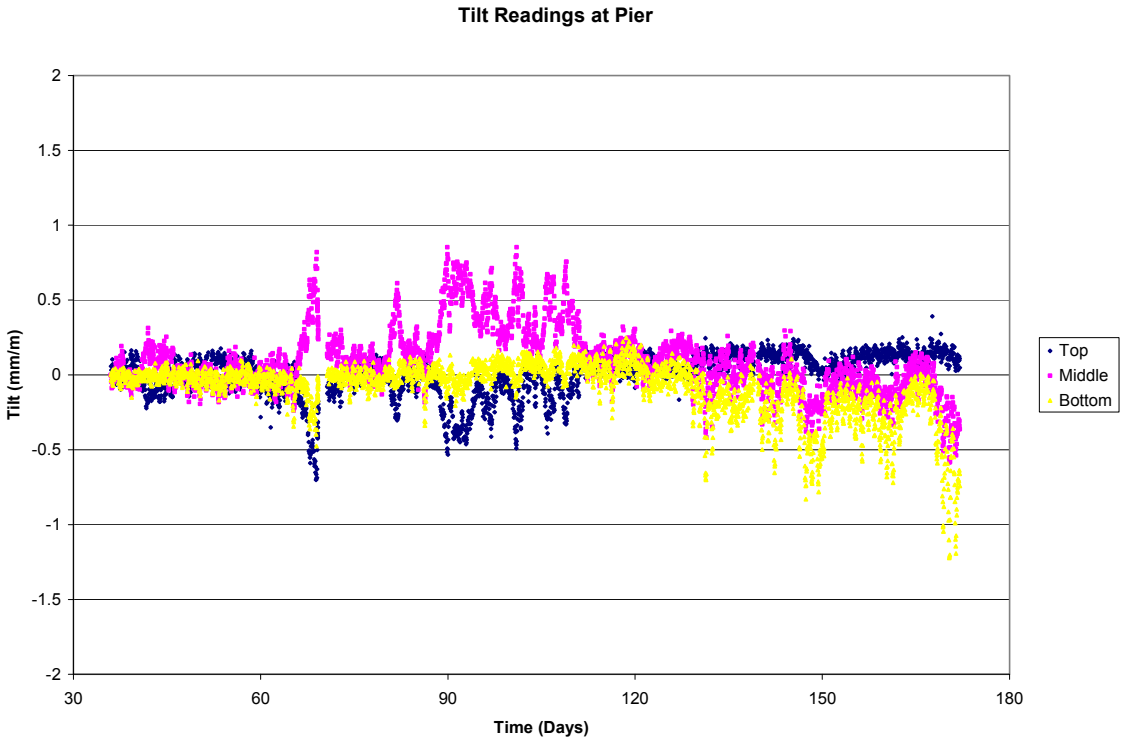

Figure 7-12. Tiltmeter data over the pier

7.5.5 LVDTs

Displacements from LVDTs installed on the south span of the bridge are shown in Figure 6-19. LVDTs on the north span did not read correctly. It should be noted that on approximately Day 215, the system was checked over and a large air bubble was found in the system, which was purged. Data up to that point is questionable. Several adjustments to the system had been made as well prior to that time.

7.5.6 Additional Data from Long-Term Monitoring

Additional plots of data that was collected during long-term monitoring can be found in Appendix A.

7.6 Results obtained from Long Term Monitoring of the Structure

Casting of the deck began on the morning of July 10th, 2004 at 6:00 am. This is used as a starting time for the long-term monitoring portion of the project. Similarly, the readings of the gages at that time used as zero values.

The effects of temperature, solar heating, and seasonal effects are discussed in the following section and the filtering developed to deal with these effects is presented in the subsequent section. Several significant observations are then discussed. Results from all of the gages are presented in Appendix A.

7.6.1 Temperature Effects

During the summer days the sun heats the top of the slab and the bridge deflection is upwards. Since the sun heats the deck directly while the girders below are shielded, a thermal gradient is introduced through the depth of the bridge. An increase in temperature causes the material the bridge is made of to expand. Since the sun is heating the top of the bridge, the top of the bridge expands, or elongates more than the bottom. The result is in an upward bending of the bridge. This effect is illustrated in Figure 7-13.

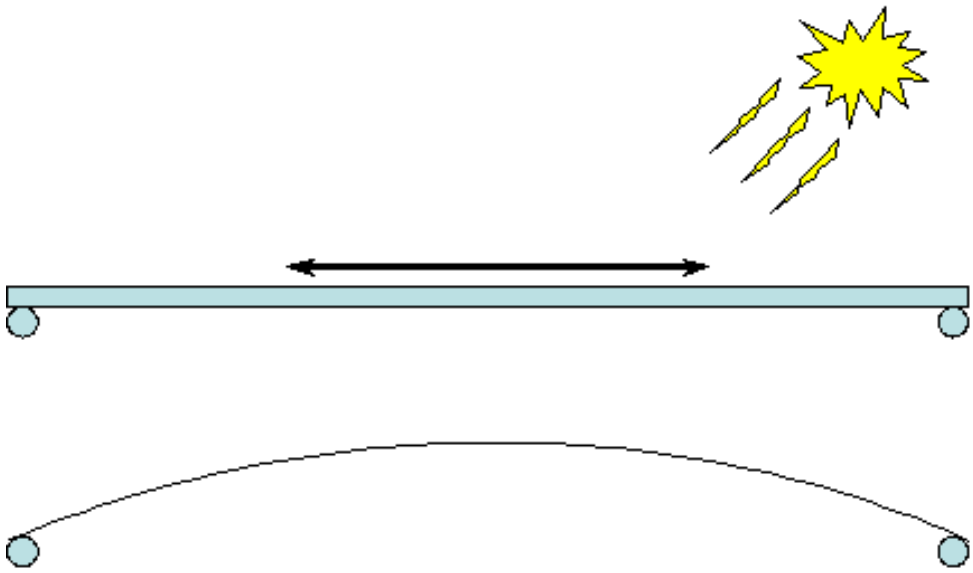

Figure 7-13. Deflection due to thermal gradient

In addition to deflection due to thermal gradient, deflection can also be in response to a change in ambient temperature. Two potential mechanisms have been identified which explain this occurrence.

The first explanation is the different coefficients of thermal expansion for steel and concrete. The values are 6.5 and 5.5 micro strain per degree Fahrenheit for steel and concrete respectively. Therefore, the steel elongates 1.0 micro strain per degree Fahrenheit more than the concrete. Since the steel is on the bottom of the structure, the bottom of the bridge elongates more than the top and the bridge deflects downwards. Notice that this is in the opposite direction as the movement due to temperature gradient. This phenomenon is illustrated in Figure 7-14.

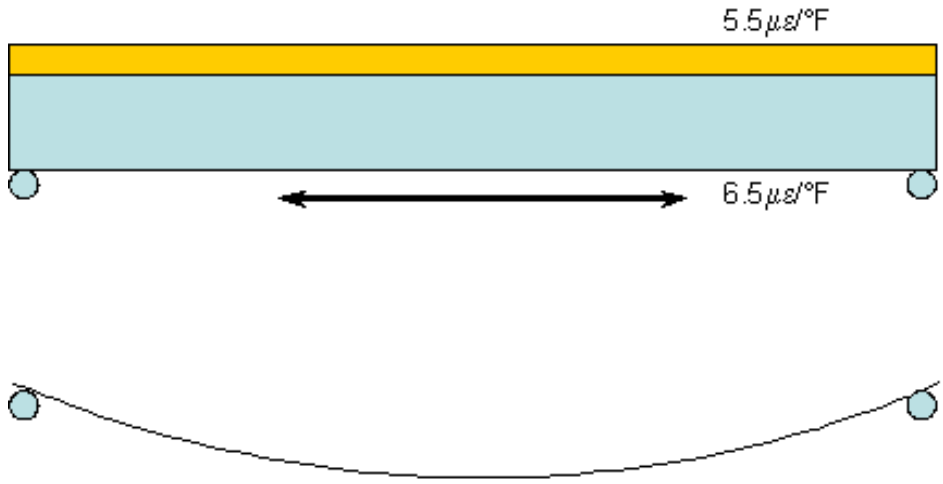

Figure 7-14. Deflection due to Uniform Temperature (Different Expansion Coefficient)

The second mechanism requires the presence of at least partial end restraint at the end of the girders which acts eccentric to the girder as shown in Figure 7-15. As the girder expands the deck is restrained from expansion while the steel girder is not. Therefore, the bottom of the bridge is free to elongate more than the top. Again, the bridge deflection is downwards.

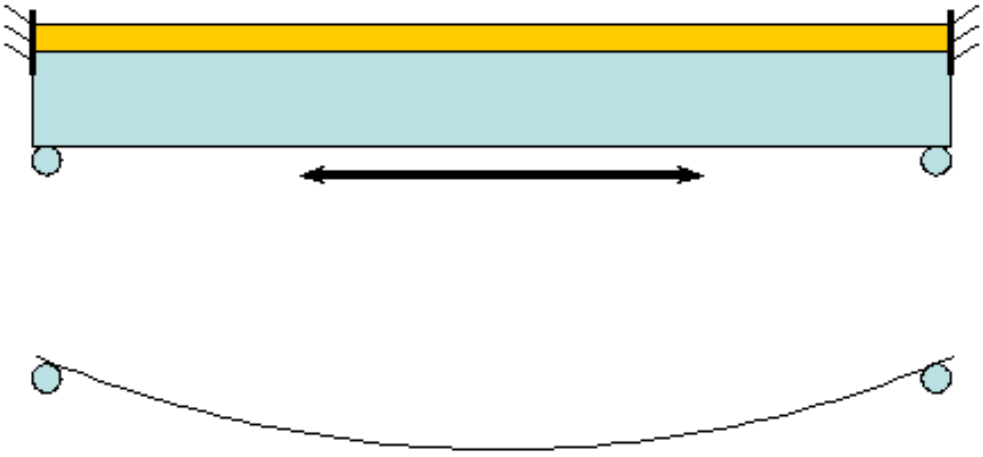

Figure 7-15. Deflection due to Uniform Temperature (End Restraint)

Three general methods were proposed for dealing with the temperature effects. The first was to fully account for all thermal effects utilizing simulation and analysis techniques. It was determined that due to the complex interaction between the various factors including additional meteorological factors not yet mentioned such as humidity, drought and precipitation this alternative was too costly given the ultimate objectives of the project.

The second alternative was to ignore the presence of the moment gradient and deal solely with the average ambient temperature at the time of a reading. As was shown in the preceding section, during the afternoon as the average ambient temperature is increasing thus forcing the bridge downwards, the thermal gradient is increasing thus forcing the bridge upwards.

The third alternative was to separate the effects and consider them separately. Studying the effect of moment gradient can be done by examining the data obtained from individual days. The goal in particular is to find a sunny day during which the ambient temperature remains relatively constant. This minimizes the effects of change in ambient temperature while exposing the response of the bridge to thermal gradient. The procedure for isolation of the bridge response to ambient temperature in absence of moment gradient is less straight forward and will be discussed in the following section.

The goal of filtering is to isolate that period of time and obtain the temperature and bridge response corresponding to a constant uniform temperature for each day. It would also be desirable to reduce to overall volume of data.

The next step is to eliminate the obvious outliers. These are the values which are so far out of range that they are obviously due to systemic error. Since future filtering steps will further eliminate outlier points the limits at this point can be very generous. These limit points have been chosen to be -30 and 50 degrees Celsius. Any reading which falls outside these limits is eliminated from the data set. These are the limits of reasonable temperatures and anything outside of these bounds is due to instrumentation errors.

The next step is to further refine the elimination of outlier data points. This step is based on the following premise. If the temperature is constant, and has been for some time, one would expect all 75 gages to give approximately the same value. Based on this, the average value and standard deviation is calculated for each reading. If the standard deviation is less than three degrees then the reading is acceptable. However, if the standard deviation is over three degrees then the individual gage reading which is furthest from the mean is eliminated and the mean and standard deviation is recalculated. This is repeated until the three degree standard deviation criterion is satisfied. At this point if there are at least ten gages remaining in the data set then the average value from the remaining gages is determined to be the average uniform temperature of the structure for the time of that reading. This is then repeated for each hour such that a single temperature is obtained for each hour.

The next step in the filtering process is to reduce to data down to a single temperature reading per day. The criteria for this operation are that the temperature range during the day must not exceed three degrees and the number of hourly reading remaining during that day be greater than or equal to five. The first criterion assures that the temperature is not changing too rapidly during the period of time. This is because the steel changes temperature quickly and closely follows the ambient temperature while the concrete slab has more thermal inertia requiring more time to respond to rapidly changing temperatures. The second criterion requires that there are a sufficient number of readings available to provide a statistically relevant result. If the specified criteria are met then a centrally weighted average is performed with the resulting temperature being the temperature for that day.

The final step in the temperature filtering process is to obtain daily values for the bridge response variables such as deflection, and strain. Minimal filtering is performed on the response variables. For each gage generous extreme outlier limits have been specified and the excessive values eliminated from the data set. Once the extreme values have been removed a centrally weighted average is performed on the admissible hourly reading values for each day. The resulting value is the response variable value for that day.

The result of temperature filtering has thus reduced the full data set into a single temperature and the corresponding response data for each day. The values are from a period each day when the thermal gradient through the depth is at a minimum. Days during which the temperature is changing rapidly have been discarded and central averaging has been utilized to further reduce the effect of variability in the response variables.

7.7 Observations

As explained earlier in this chapter, in order to access the long-term bridge behavior from the strain gages, the general trend of the strain data is of interest. In fact, since the strain data has large fluctuations over time (depending to the temperature, season, etc.), it is rational to access them and the bridge behavior over a long period of time based on the whole trend of the data. Therefore, in the case that the measured strains do not significantly change over the data logging period, it can be concluded that the bridge responses to loading remains stationary.

The long-term monitoring filtered plots from the installed gages can be found in Appendix A. Here, some of the most significant observations from these plots are presented.

Having a look at the long-term monitoring plots, the majority of the significant changes in the strain data happen in the gages installed in the concrete. Most of the significant changes on the other hand, have taken place in the first two years. These changes can be interpreted as being due to concrete shrinkage and/or creep. Figure 7-16 through Figure 7-20 are some examples showing the changes in the long-term response due to the concrete shrinkage/creep.

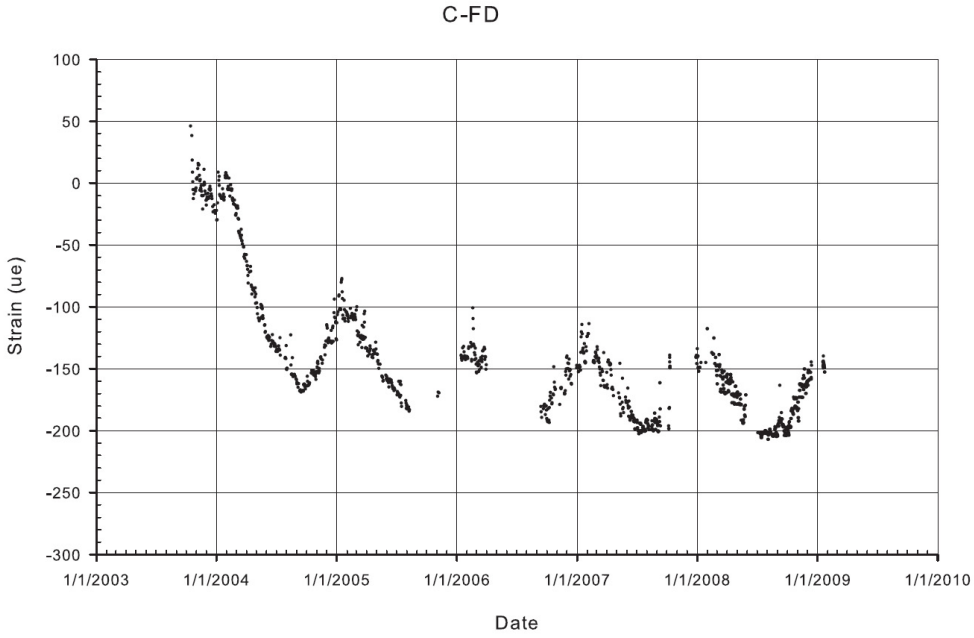

Figure 7-16. Strain from concrete embedment gages located in the bottom flange concrete diaphragm over the pier, Girder C, Section F

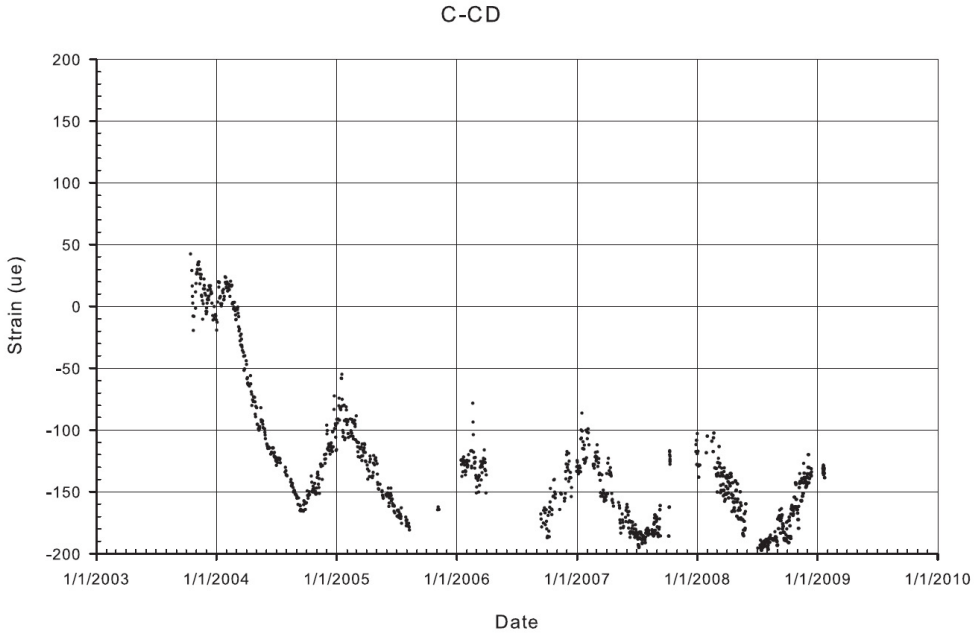

Figure 7-17. Strain from concrete embedment gages located in the bottom flange concrete diaphragm over the pier, Girder C, Section C

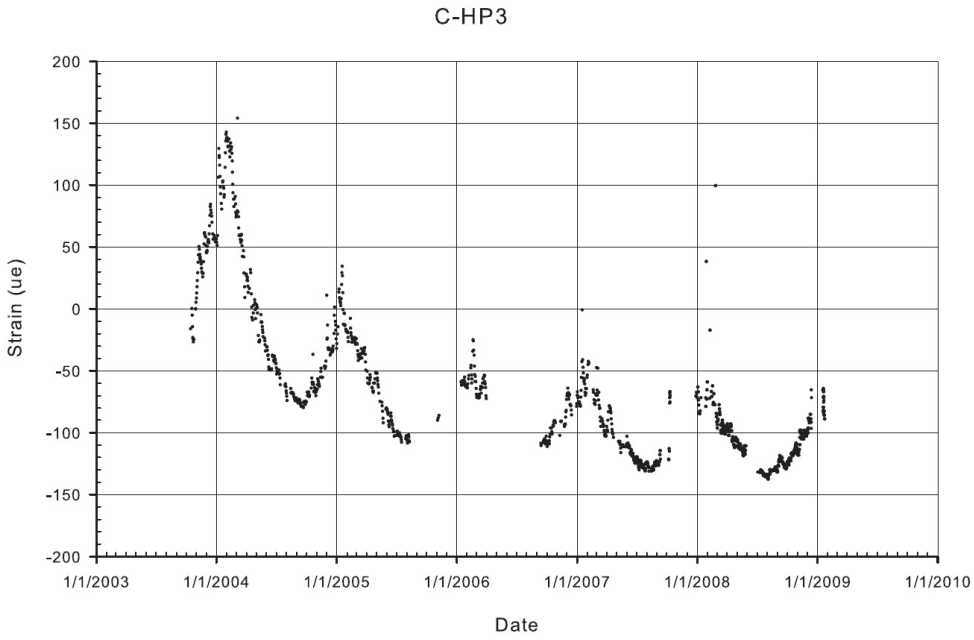

Figure 7-18. Strain from concrete embedment gages located in concrete diaphragm over the pier, Girder C, Section H

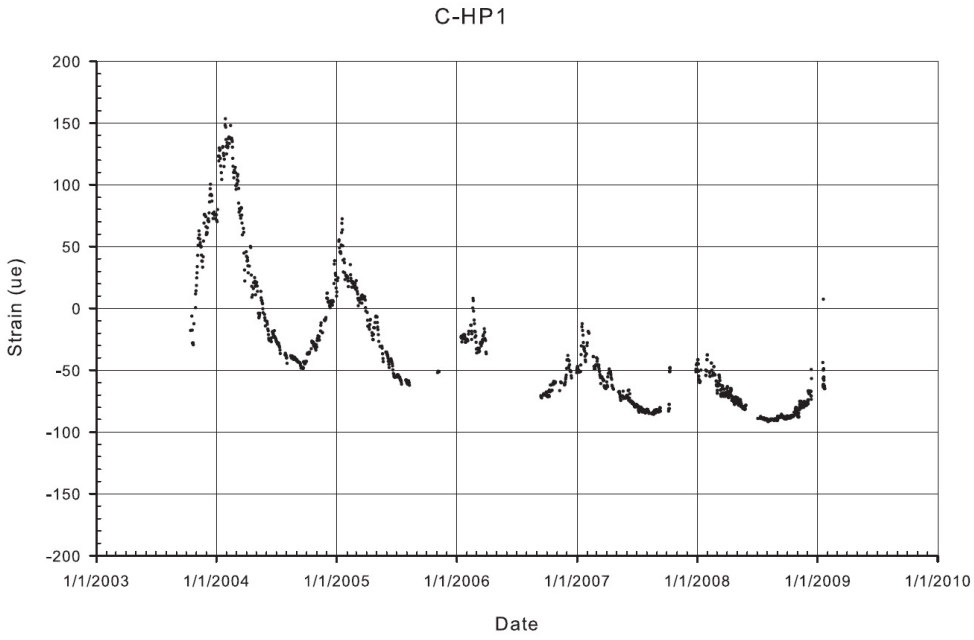

Figure 7-19. Strain from concrete embedment gages located in concrete diaphragm over the pier, Girder C, Section H

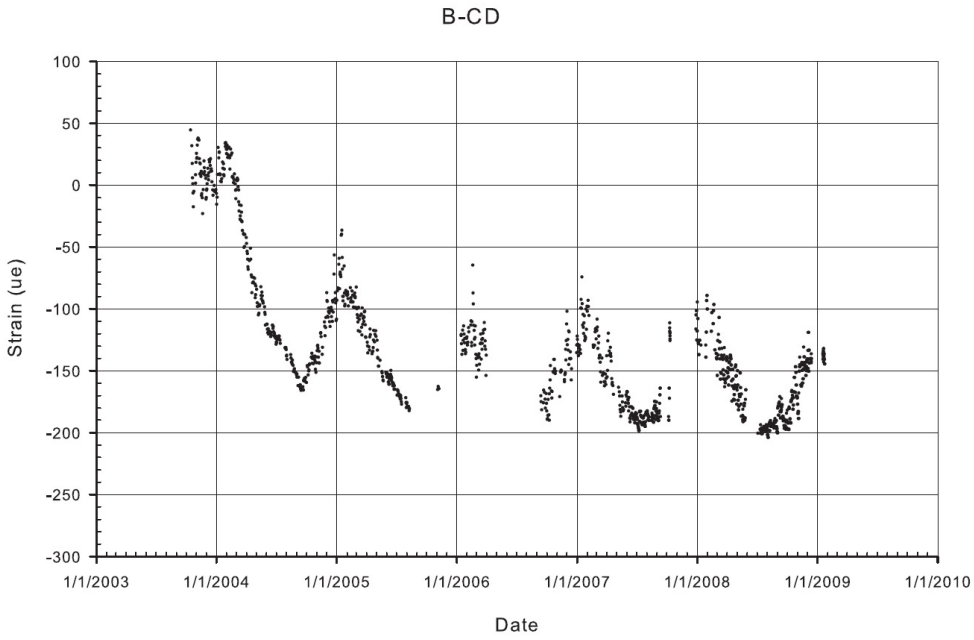

Figure 7-20. Strain from concrete embedment gages located in the bottom flange concrete diaphragm over the pier, Girder B Section C

A major trend seen in almost all of the long-term strain plots is the seasonal fluctuations. The strains in almost all strain gages show an increase in the strain in the winter seasons. In other words, for the strain gages with positive strains (top flanges), the measured strains in the winters are larger comparing to the ones in the summers and, for the strain gages with negative strains (bottom flanges), the measured strains in the winters are closer to zero comparing to the ones in the summers. This observation can be related to two major reasons.

The first reason is the partial restraint effects of the abutments. Since the bridge is an integral abutment bridge, they restraint the movements of the bottom flanges of the girders. Temperature changes on the other hand tend to elongate or shorten the bridge length which results in a moment in the bridge due to the eccentricity of the restraint forces and the neutral axis of the bridge. (Figure 7-21)

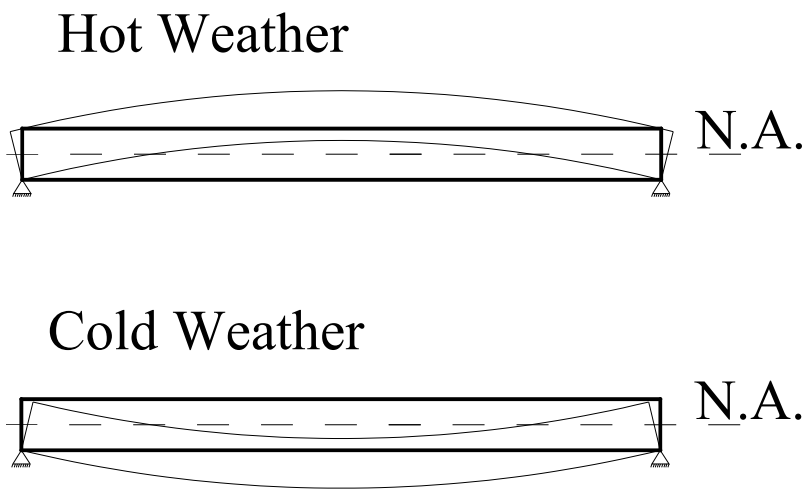

Figure 7-21. Bending modes of the girder with supports at both ends due to temperature effects

The second possible reason is the different coefficients of thermal expansion for steel and concrete. The values are 6.5 and 5.5 micro strain per degree Fahrenheit for steel and concrete respectively. Therefore, the steel elongates 1.0 micro strain per degree Fahrenheit more than the concrete. Since the steel is on the bottom of the structure, the bottom of the bridge elongates more than the top and the bridge deflects downwards. Notice that this is in the opposite direction as the movement due to temperature gradient. This phenomenon is illustrated in Figure 7-14.

Some sections do not experience any strain. Examples of those sections are the top flanges of the girders at section F (which indicates the end of the girders). This is because in the system used the top rebars provide the needed connectivity of the connection and the top flanges are not connected in that section. As can be seen in Figure 7-22 and Figure 7-23, the strain gages show more or less no strain in the whole monitoring time of the bridge.

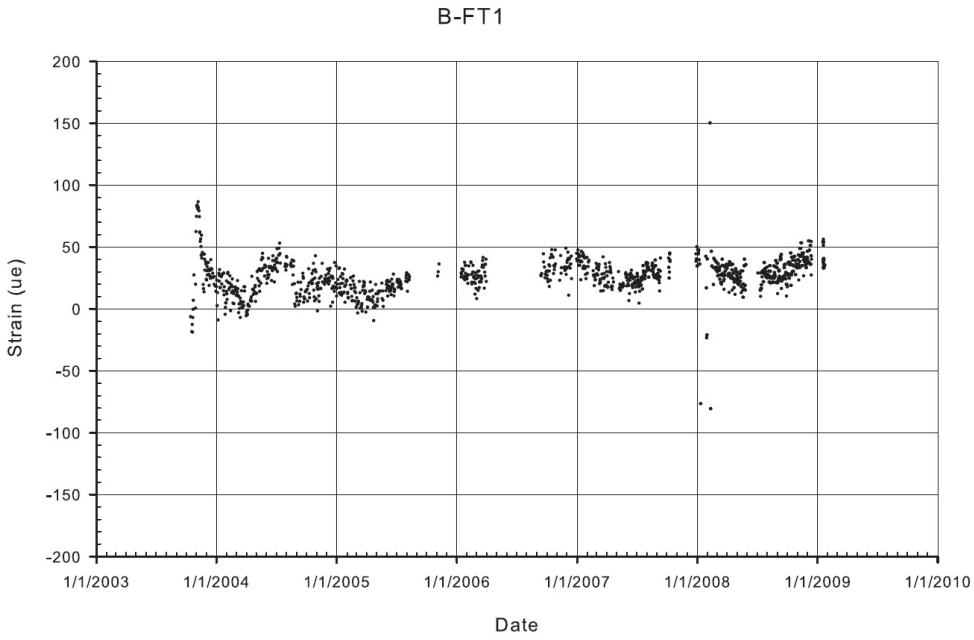

Figure 7-22. Strain at section F girder B on top flange

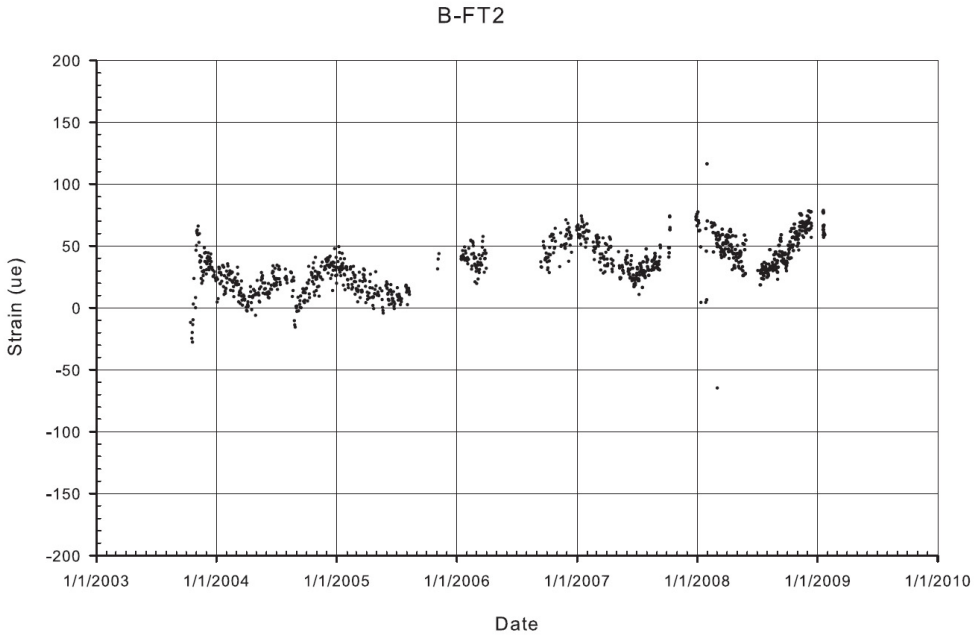

Figure 7-23. Strain at section F girder B on top flange

One of the other strain data are those from the sister bars which are basically measuring the strains of the concrete. Again, due to the shrinkage and creep in the concrete, these gages show increase in the magnitude of strain in the first year. An example of this effect is shown in Figure 7-24.

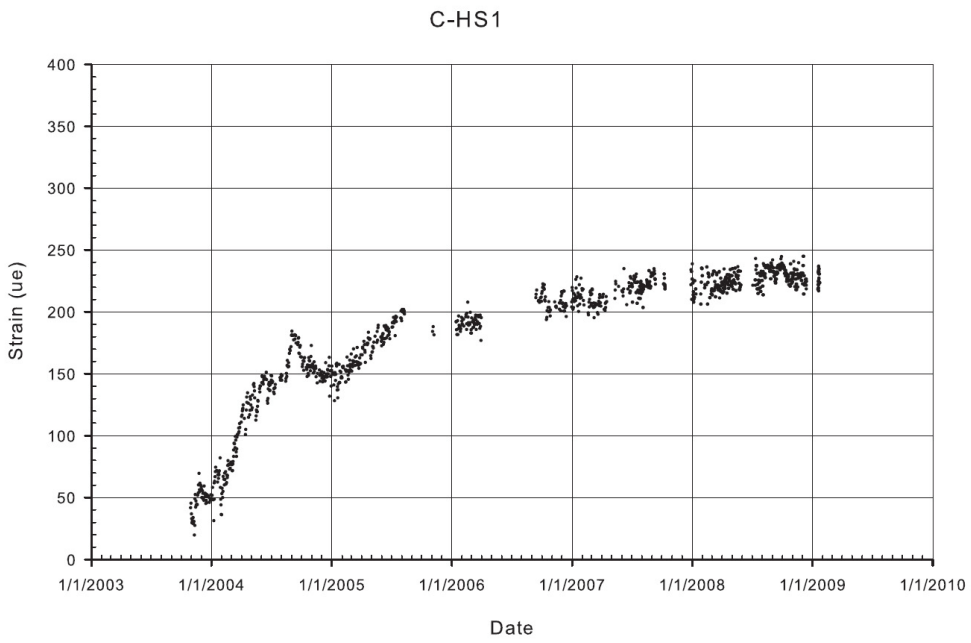

Figure 7-24. Strain measured from sister bar at section H girder C

Chapter 8
Summary and Conclusions

Construction and long term monitoring of the N-2 over I-80 Bridge in Nebraska provided an opportunity to monitor a bridge constructed using Simple-Dead-Continuous-Live technique both during construction and beyond. To determine the behavior of the structure, various types of instrumentation were used on the structure to monitor strains, deflections, and various climatic effects.

Bridge responses were monitored during construction using the data collected from instrumentation. In order to ensure the satisfactory behavior of the bridge under the real life loading, determine the load rating of the bridge, and also check the validity of the design assumptions, a live load testing was carried out using three trucks. The bridge was then monitored between October 2003 and December 2008 under daily traffic loads.

During construction, the majority of monitored deflections were predictable and attributable to discreet events.

The bridge components remain well in the elastic range of behavior during the live load testing and the resulted deflections from finite element modeling closely follow the ones resulted from live load testing of the bridge. The finite element deflections at sections close to mid-span are slightly larger than the deflections from the live load testing which insures that the design procedure will be in the conservative margins. Calculated neutral axis depths are less that the measured one from the testing for all cases and the differences between the calculated values and the measured values are larger in the negative region values. Neutral Axis is higher at exterior girders due to the contribution of railing.

Long term monitoring of the bridge showed that the full actual deformation due to temperature variation is safely within the design limits. Having a look at the long-term monitoring plots, the majority of the significant changes in the strain data happen in the gages installed in the concrete. Most of the significant changes on the other hand, have taken place in the first two years. These changes can be interpreted as being due to concrete shrinkage and/or creep. The strains created in the girder due to temperature and thermal gradient are very small in comparison with strains due to dead load during construction.

Identification of the underlying mechanism driving the seasonal deformation is a topic for future research.

Chapter 9
References

American Association of State Highway Transportation Officials (AASHTO). (2007). *Load and resistance factor design bridge design specifications*, 4th Ed., Washington, D.C.

Lampe, N. and Azizinamini, A. (2000). "Steel Bridge System, Simple for Dead Load and Continuous for Live Load." *Steel Bridge Design and Construction for the New Millennium with emphasis on High Performance Steel*, Baltimore, MD, November 30-December 1.

Stallings, J.M. and Yoo, C.H. (1993). "Tests and Ratings of Short-Span Steel Bridges." *Journal of Structural Engineering, ASCE*, 119(7), pp. 2150-2168.

Swendroski, J.P. (2001). "Field Monitoring of a Staged Construction Bridge Project." *M.S. thesis, University of Nebraska, Lincoln*, NE, 626 pp.

Yakel, A.J., Marchon, P., and Azizinamini, A. (2005). "Long Term Monitoring of a Steel Bridge Constructed Using Phase Construction." *NDOR Research Project Number SPR-PL-1 (038) P530*, by National Bridge Research Organization (NaBRO), University of Nebraska-Lincoln, Lincoln, NE.

Appendix A

Long-Term Monitoring Graphs

C-CW

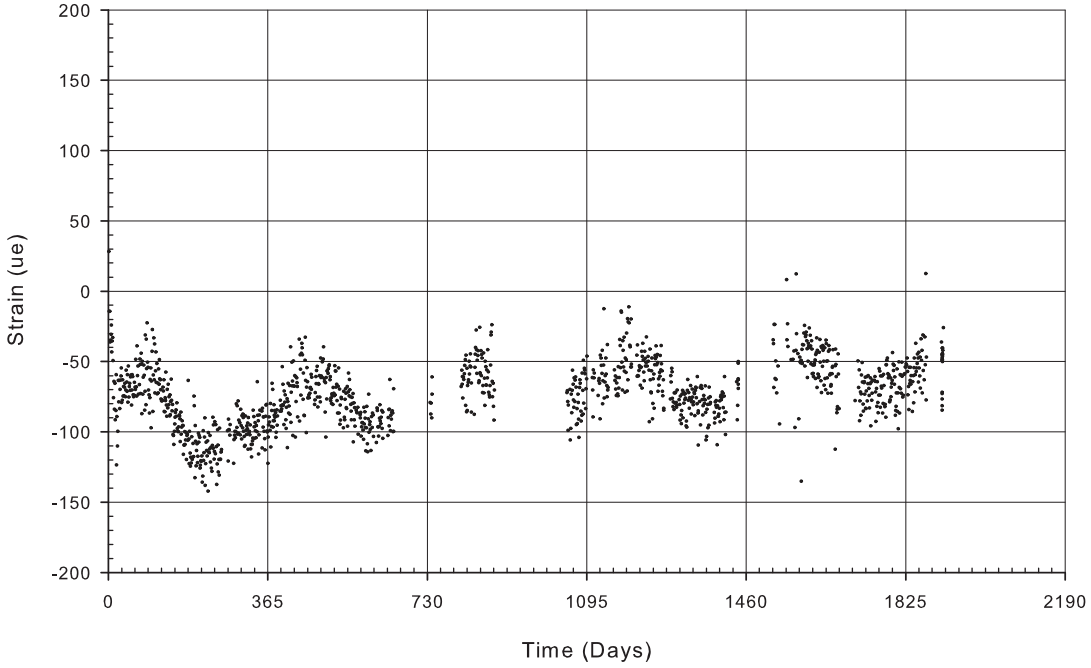
200
150
100
50
0
-50
-100
-150
-200
Strain (ue)
0
365
730
1095
1460
1825
2190
Time (Days)

C-CT

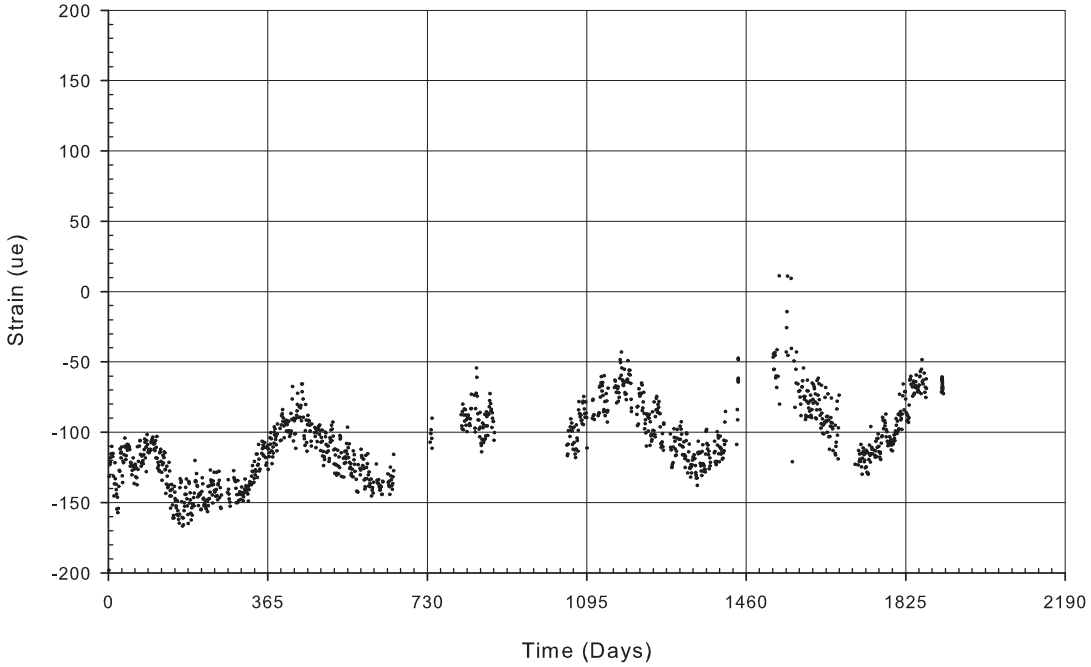
200
150
100
50
0
-50
-100
-150
-200
Strain (ue)
0
365
730
1095
1460
1825
2190
Time (Days)

C-FD

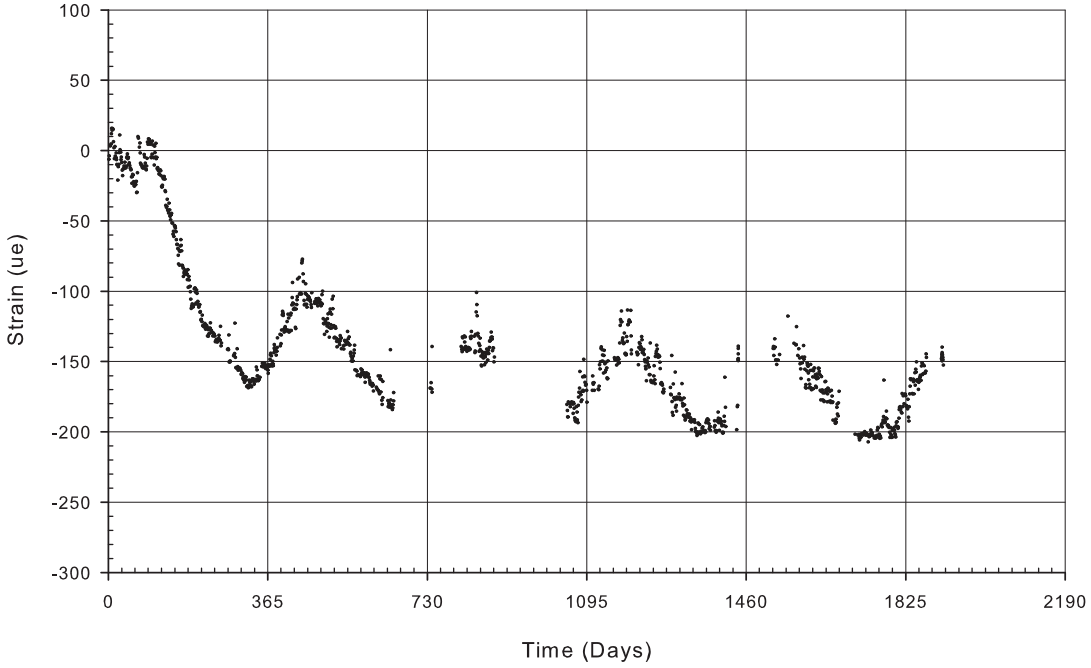
100
50
0
-50
-100
-150
-200
-250
-300
Strain (ue)
0
365
730
1095
1460
1825
2190
Time (Days)

C-FW

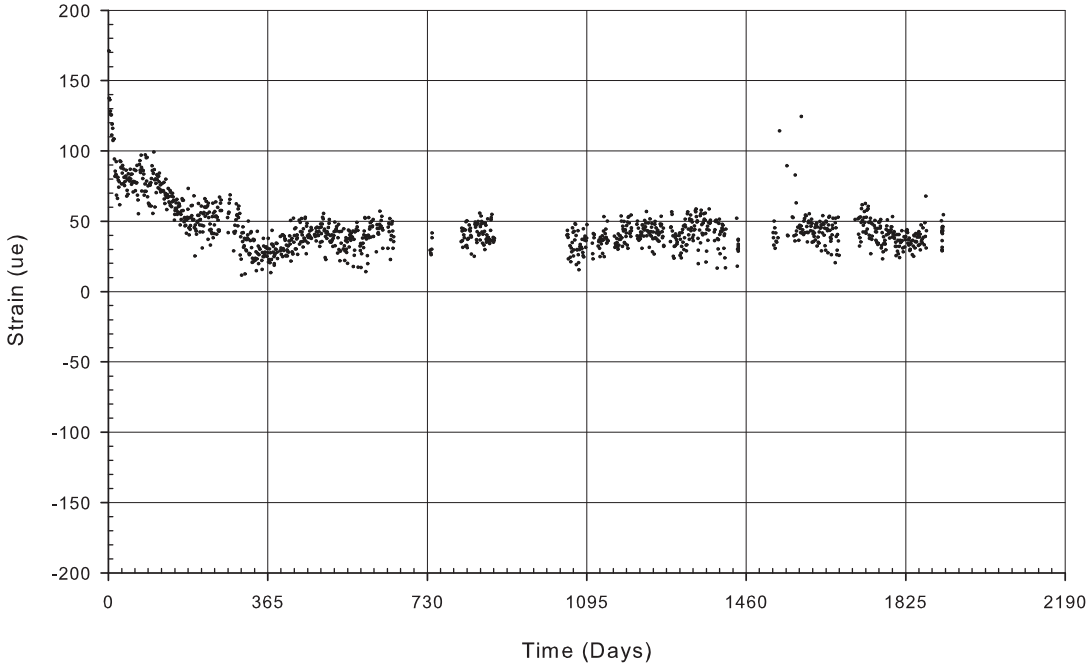
200
150
100
50
0
-50
-100
-150
-200
Strain (ue)
0
365
730
1095
1460
1825
2190
Time (Days)

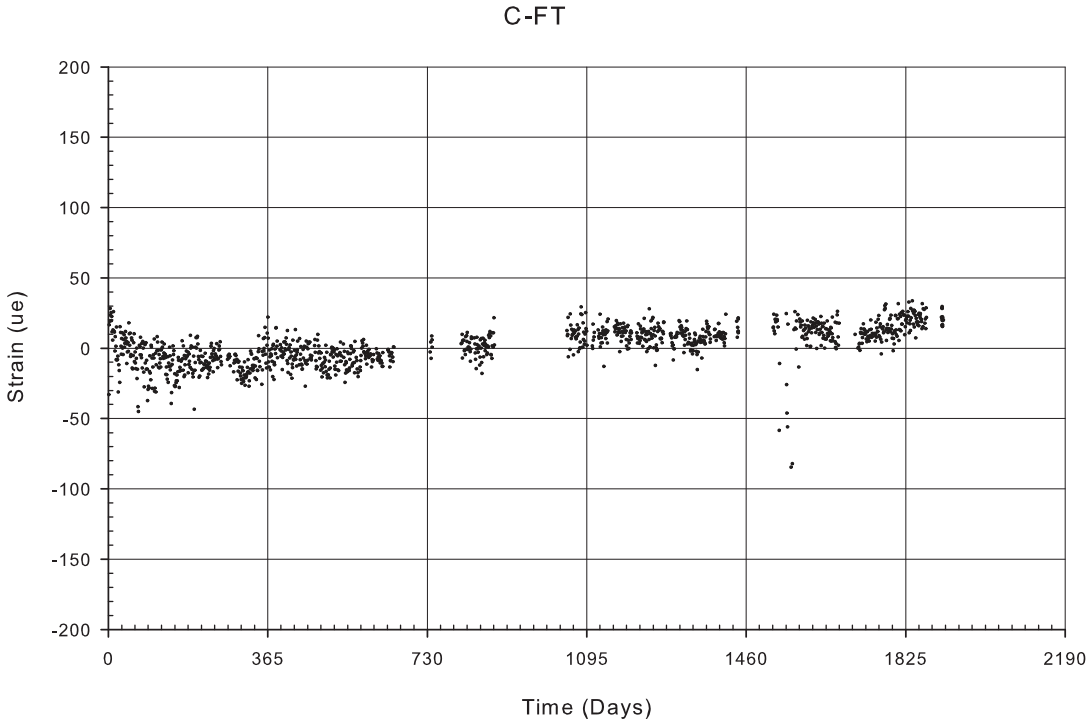
C-FT
200
150
100
50
0
-50
-100
-150
-200
Strain (ue)
0
365
730
1095
1460
1825
2190
Time (Days)

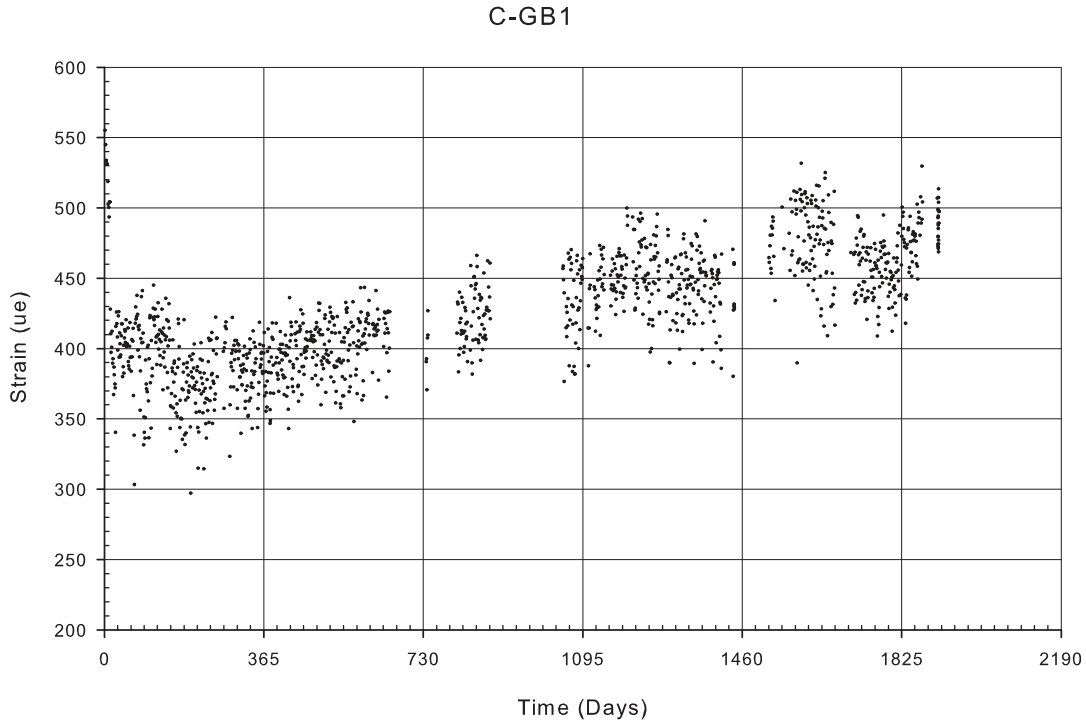
C-GB1
600
550
500
450
400
350
300
250
200
Strain (ue)
0
365
730
1095
1460
1825
2190
Time (Days)

C-GB2

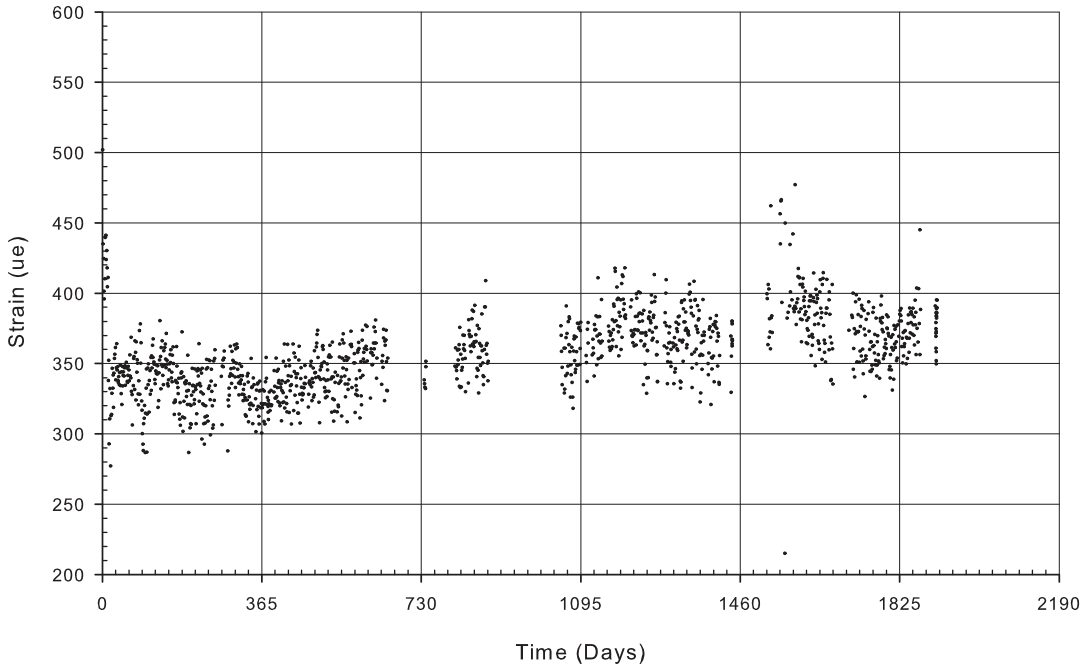
600
550
500
450
400
350
300
250
200
Strain (ue)
0
365
730
1095
1460
1825
2190
Time (Days)

C-GP1

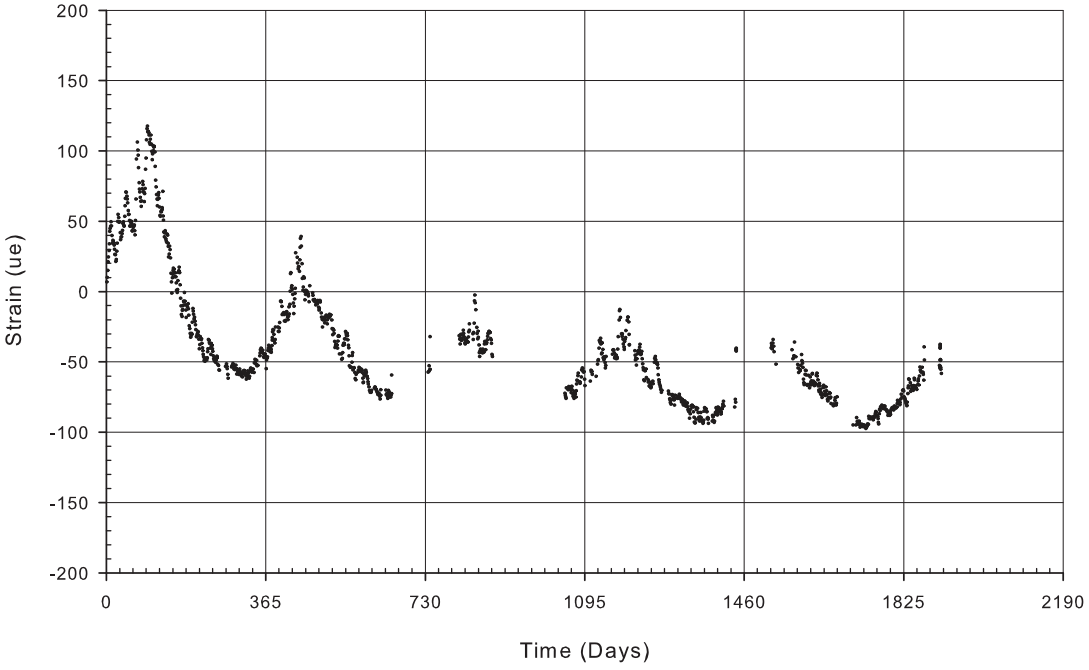
200
150
100
50
0
-50
-100
-150
-200
Strain (ue)
0
365
730
1095
1460
1825
2190
Time (Days)

C-GP2

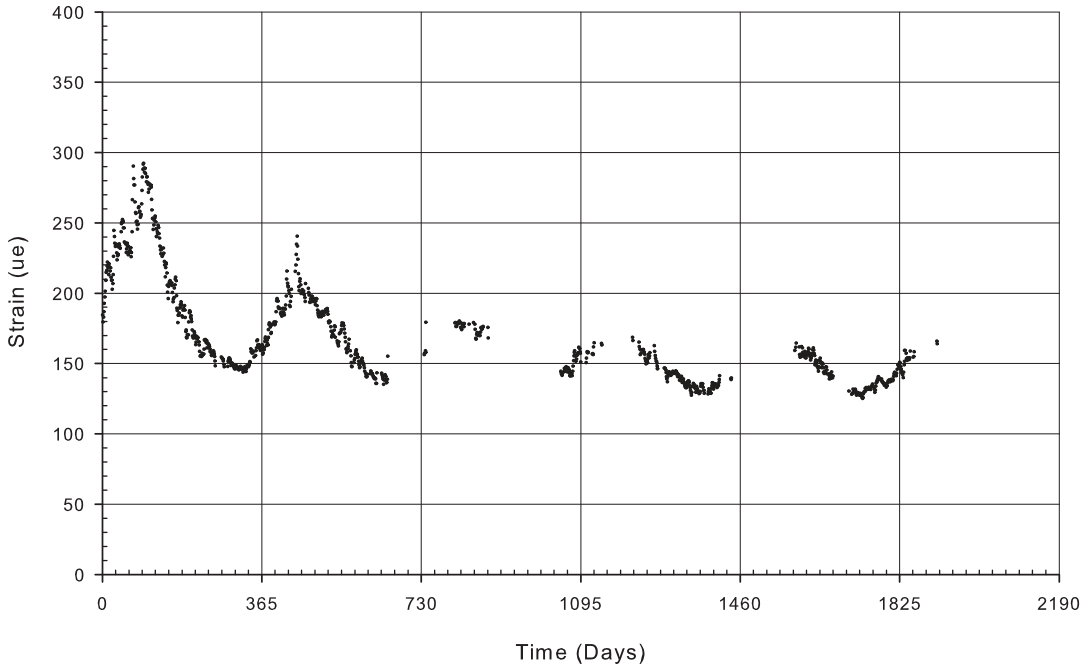
400
350
300
250
200
150
100
50
0
Strain (ue)
0
365
730
1095
1460
1825
2190
Time (Days)

C-AB

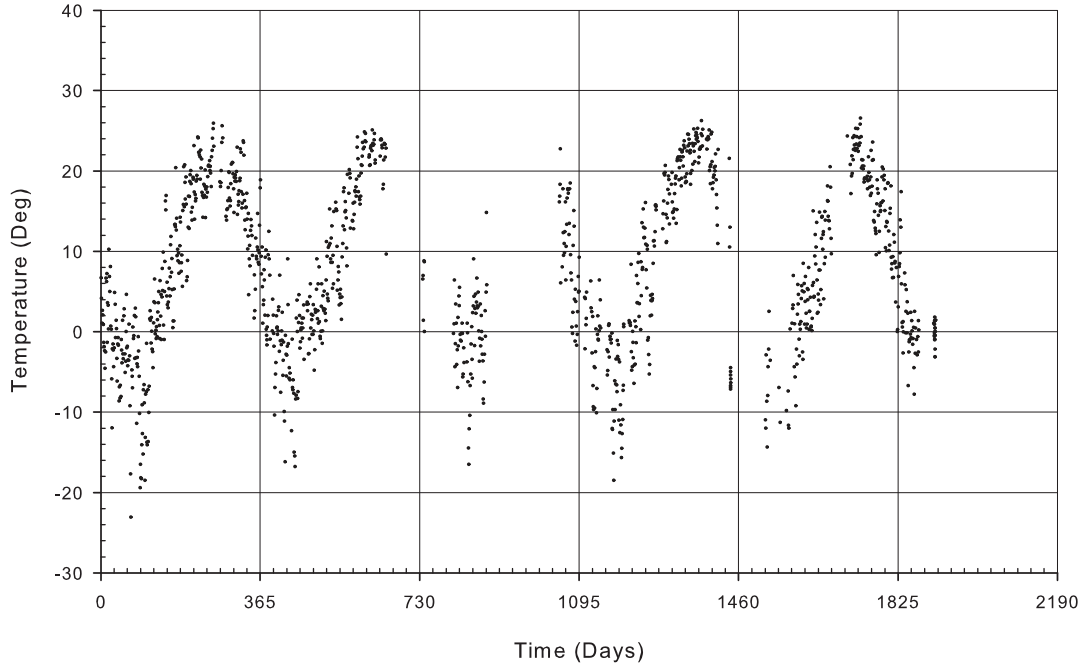
40
30
20
10
0
-10
-20
-30
Temperature (Deg)
0
365
730
1095
1460
1825
2190
Time (Days)

C-AW

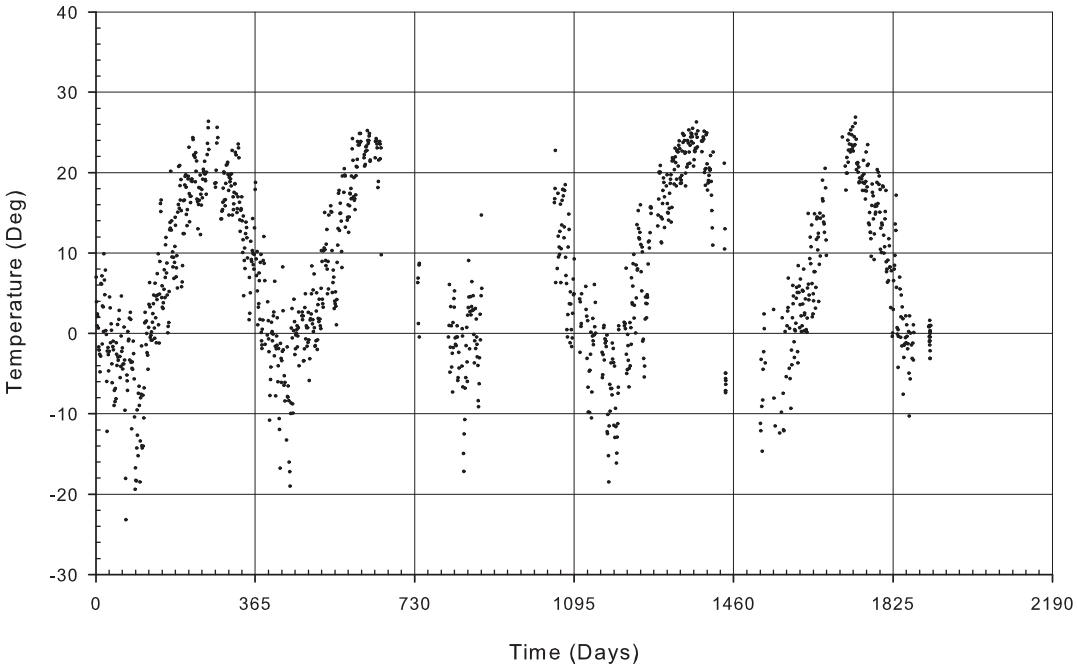
40
30
20
10
0
-10
-20
-30
Temperature (Deg)
0
365
730
1095
1460
1825
2190
Time (Days)

C-AT

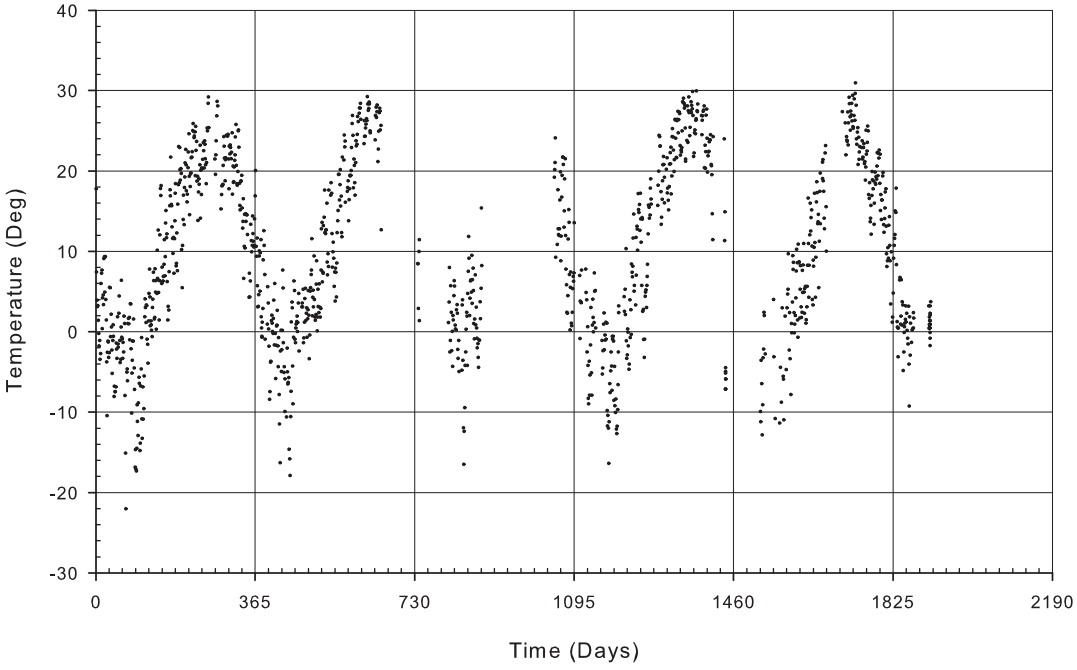
40
30
20
10
0
-10
-20
-30
Temperature (Deg)
0
365
730
1095
1460
1825
2190
Time (Days)

C-BB

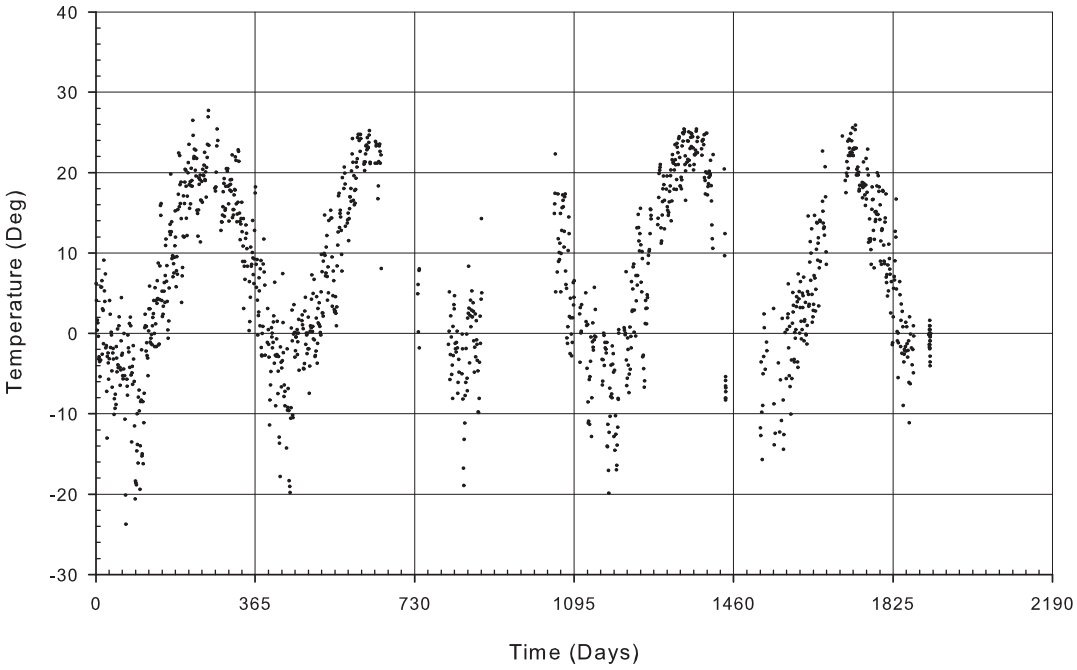
40
30
20
10
0
-10
-20
-30
Temperature (Deg)
0
365
730
1095
1460
1825
2190
Time (Days)

C-BW

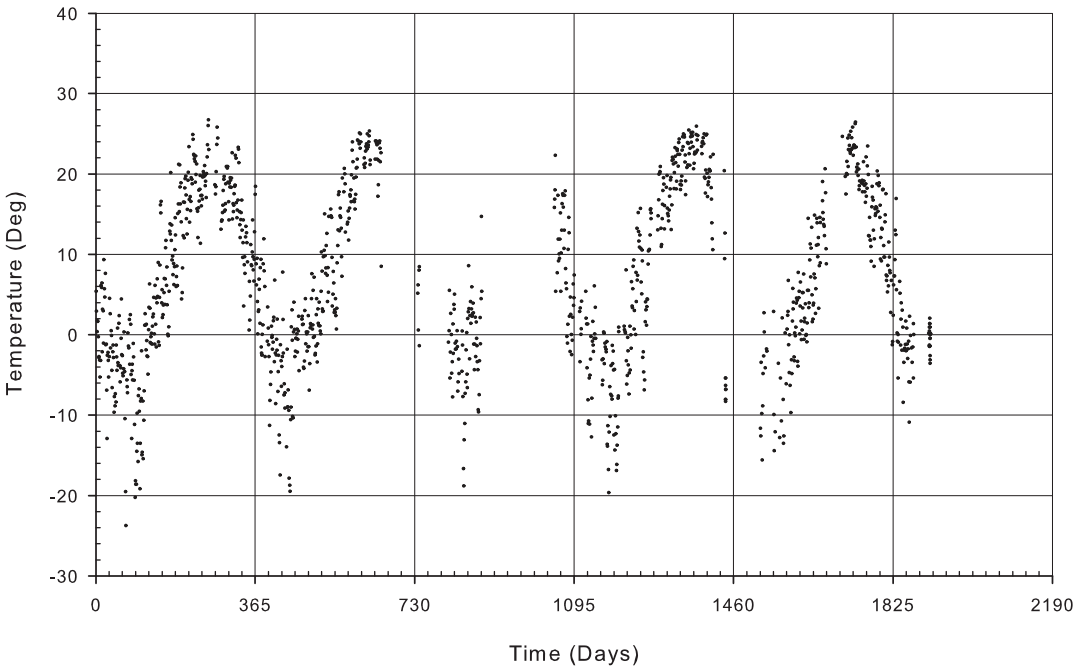
40
30
20
10
0
-10
-20
-30
Temperature (Deg)
0
365
730
1095
1460
1825
2190
Time (Days)

C-BT

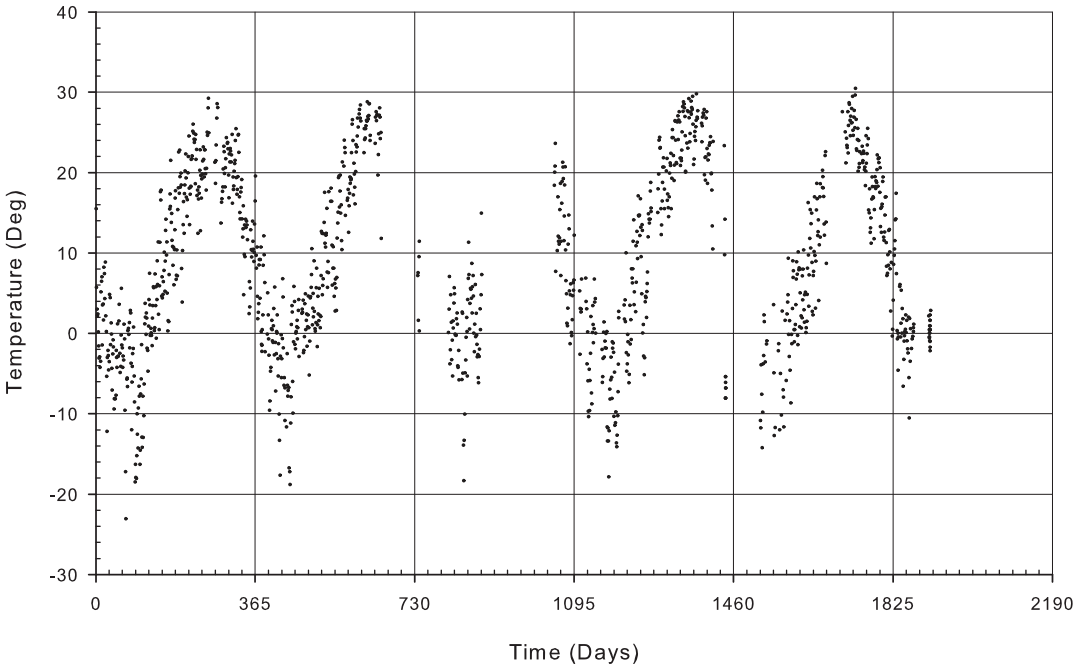
40
30
20
10
0
-10
-20
-30
Temperature (Deg)
0
365
730
1095
1460
1825
2190
Time (Days)

C-CD

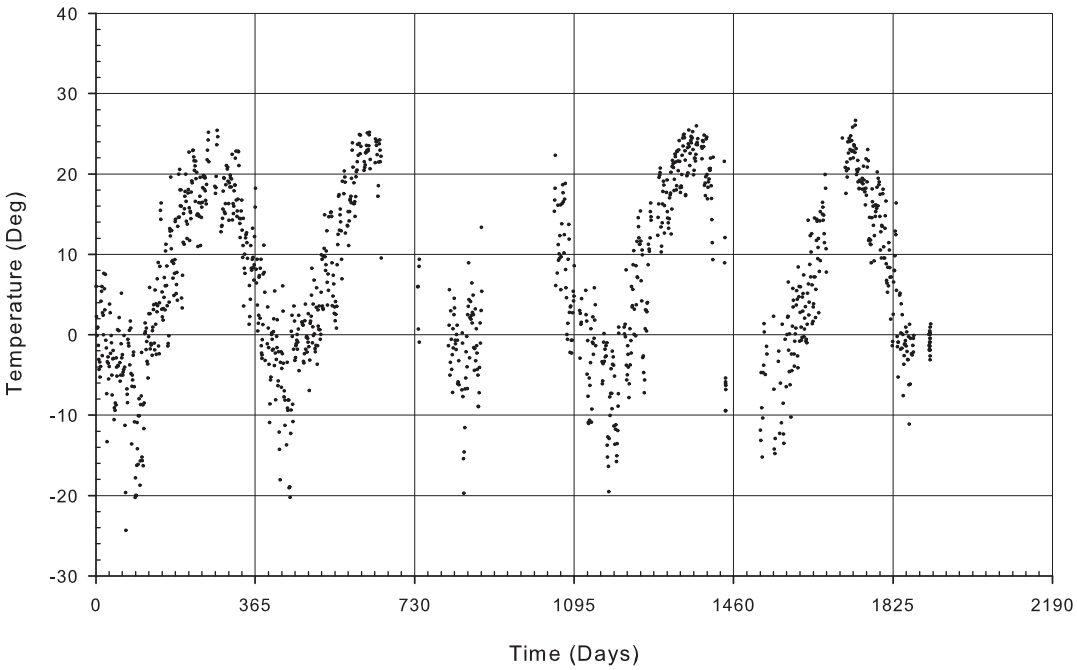
40
30
20
10
0
-10
-20
-30
Temperature (Deg)
0
365
730
1095
1460
1825
2190
Time (Days)

C-CW

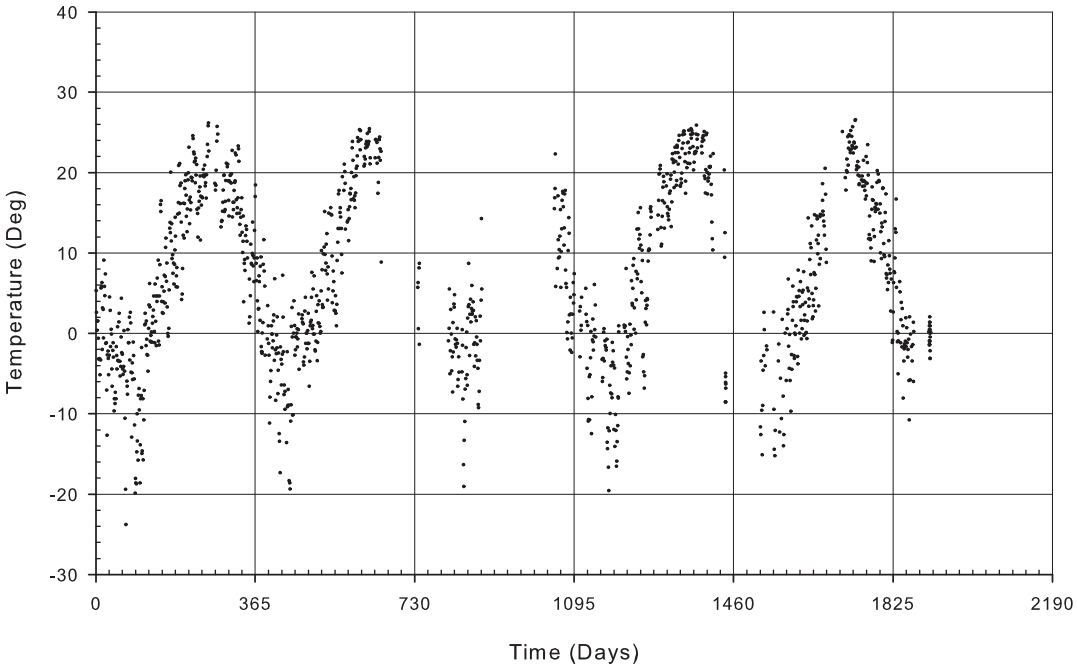
40
30
20
10
0
-10
-20
-30
Temperature (Deg)
0
365
730
1095
1460
1825
2190
Time (Days)

C-CT

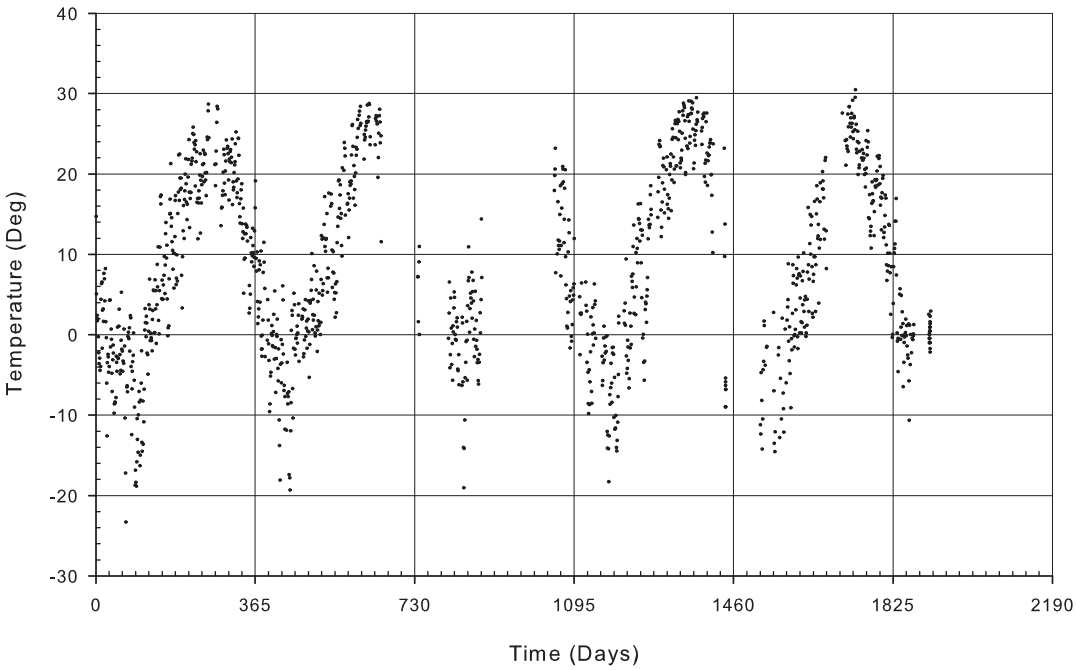
40
30
20
10
0
-10
-20
-30
Temperature (Deg)
0
365
730
1095
1460
1825
2190
Time (Days)

C-FD

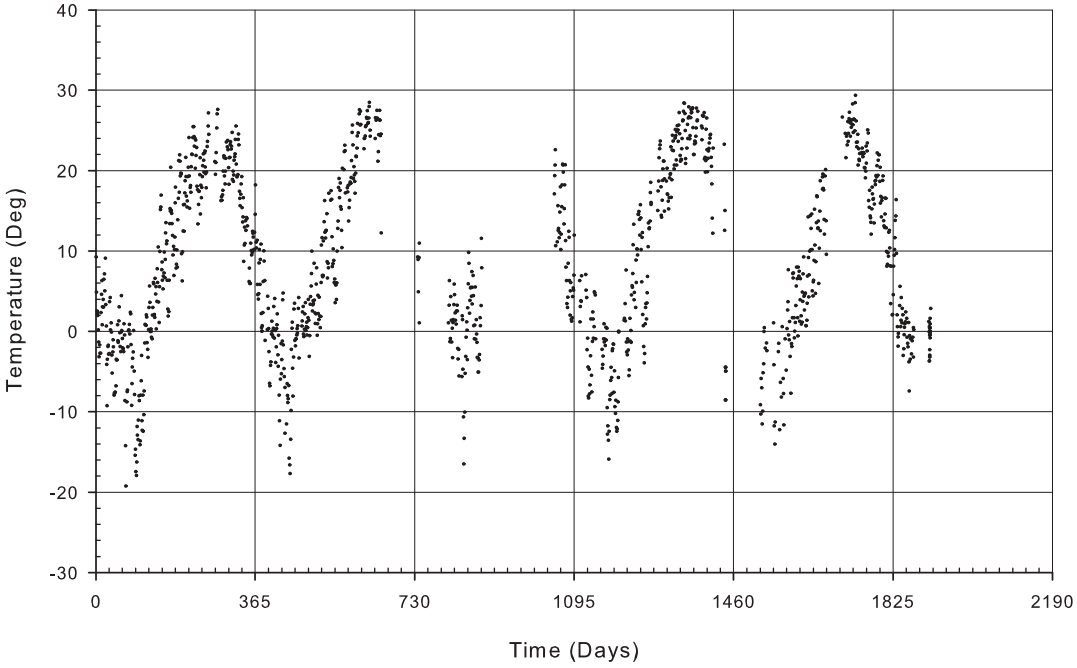
40
30
20
10
0
-10
-20
-30
Temperature (Deg)
0
365
730
1095
1460
1825
2190
Time (Days)

C-FW

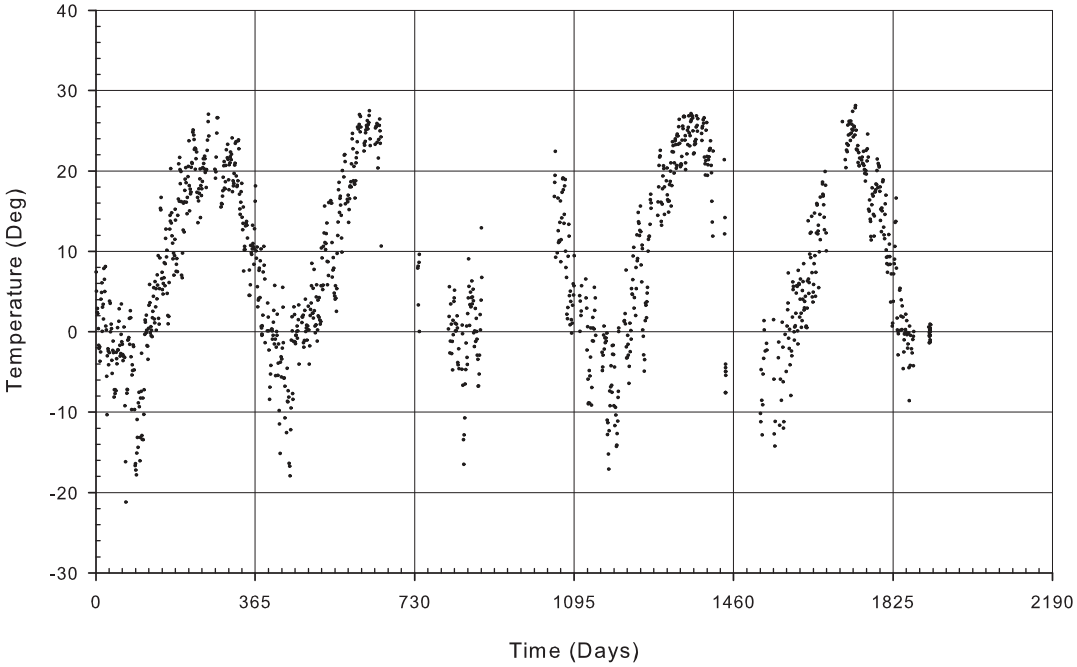
40
30
20
10
0
-10
-20
-30
Temperature (Deg)
0
365
730
1095
1460
1825
2190
Time (Days)

C-FT

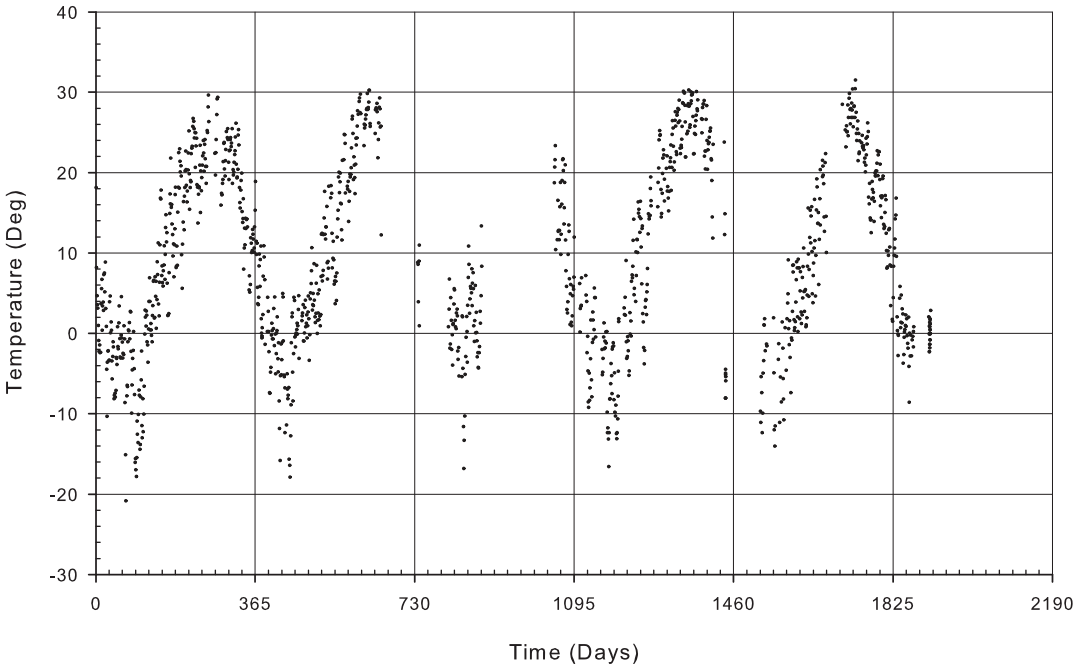
40
30
20
10
0
-10
-20
-30
Temperature (Deg)
0
365
730
1095
1460
1825
2190
Time (Days)

C-GB1

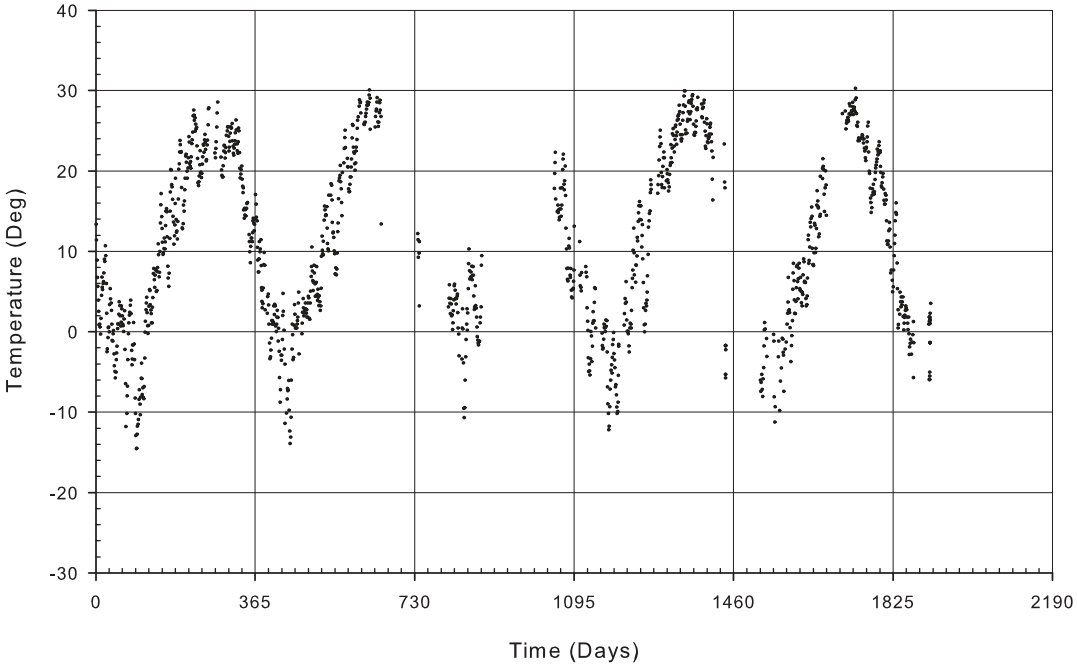
40
30
20
10
0
-10
-20
-30
Temperature (Deg)
0
365
730
1095
1460
1825
2190
Time (Days)

C-GB2

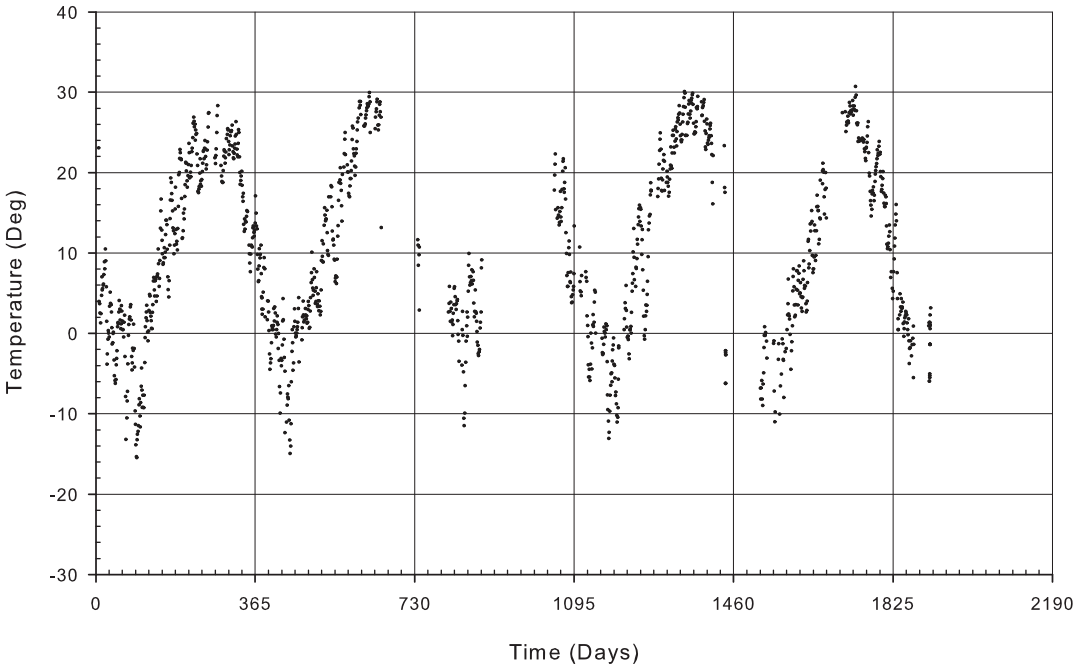
40
30
20
10
0
-10
-20
-30
Temperature (Deg)
0
365
730
1095
1460
1825
2190
Time (Days)

C-GP1

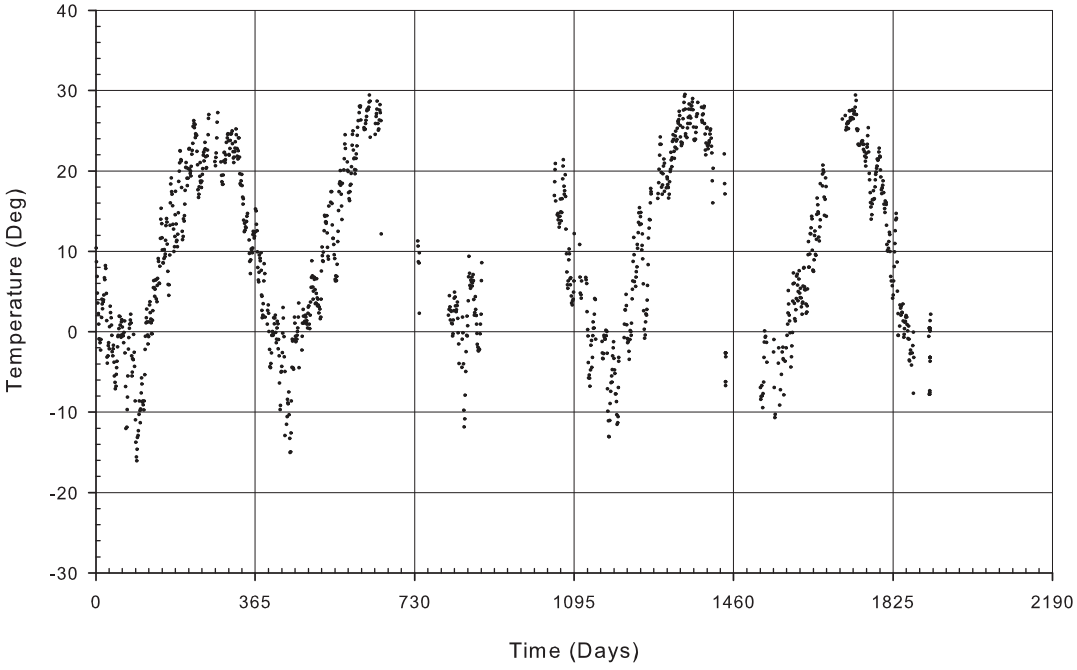
40
30
20
10
0
-10
-20
-30
Temperature (Deg)
0
365
730
1095
1460
1825
2190
Time (Days)

C-GP2

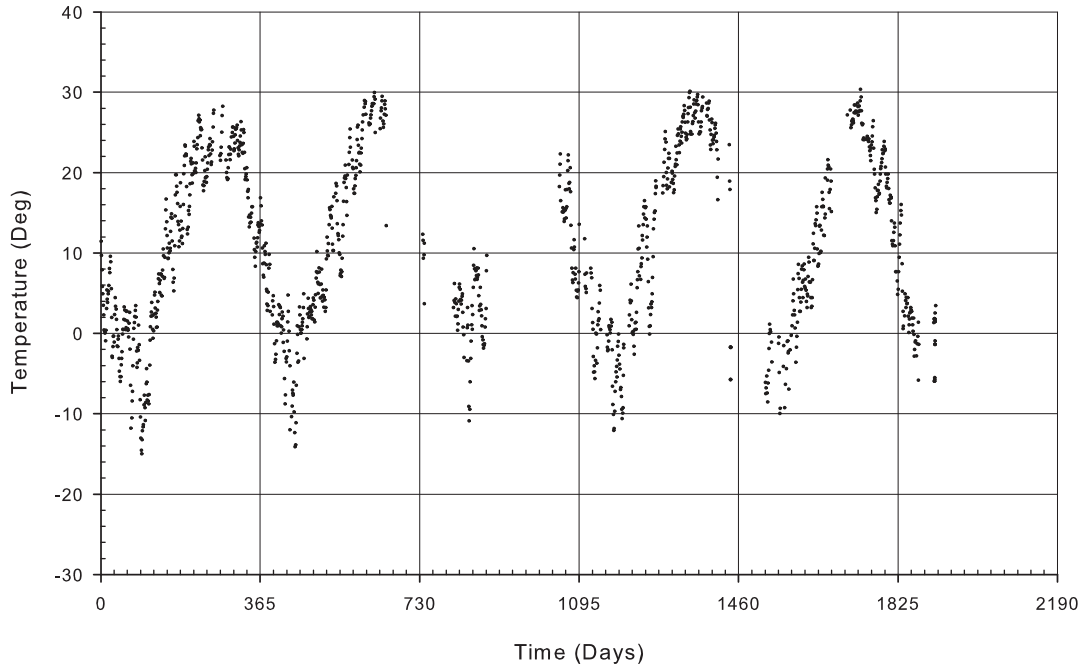
40
30
20
10
0
-10
-20
-30
Temperature (Deg)
0
365
730
1095
1460
1825
2190
Time (Days)

C-CB

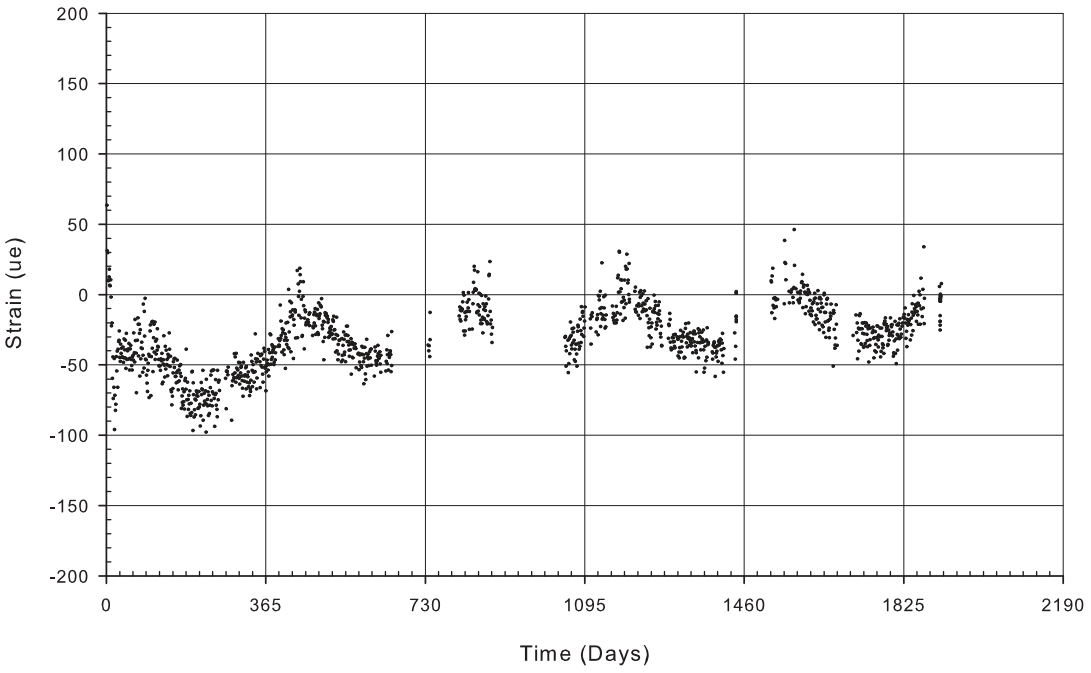
200
150
100
50
0
-50
-100
-150
-200
Strain (ue)
0
365
730
1095
1460
1825
2190
Time (Days)

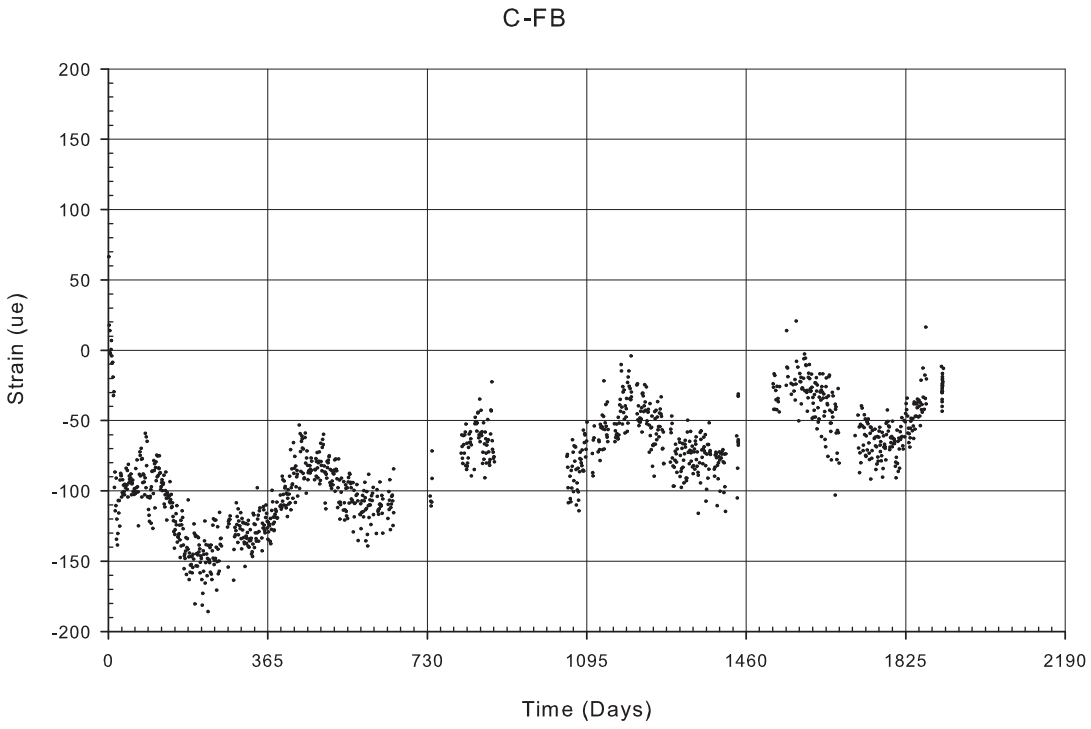
C-FB
Strain (ue)
200
150
100
50
0
-50
-100
-150
-200
0
365
730
1095
1460
1825
2190
Time (Days)

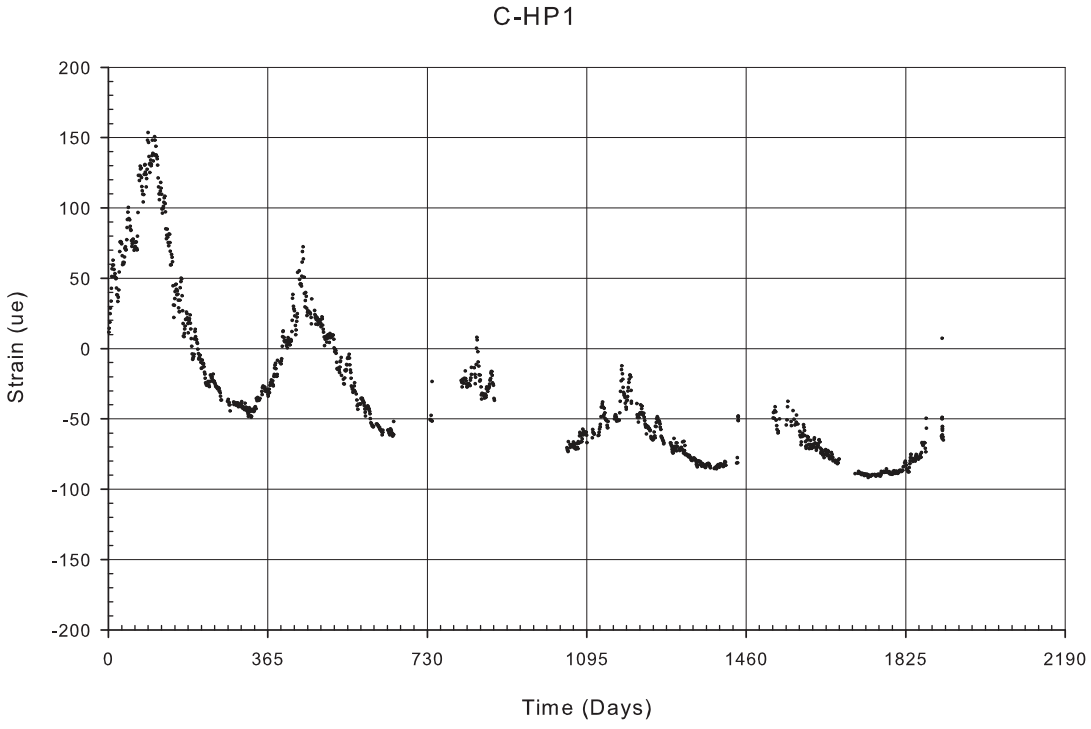
C-HP1
Strain (ue)
200
150
100
50
0
-50
-100
-150
-200
0
365
730
1095
1460
1825
2190
Time (Days)

C-HP2

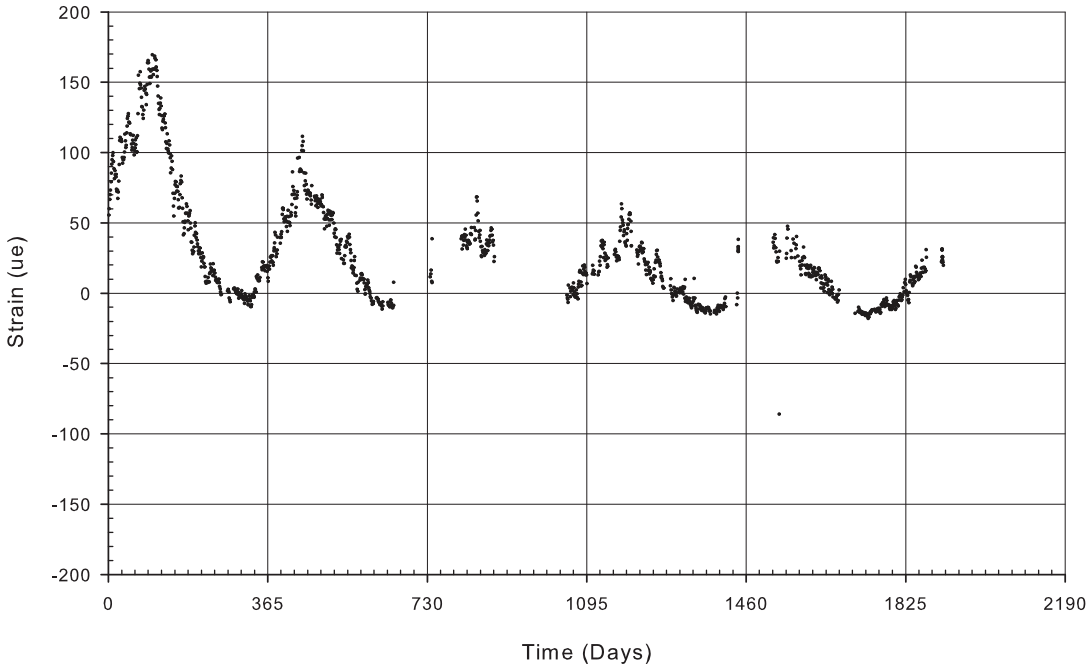
200
150
100
50
0
-50
-100
-150
-200
Strain (ue)
0
365
730
1095
1460
1825
2190
Time (Days)

C-HP3

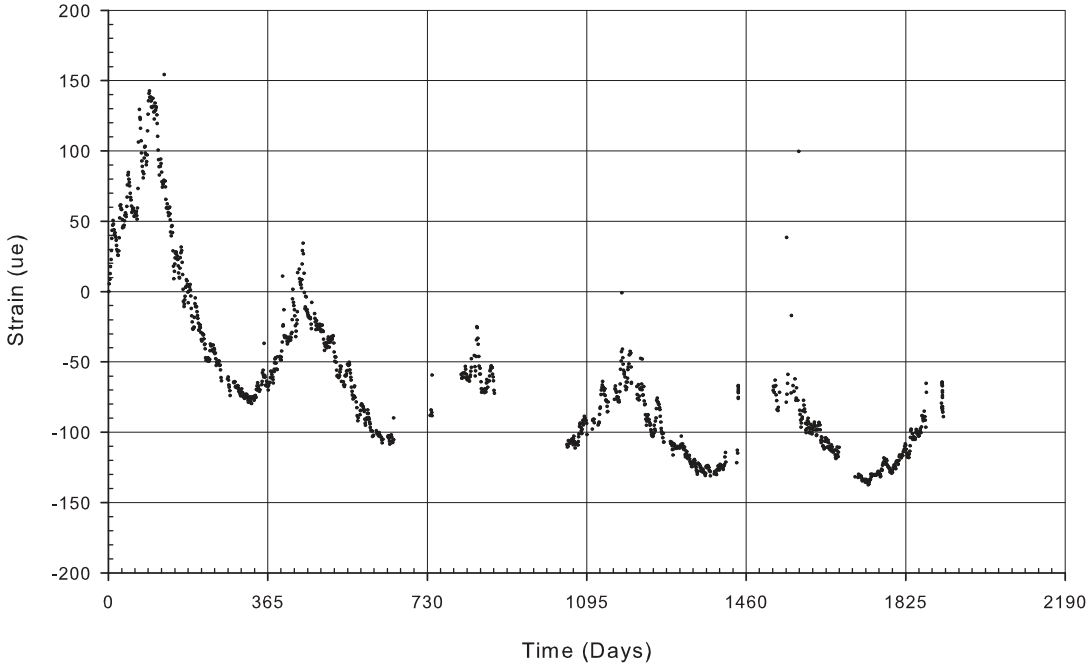
200
150
100
50
0
-50
-100
-150
-200
Strain (ue)
0
365
730
1095
1460
1825
2190
Time (Days)

C-HP6

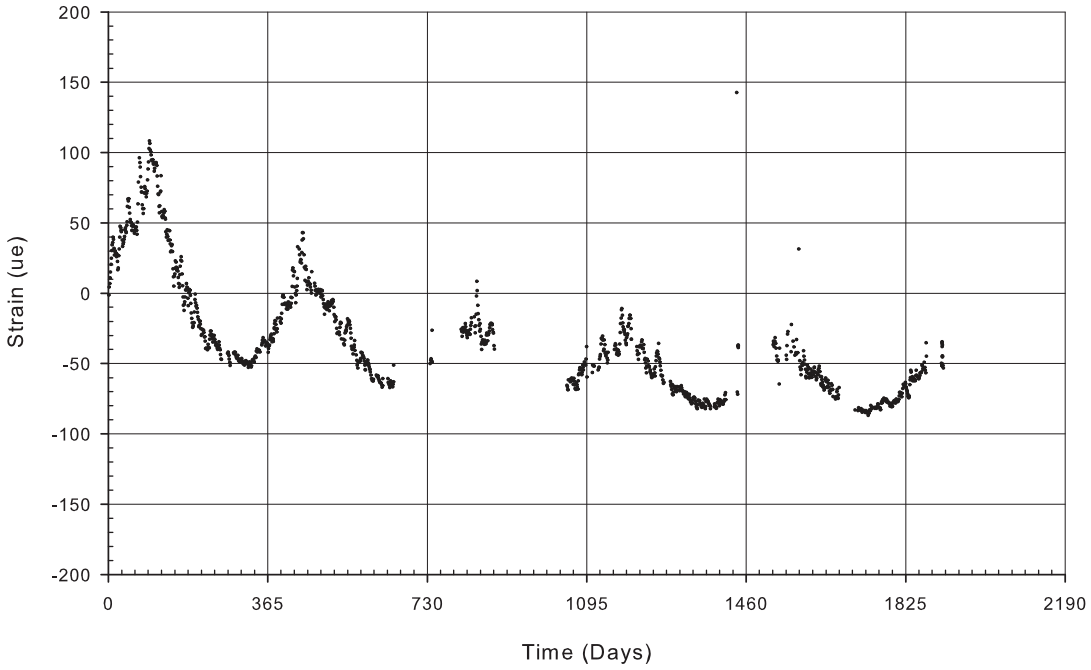
200
150
100
50
0
-50
-100
-150
-200
Strain (ue)
0
365
730
1095
1460
1825
2190
Time (Days)

B-CB

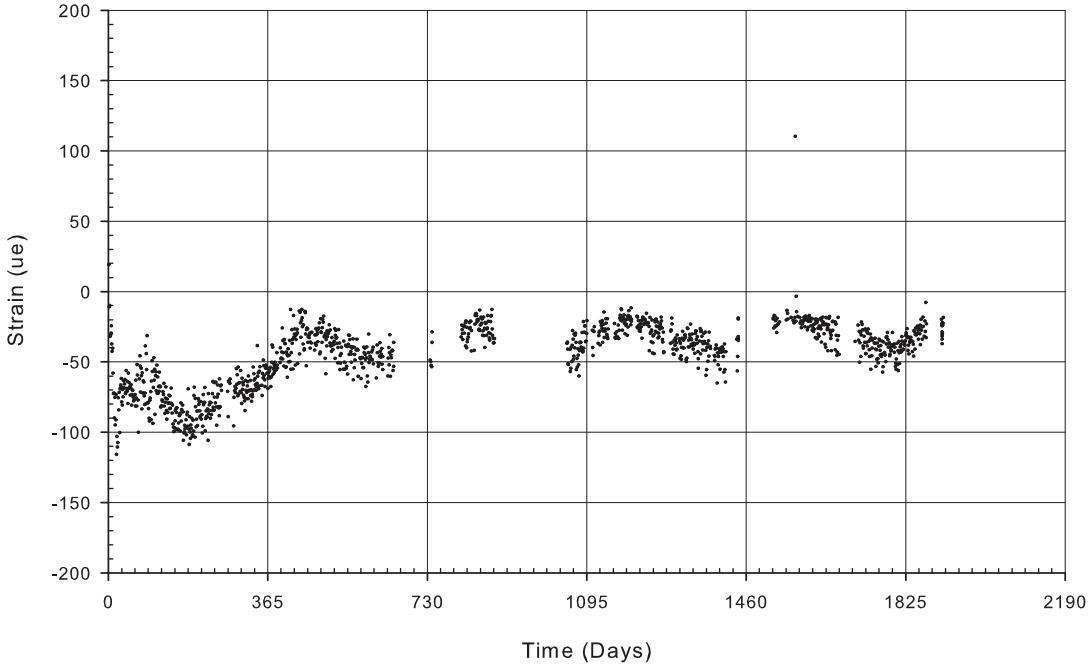
200
150
100
50
0
-50
-100
-150
-200
Strain (ue)
0
365
730
1095
1460
1825
2190
Time (Days)

B-DB

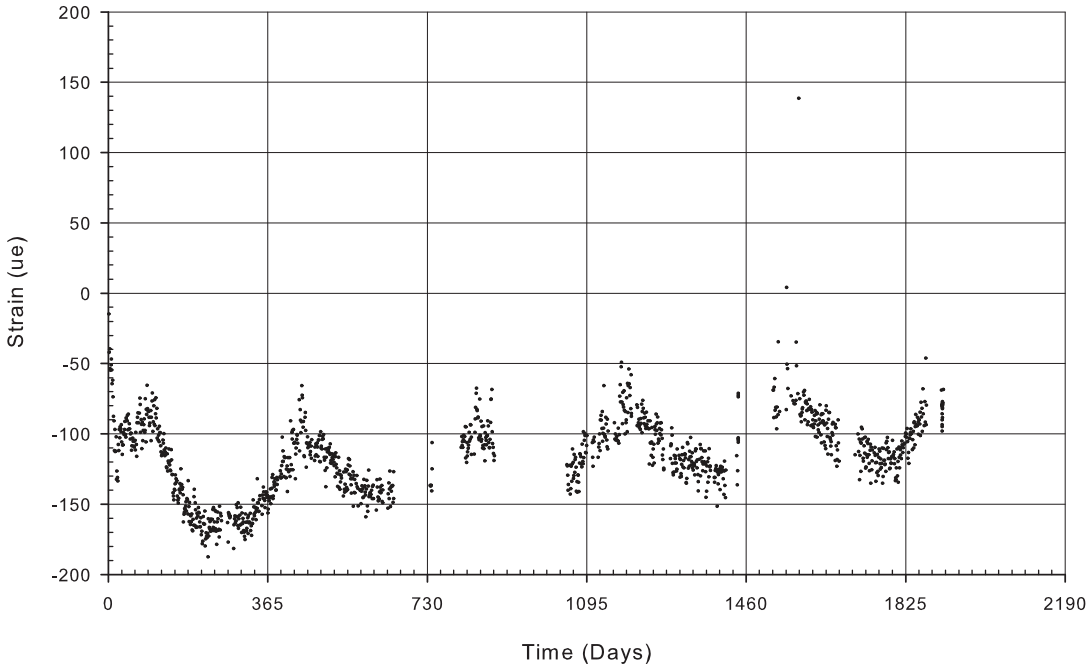
200
150
100
50
0
-50
-100
-150
-200
Strain (ue)
0
365
730
1095
1460
1825
2190
Time (Days)

B-EB

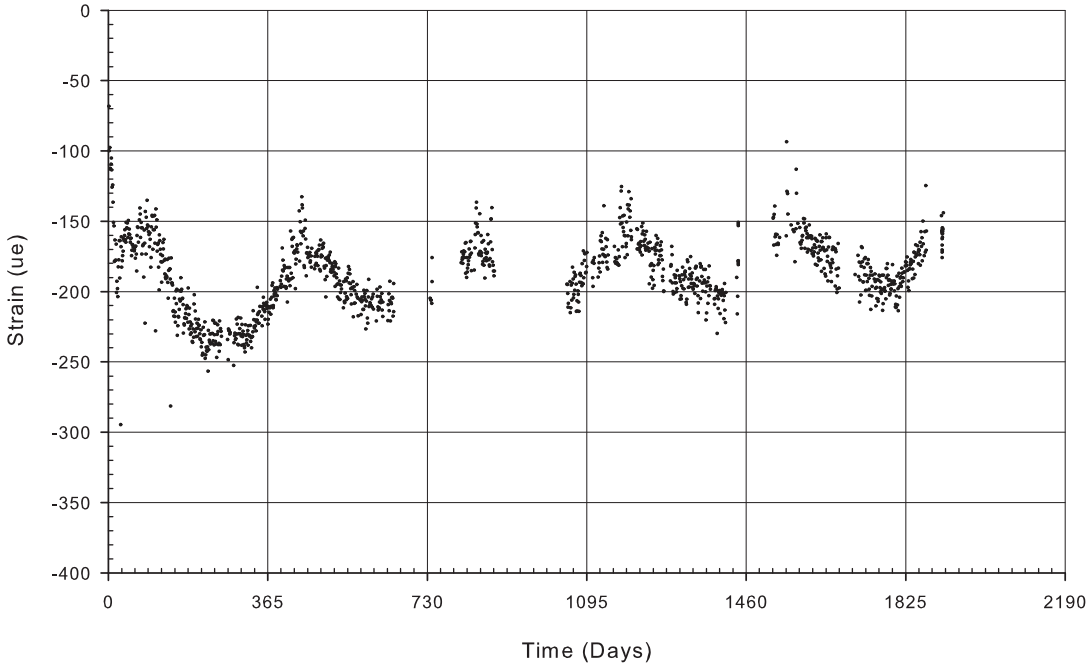
0
-50
-100
-150
-200
-250
-300
-350
-400
Strain (ue)
0
365
730
1095
1460
1825
2190
Time (Days)

B-FB1

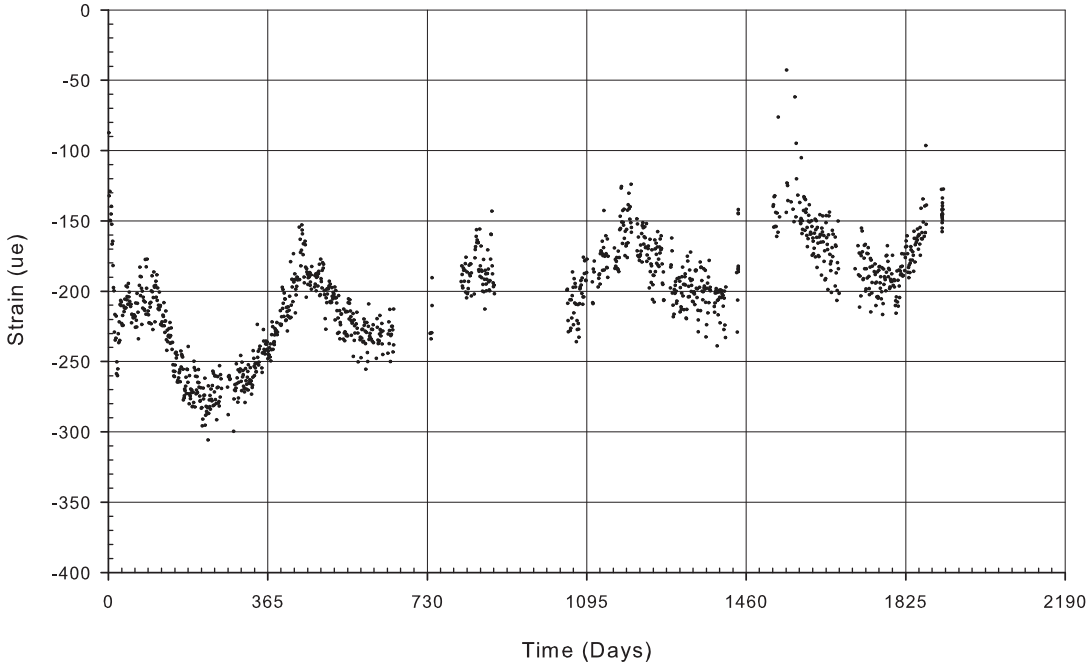
0
-50
-100
-150
-200
-250
-300
-350
-400
Strain (ue)
0
365
730
1095
1460
1825
2190
Time (Days)

B-FB2

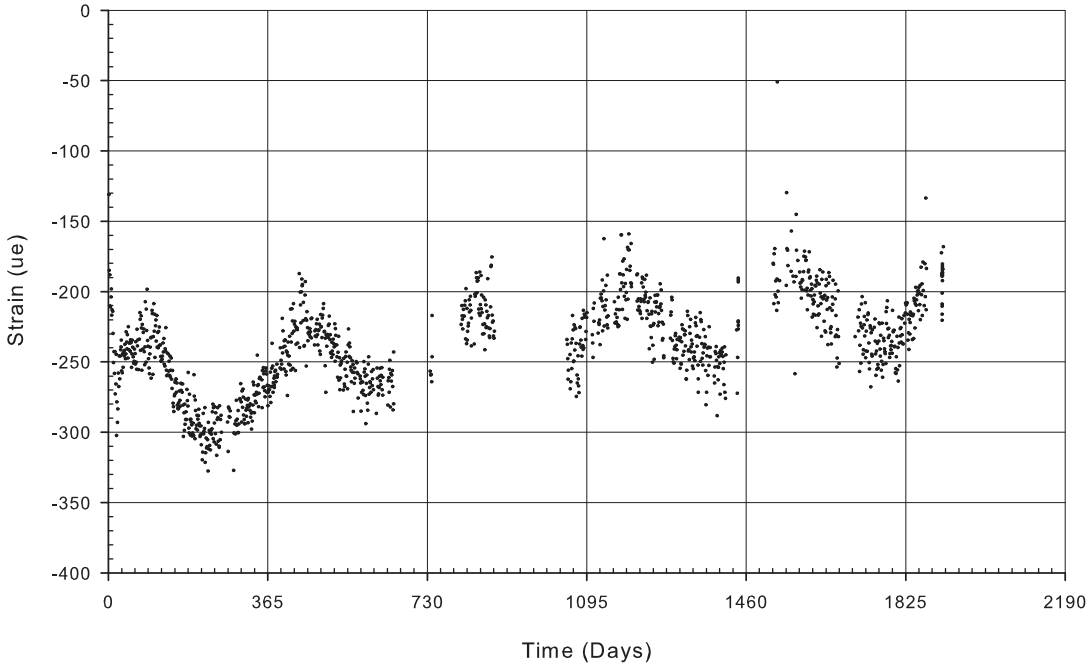
0
-50
-100
-150
-200
-250
-300
-350
-400
Strain (ue)
0
365
730
1095
1460
1825
2190
Time (Days)

B-KB

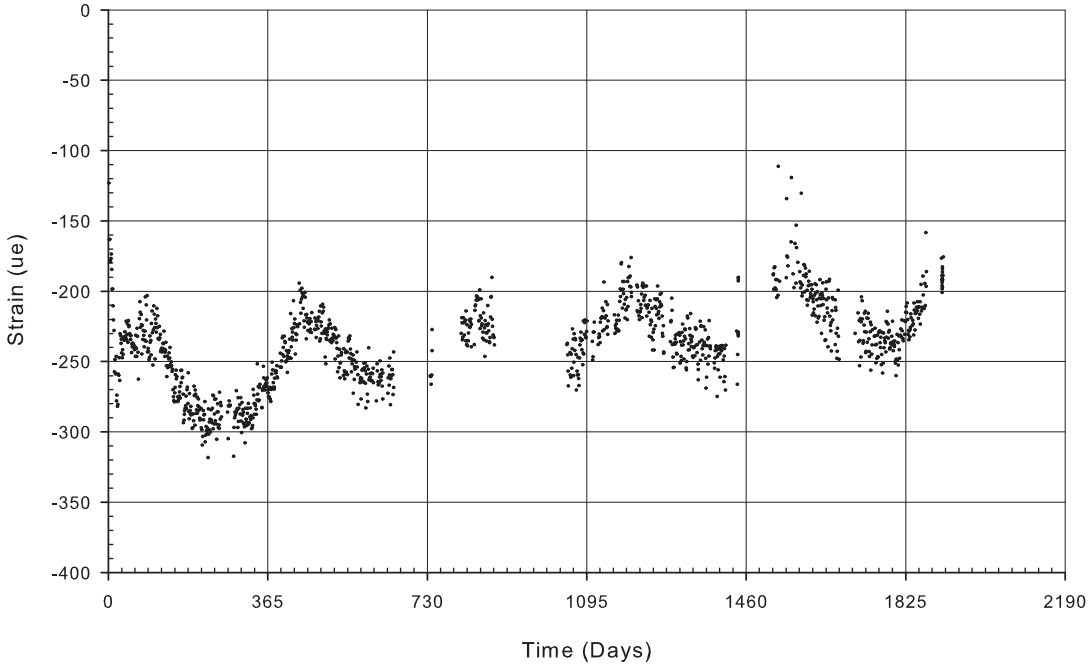
0
-50
-100
-150
-200
-250
-300
-350
-400
Strain (ue)
0
365
730
1095
1460
1825
2190
Time (Days)

B-LB

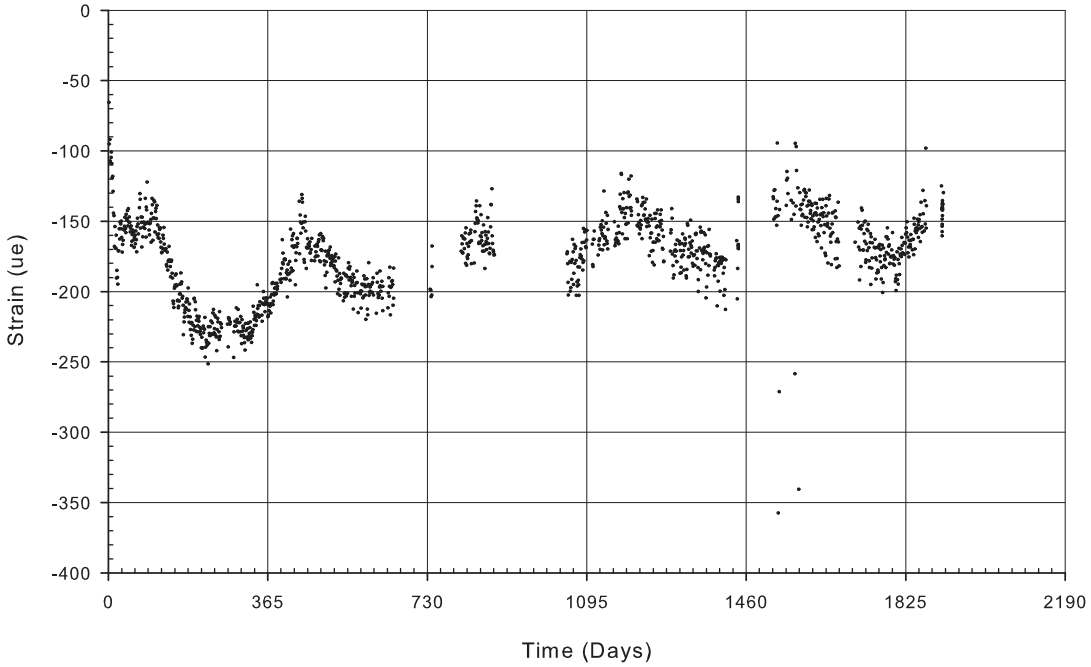
0
-50
-100
-150
-200
-250
-300
-350
-400
Strain (ue)
0
365
730
1095
1460
1825
2190
Time (Days)

B-MB

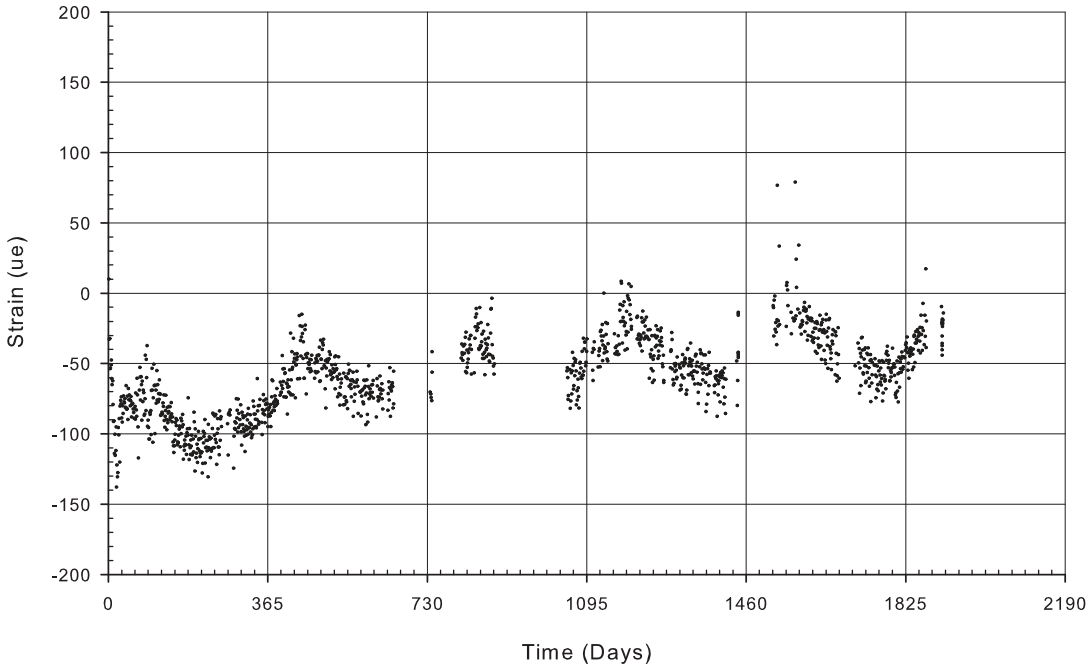
200
150
100
50
0
-50
-100
-150
-200
Strain (ue)
0
365
730
1095
1460
1825
2190
Time (Days)

B-HC1

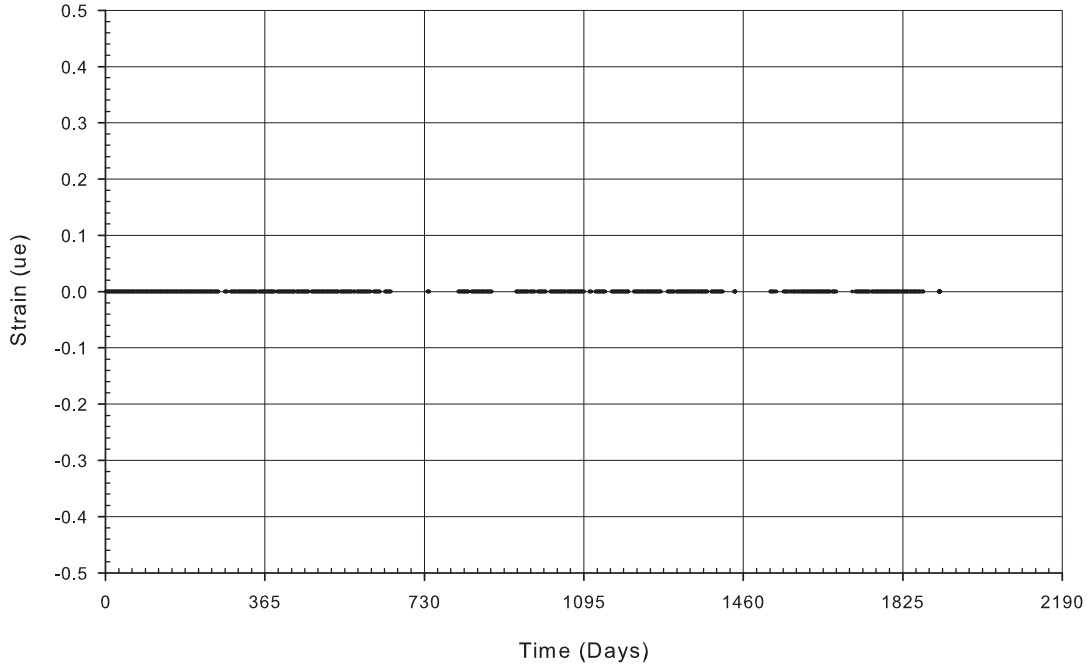
0.5
0.4
0.3
0.2
0.1
0.0
-0.1
-0.2
-0.3
-0.4
-0.5
Strain (ue)
0
365
730
1095
1460
1825
2190
Time (Days)

B-HC2

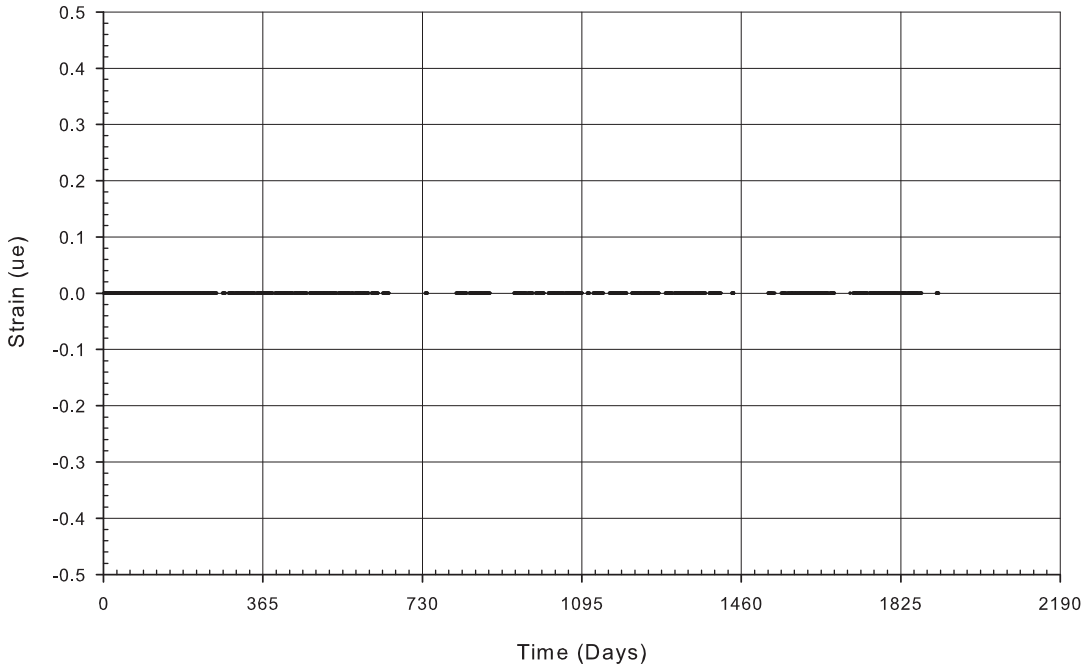
0.5
0.4
0.3
0.2
0.1
0.0
-0.1
-0.2
-0.3
-0.4
-0.5
Strain (ue)
0
365
730
1095
1460
1825
2190
Time (Days)

C-CB

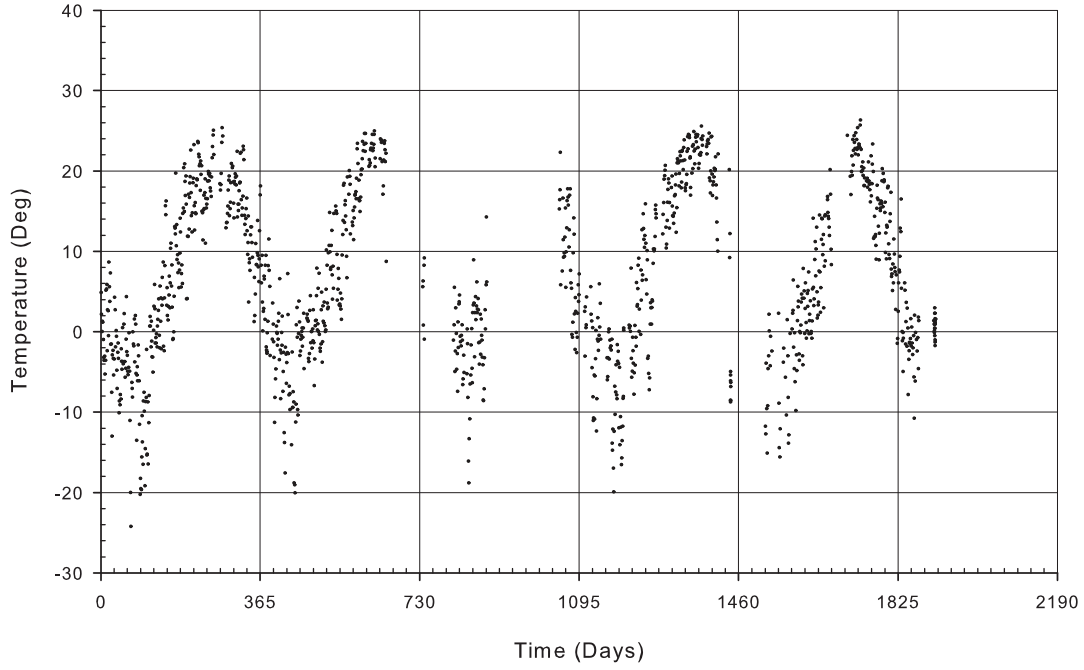
40
30
20
10
0
-10
-20
-30
Temperature (Deg)
0
365
730
1095
1460
1825
2190
Time (Days)

C-FB

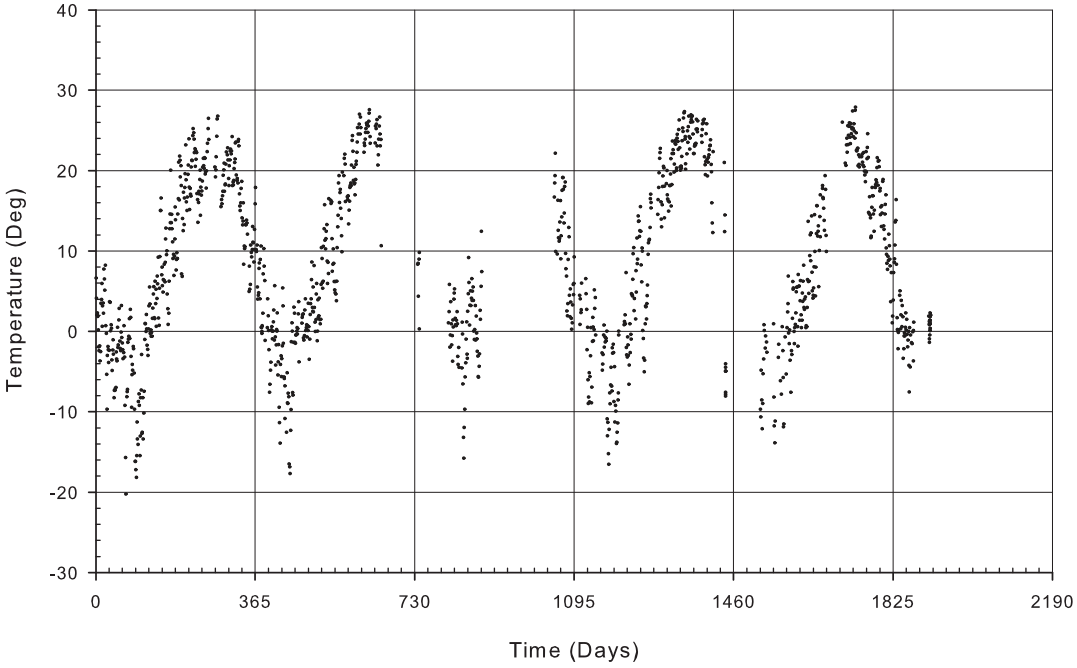
40
30
20
10
0
-10
-20
-30
Temperature (Deg)
0
365
730
1095
1460
1825
2190
Time (Days)

C-HP1

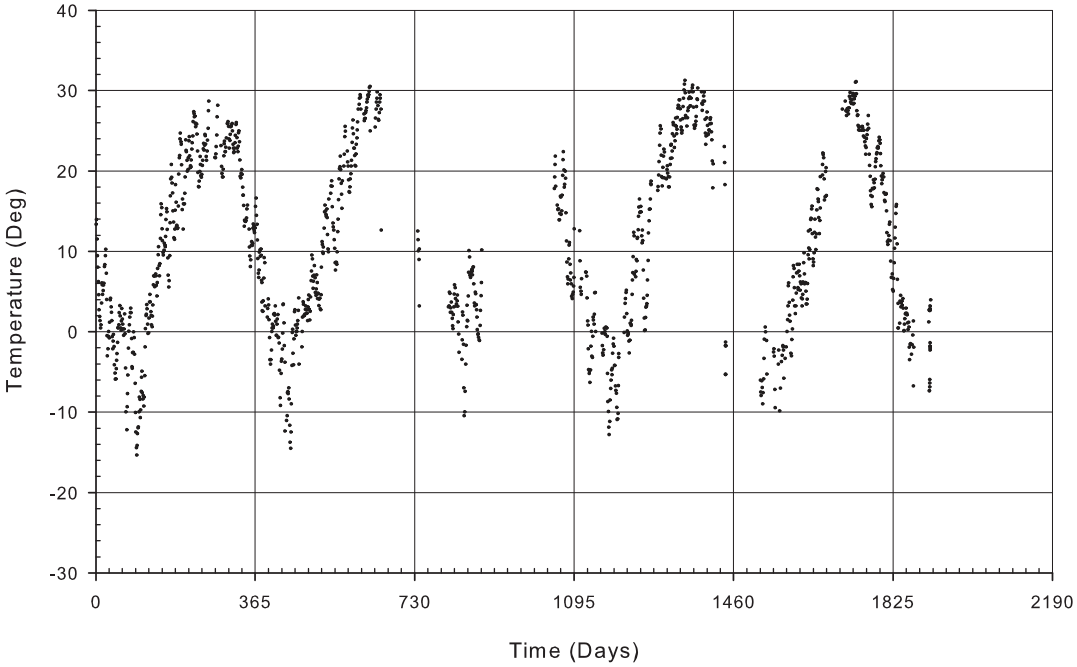
40
30
20
10
0
-10
-20
-30
Temperature (Deg)
0
365
730
1095
1460
1825
2190
Time (Days)

C-HP2

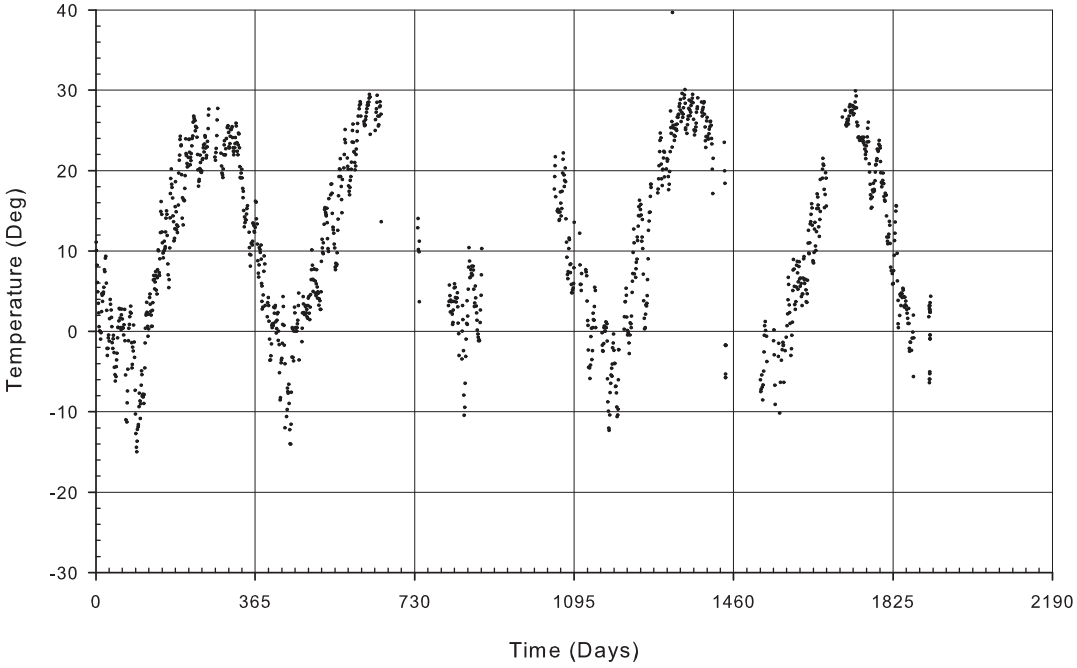
40
30
20
10
0
-10
-20
-30
Temperature (Deg)
0
365
730
1095
1460
1825
2190
Time (Days)

C-HP3

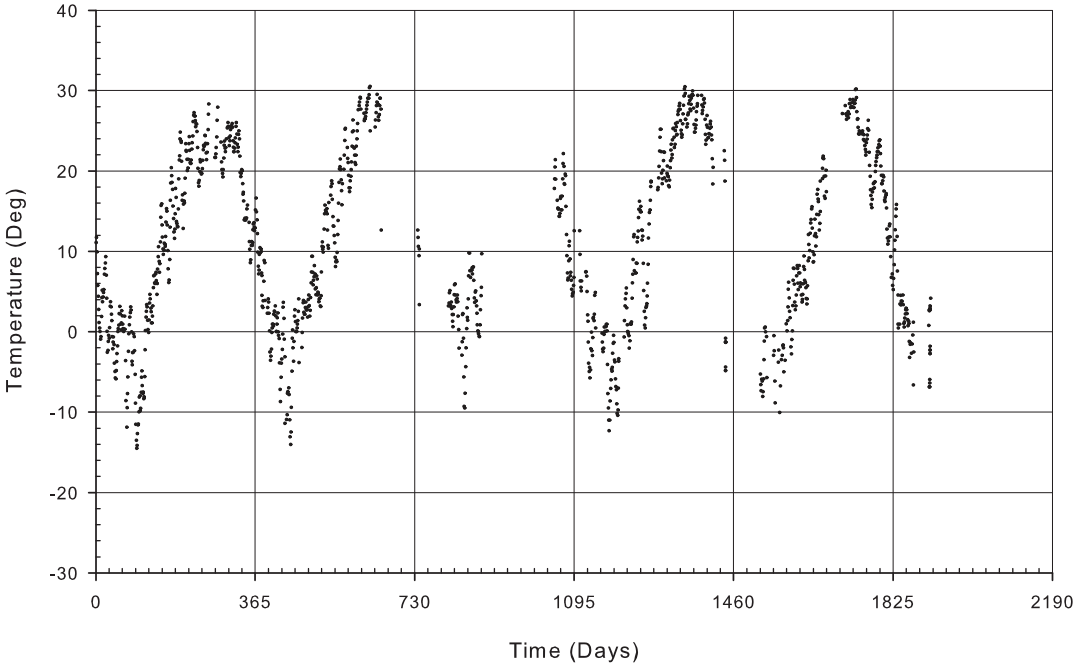
40
30
20
10
0
-10
-20
-30
Temperature (Deg)
0
365
730
1095
1460
1825
2190
Time (Days)

C-HP6

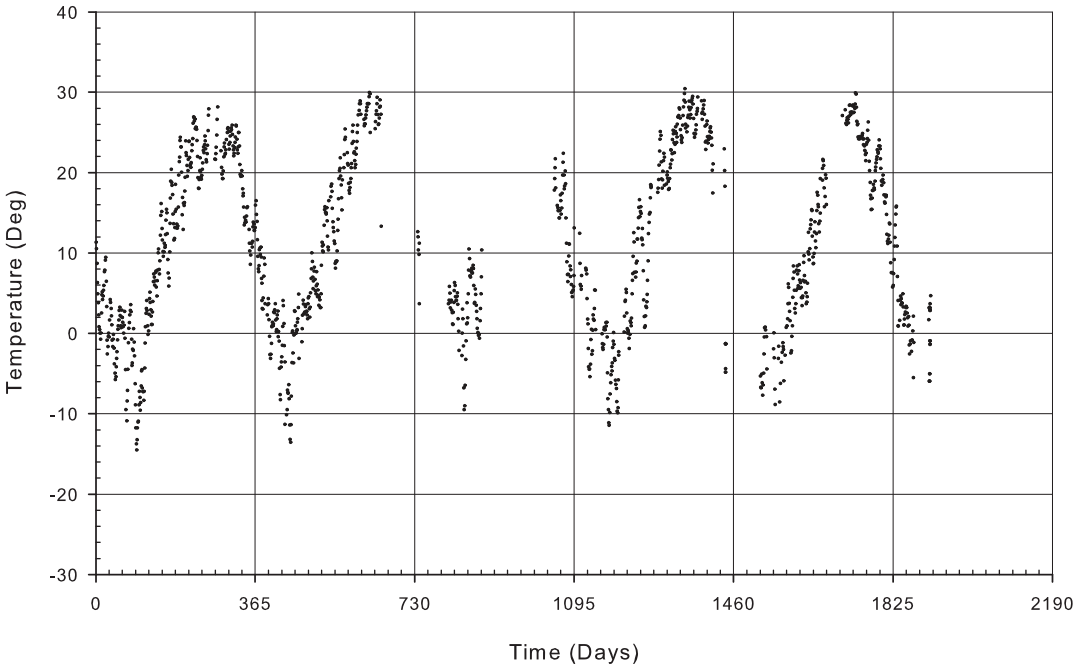
40
30
20
10
0
-10
-20
-30
Temperature (Deg)
0
365
730
1095
1460
1825
2190
Time (Days)

B-CB

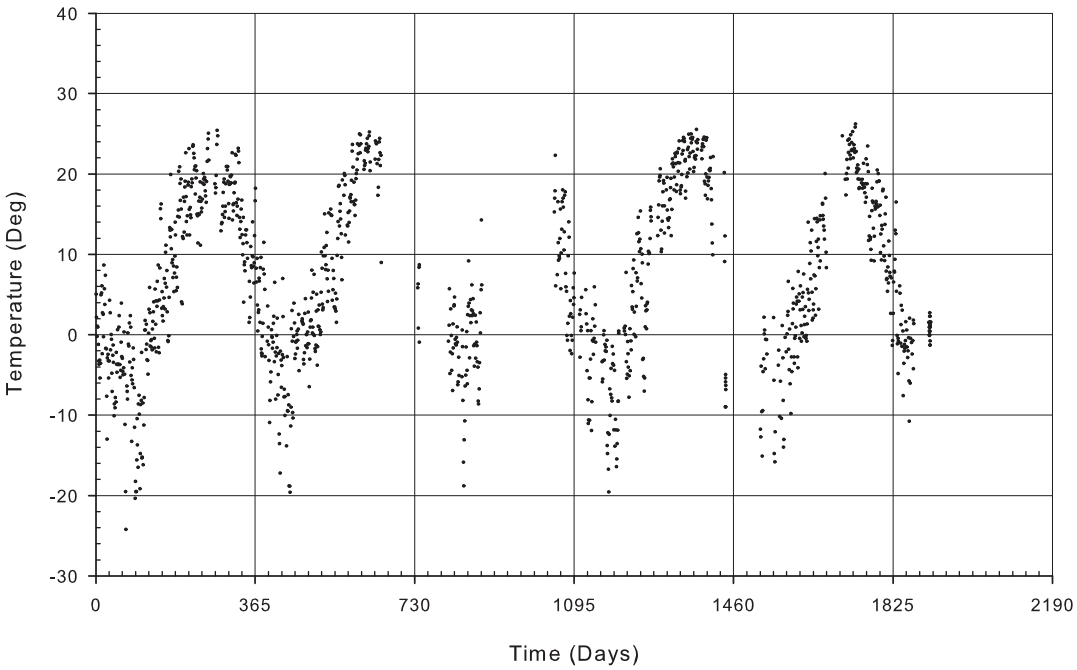
40
30
20
10
0
-10
-20
-30
Temperature (Deg)
0
365
730
1095
1460
1825
2190
Time (Days)

B-DB

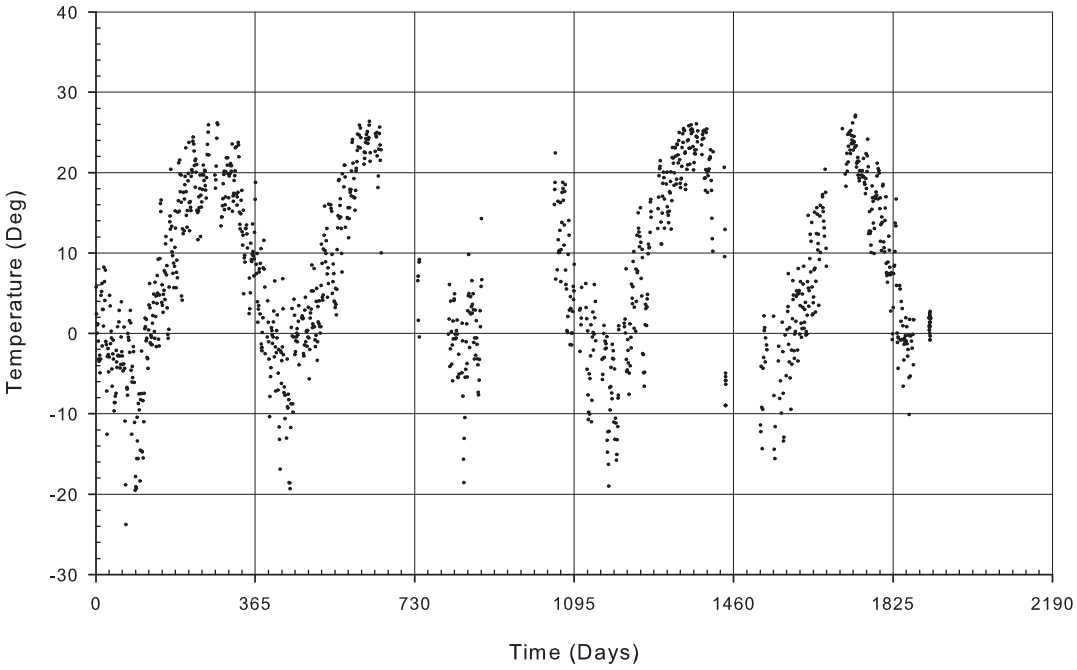
40
30
20
10
0
-10
-20
-30
Temperature (Deg)
0
365
730
1095
1460
1825
2190
Time (Days)

B-EB

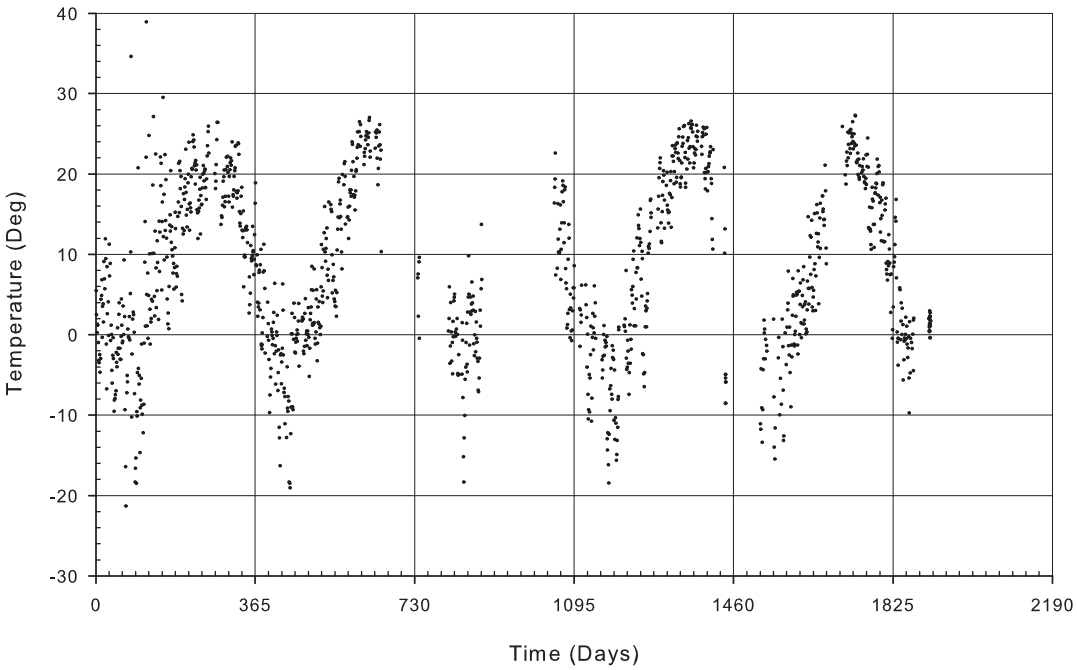
40
30
20
10
0
-10
-20
-30
Temperature (Deg)
0
365
730
1095
1460
1825
2190
Time (Days)

B-FB1

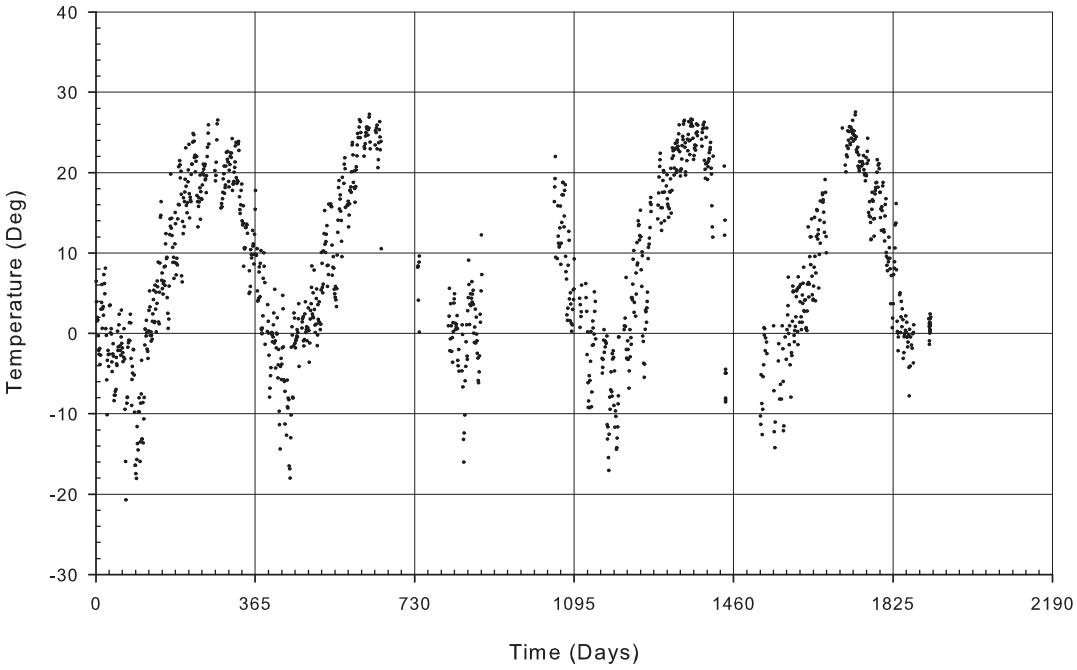
40
30
20
10
0
-10
-20
-30
Temperature (Deg)
0
365
730
1095
1460
1825
2190
Time (Days)

B-FB2

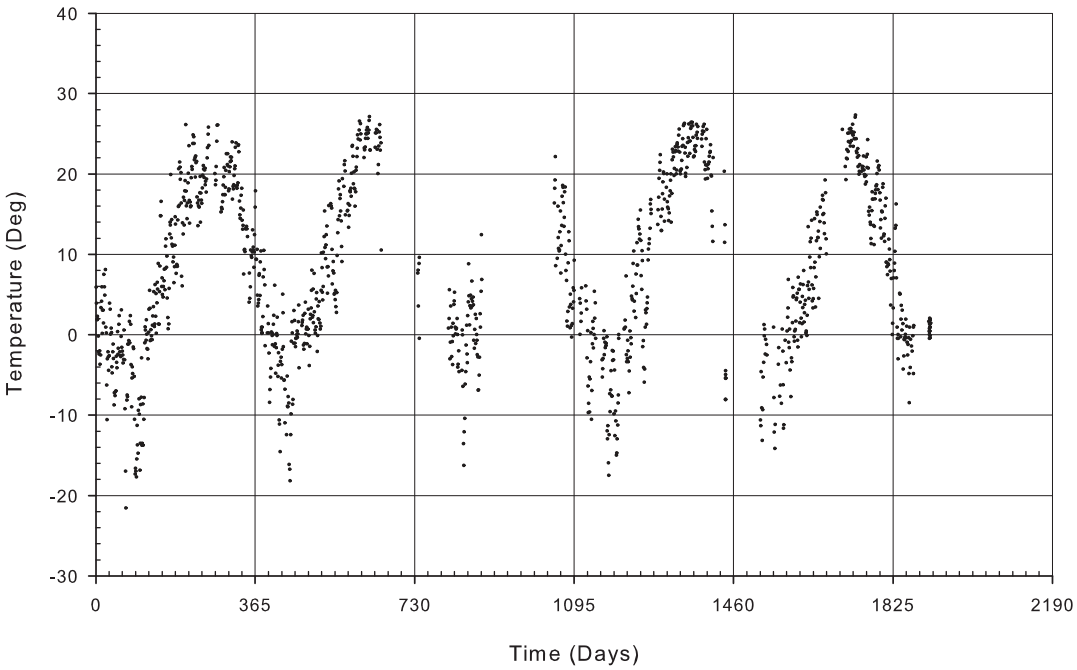
40
30
20
10
0
-10
-20
-30
Temperature (Deg)
0
365
730
1095
1460
1825
2190
Time (Days)

B-KB

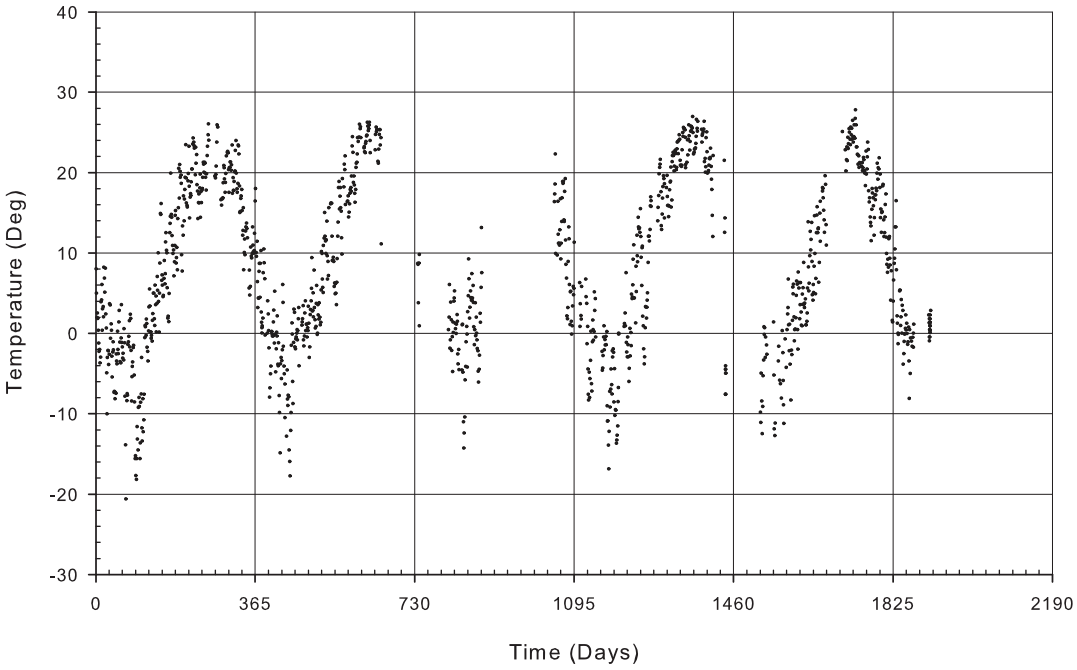
40
30
20
10
0
-10
-20
-30
Temperature (Deg)
0
365
730
1095
1460
1825
2190
Time (Days)

B-LB

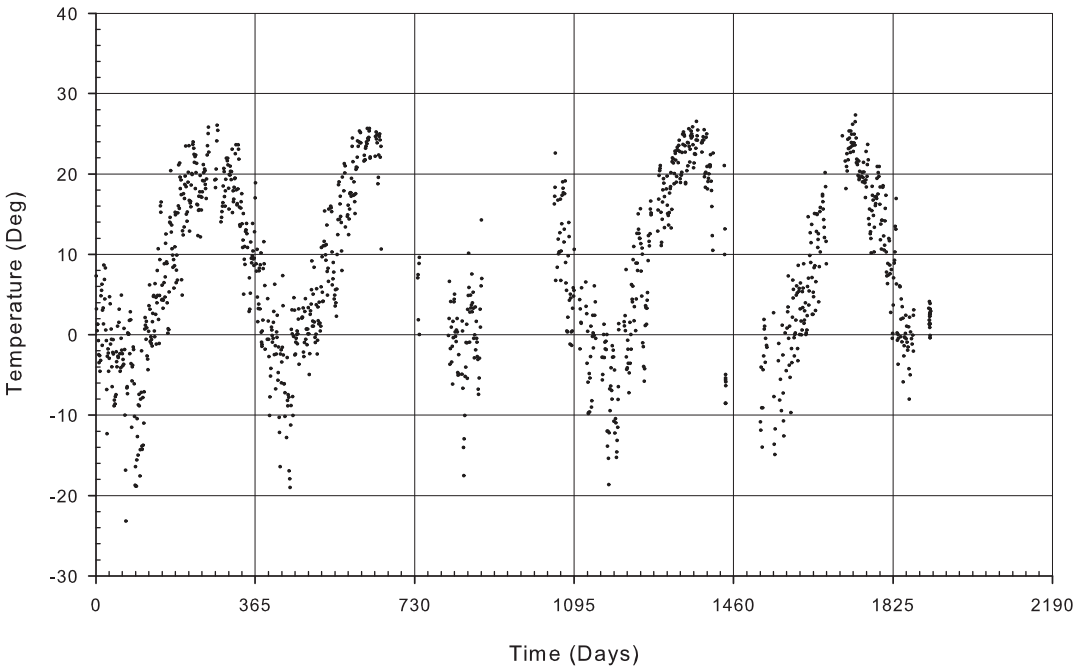
40
30
20
10
0
-10
-20
-30
Temperature (Deg)
0
365
730
1095
1460
1825
2190
Time (Days)

B-MB

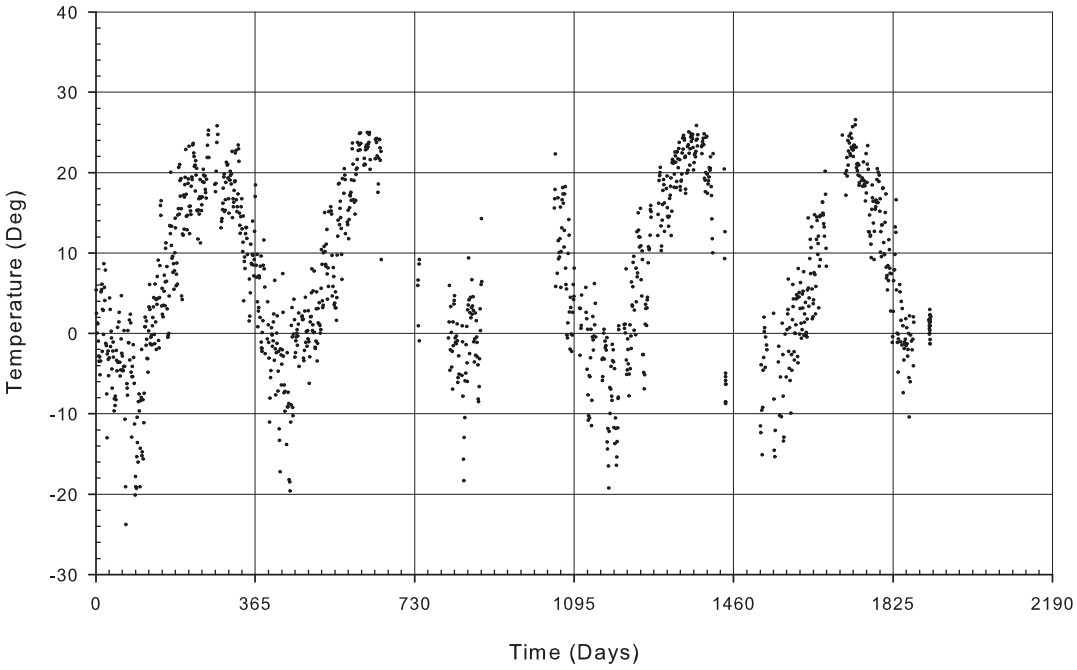
40
30
20
10
0
-10
-20
-30
Temperature (Deg)
0
365
730
1095
1460
1825
2190
Time (Days)

B-HC1

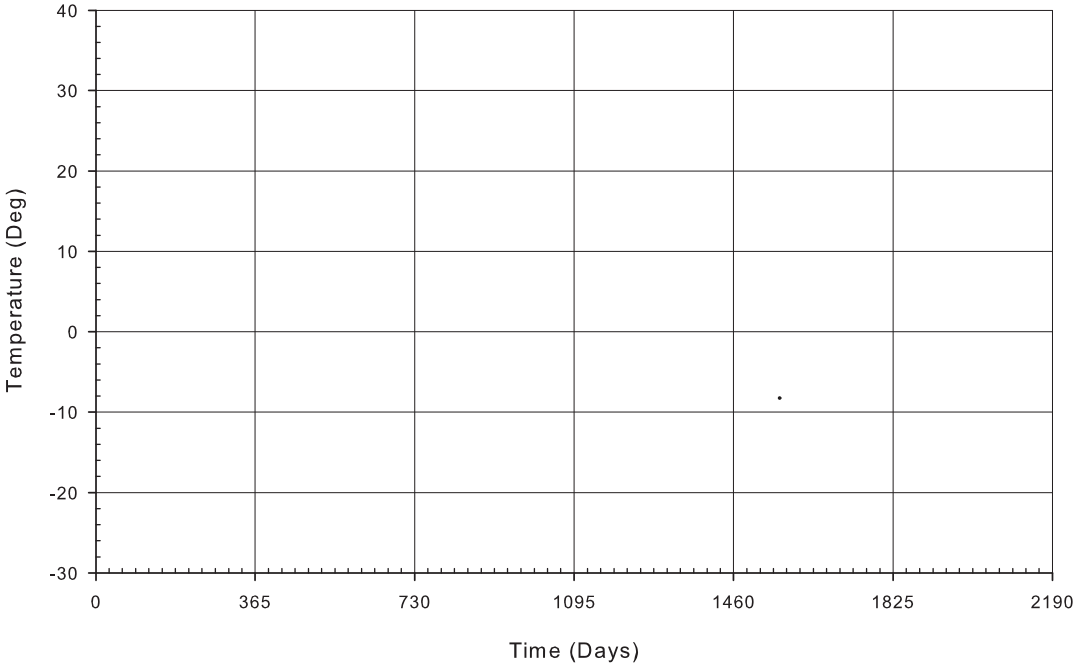
40
30
20
10
0
-10
-20
-30
Temperature (Deg)
0
365
730
1095
1460
1825
2190
Time (Days)

B-HC2

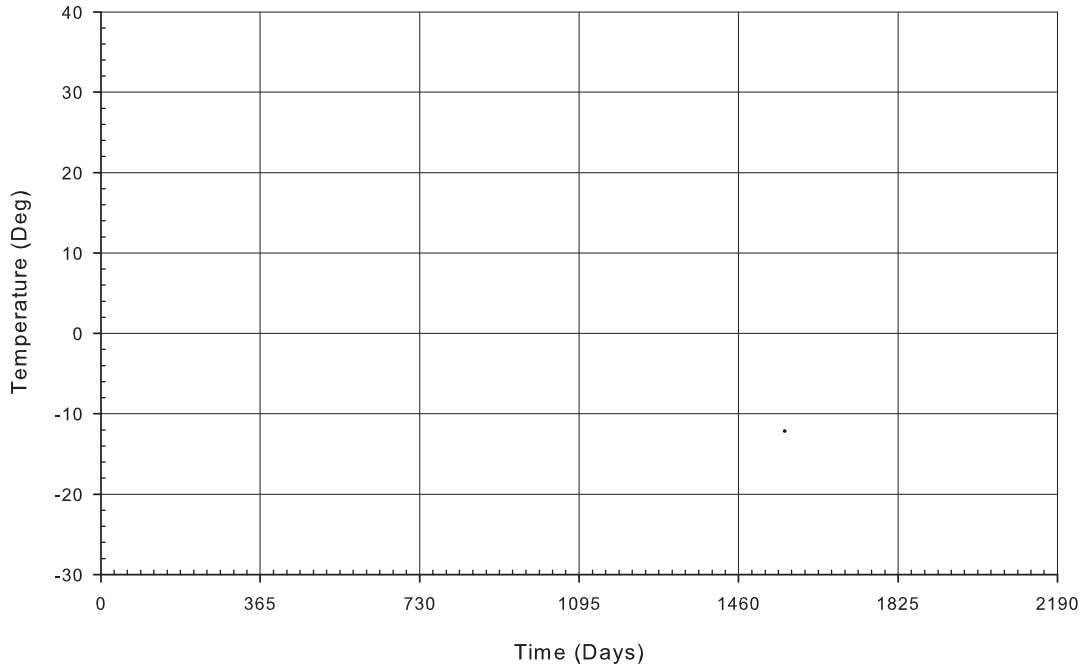
40
30
20
10
0
-10
-20
-30
Temperature (Deg)
0
365
730
1095
1460
1825
2190
Time (Days)

B-XL1

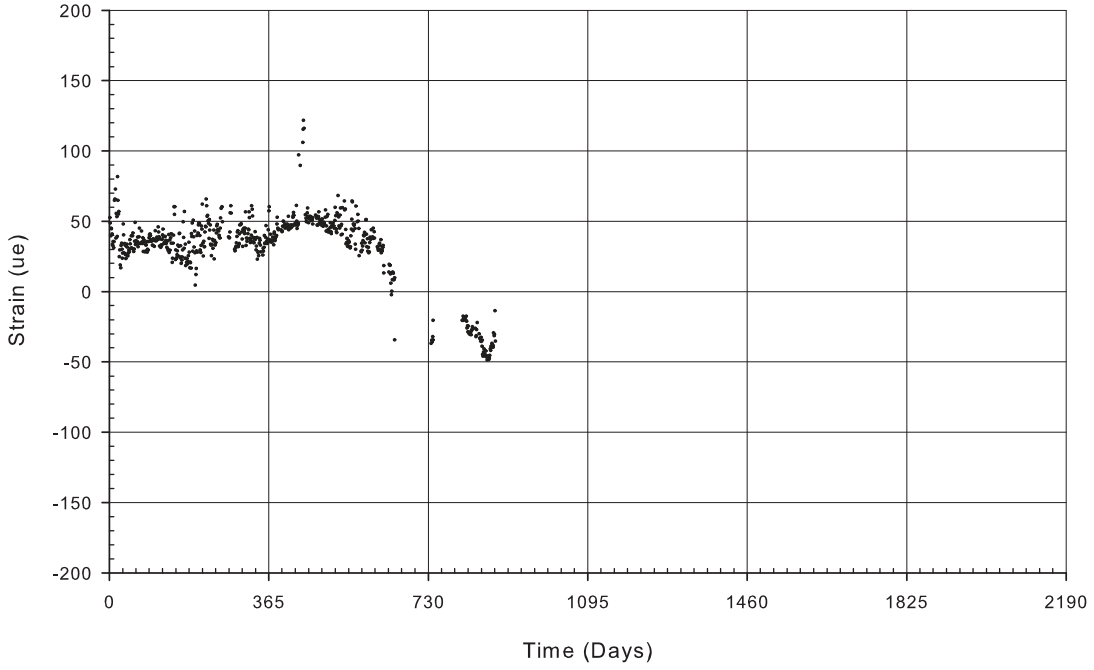
200
150
100
50
0
-50
-100
-150
-200
Strain (ue)
0
365
730
1095
1460
1825
2190
Time (Days)

B-XL2

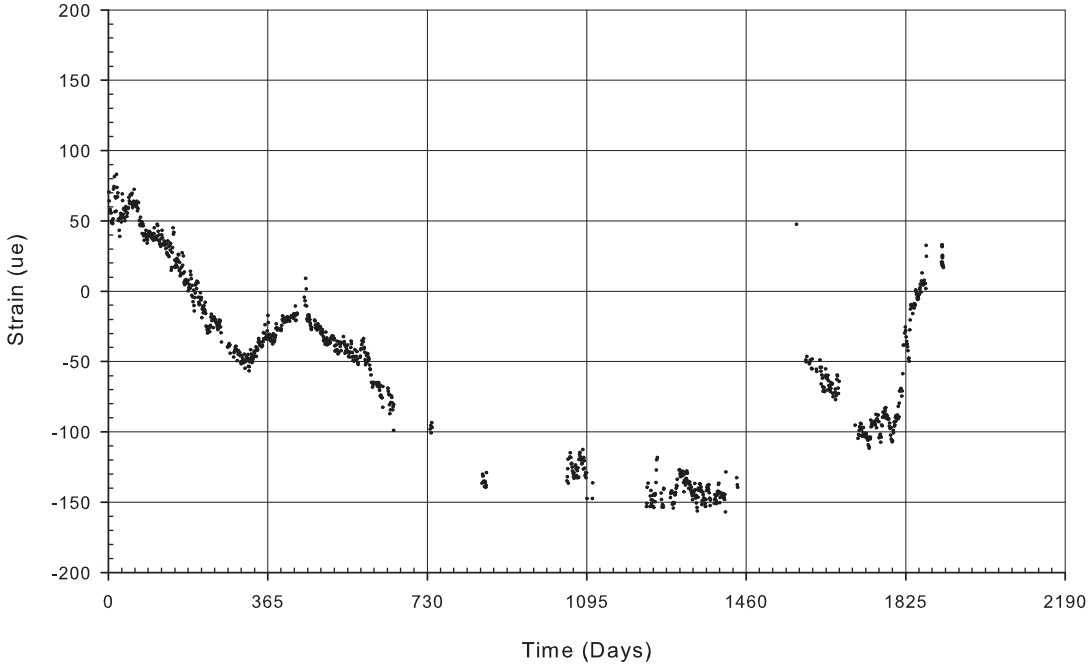
200
150
100
50
0
-50
-100
-150
-200
Strain (ue)
0
365
730
1095
1460
1825
2190
Time (Days)

B-XL3

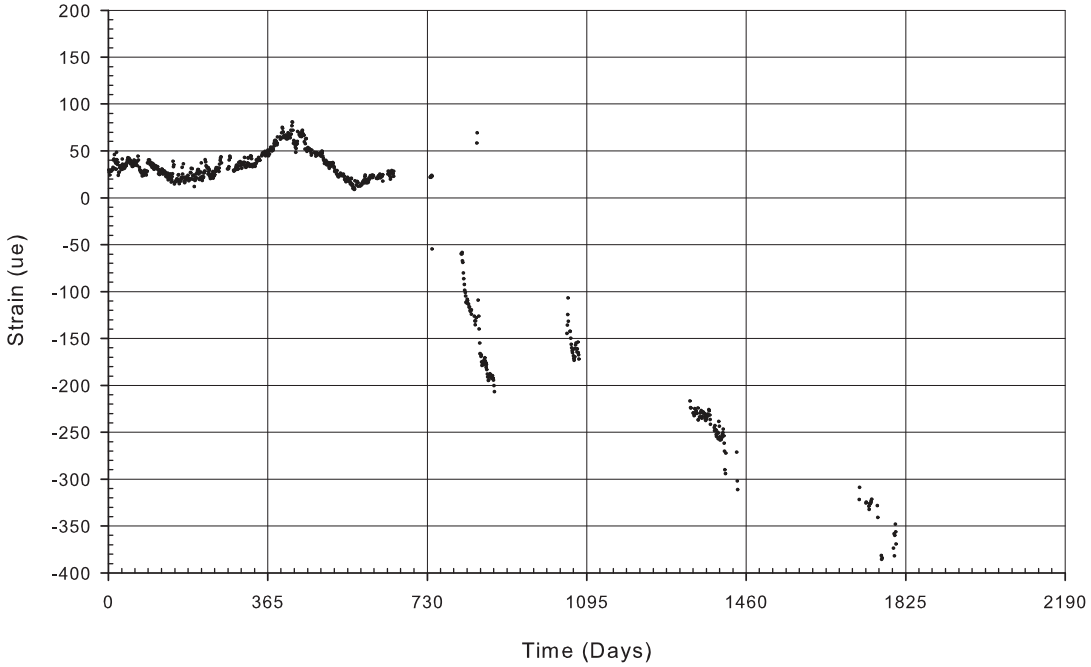
200
150
100
50
0
-50
-100
-150
-200
-250
-300
-350
-400
Strain (ue)
0
365
730
1095
1460
1825
2190
Time (Days)

B-XL4

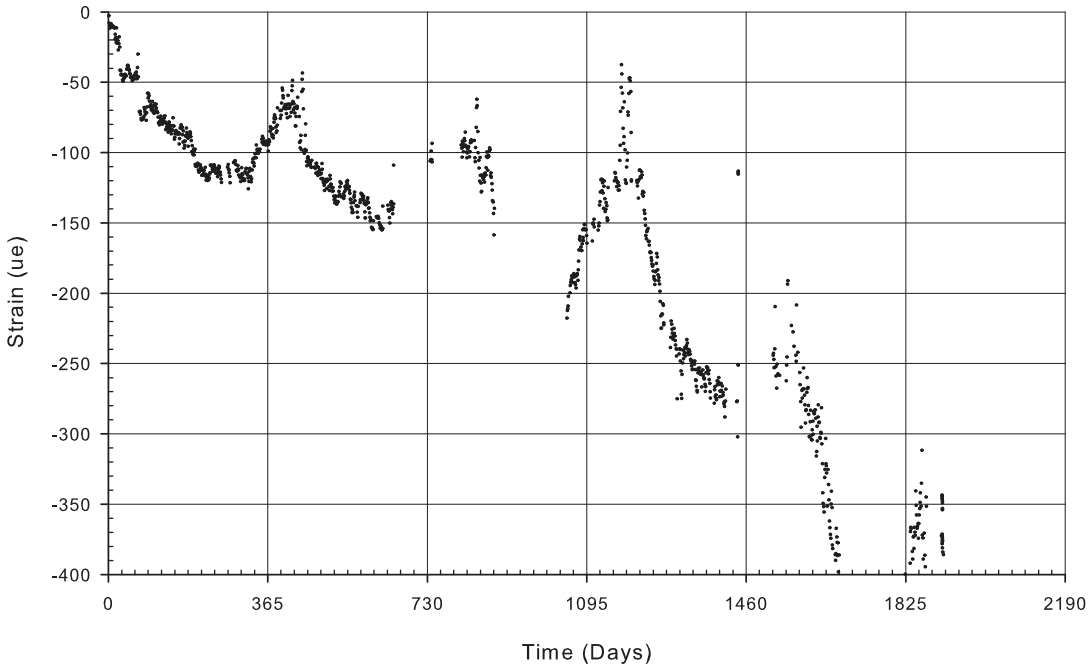
0
-50
-100
-150
-200
-250
-300
-350
-400
Strain (ue)
0
365
730
1095
1460
1825
2190
Time (Days)

B-AB

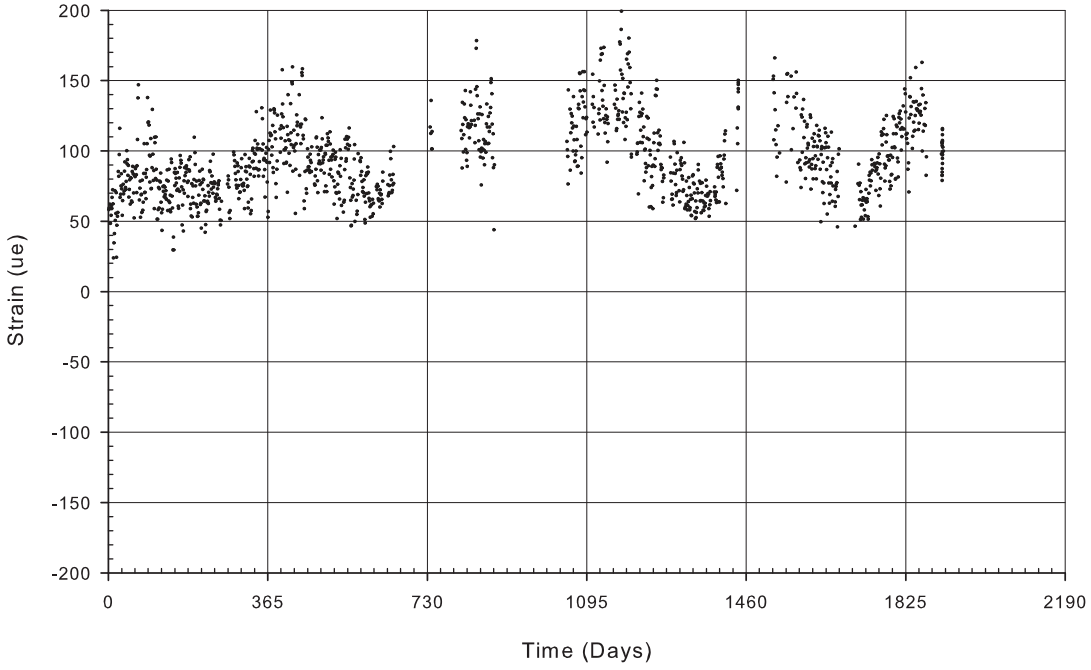
200
150
100
50
0
-50
-100
-150
-200
Strain (ue)
0
365
730
1095
1460
1825
2190
Time (Days)

B-AW

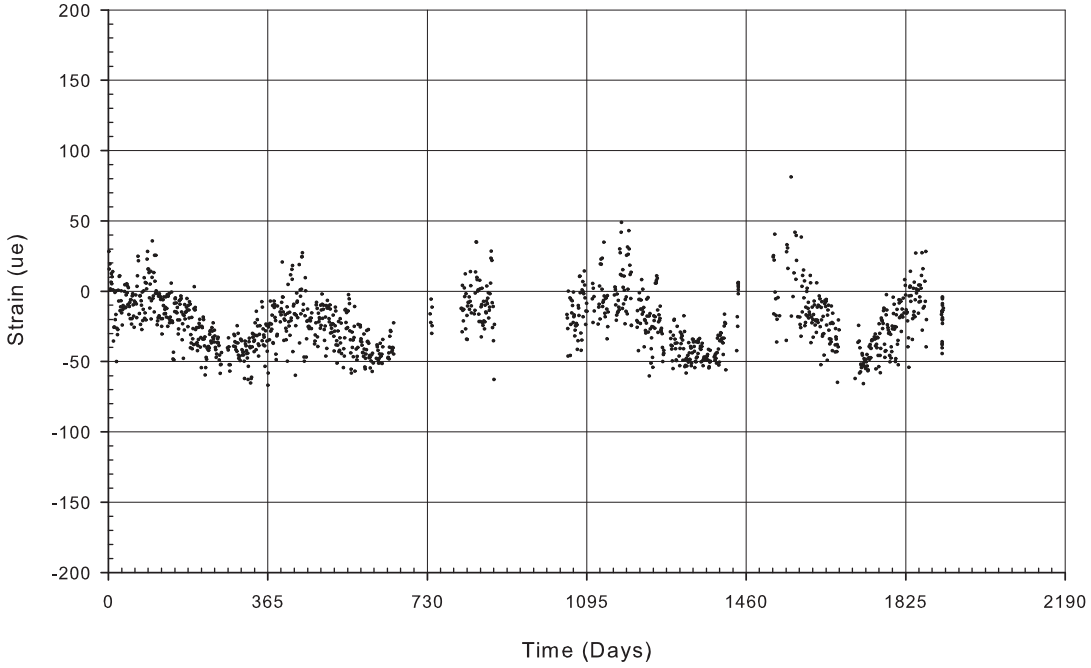
200
150
100
50
0
-50
-100
-150
-200
Strain (ue)
0
365
730
1095
1460
1825
2190
Time (Days)

B-AT

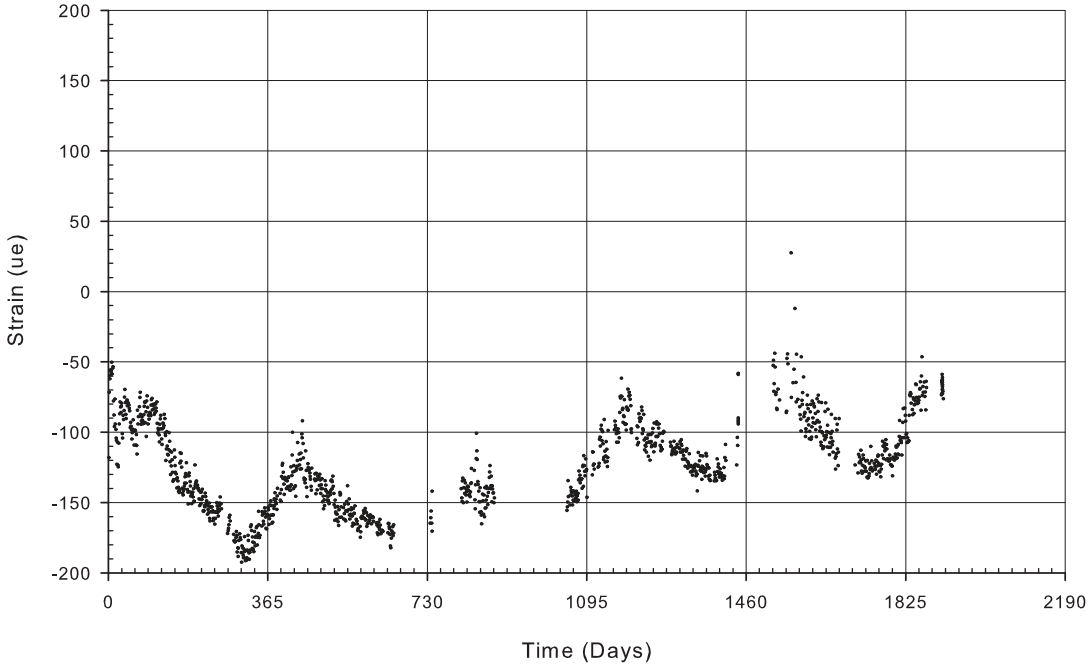
200
150
100
50
0
-50
-100
-150
-200
Strain (ue)
0
365
730
1095
1460
1825
2190
Time (Days)

B-BB1

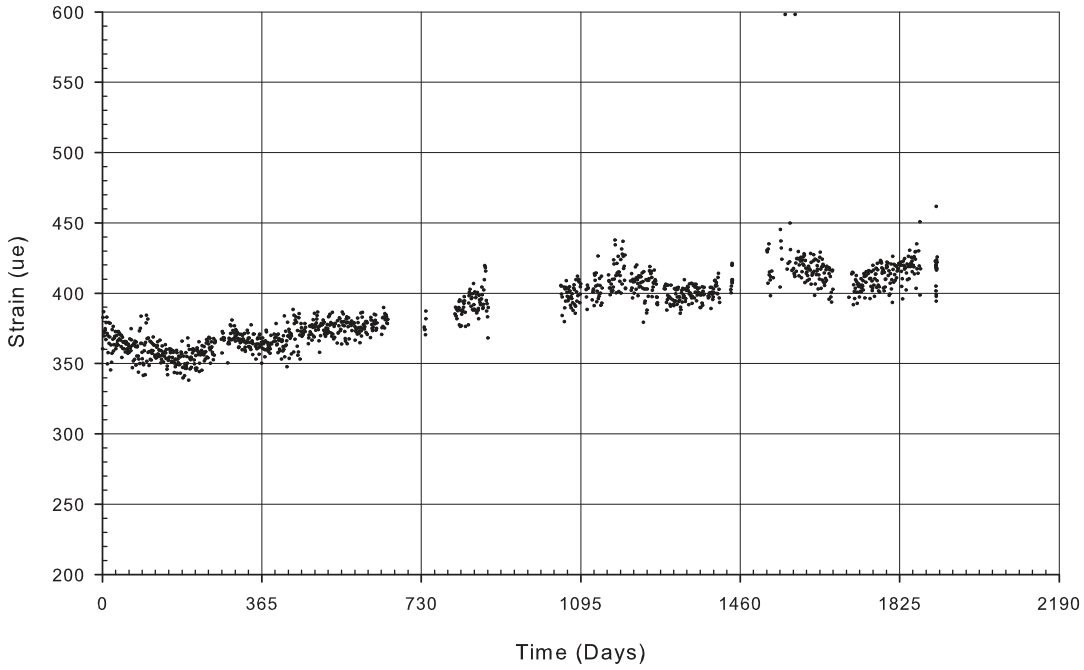
600
550
500
450
400
350
300
250
200
Strain (ue)
0
365
730
1095
1460
1825
2190
Time (Days)

B-BB2

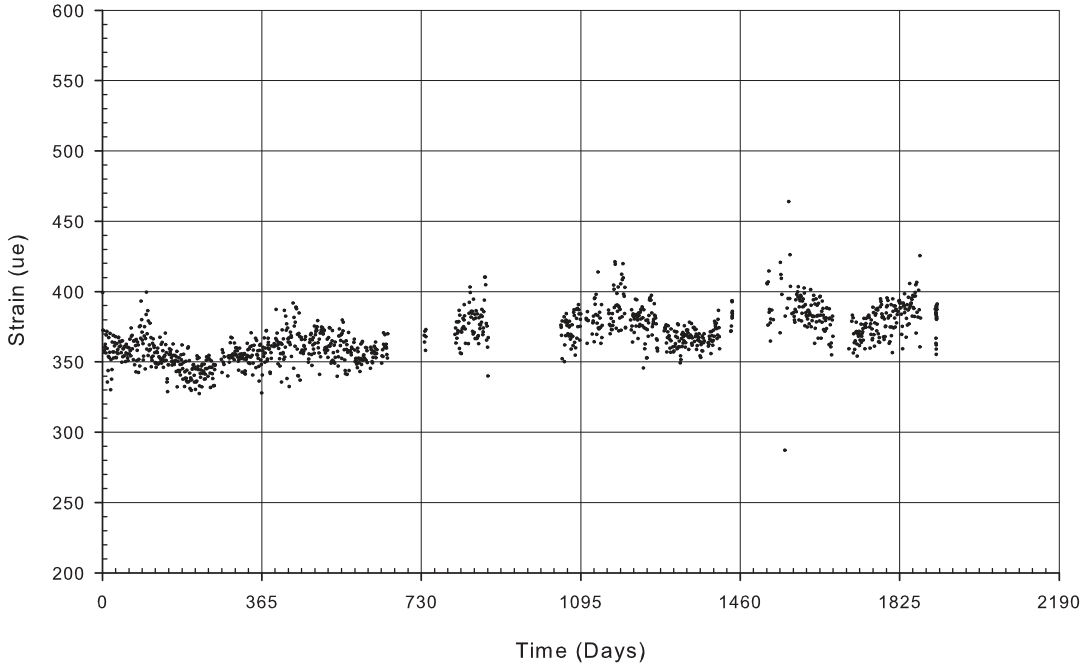
600
550
500
450
400
350
300
250
200
Strain (ue)
0
365
730
1095
1460
1825
2190
Time (Days)

B-BW

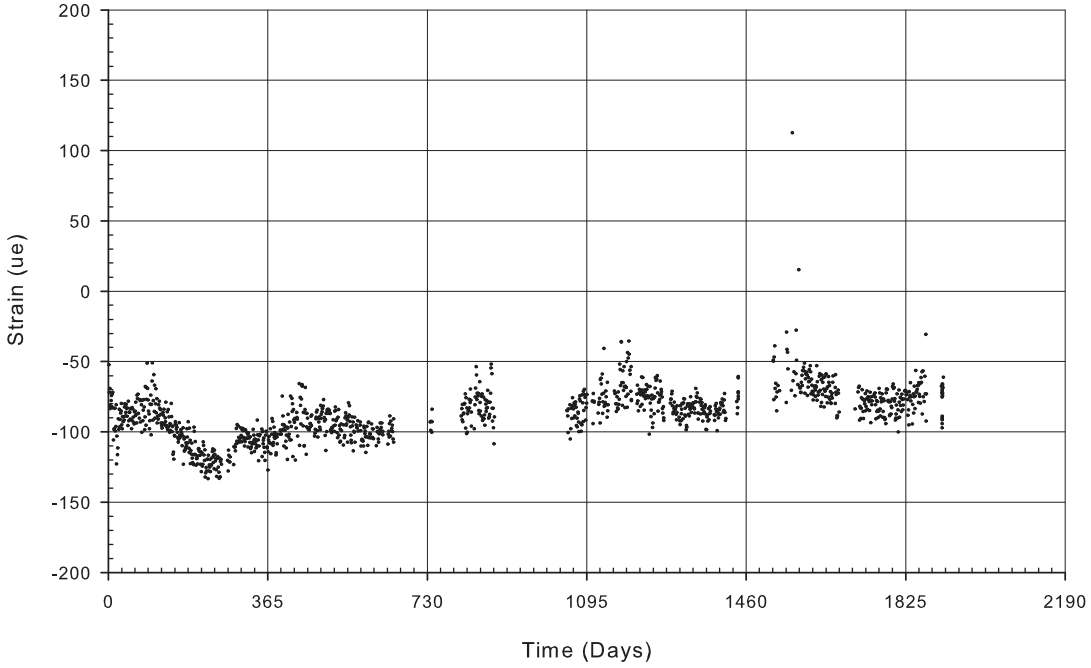
200
150
100
50
0
-50
-100
-150
-200
Strain (ue)
0
365
730
1095
1460
1825
2190
Time (Days)

B-BT

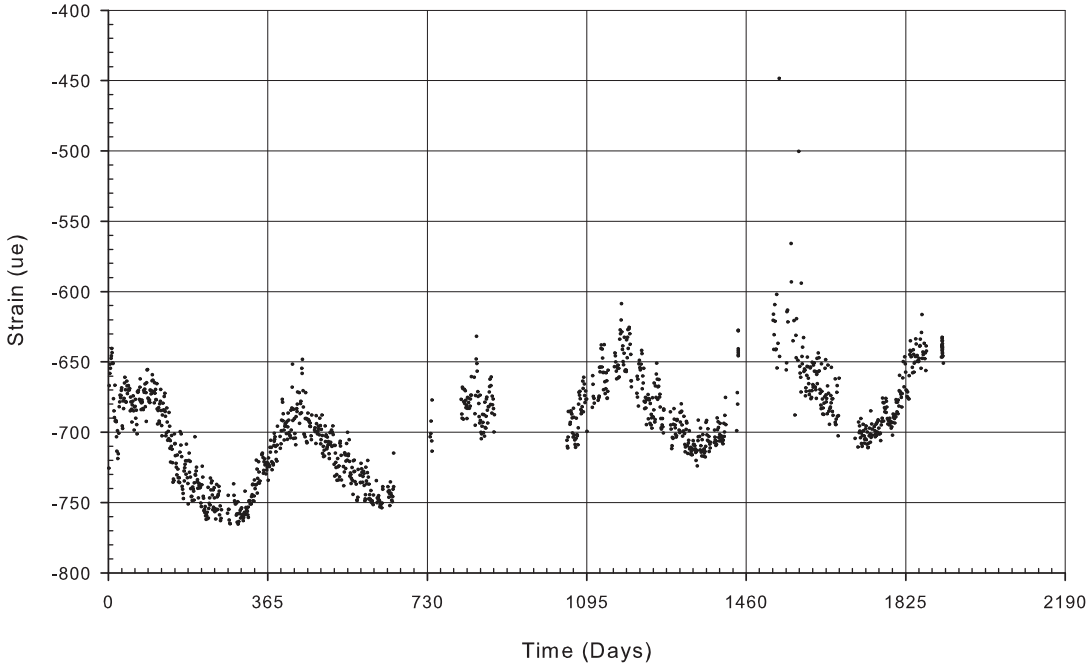
-400
-450
-500
-550
-600
-650
-700
-750
-800
Strain (ue)
0
365
730
1095
1460
1825
2190
Time (Days)

B-CD

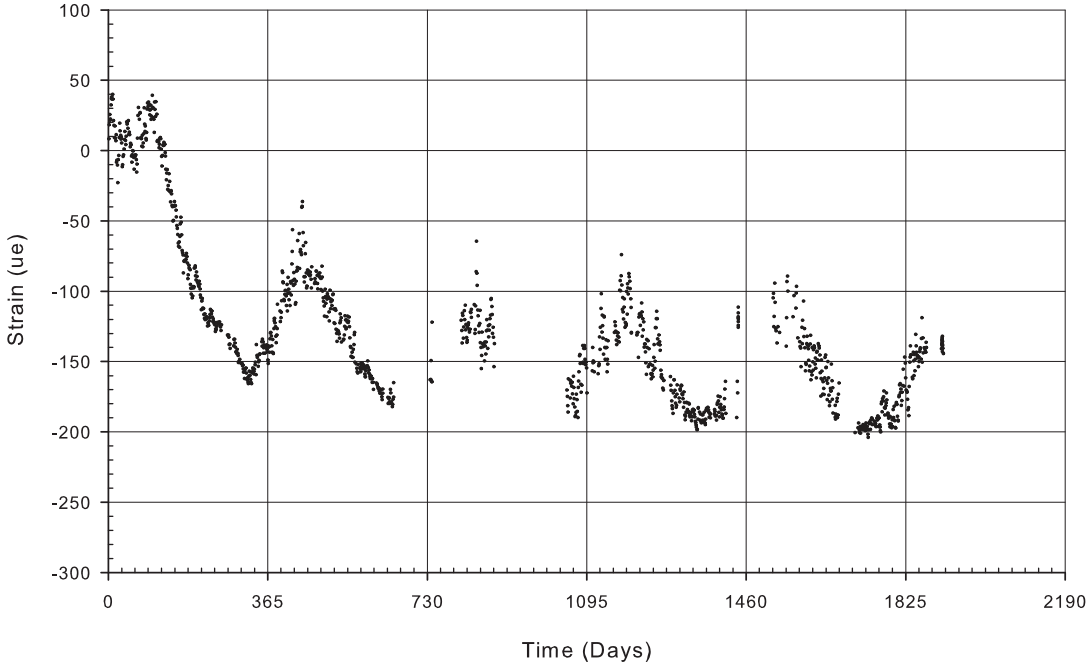
100
50
0
-50
-100
-150
-200
-250
-300
Strain (ue)
0
365
730
1095
1460
1825
2190
Time (Days)

B-CW

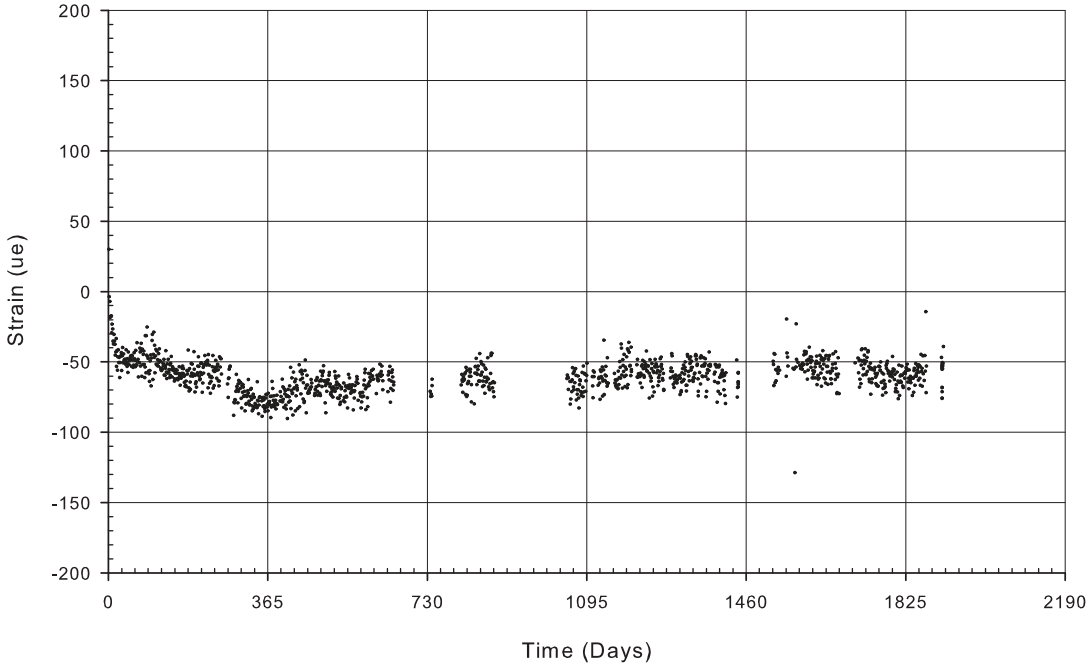
200
150
100
50
0
-50
-100
-150
-200
Strain (ue)
0
365
730
1095
1460
1825
2190
Time (Days)

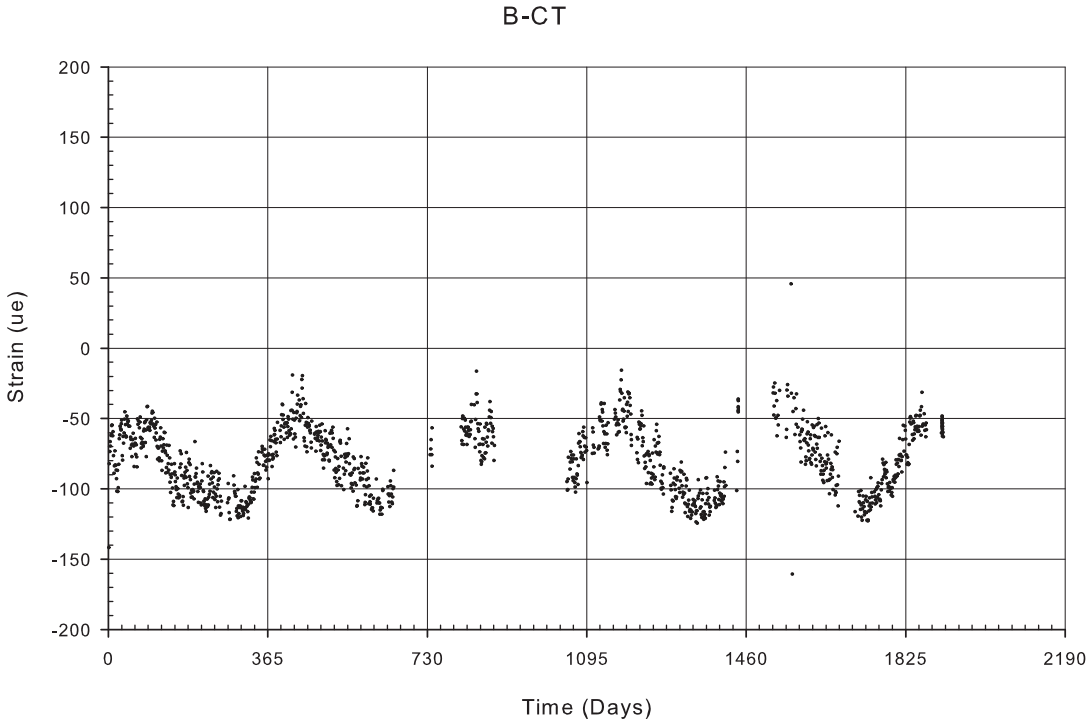
B-CT
Strain (ue)
200
150
100
50
0
-50
-100
-150
-200
0
365
730
1095
1460
1825
2190
Time (Days)

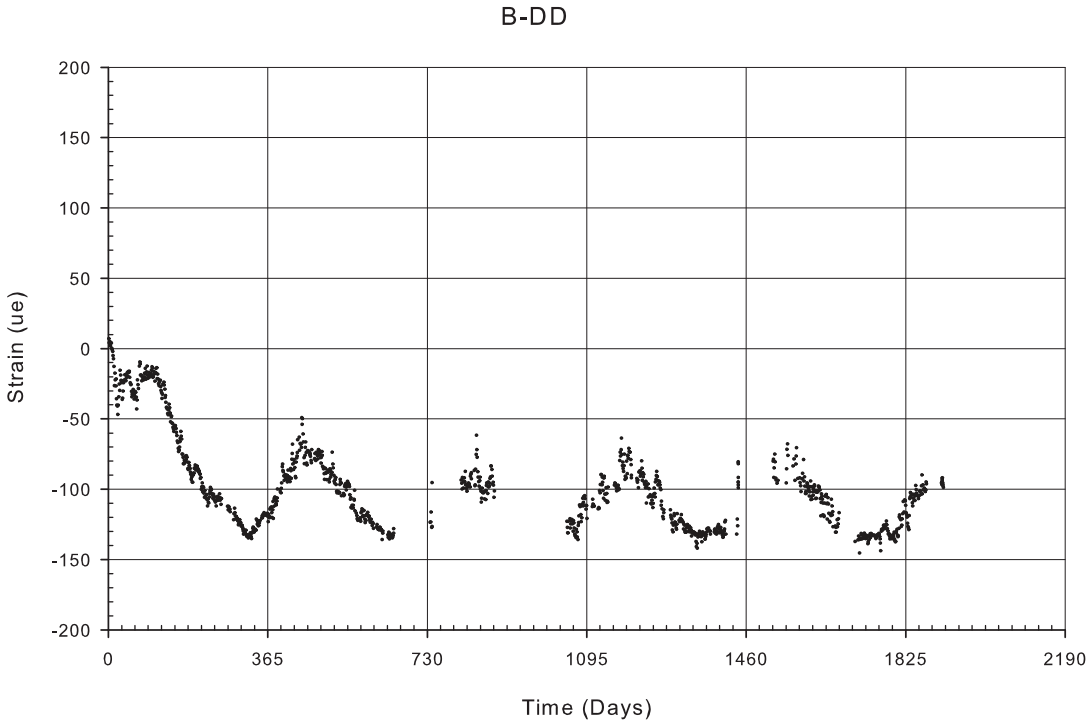
B-DD
Strain (ue)
200
150
100
50
0
-50
-100
-150
-200
0
365
730
1095
1460
1825
2190
Time (Days)

B-DT

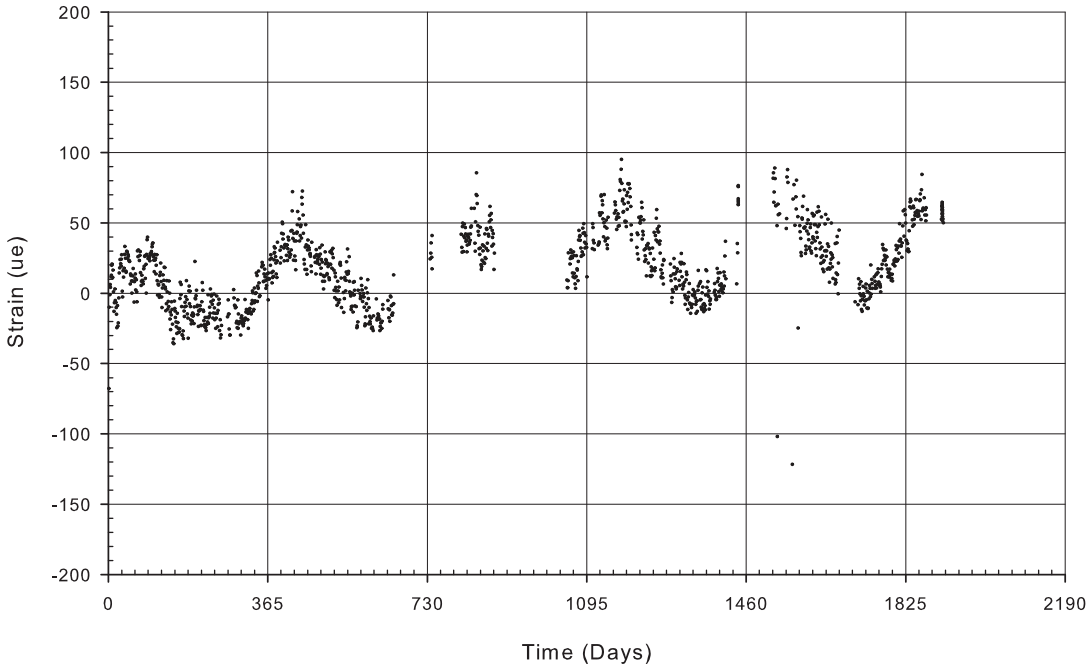
200
150
100
50
0
-50
-100
-150
-200
Strain (ue)
0
365
730
1095
1460
1825
2190
Time (Days)

B-XL1

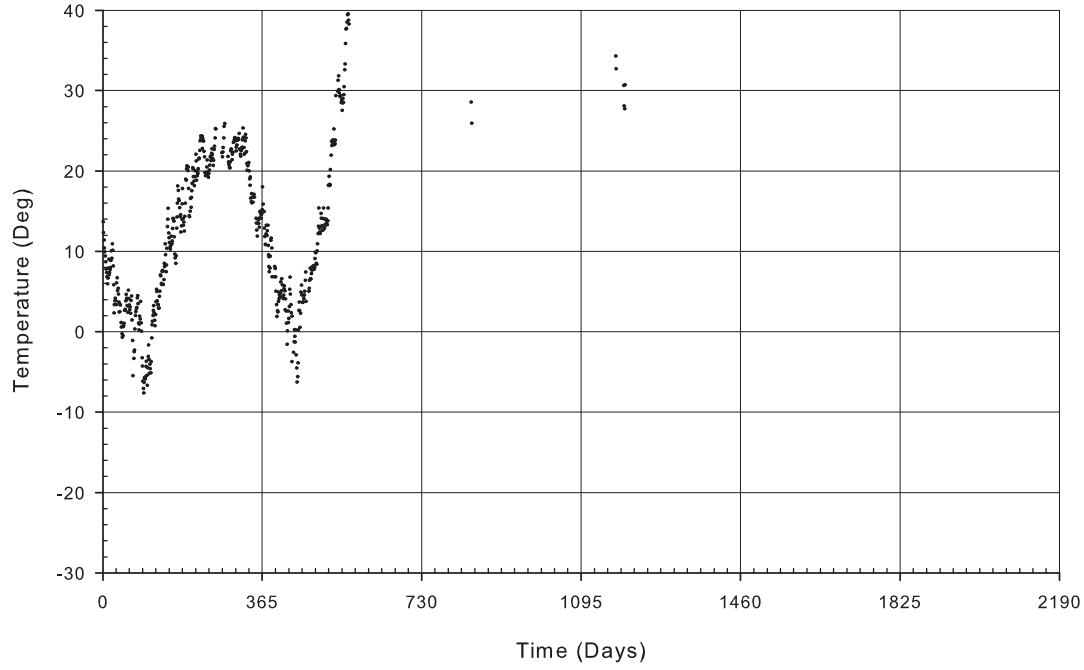
40
30
20
10
0
-10
-20
-30
Temperature (Deg)
0
365
730
1095
1460
1825
2190
Time (Days)

B-XL2

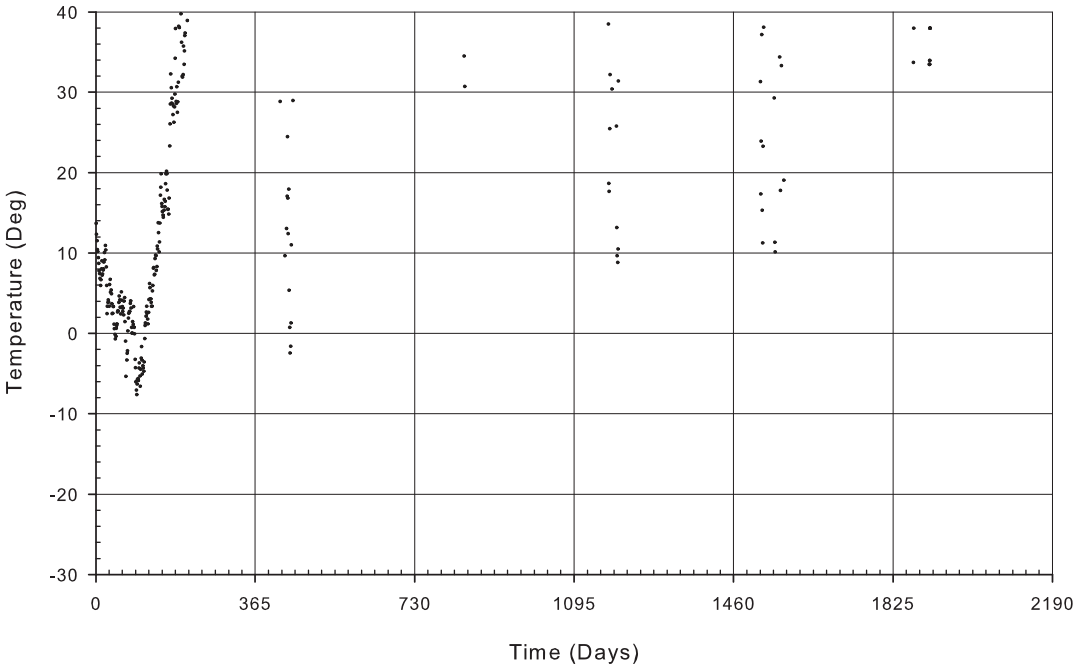
40
30
20
10
0
-10
-20
-30
Temperature (Deg)
0
365
730
1095
1460
1825
2190
Time (Days)

B-XL3

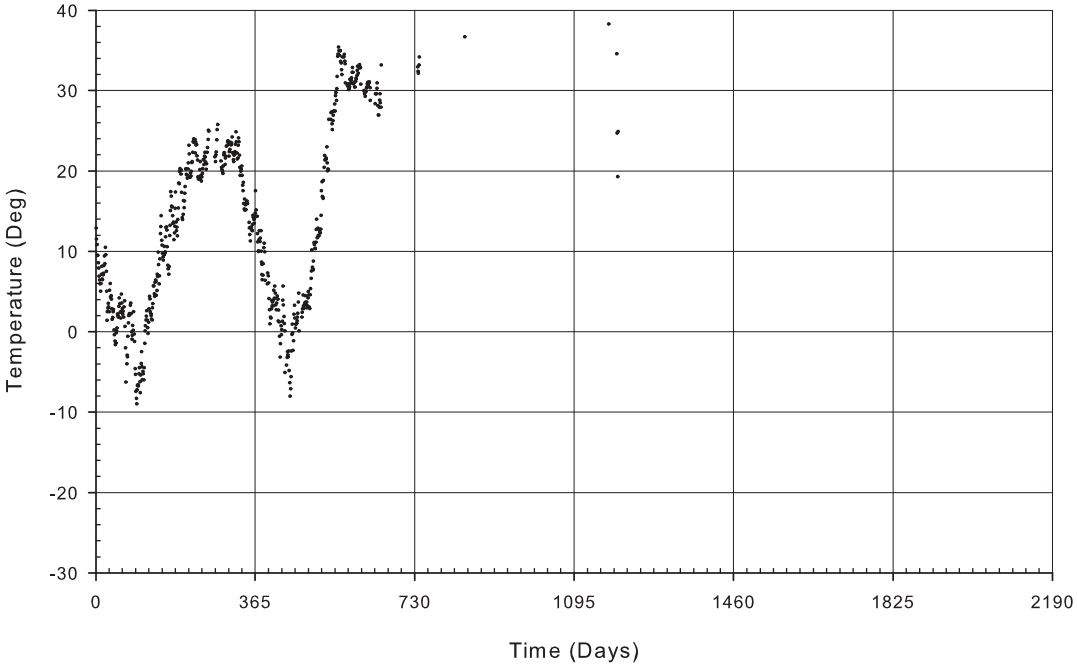
40
30
20
10
0
-10
-20
-30
Temperature (Deg)
0
365
730
1095
1460
1825
2190
Time (Days)

B-XL4

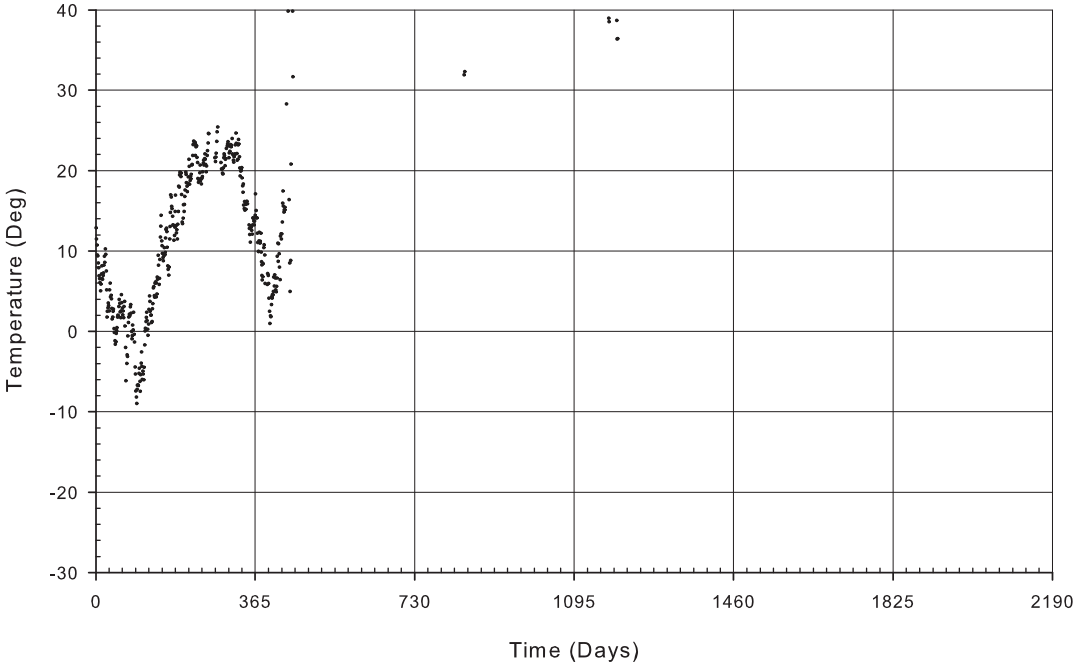
40
30
20
10
0
-10
-20
-30
Temperature (Deg)
0
365
730
1095
1460
1825
2190
Time (Days)

B-AB

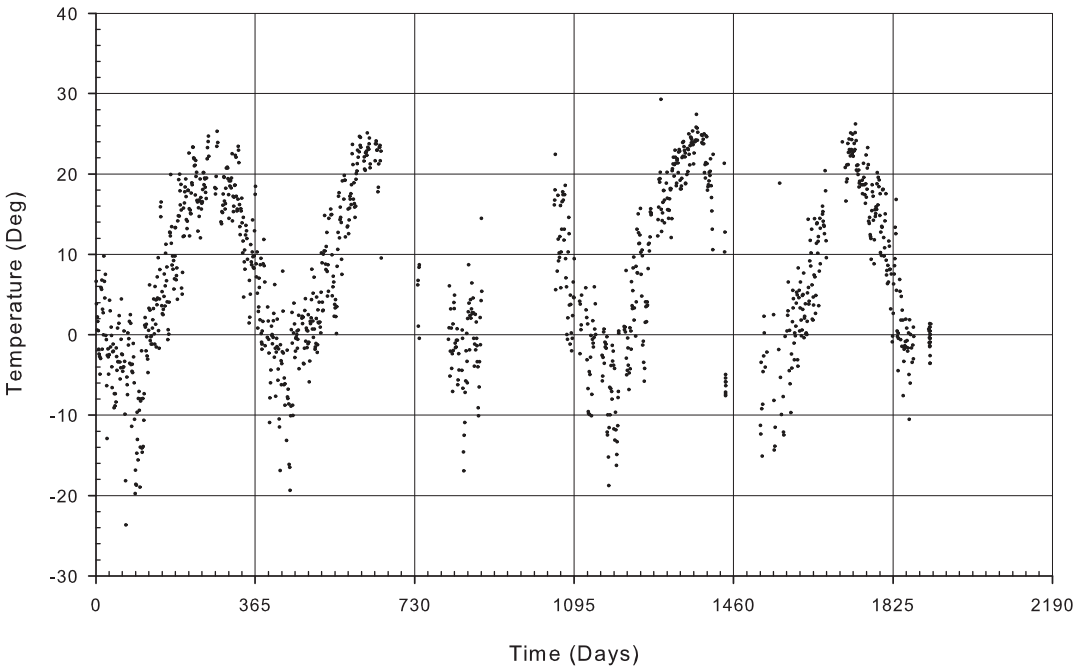
40
30
20
10
0
-10
-20
-30
Temperature (Deg)
0
365
730
1095
1460
1825
2190
Time (Days)

B-AW

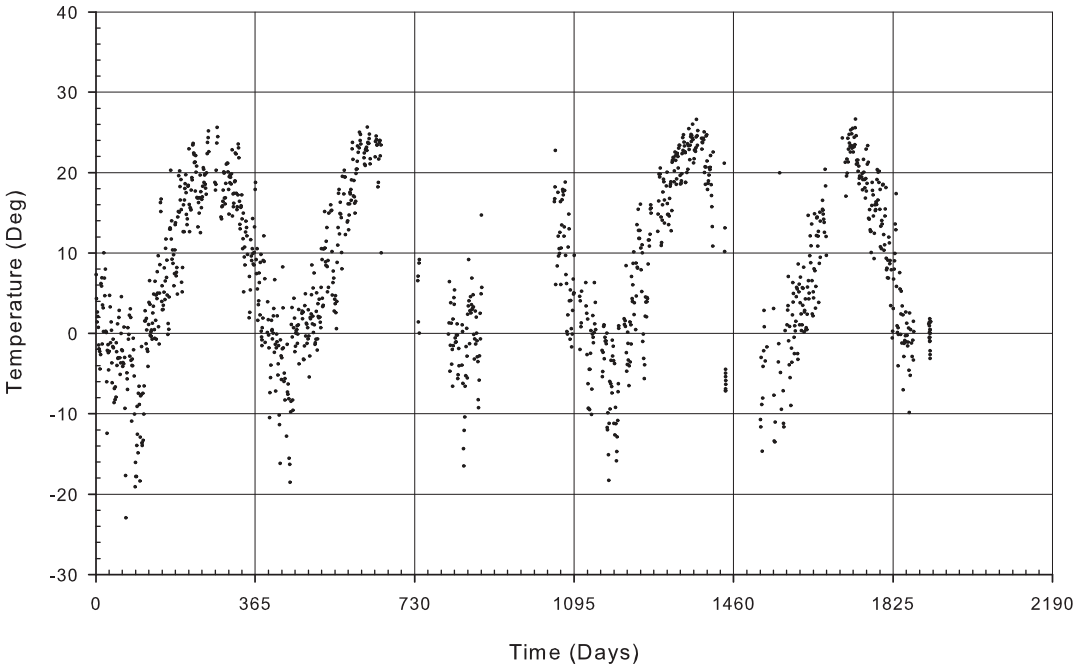
40
30
20
10
0
-10
-20
-30
Temperature (Deg)
0
365
730
1095
1460
1825
2190
Time (Days)

B-AT

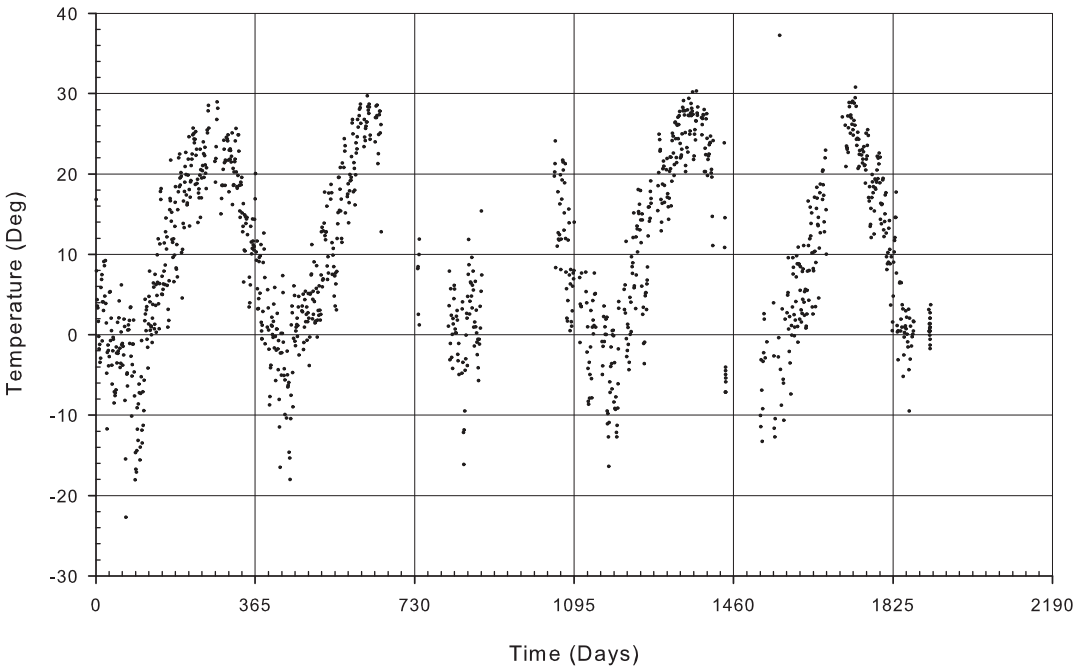
40
30
20
10
0
-10
-20
-30
Temperature (Deg)
0
365
730
1095
1460
1825
2190
Time (Days)

B-BB1

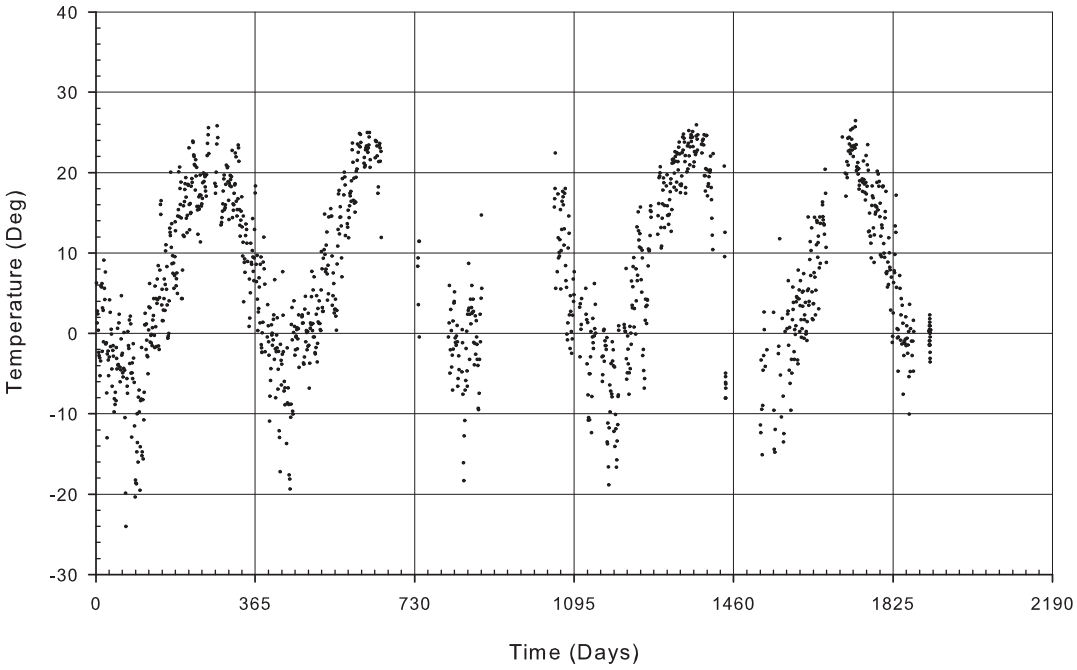
40
30
20
10
0
-10
-20
-30
Temperature (Deg)
0
365
730
1095
1460
1825
2190
Time (Days)

B-BB2

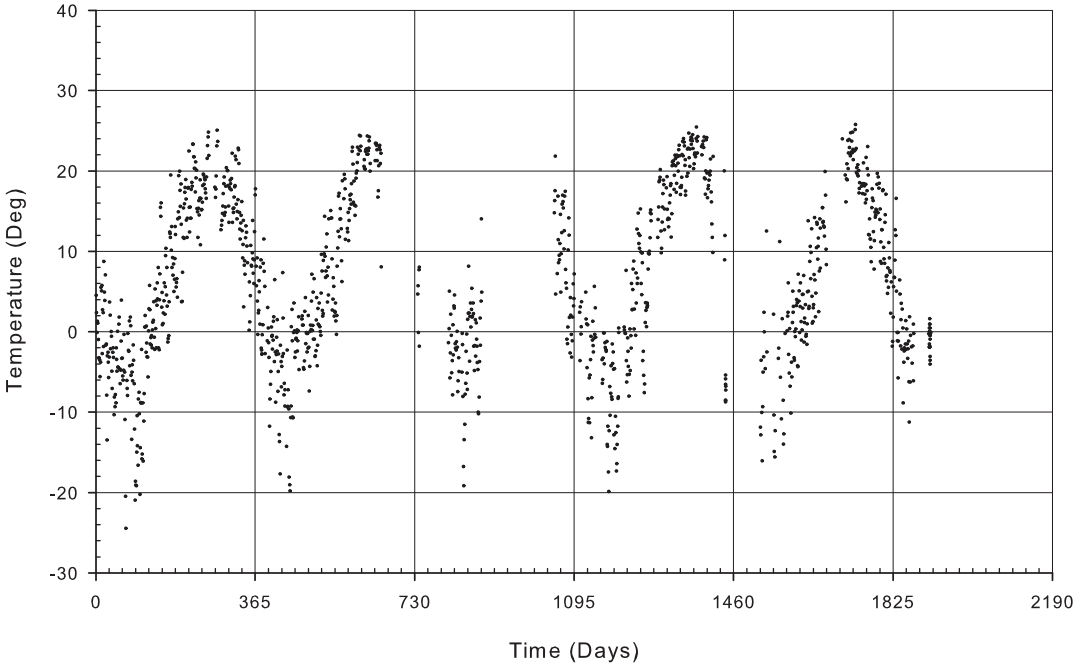
40
30
20
10
0
-10
-20
-30
Temperature (Deg)
0
365
730
1095
1460
1825
2190
Time (Days)

B-BW

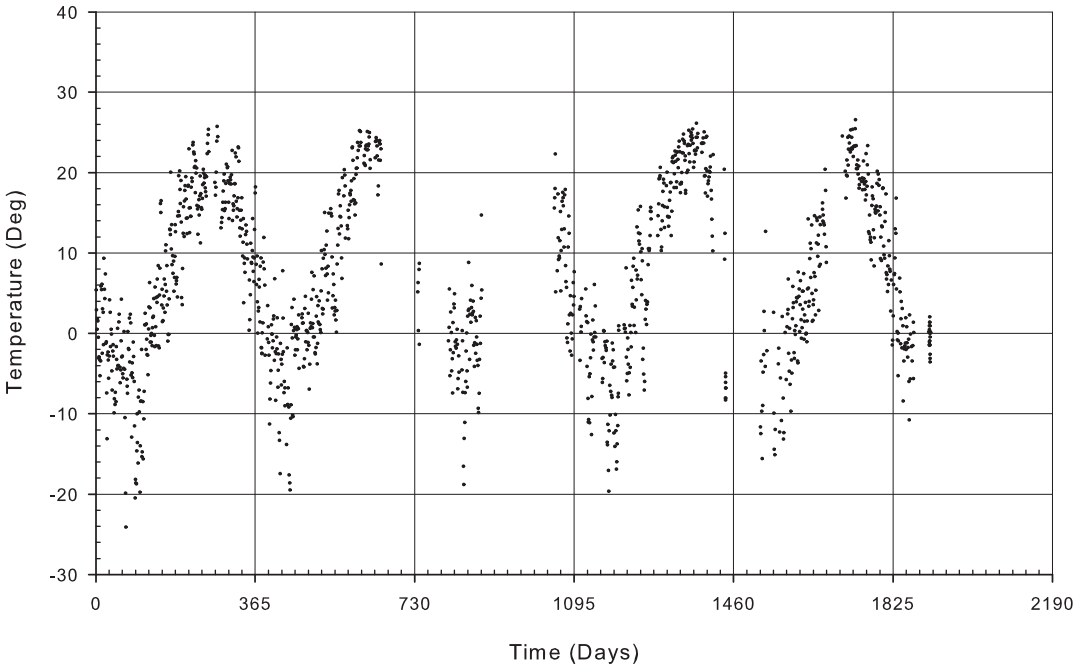
40
30
20
10
0
-10
-20
-30
Temperature (Deg)
0
365
730
1095
1460
1825
2190
Time (Days)

B-BT

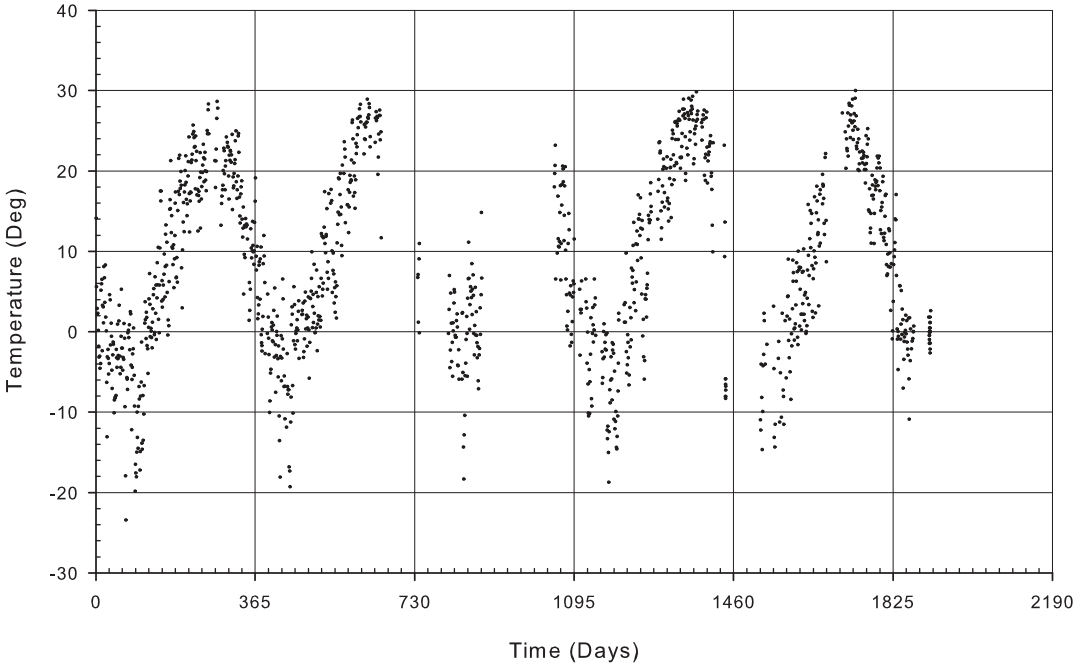
40
30
20
10
0
-10
-20
-30
Temperature (Deg)
0
365
730
1095
1460
1825
2190
Time (Days)

B-CD

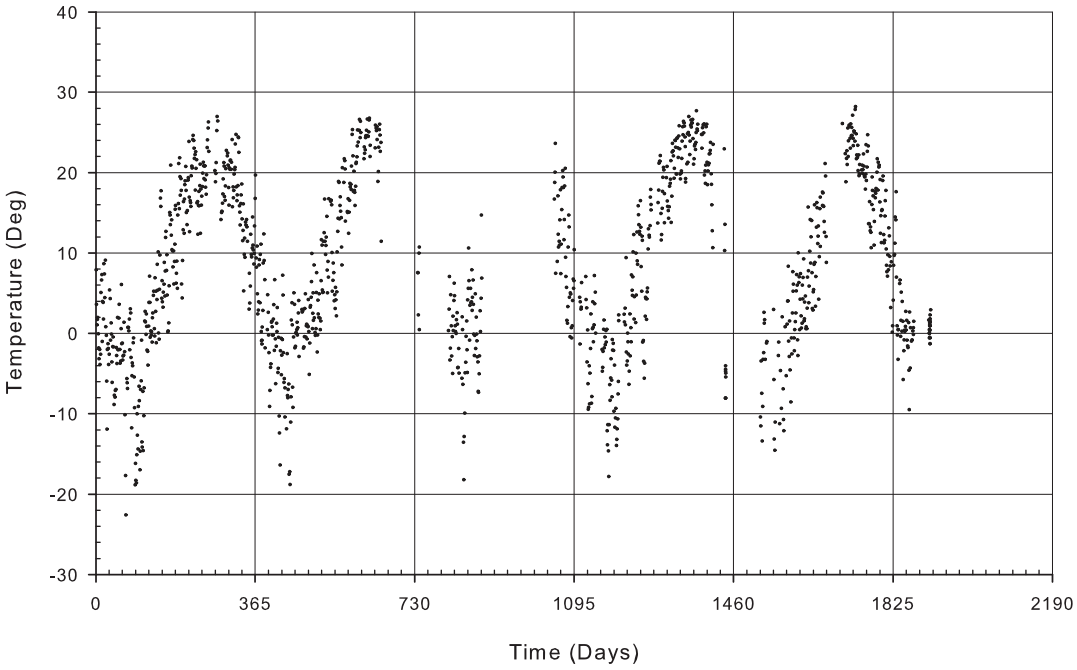
40
30
20
10
0
-10
-20
-30
Temperature (Deg)
0
365
730
1095
1460
1825
2190
Time (Days)

B-CW

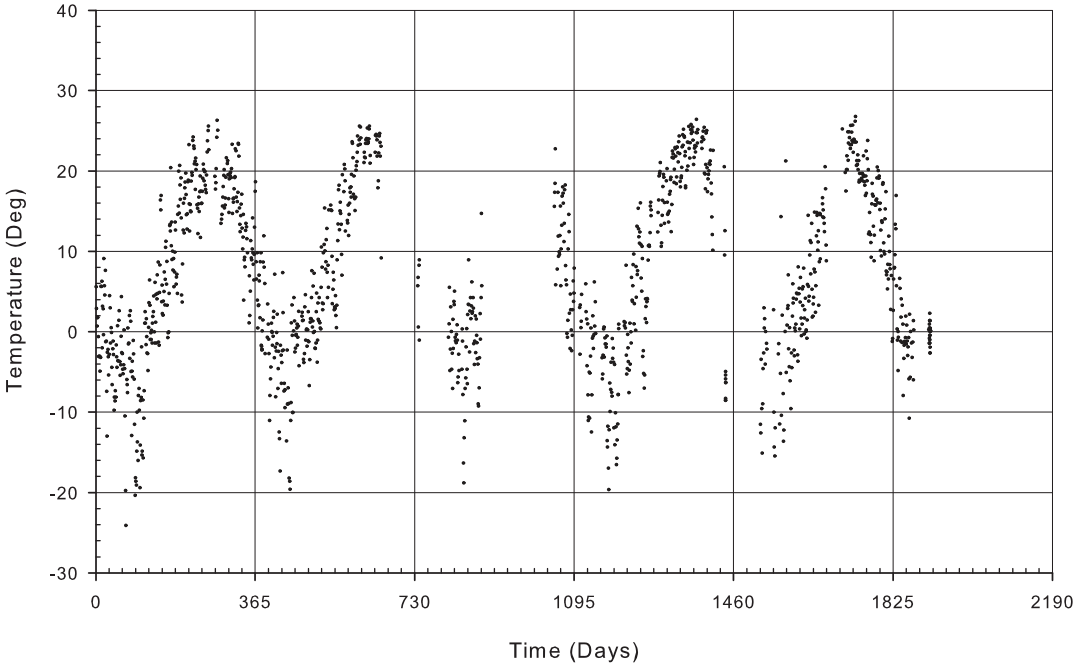
40
30
20
10
0
-10
-20
-30
Temperature (Deg)
0
365
730
1095
1460
1825
2190
Time (Days)

B-CT

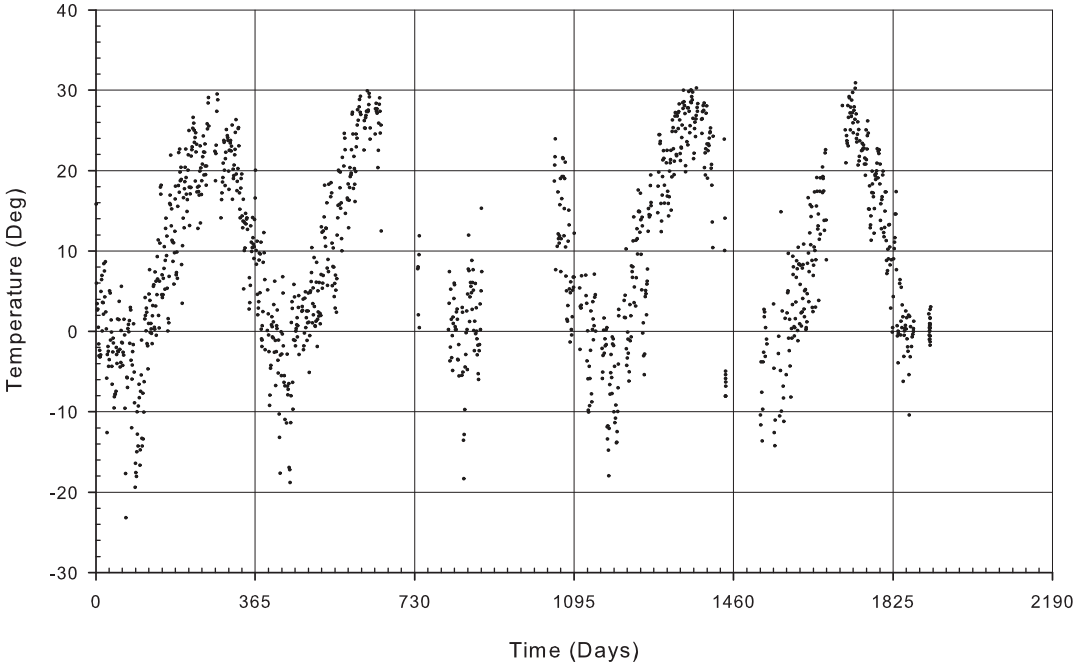
40
30
20
10
0
-10
-20
-30
Temperature (Deg)
0
365
730
1095
1460
1825
2190
Time (Days)

B-DD

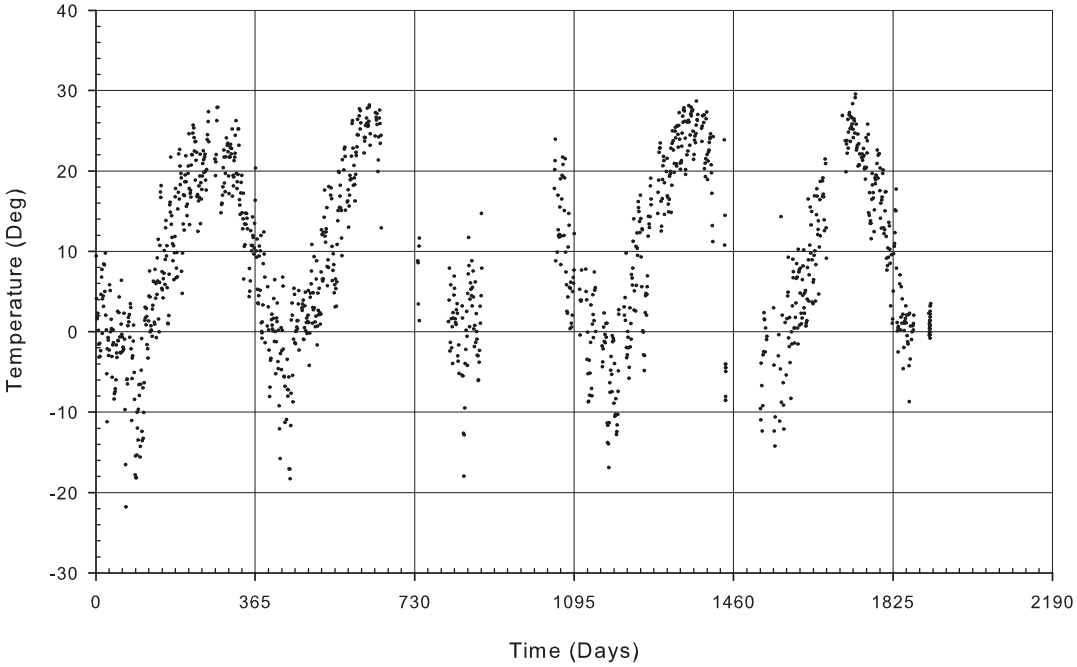
40
30
20
10
0
-10
-20
-30
Temperature (Deg)
0
365
730
1095
1460
1825
2190
Time (Days)

B-DT

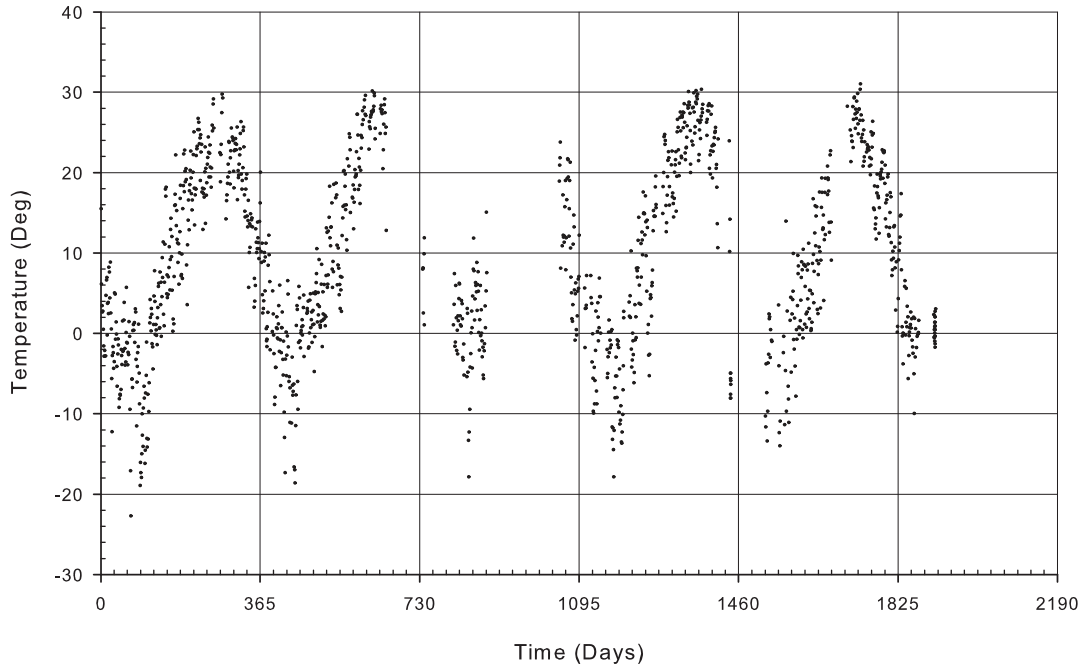
40
30
20
10
0
-10
-20
-30
Temperature (Deg)
0
365
730
1095
1460
1825
2190
Time (Days)

B-ED

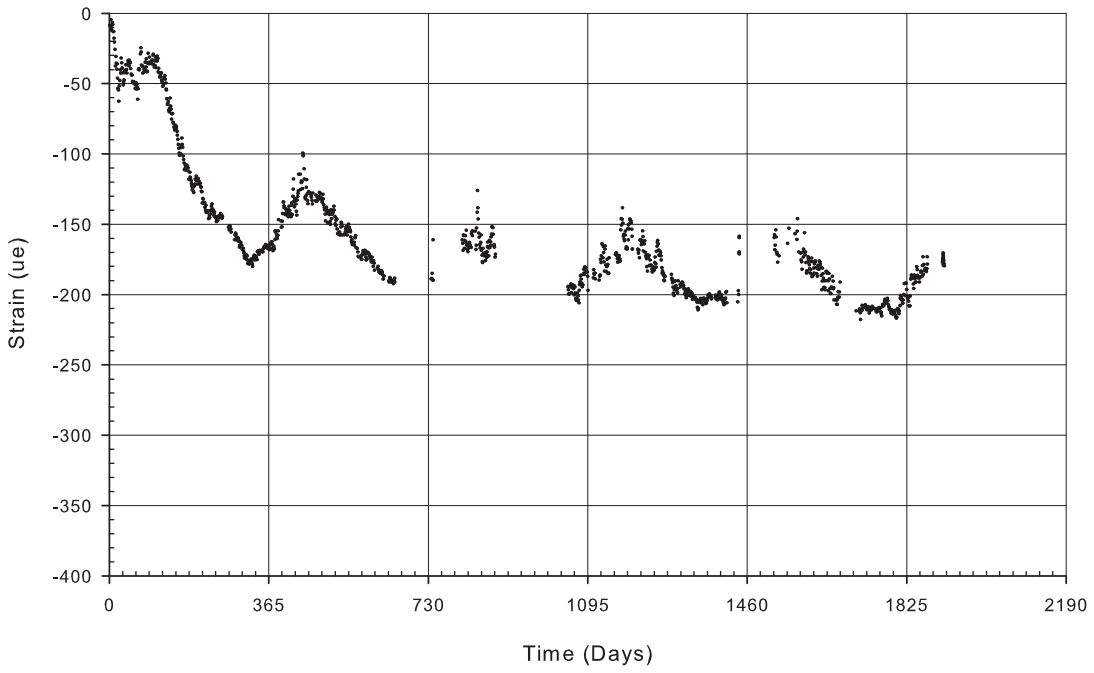
0
-50
-100
-150
-200
-250
-300
-350
-400
Strain (ue)
0
365
730
1095
1460
1825
2190
Time (Days)

B-ET

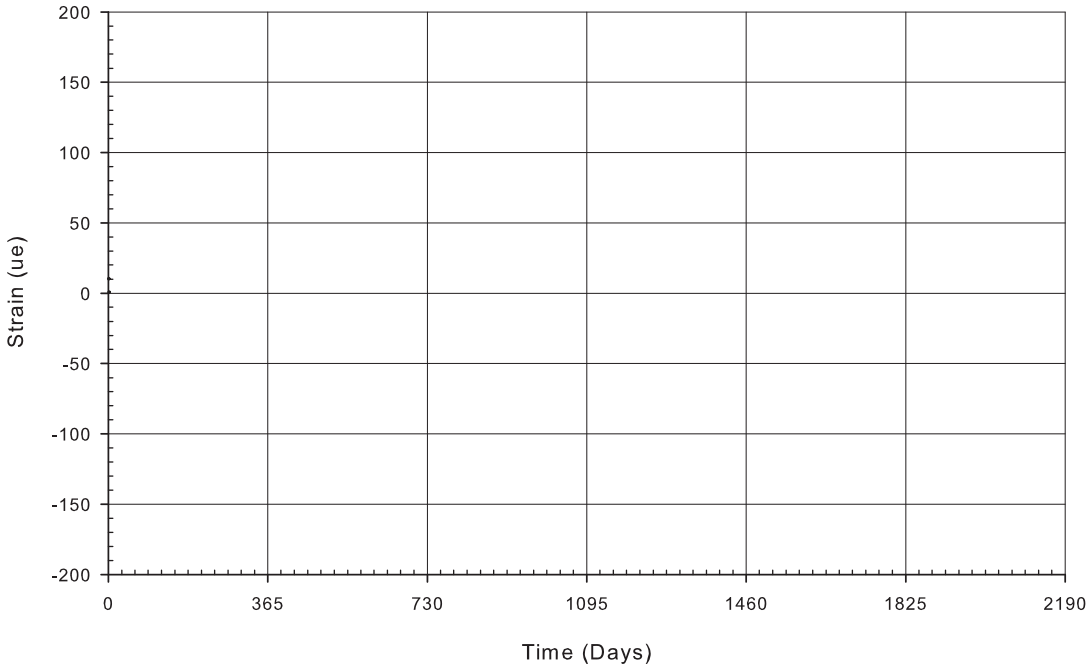
200
150
100
50
0
-50
-100
-150
-200
Strain (ue)
0
365
730
1095
1460
1825
2190
Time (Days)

B-FD1

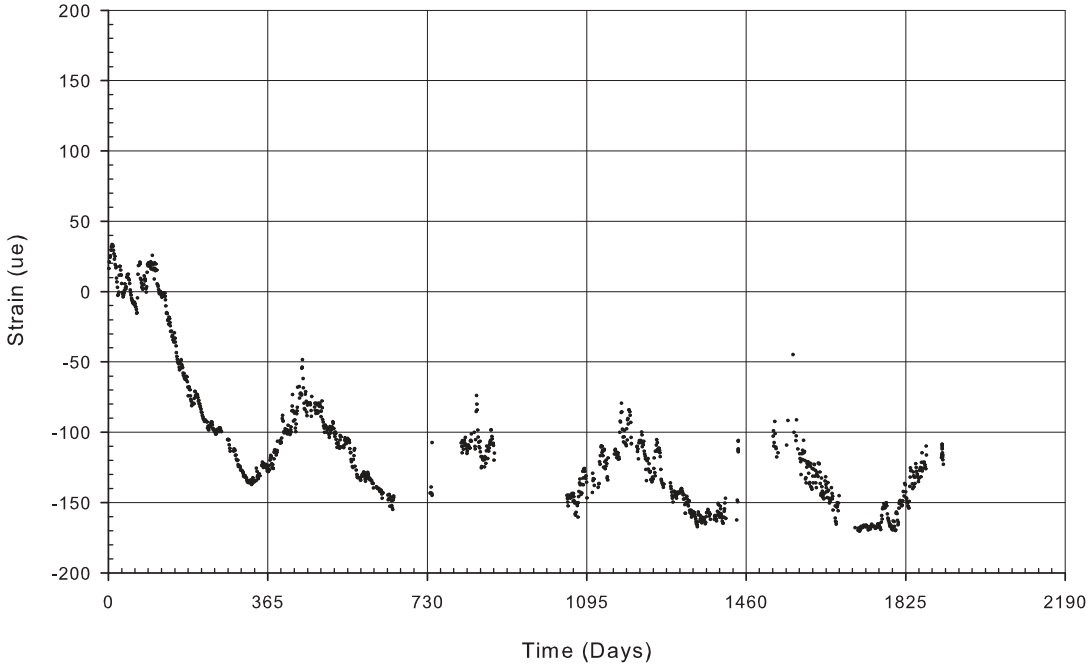
200
150
100
50
0
-50
-100
-150
-200
Strain (ue)
0
365
730
1095
1460
1825
2190
Time (Days)

B-FD2

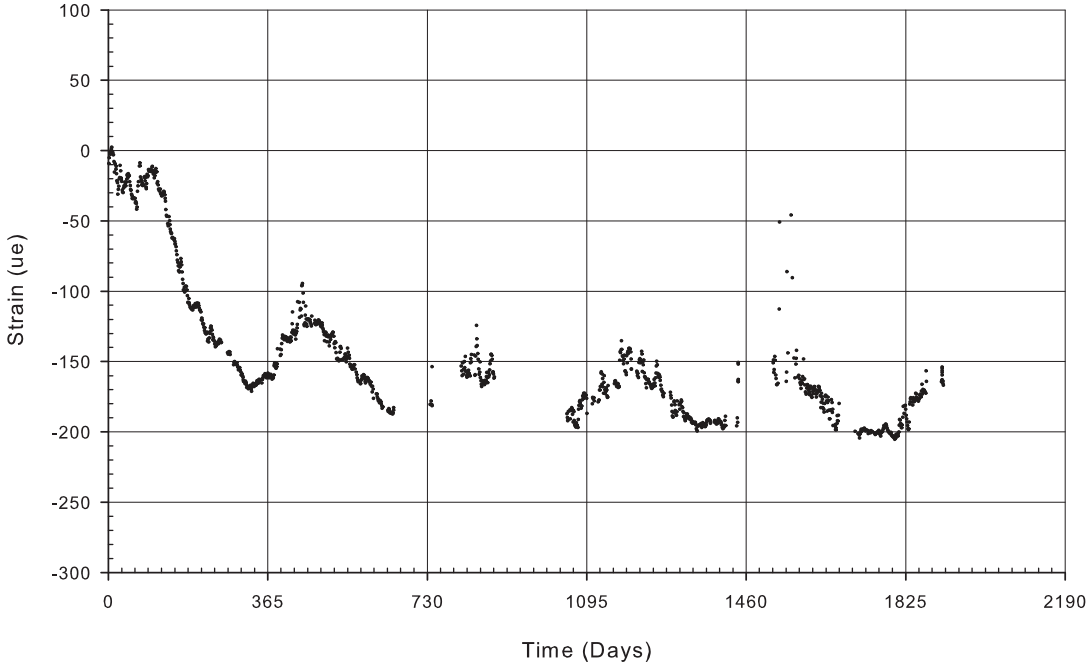
100
50
0
-50
-100
-150
-200
-250
-300
Strain (ue)
0
365
730
1095
1460
1825
2190
Time (Days)

B-FW1

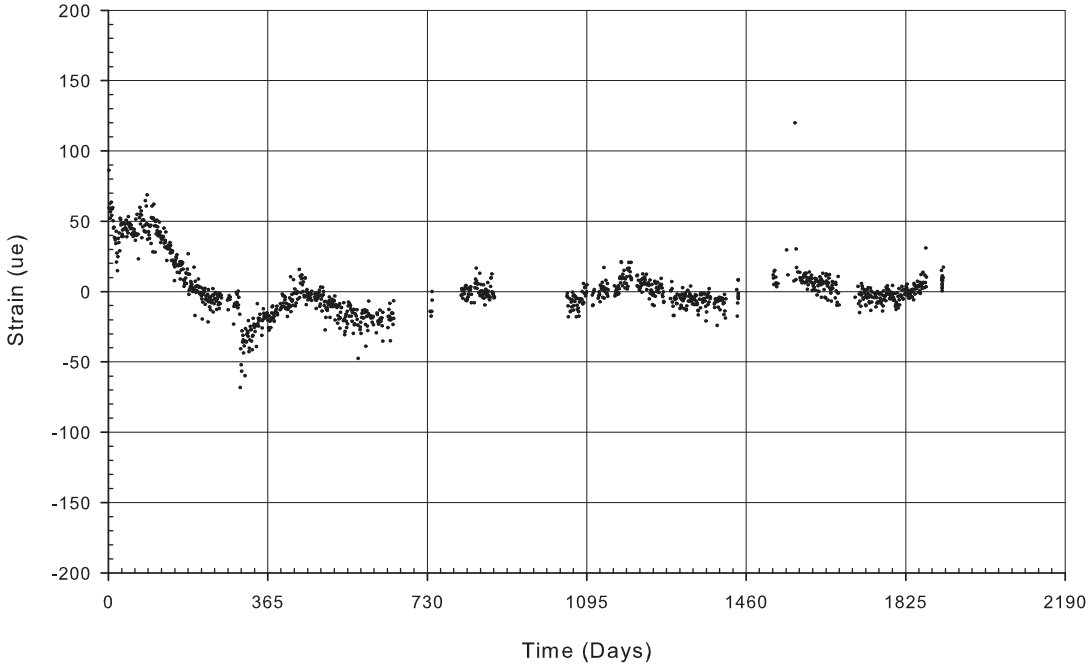
200
150
100
50
0
-50
-100
-150
-200
Strain (ue)
0
365
730
1095
1460
1825
2190
Time (Days)

B-FW2

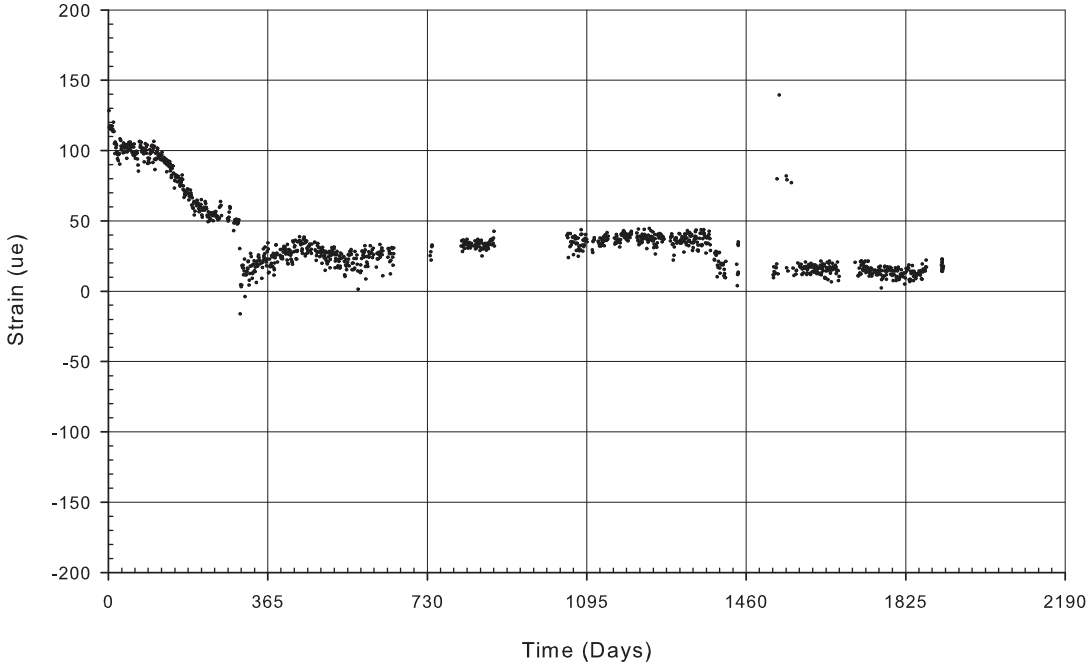
200
150
100
50
0
-50
-100
-150
-200
Strain (ue)
0
365
730
1095
1460
1825
2190
Time (Days)

B-FT1

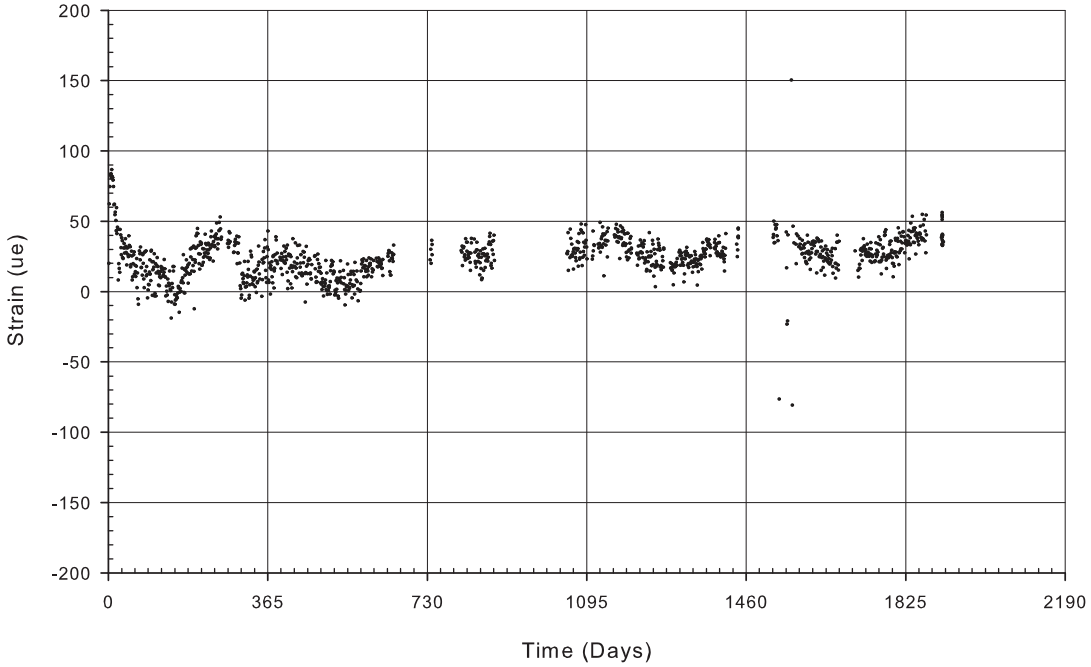
200
150
100
50
0
-50
-100
-150
-200
Strain (ue)
0
365
730
1095
1460
1825
2190
Time (Days)

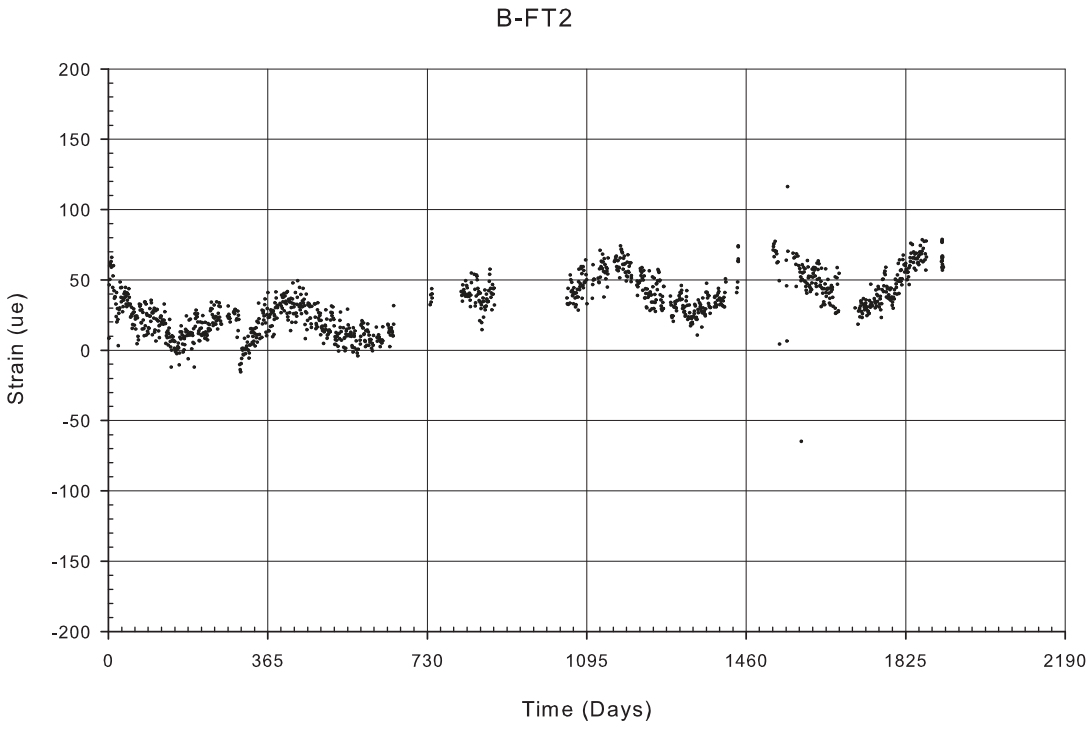
B-FT2
Strain (ue)
200
150
100
50
0
-50
-100
-150
-200
0
365
730
1095
1460
1825
2190
Time (Days)

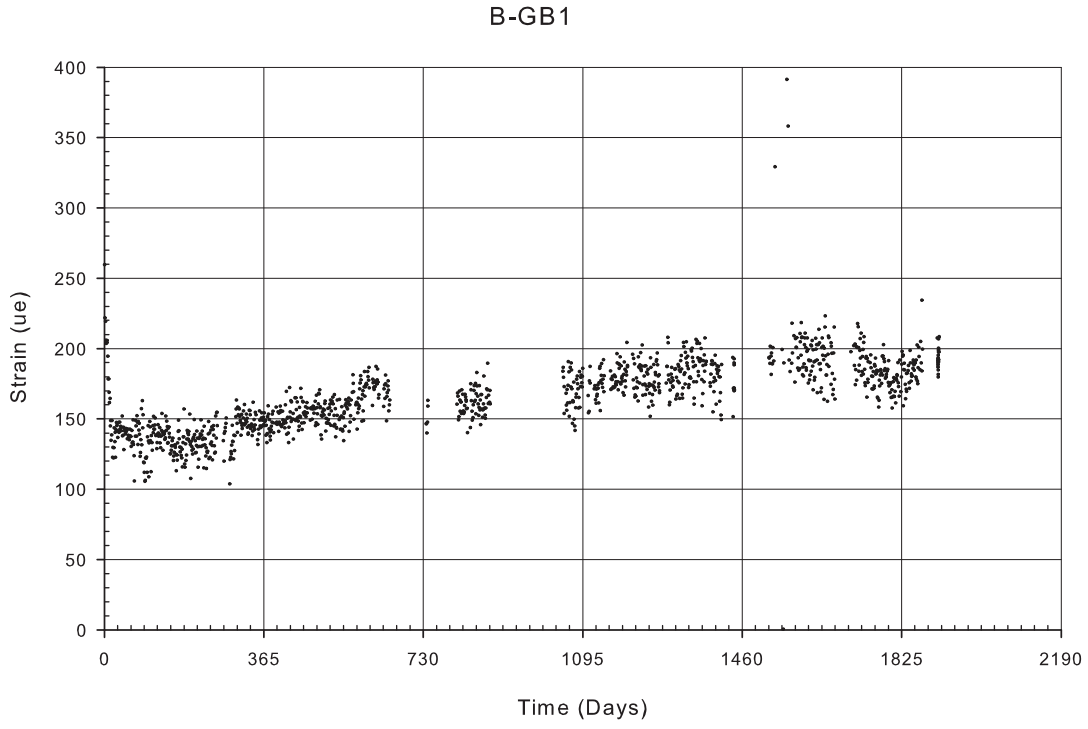
B-GB1
Strain (ue)
400
350
300
250
200
150
100
50
0
0
365
730
1095
1460
1825
2190
Time (Days)

B-GB2

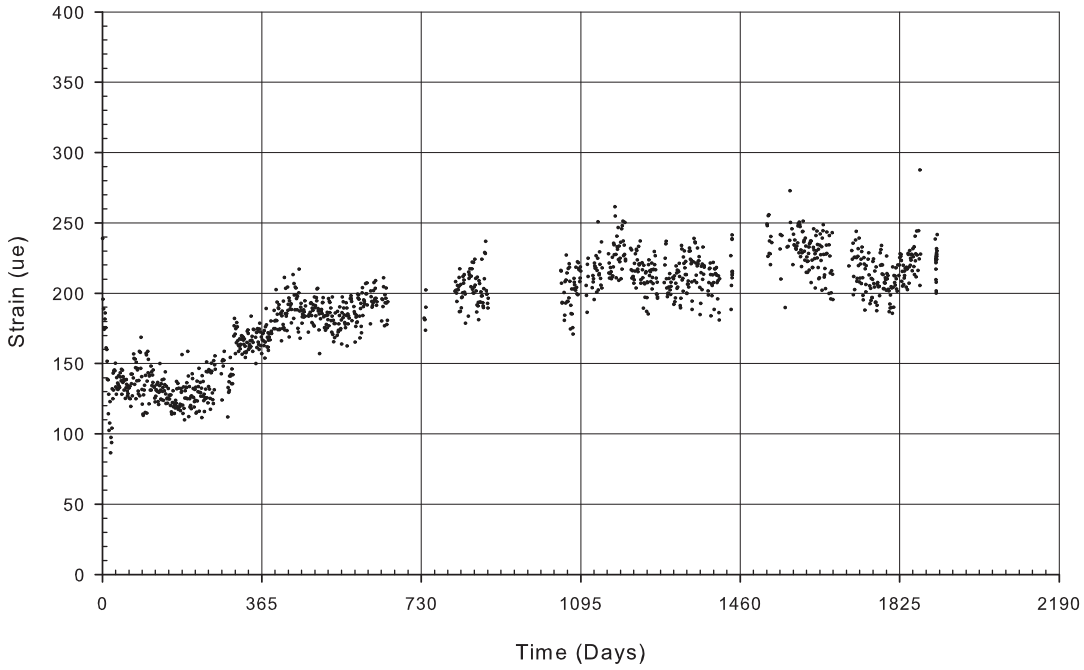
Strain (ue)
400
350
300
250
200
150
100
50
0
0
365
730
1095
1460
1825
2190
Time (Days)

B-GP1

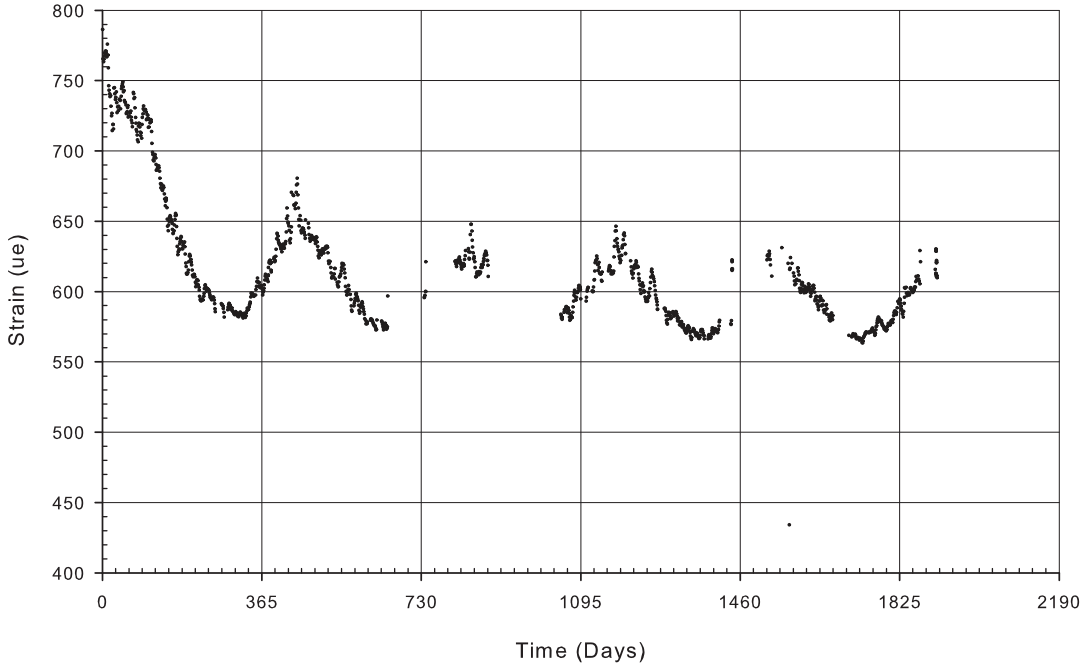
Strain (ue)
800
750
700
650
600
550
500
450
400
0
365
730
1095
1460
1825
2190
Time (Days)

B-GP2

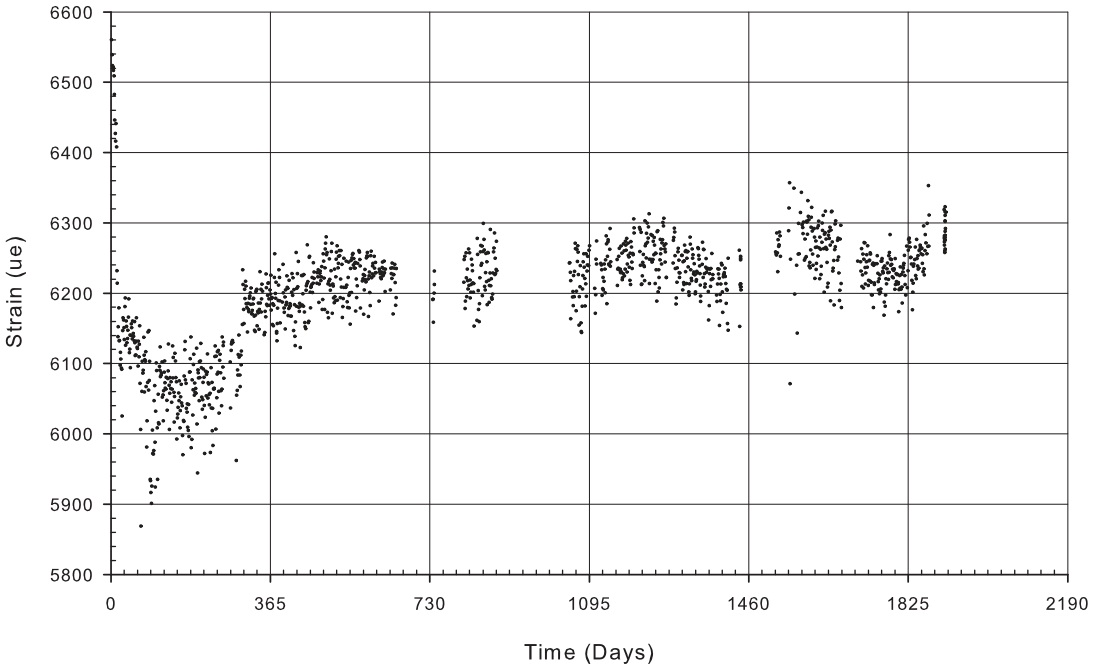
6600
6500
6400
6300
6200
6100
6000
5900
5800
Strain (ue)
0
365
730
1095
1460
1825
2190
Time (Days)

B-JB

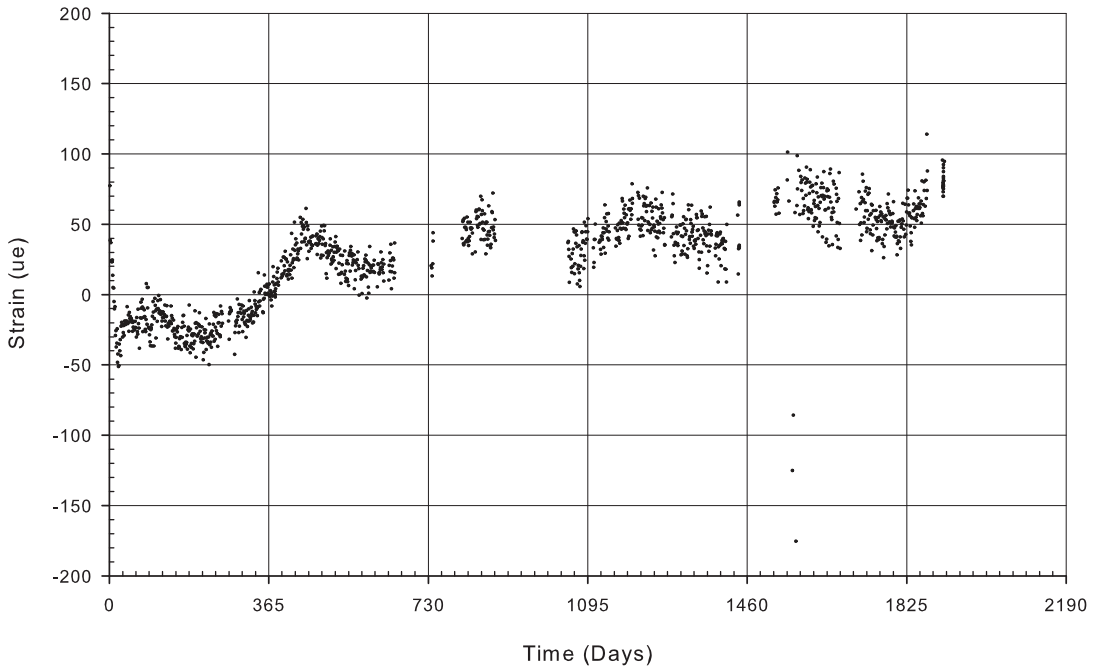
200
150
100
50
0
-50
-100
-150
-200
Strain (ue)
0
365
730
1095
1460
1825
2190
Time (Days)

B-JP

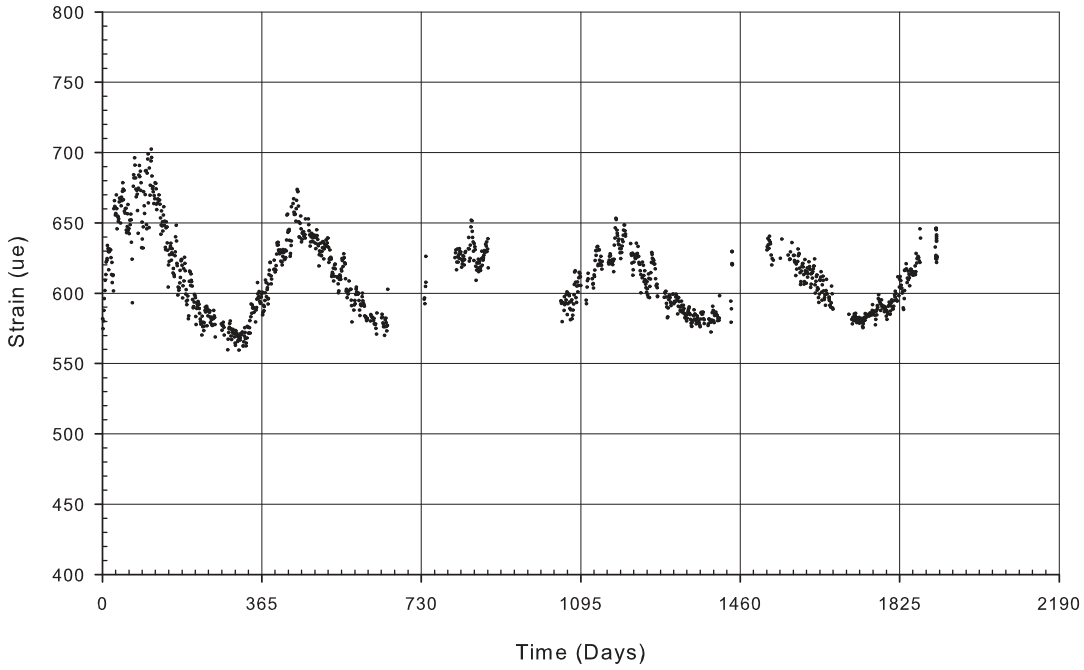
800
750
700
650
600
550
500
450
400
Strain (ue)
0
365
730
1095
1460
1825
2190
Time (Days)

B-KD

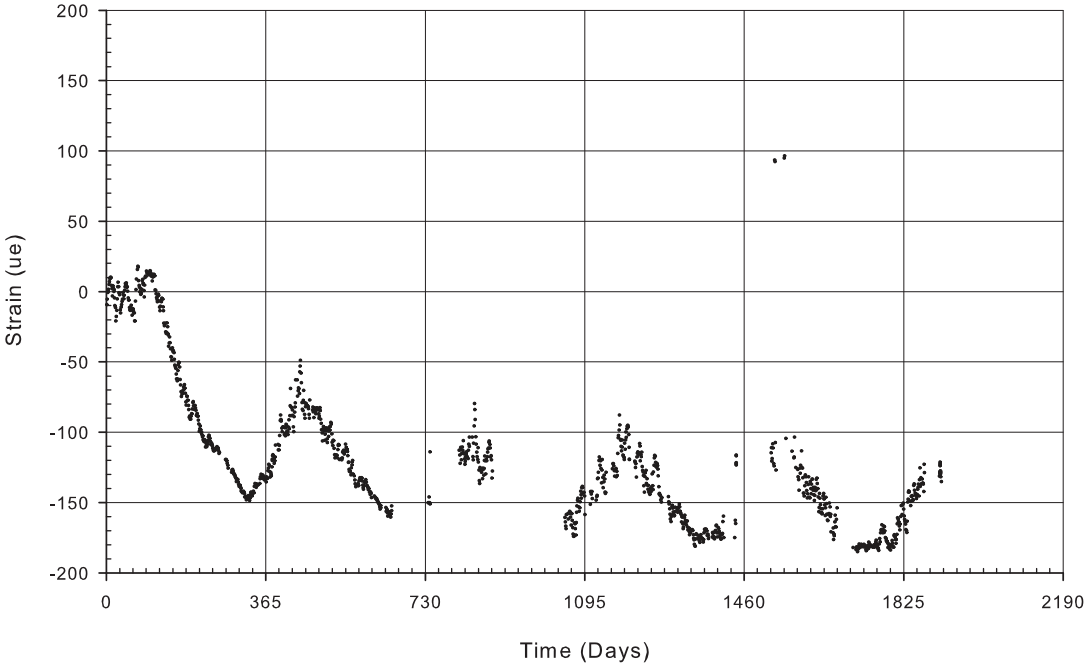
200
150
100
50
0
-50
-100
-150
-200
Strain (ue)
0
365
730
1095
1460
1825
2190
Time (Days)

B-HP7

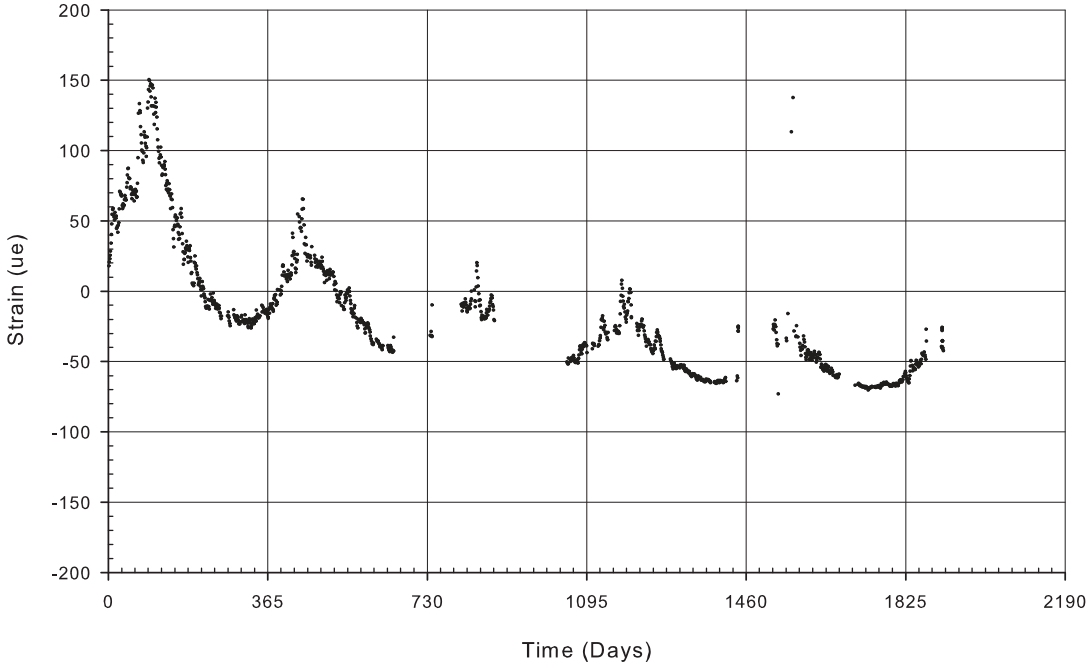
200
150
100
50
0
-50
-100
-150
-200
Strain (ue)
0
365
730
1095
1460
1825
2190
Time (Days)

B-ED

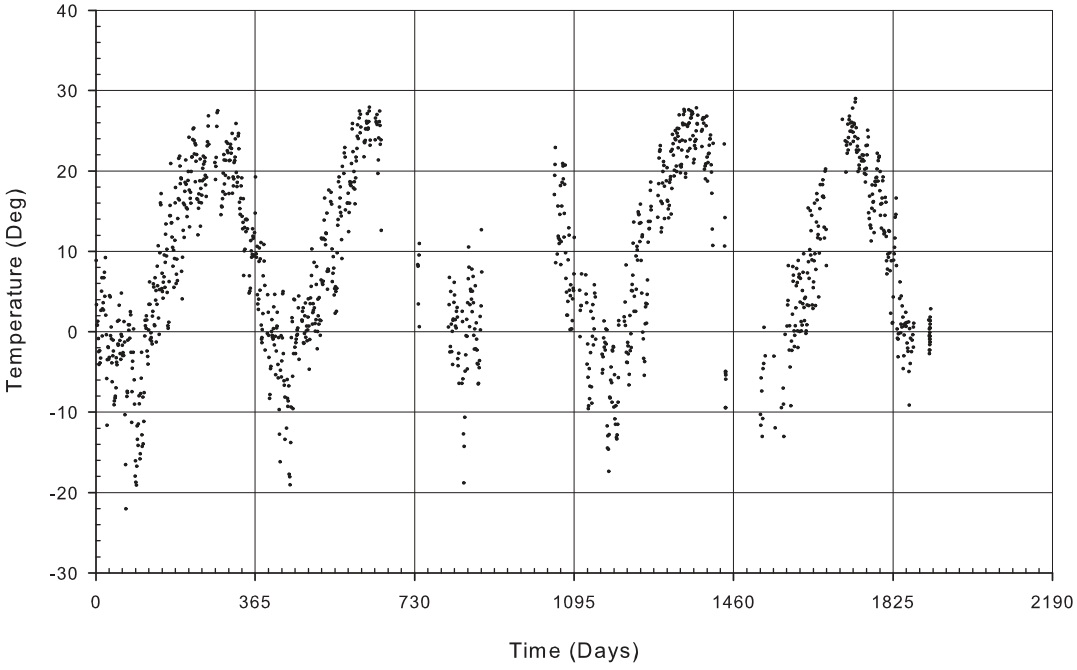
40
30
20
10
0
-10
-20
-30
Temperature (Deg)
0
365
730
1095
1460
1825
2190
Time (Days)

B-ET

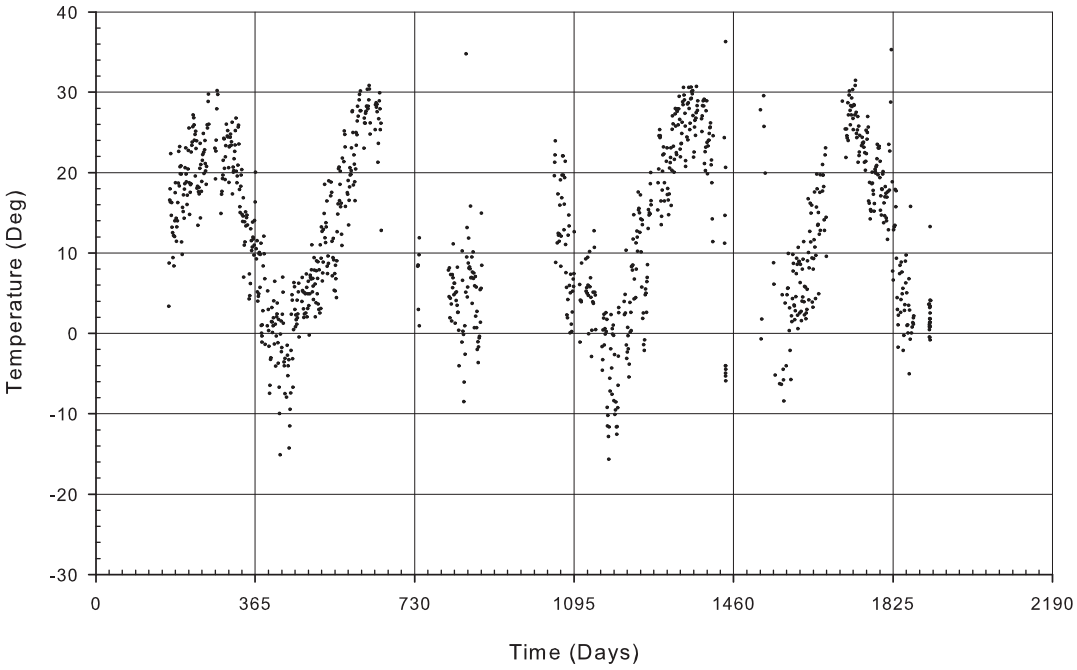
40
30
20
10
0
-10
-20
-30
Temperature (Deg)
0
365
730
1095
1460
1825
2190
Time (Days)

B-FD1

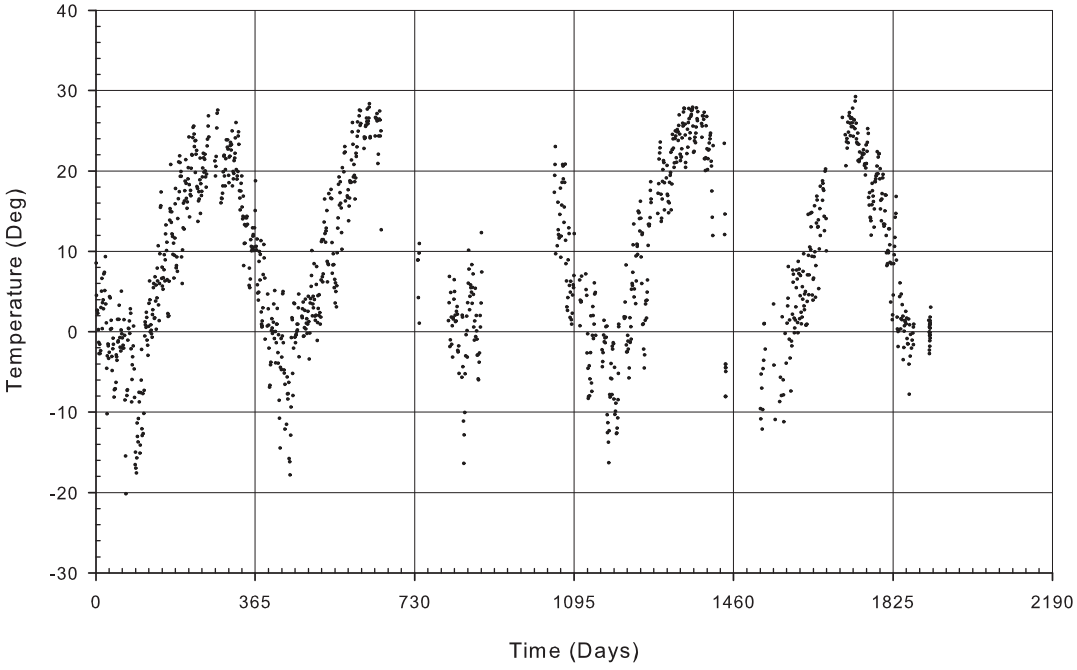
40
30
20
10
0
-10
-20
-30
Temperature (Deg)
0
365
730
1095
1460
1825
2190
Time (Days)

B-FD2

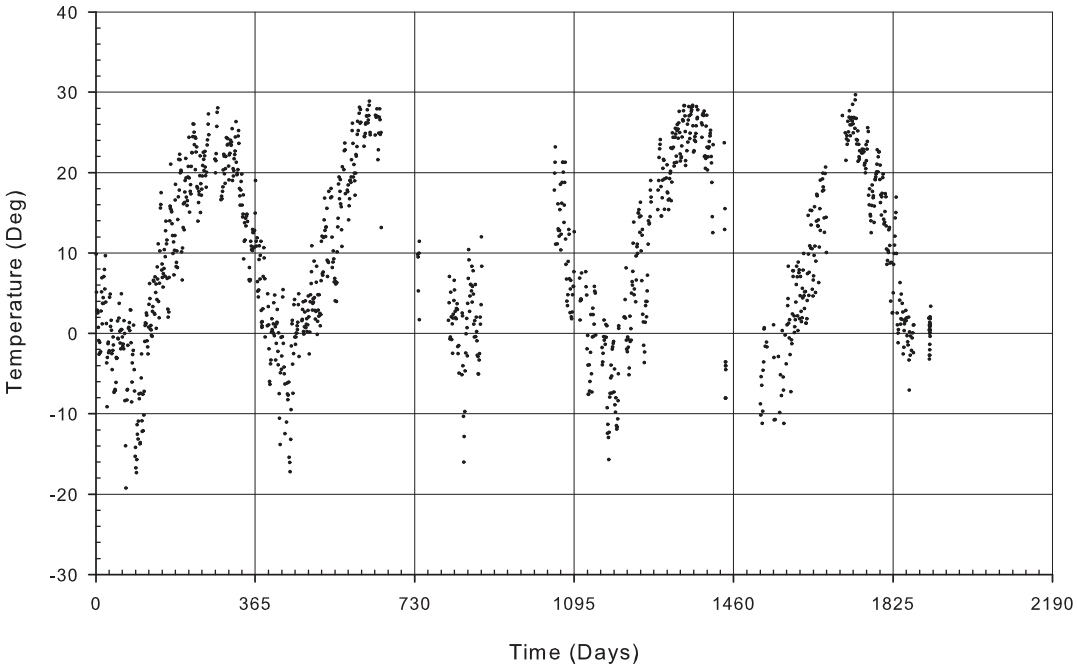
40
30
20
10
0
-10
-20
-30
Temperature (Deg)
0
365
730
1095
1460
1825
2190
Time (Days)

B-FW1

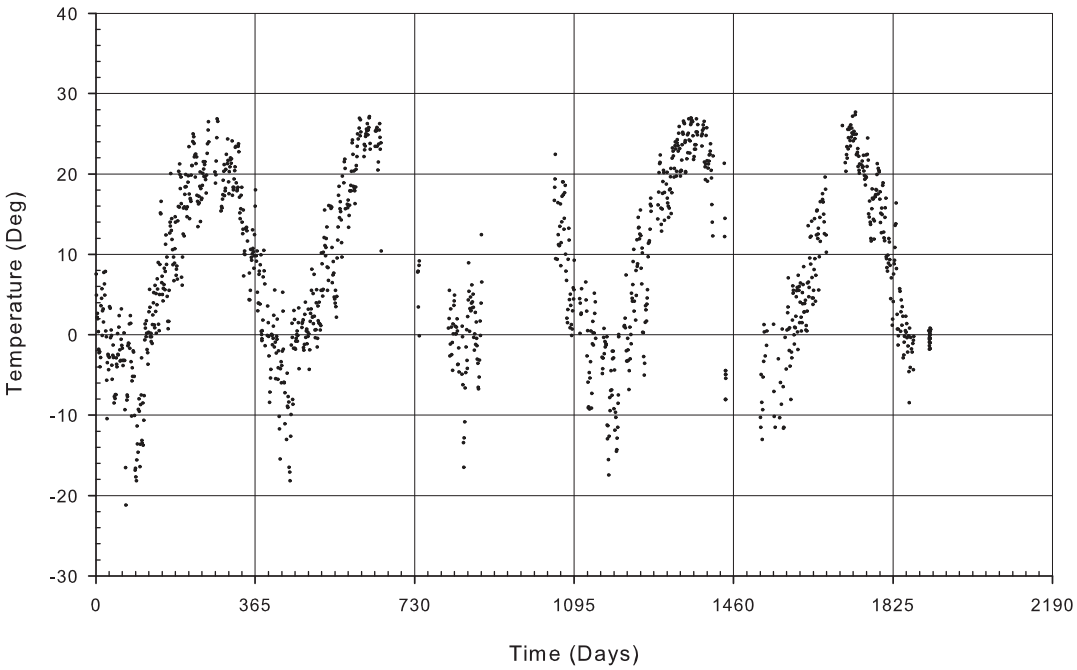
40
30
20
10
0
-10
-20
-30
Temperature (Deg)
0
365
730
1095
1460
1825
2190
Time (Days)

B-FW2

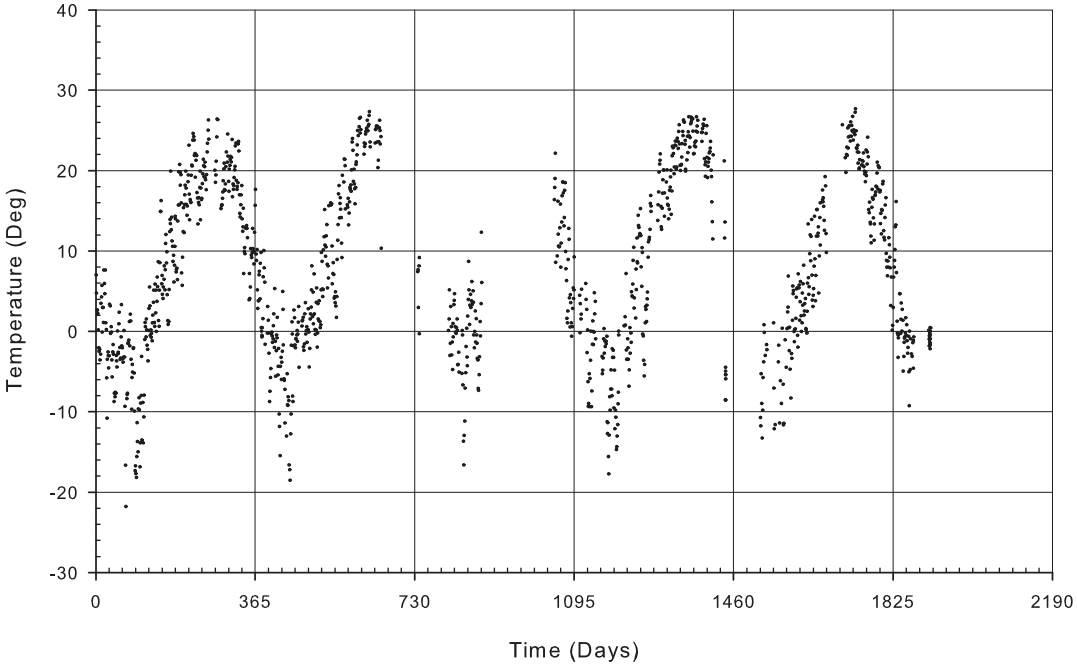
40
30
20
10
0
-10
-20
-30
Temperature (Deg)
0
365
730
1095
1460
1825
2190
Time (Days)

B-FT1

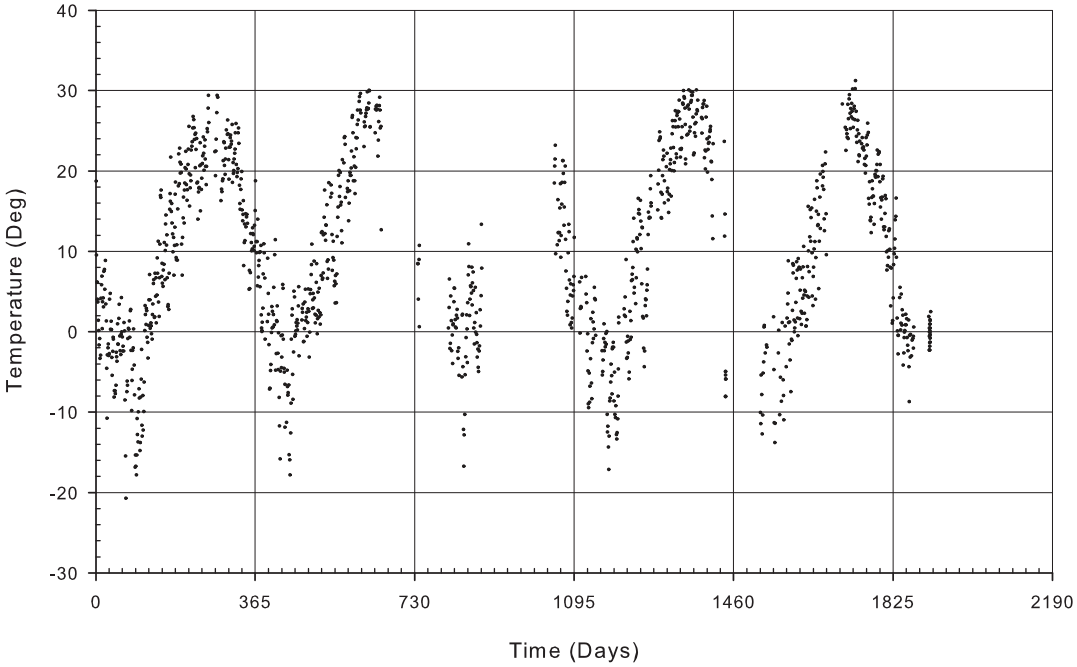
40
30
20
10
0
-10
-20
-30
Temperature (Deg)
0
365
730
1095
1460
1825
2190
Time (Days)

B-FT2

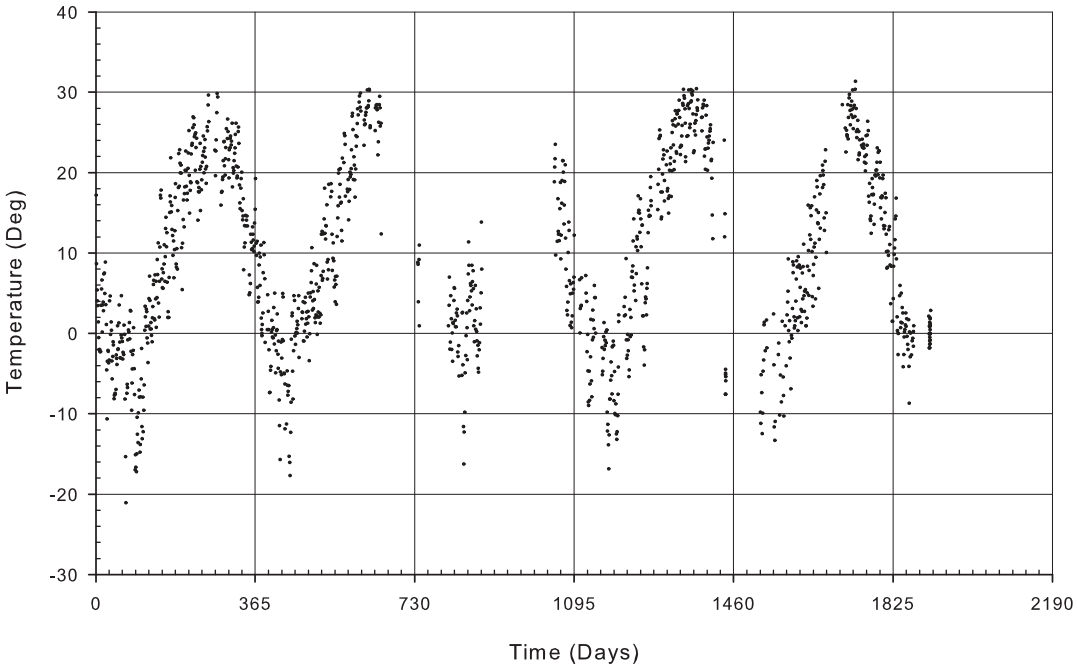
40
30
20
10
0
-10
-20
-30
Temperature (Deg)
0
365
730
1095
1460
1825
2190
Time (Days)

B-GB1

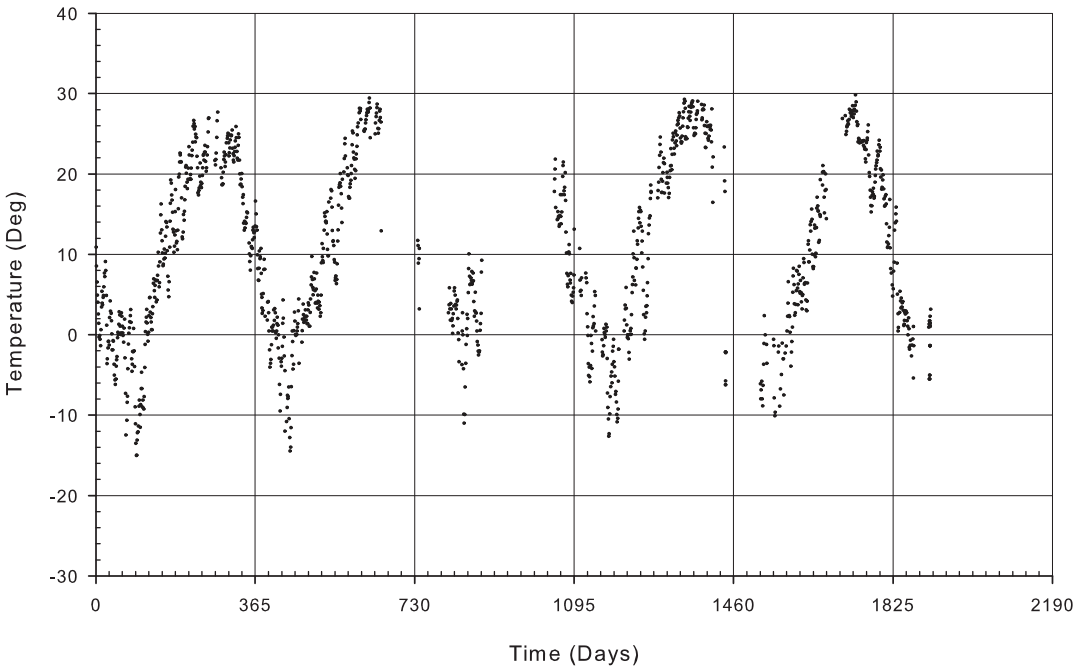
40
30
20
10
0
-10
-20
-30
Temperature (Deg)
0
365
730
1095
1460
1825
2190
Time (Days)

B-GB2

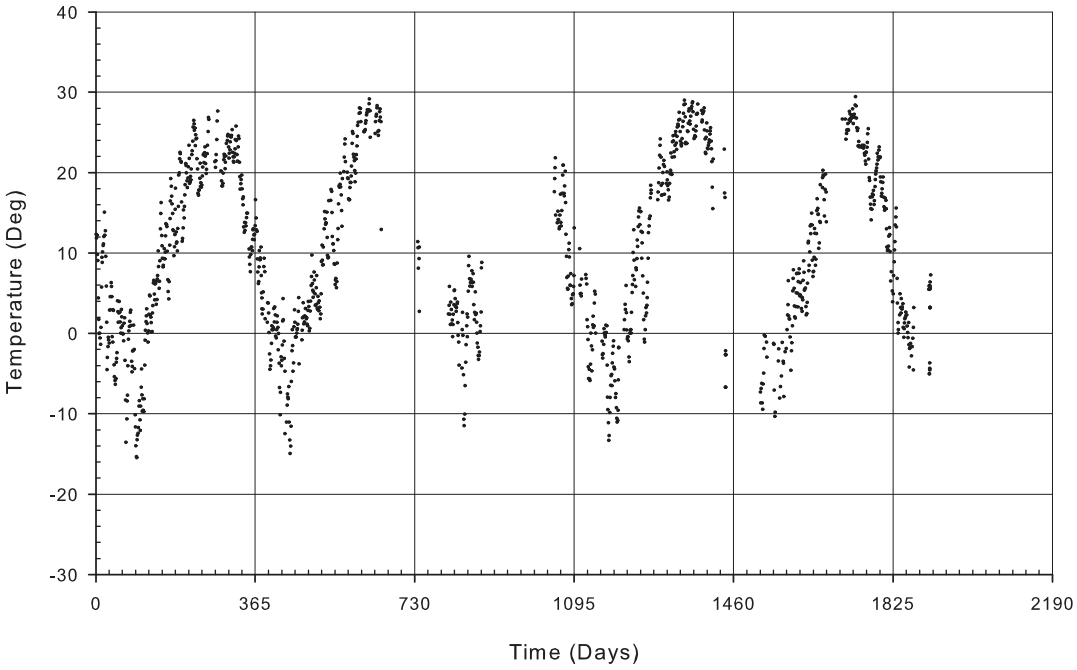
40
30
20
10
0
-10
-20
-30
Temperature (Deg)
0
365
730
1095
1460
1825
2190
Time (Days)

B-GP1

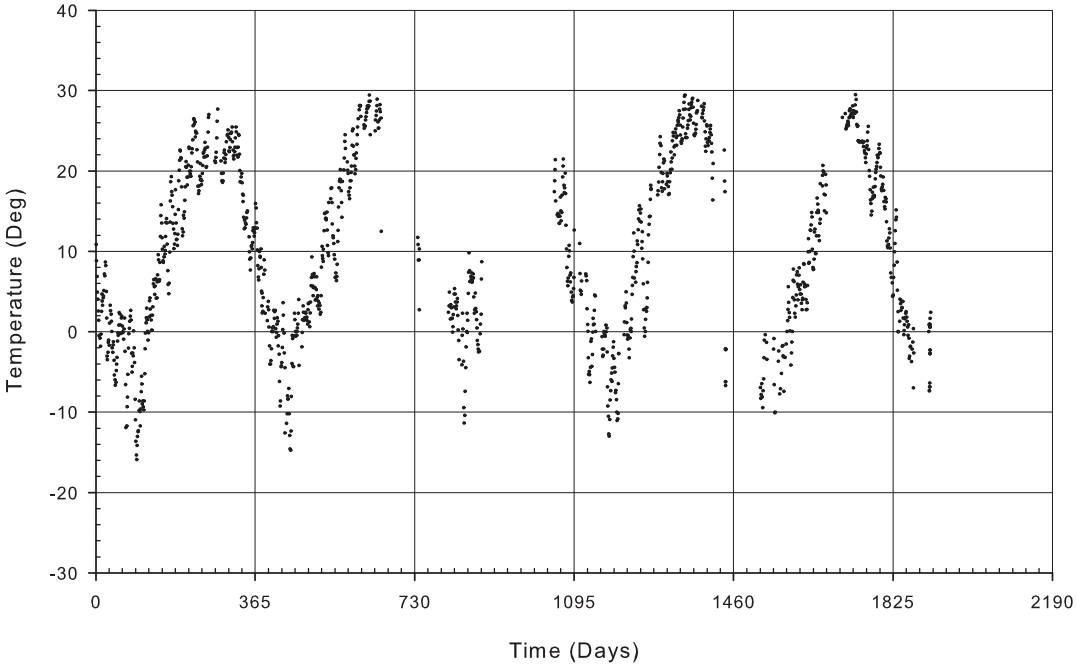
40
30
20
10
0
-10
-20
-30
Temperature (Deg)
0
365
730
1095
1460
1825
2190
Time (Days)

B-GP2

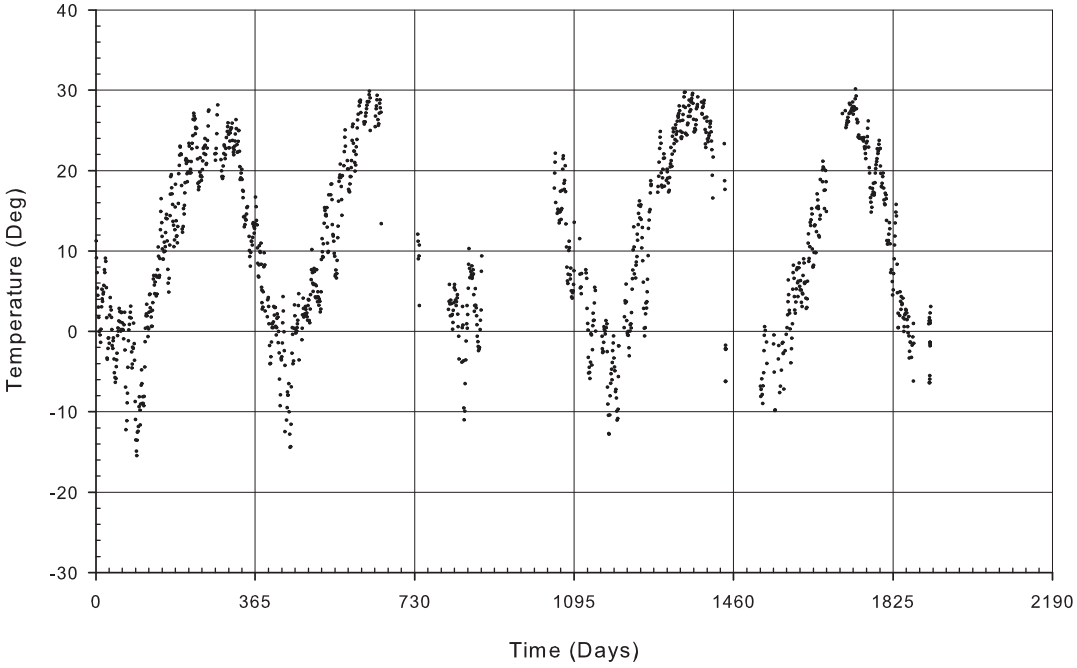
40
30
20
10
0
-10
-20
-30
Temperature (Deg)
0
365
730
1095
1460
1825
2190
Time (Days)

B-JB

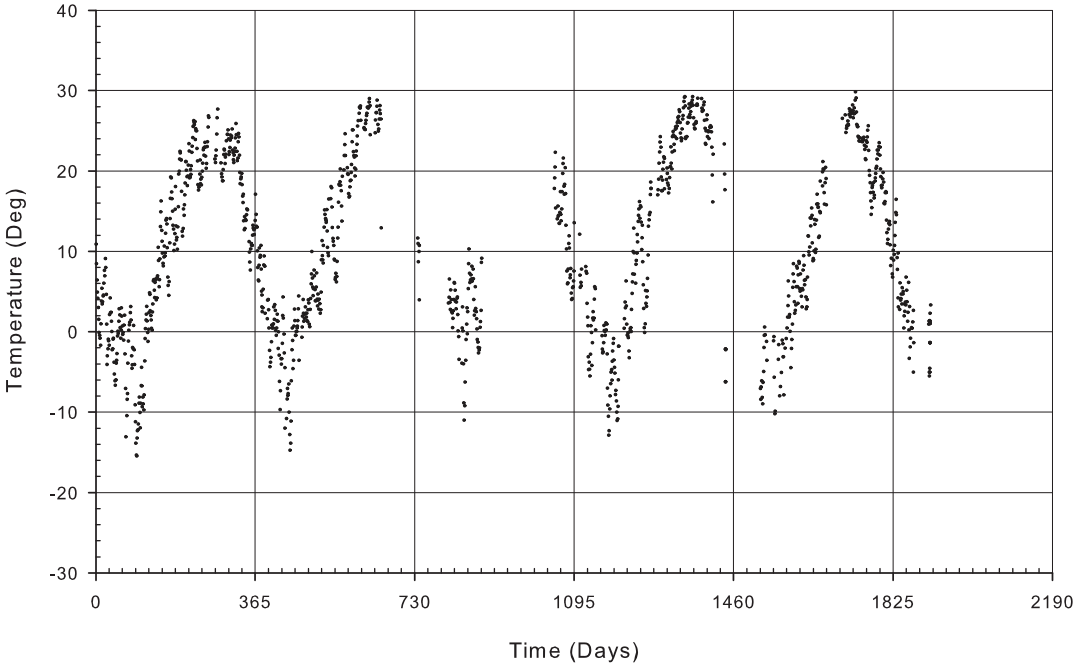
40
30
20
10
0
-10
-20
-30
Temperature (Deg)
0
365
730
1095
1460
1825
2190
Time (Days)

B-JP

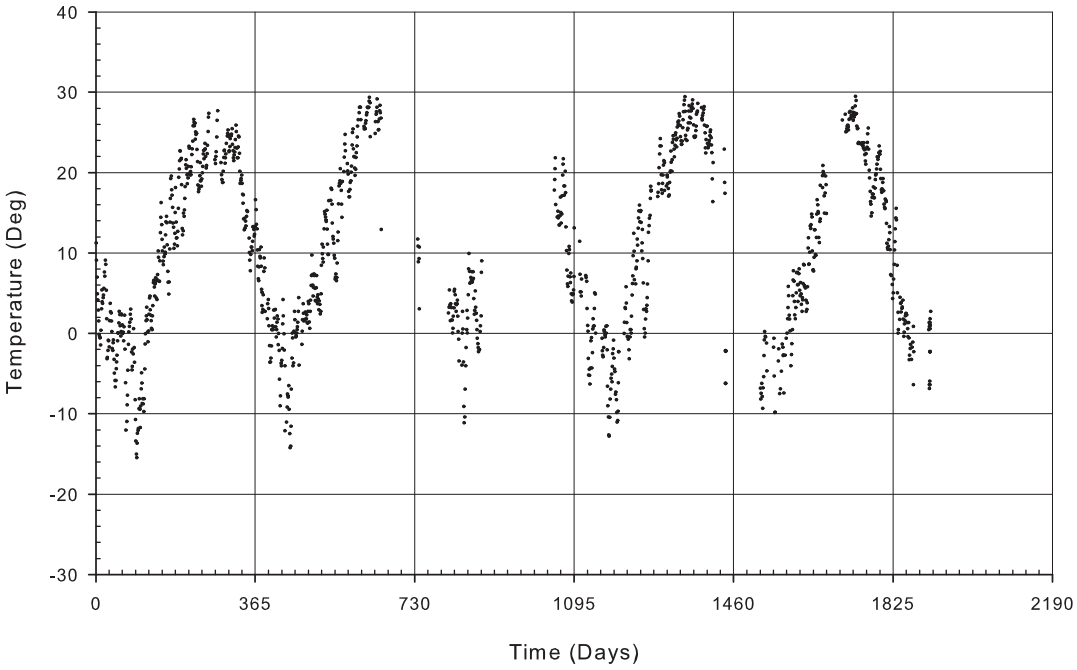
40
30
20
10
0
-10
-20
-30
Temperature (Deg)
0
365
730
1095
1460
1825
2190
Time (Days)

B-KD

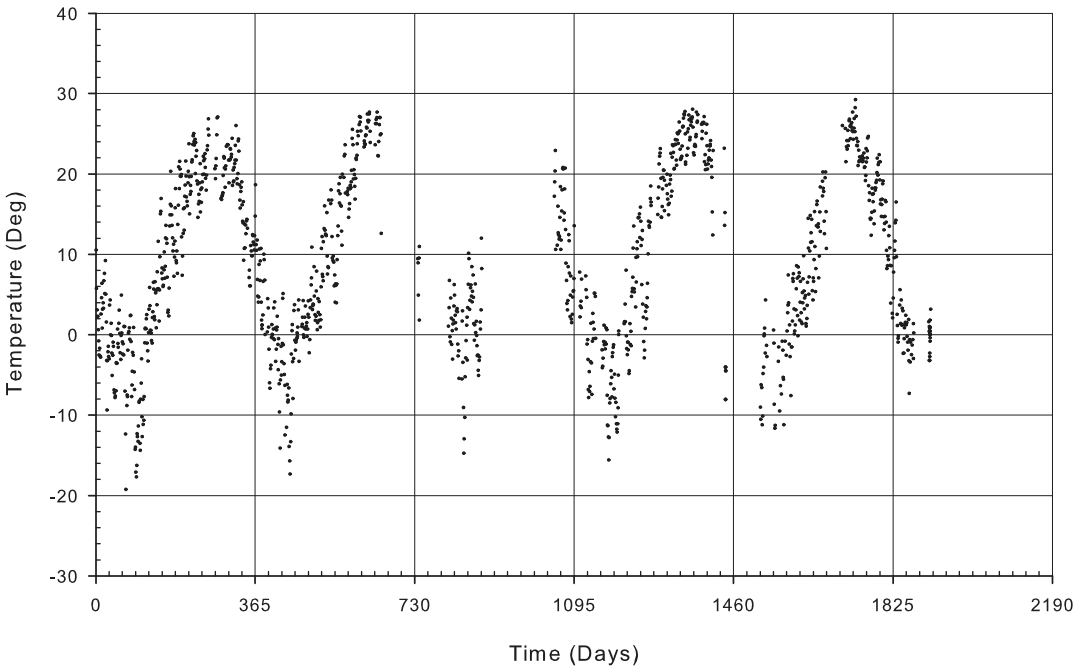
40
30
20
10
0
-10
-20
-30
Temperature (Deg)
0
365
730
1095
1460
1825
2190
Time (Days)

B-HP7

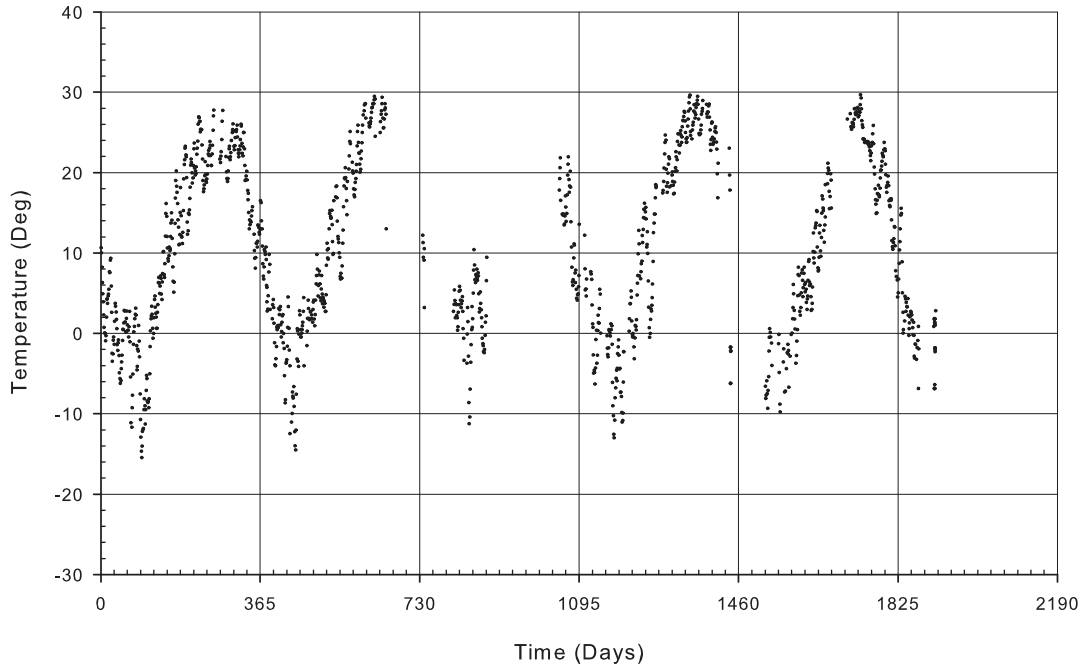
40
30
20
10
0
-10
-20
-30
Temperature (Deg)
0
365
730
1095
1460
1825
2190
Time (Days)

B-LD

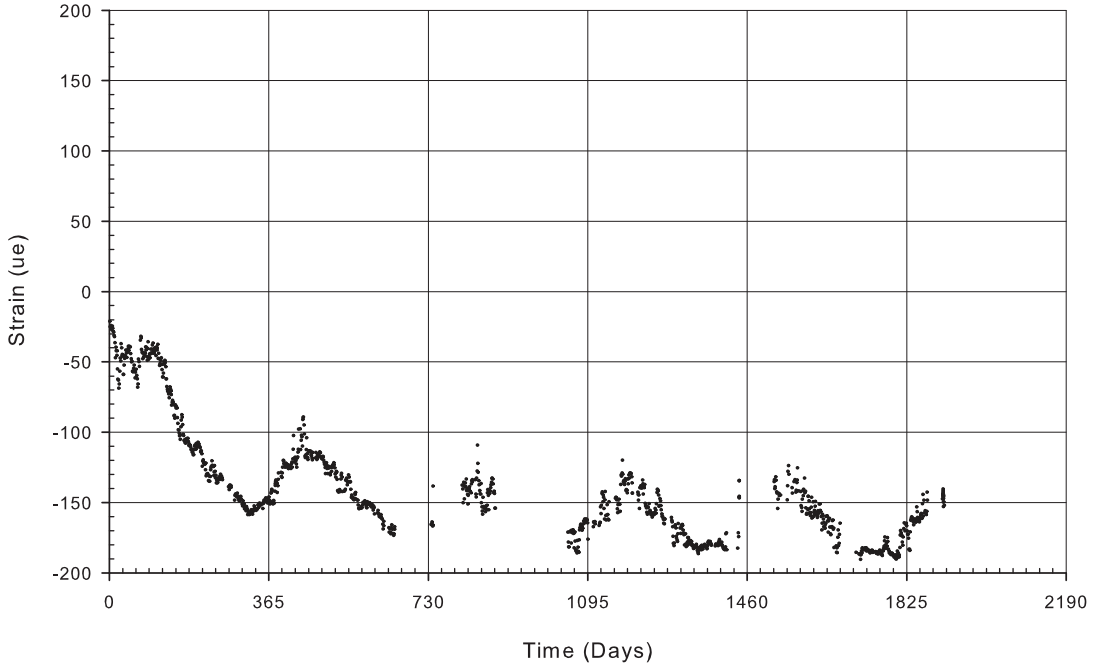
200
150
100
50
0
-50
-100
-150
-200
Strain (ue)
0
365
730
1095
1460
1825
2190
Time (Days)

B-LT

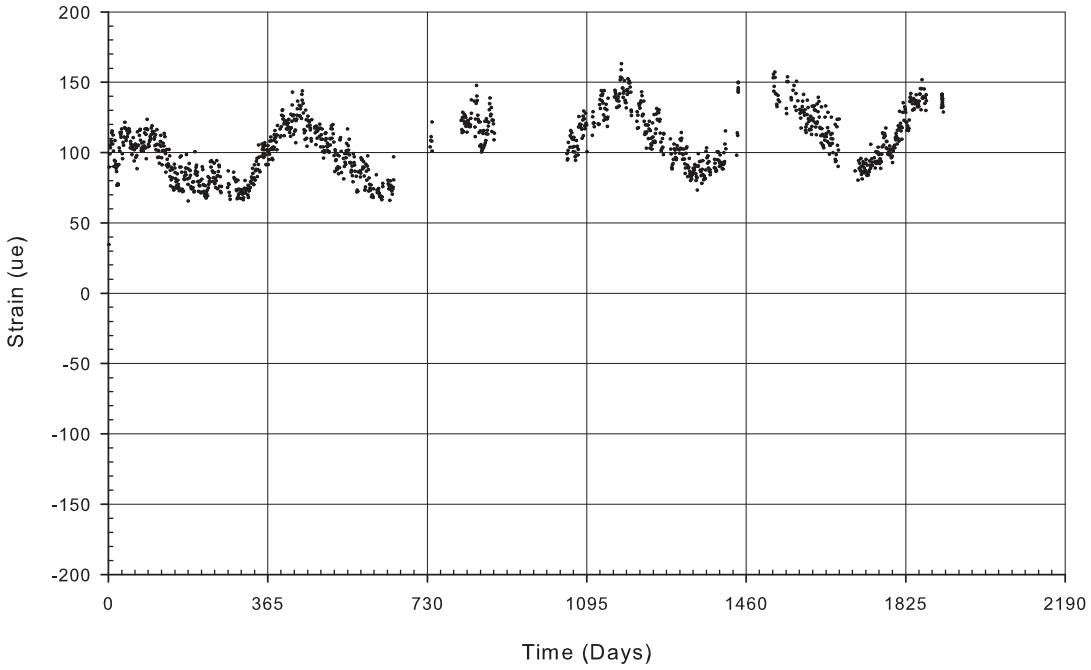
200
150
100
50
0
-50
-100
-150
-200
Strain (ue)
0
365
730
1095
1460
1825
2190
Time (Days)

B-MD

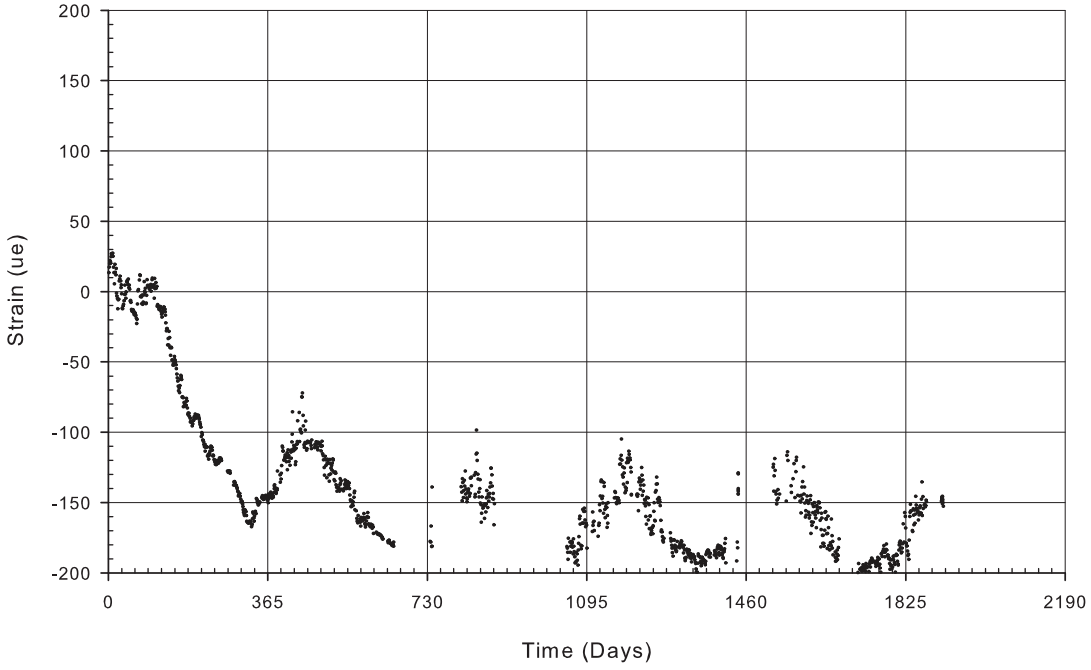
200
150
100
50
0
-50
-100
-150
-200
Strain (ue)
0
365
730
1095
1460
1825
2190
Time (Days)

B-MT

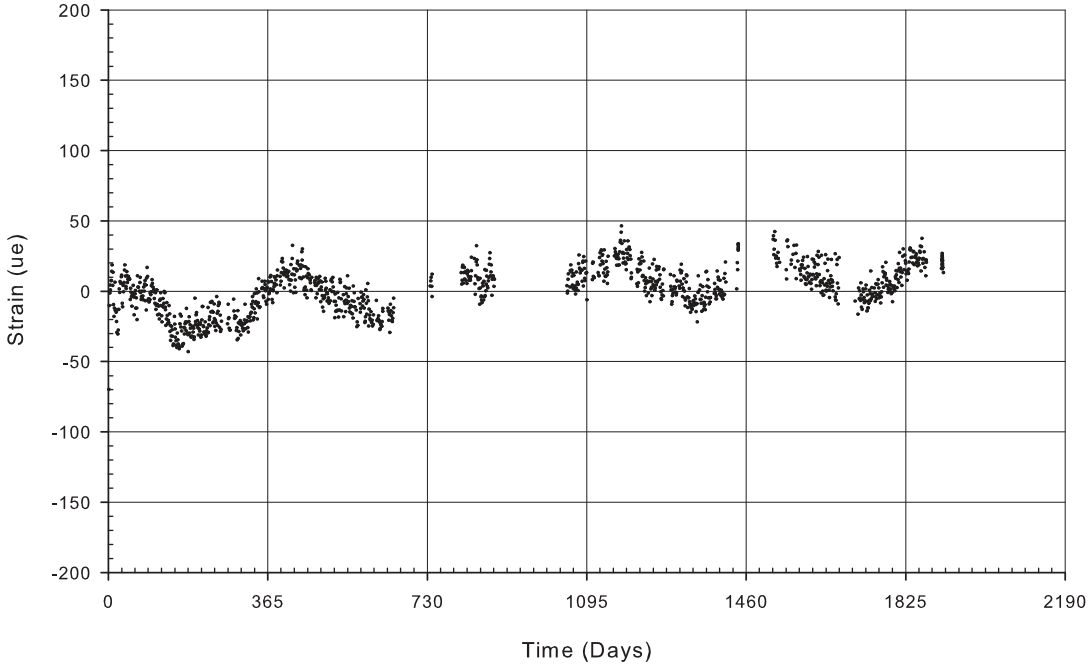
200
150
100
50
0
-50
-100
-150
-200
Strain (ue)
0
365
730
1095
1460
1825
2190
Time (Days)

B-NB1

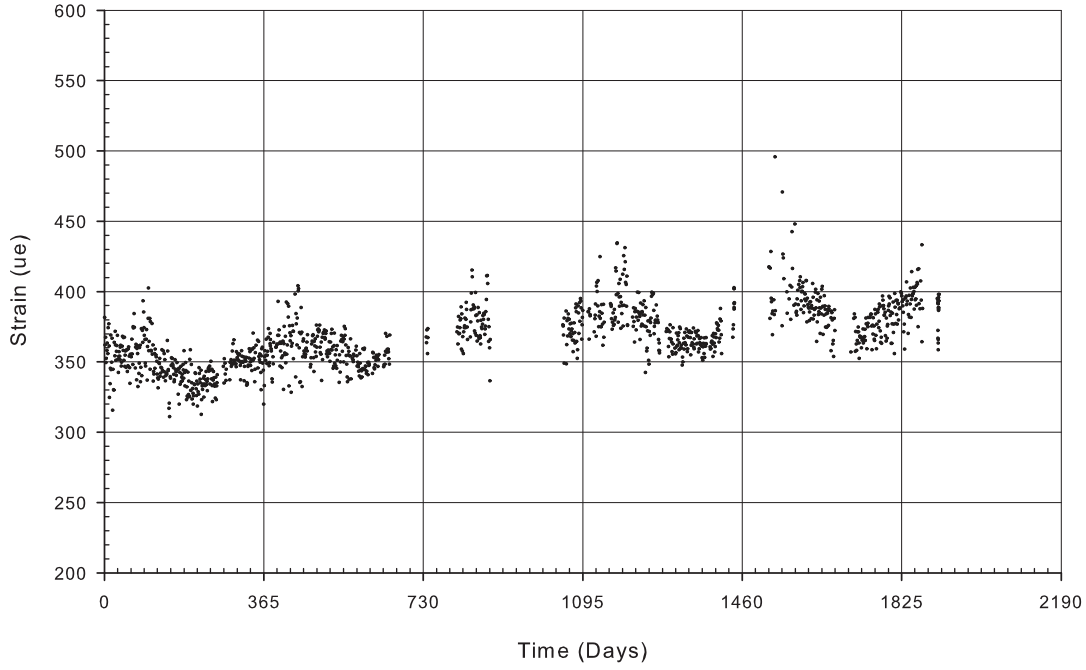
600
550
500
450
400
350
300
250
200
Strain (ue)
0
365
730
1095
1460
1825
2190
Time (Days)

B-NB2

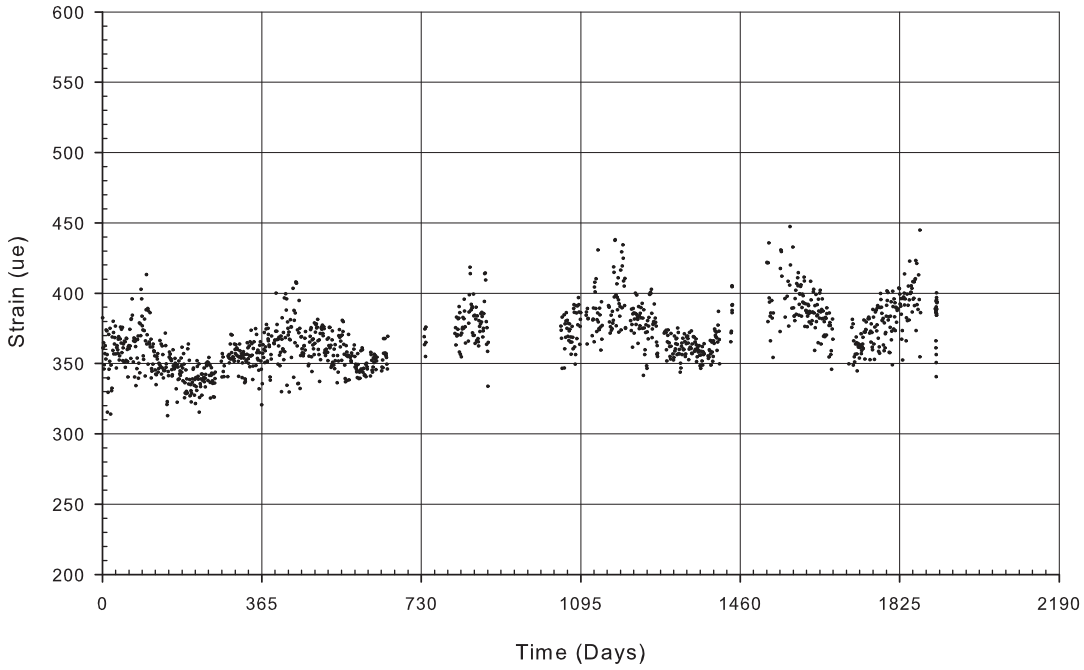
600
550
500
450
400
350
300
250
200
Strain (ue)
0
365
730
1095
1460
1825
2190
Time (Days)

B-NW

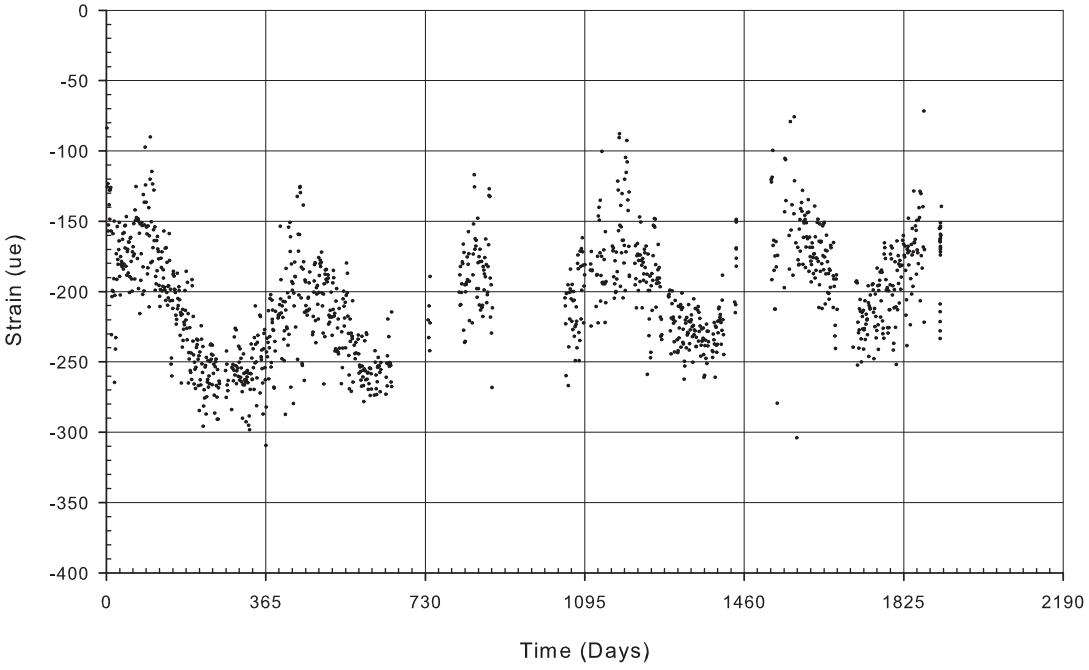
0
-50
-100
-150
-200
-250
-300
-350
-400
Strain (ue)
0
365
730
1095
1460
1825
2190
Time (Days)

B-NT

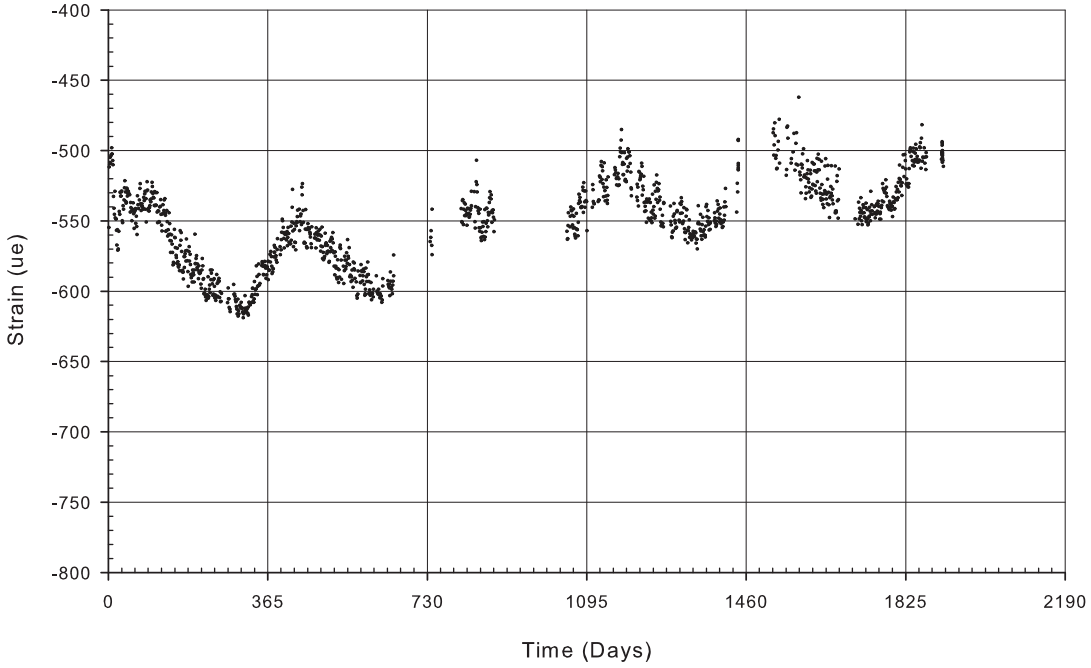
-400
-450
-500
-550
-600
-650
-700
-750
-800
Strain (ue)
0
365
730
1095
1460
1825
2190
Time (Days)

B-PB

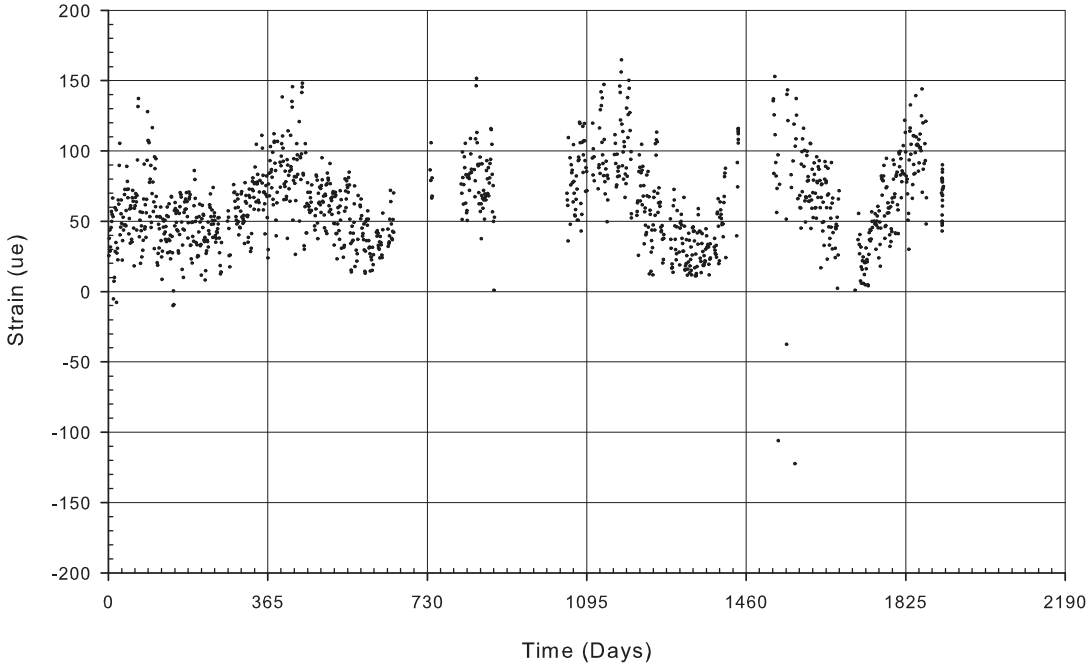
200
150
100
50
0
-50
-100
-150
-200
Strain (ue)
0
365
730
1095
1460
1825
2190
Time (Days)

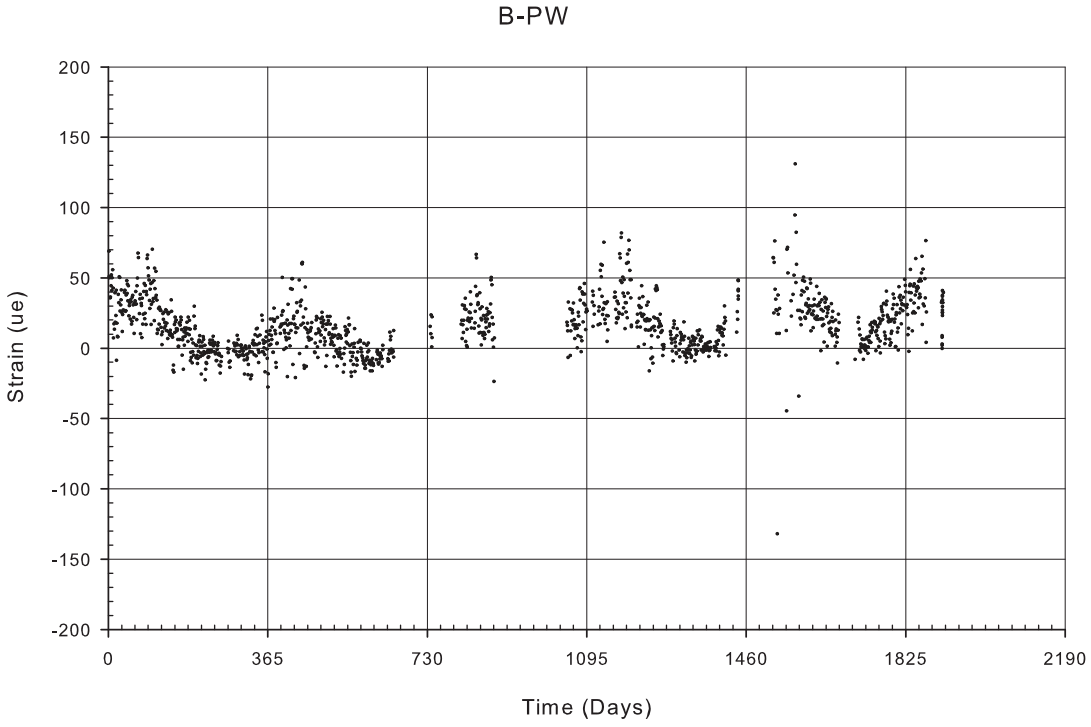
B-PW
200
150
100
50
0
-50
-100
-150
-200
Strain (ue)
0
365
730
1095
1460
1825
2190
Time (Days)

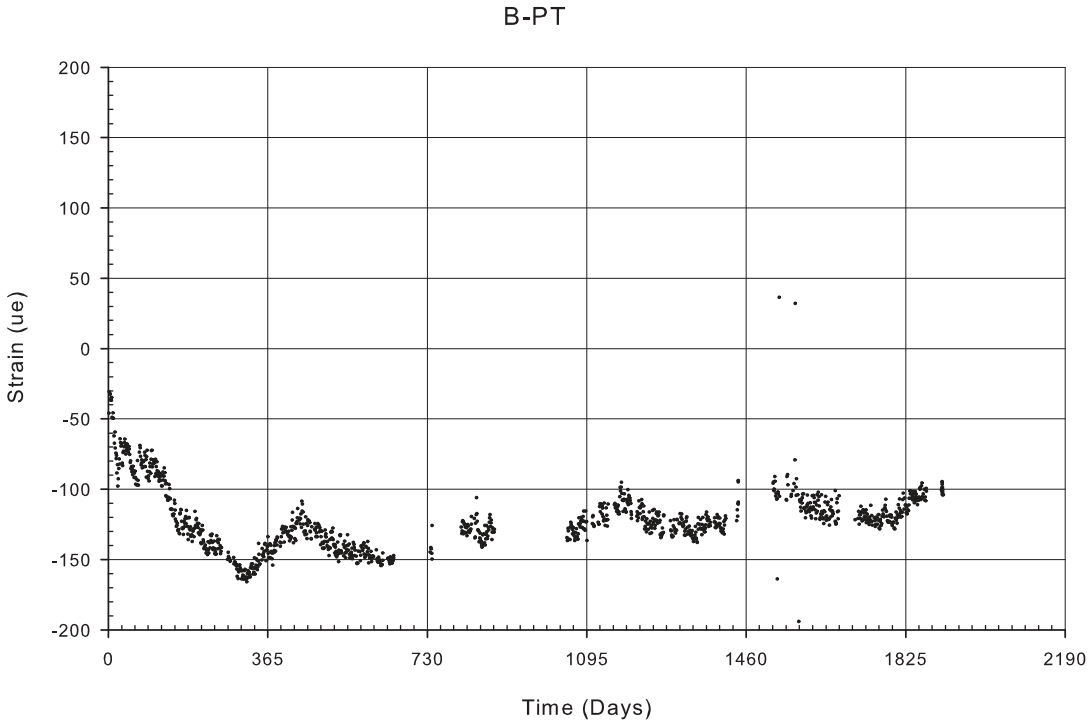
B-PT
200
150
100
50
0
-50
-100
-150
-200
Strain (ue)
0
365
730
1095
1460
1825
2190
Time (Days)

B-ZL1

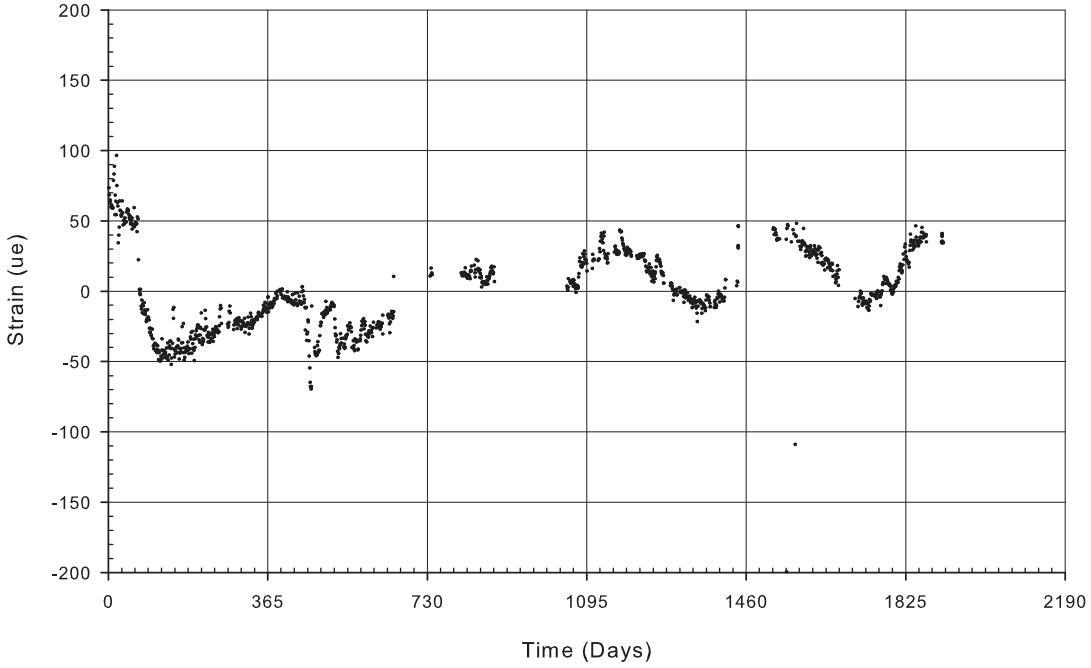
200
150
100
50
0
-50
-100
-150
-200
Strain (ue)
0
365
730
1095
1460
1825
2190
Time (Days)

B-ZL2

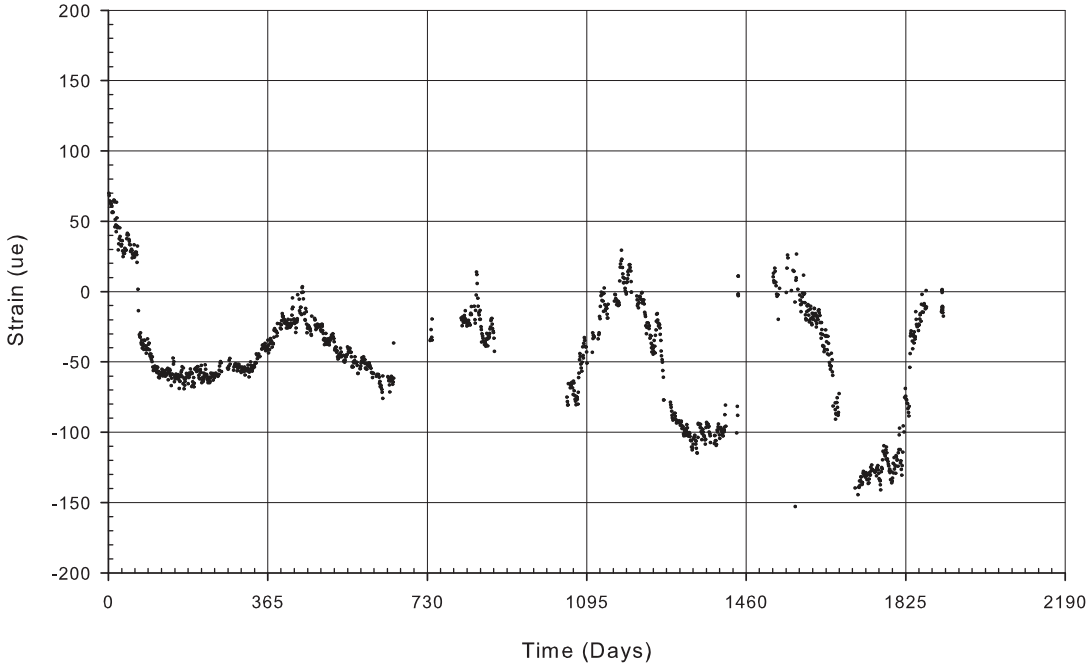
200
150
100
50
0
-50
-100
-150
-200
Strain (ue)
0
365
730
1095
1460
1825
2190
Time (Days)

B-ZL3

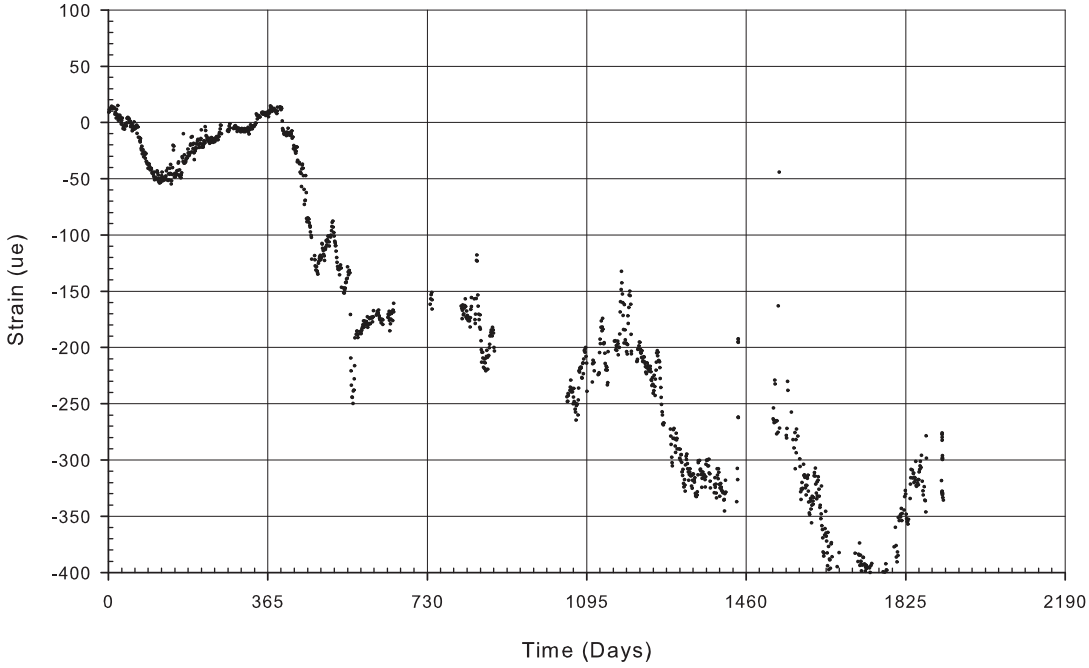
100
50
0
-50
-100
-150
-200
-250
-300
-350
-400
Strain (ue)
0
365
730
1095
1460
1825
2190
Time (Days)

B-ZL4

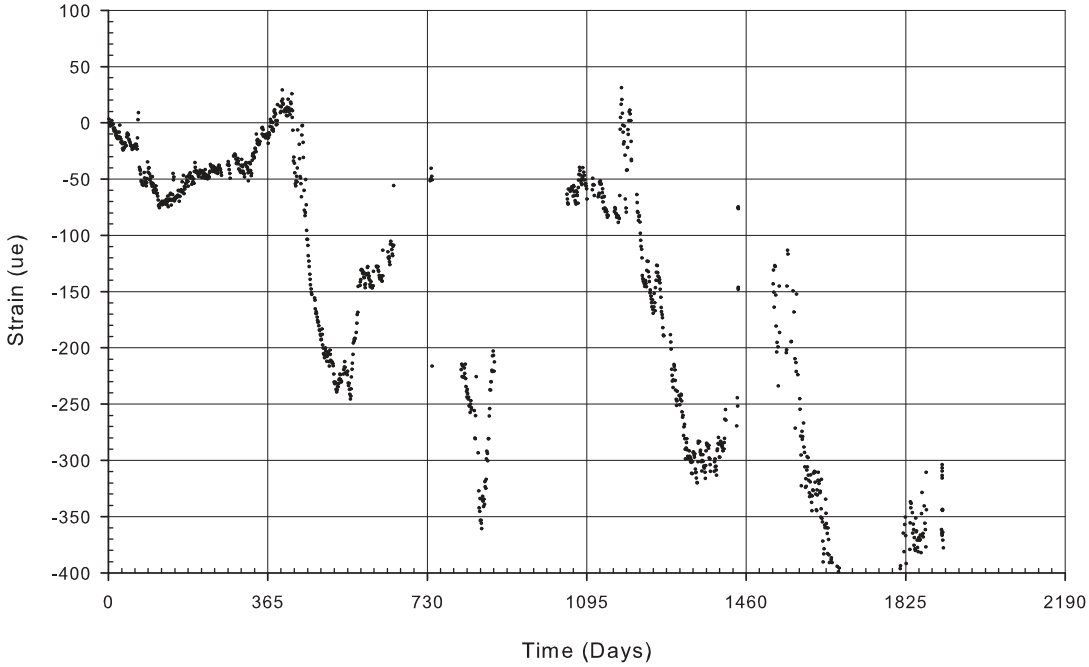
100
50
0
-50
-100
-150
-200
-250
-300
-350
-400
Strain (ue)
0
365
730
1095
1460
1825
2190
Time (Days)

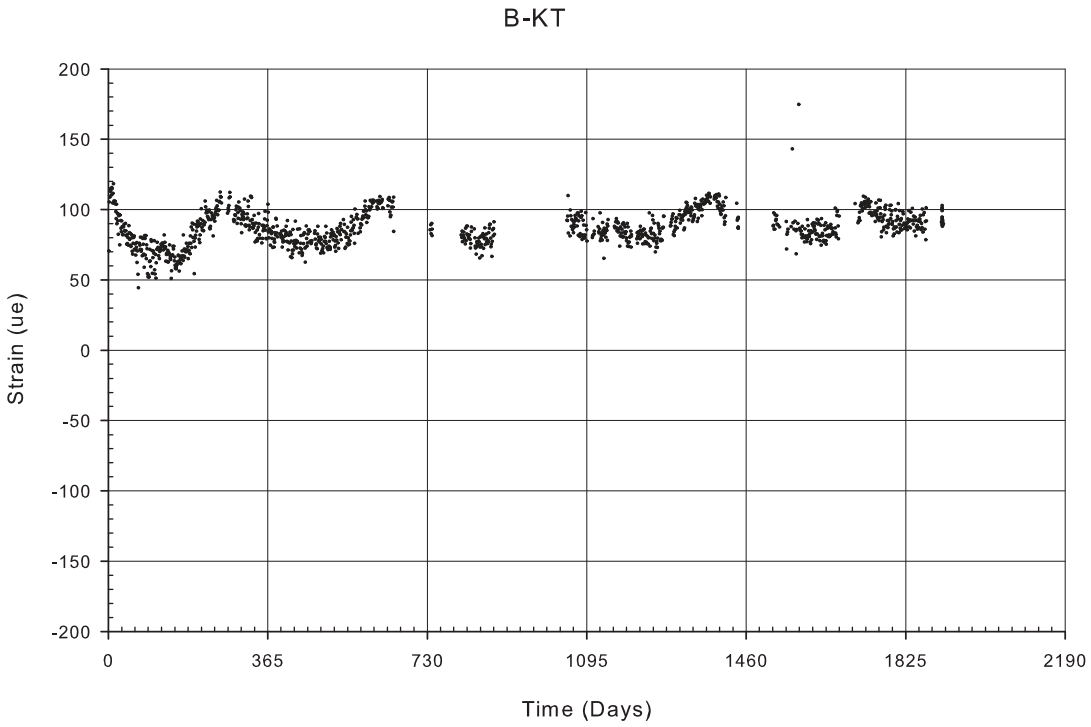
B-KT
Strain (ue)
200
150
100
50
0
-50
-100
-150
-200
0
365
730
1095
1460
1825
2190
Time (Days)

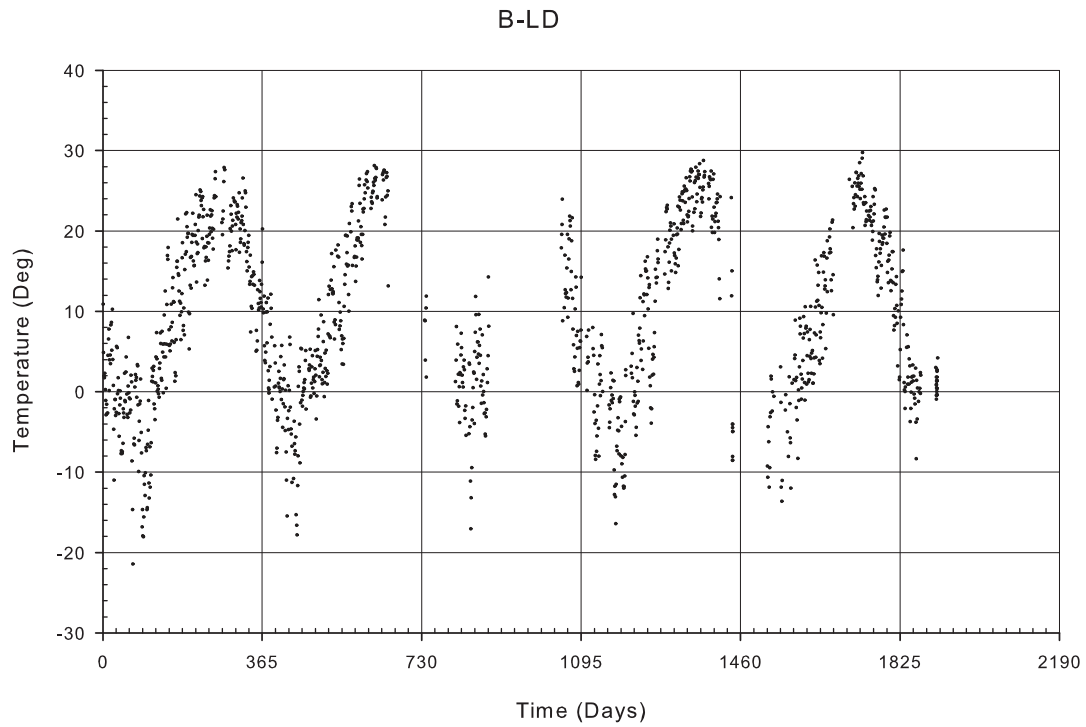
B-LD
Temperature (Deg)
40
30
20
10
0
-10
-20
-30
0
365
730
1095
1460
1825
2190
Time (Days)

B-LT

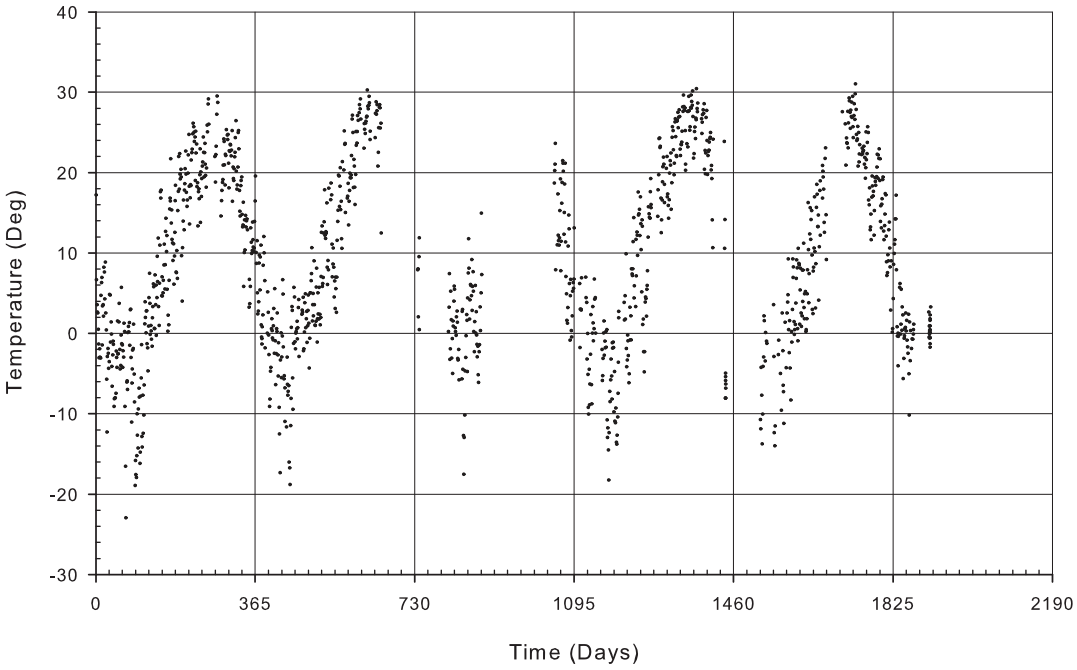
40
30
20
10
0
-10
-20
-30
Temperature (Deg)
0
365
730
1095
1460
1825
2190
Time (Days)

B-MD

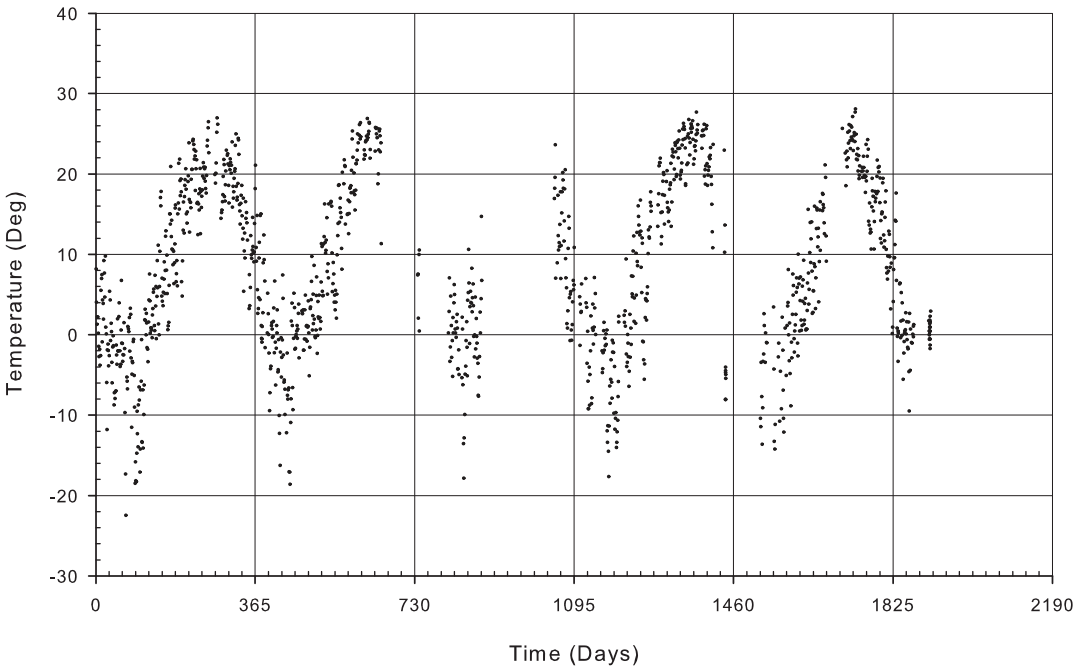
40
30
20
10
0
-10
-20
-30
Temperature (Deg)
0
365
730
1095
1460
1825
2190
Time (Days)

B-MT

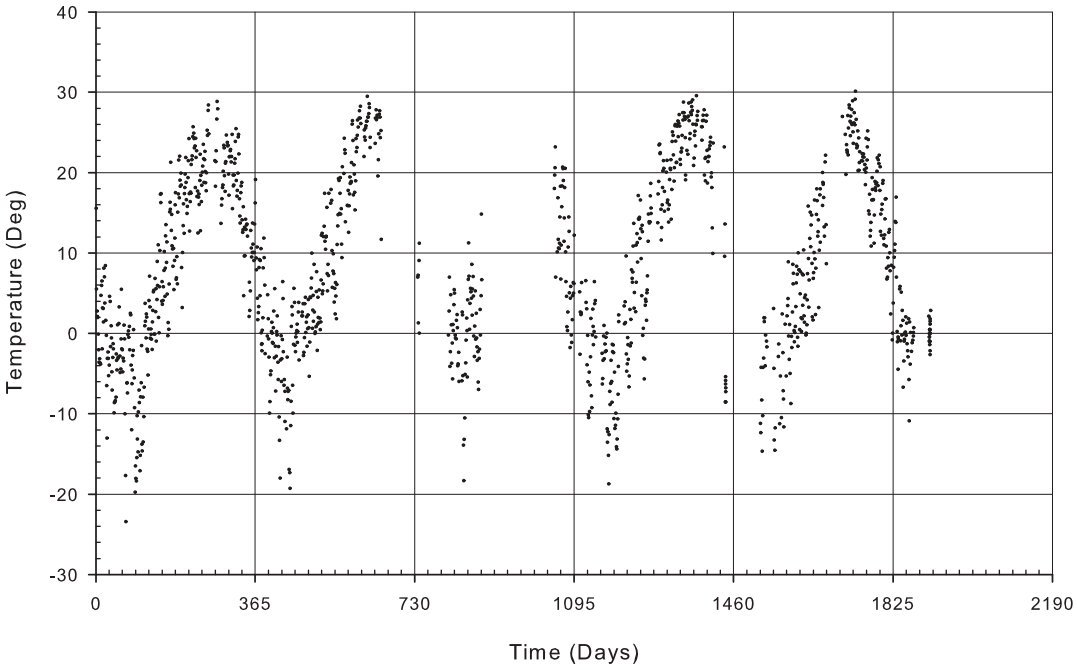
40
30
20
10
0
-10
-20
-30
Temperature (Deg)
0
365
730
1095
1460
1825
2190
Time (Days)

B-NB1

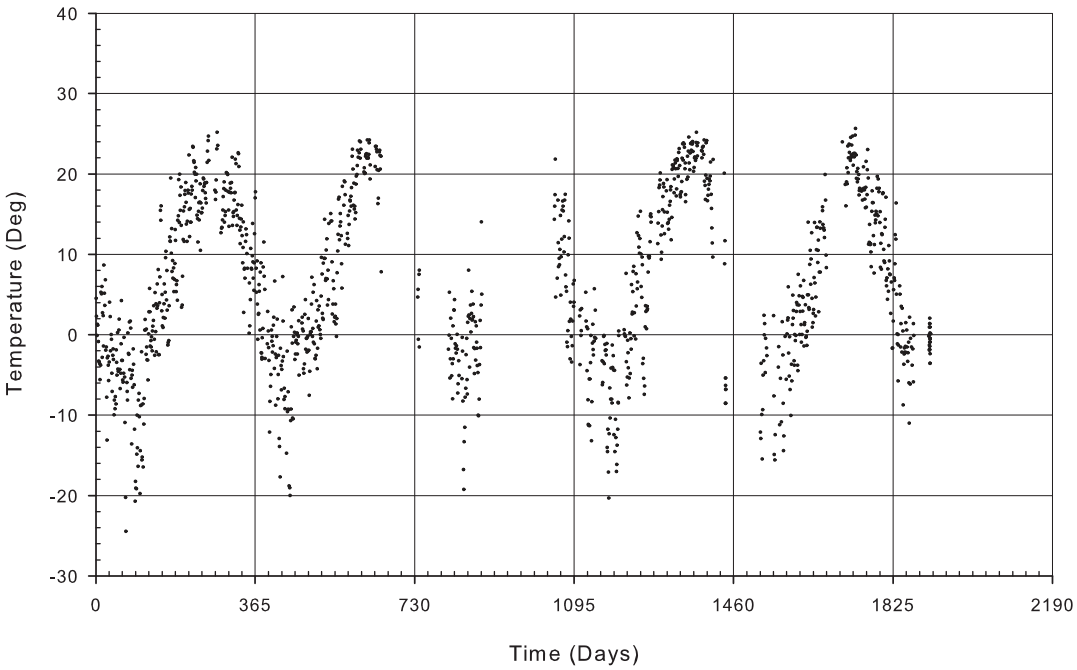
40
30
20
10
0
-10
-20
-30
Temperature (Deg)
0
365
730
1095
1460
1825
2190
Time (Days)

B-NB2

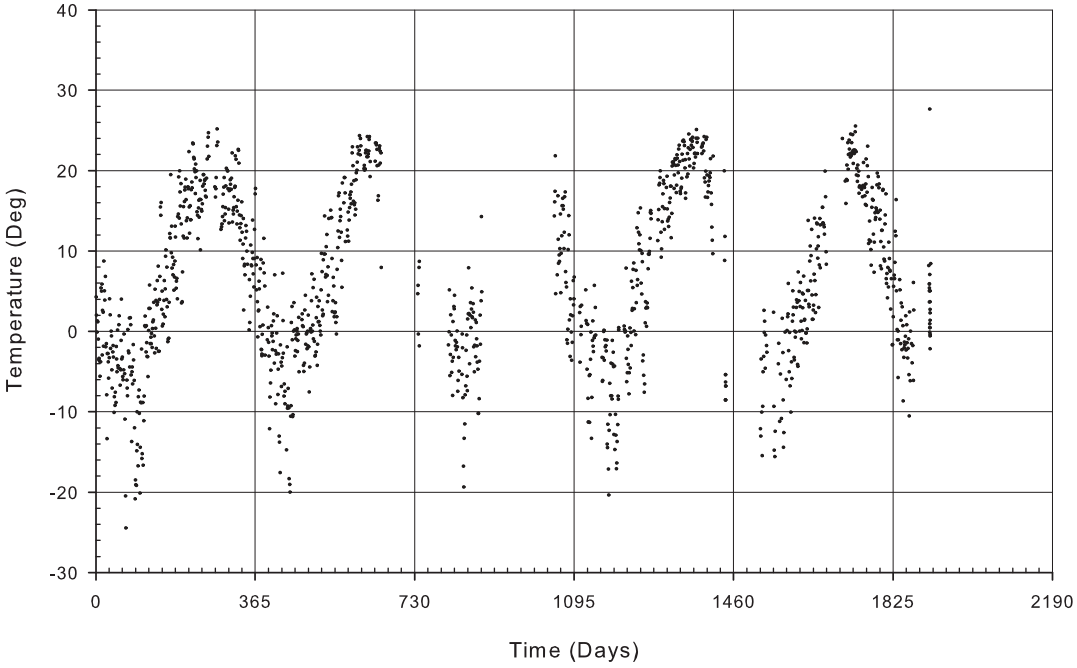
40
30
20
10
0
-10
-20
-30
Temperature (Deg)
0
365
730
1095
1460
1825
2190
Time (Days)

B-NW

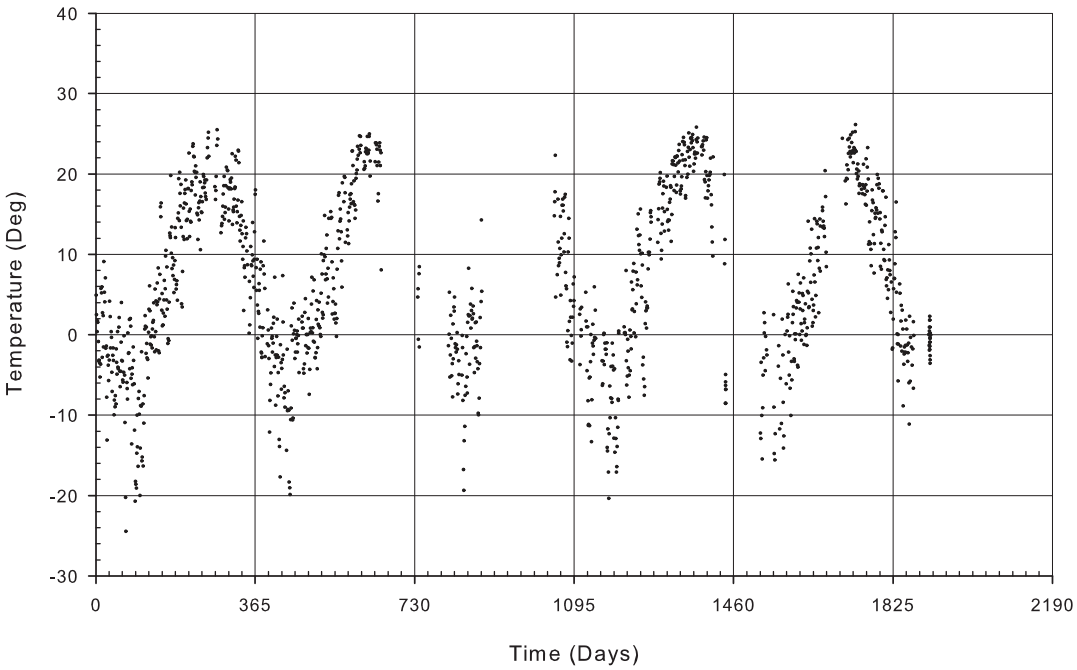
40
30
20
10
0
-10
-20
-30
Temperature (Deg)
0
365
730
1095
1460
1825
2190
Time (Days)

B-NT

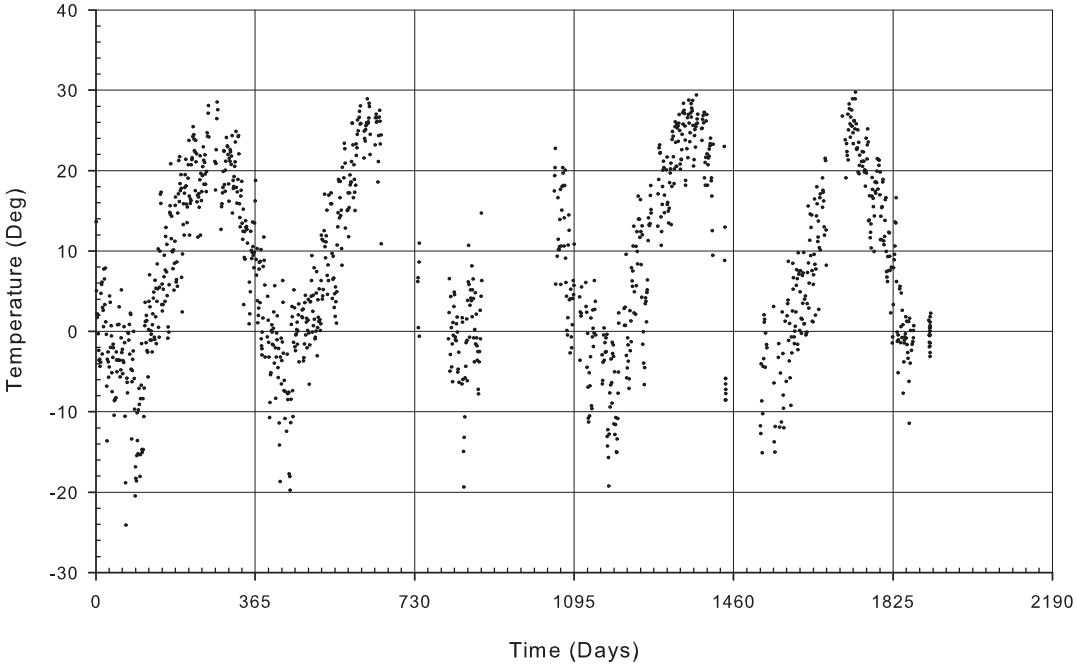
40
30
20
10
0
-10
-20
-30
Temperature (Deg)
0
365
730
1095
1460
1825
2190
Time (Days)

B-PB

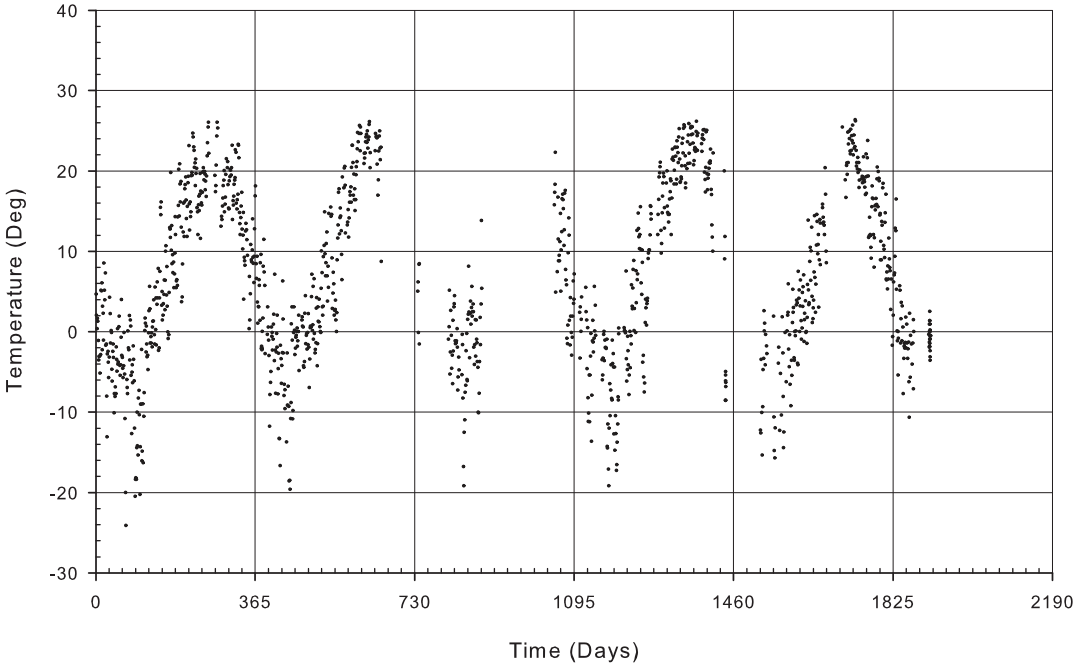
40
30
20
10
0
-10
-20
-30
Temperature (Deg)
0
365
730
1095
1460
1825
2190
Time (Days)

B-PW

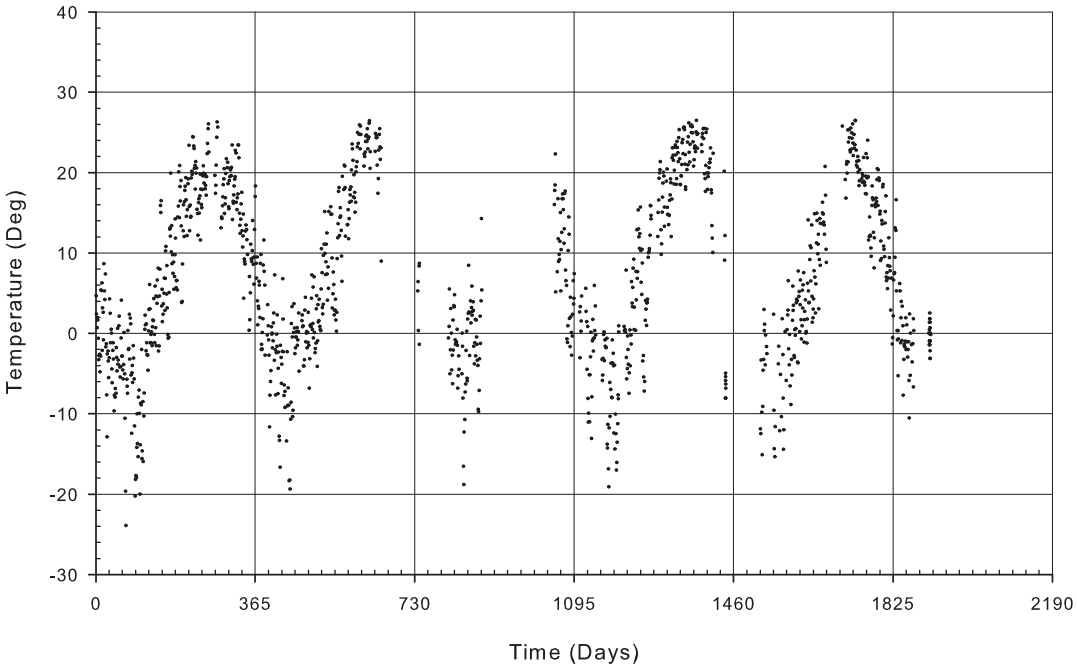
40
30
20
10
0
-10
-20
-30
Temperature (Deg)
0
365
730
1095
1460
1825
2190
Time (Days)

B-PT

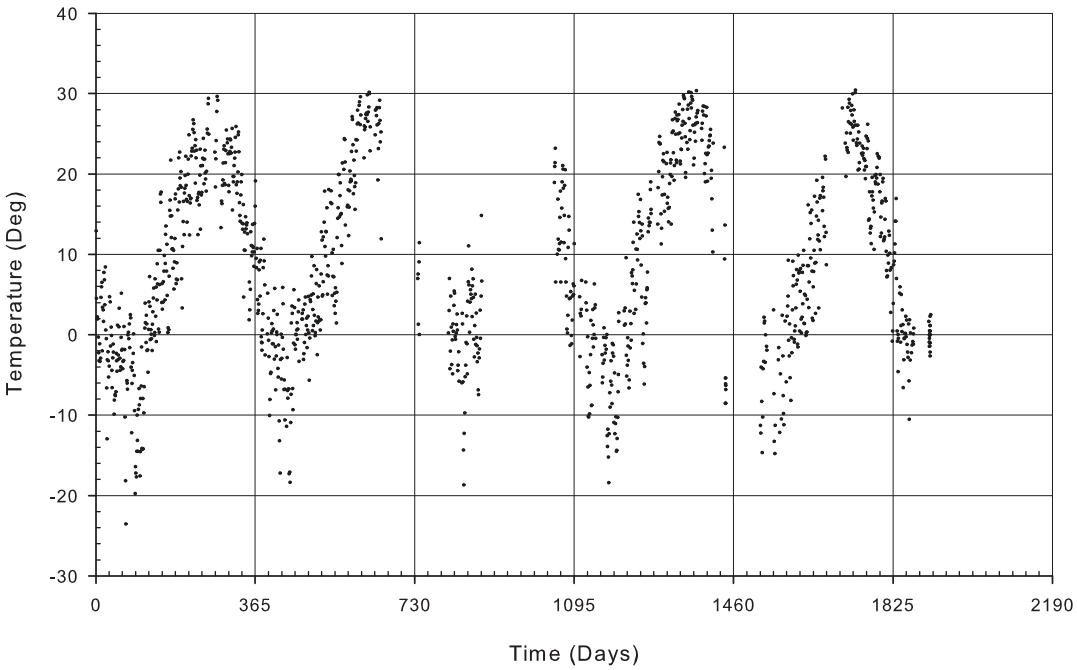
40
30
20
10
0
-10
-20
-30
Temperature (Deg)
0
365
730
1095
1460
1825
2190
Time (Days)

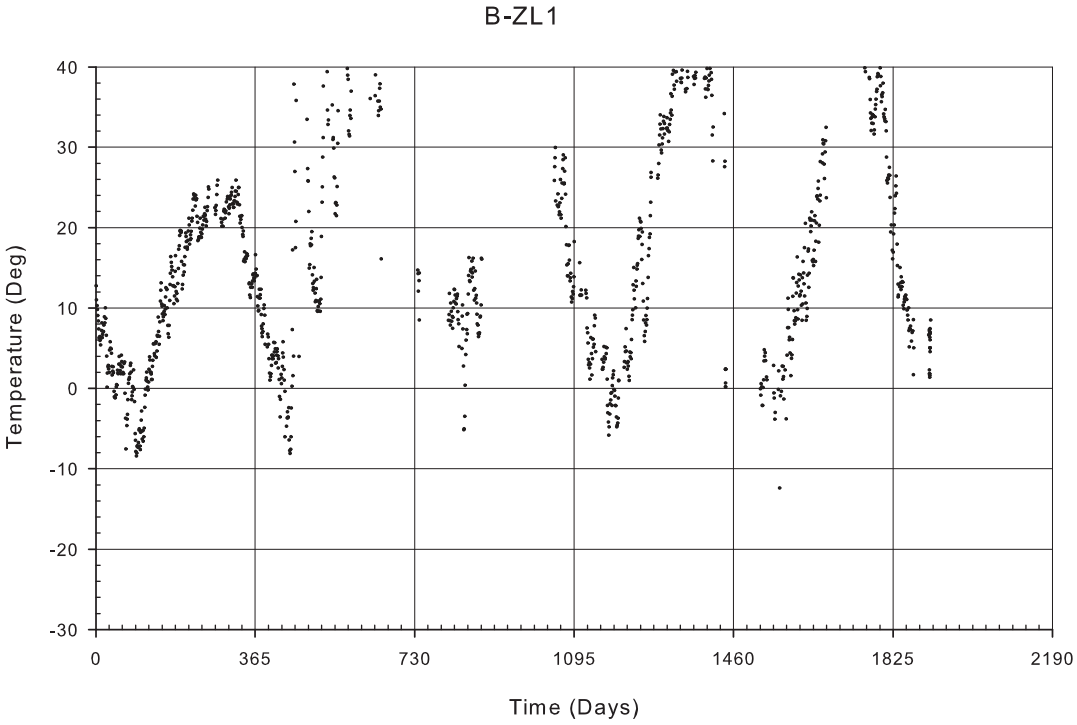
B-ZL1
Temperature (Deg)
40
30
20
10
0
-10
-20
-30
0
365
730
1095
1460
1825
2190
Time (Days)

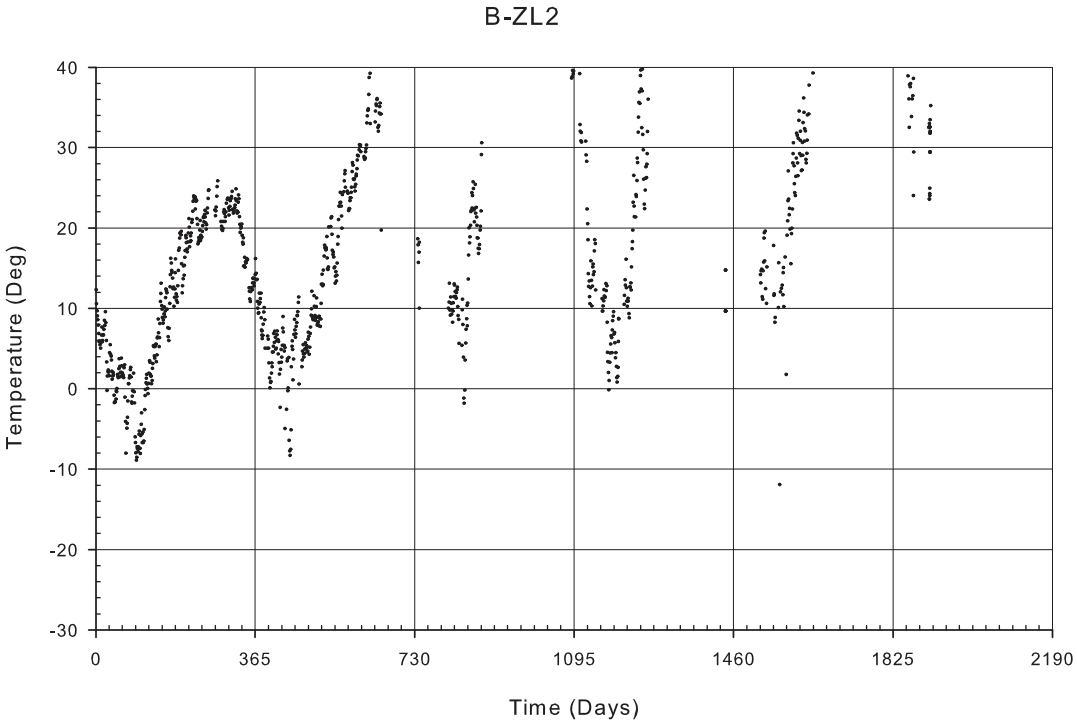
B-ZL2
Temperature (Deg)
40
30
20
10
0
-10
-20
-30
0
365
730
1095
1460
1825
2190
Time (Days)

B-ZL3

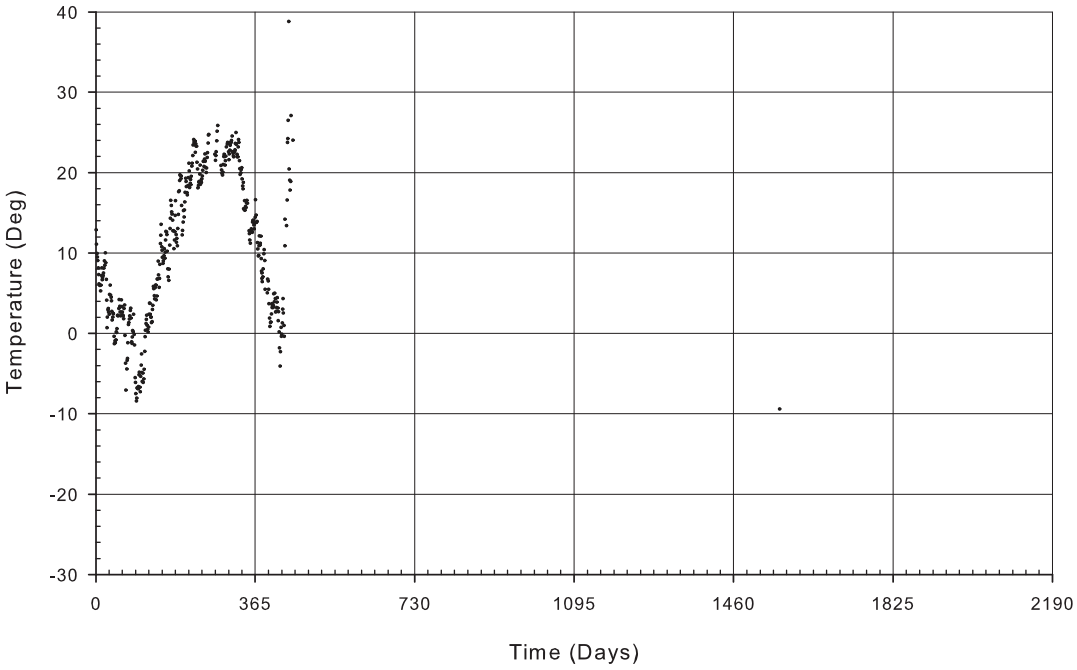
40
30
20
10
0
-10
-20
-30
Temperature (Deg)
0
365
730
1095
1460
1825
2190
Time (Days)

B-ZL4

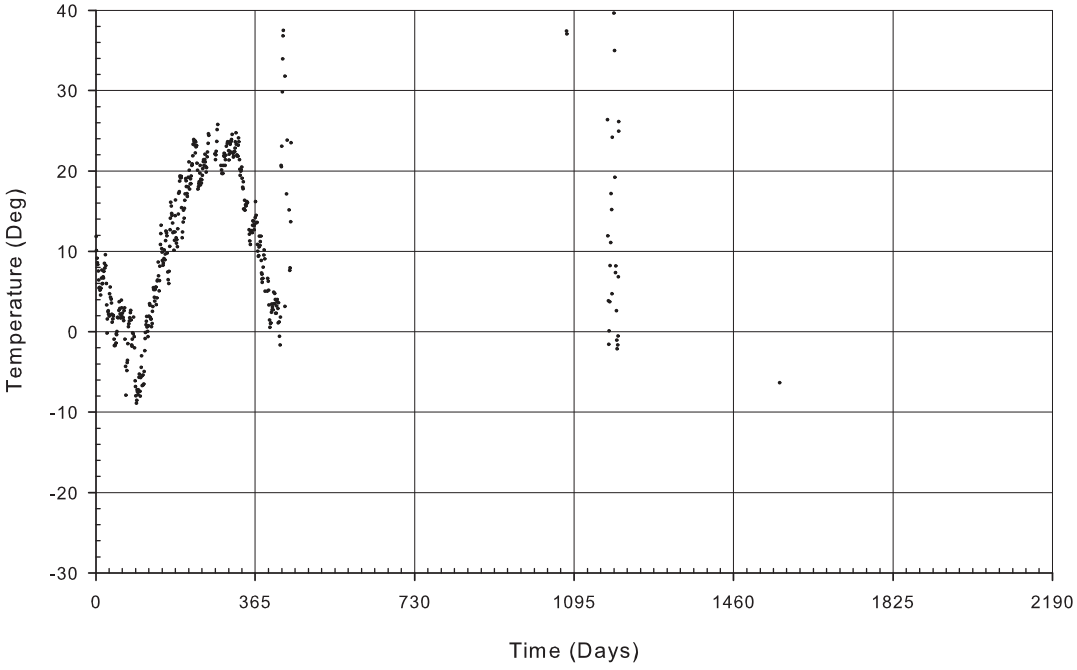
40
30
20
10
0
-10
-20
-30
Temperature (Deg)
0
365
730
1095
1460
1825
2190
Time (Days)

B-KT

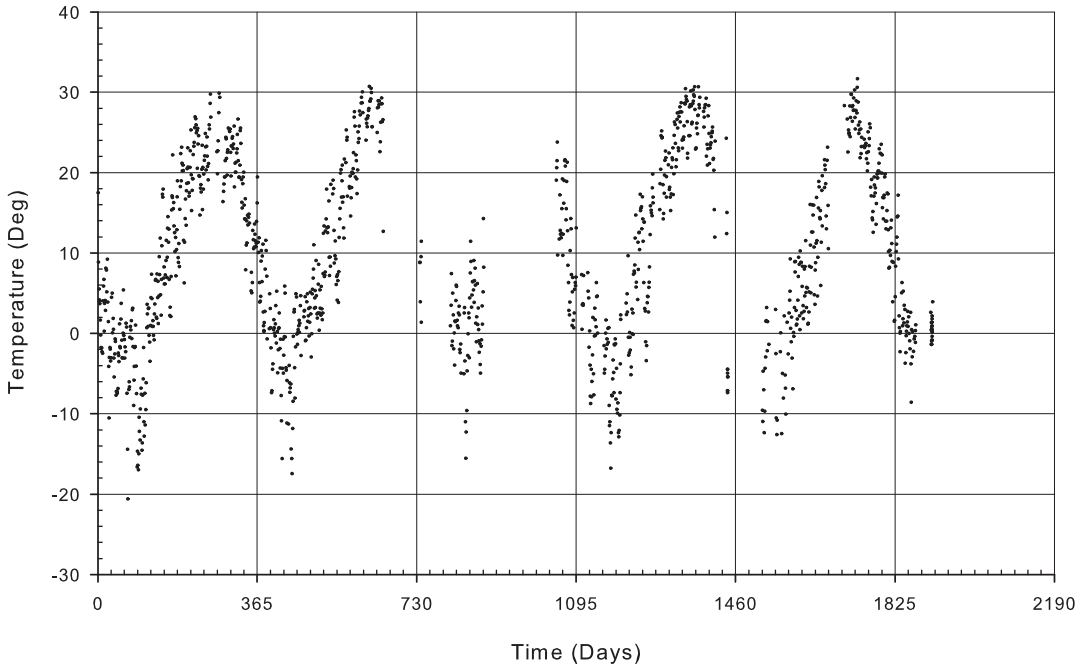
40
30
20
10
0
-10
-20
-30
Temperature (Deg)
0
365
730
1095
1460
1825
2190
Time (Days)

C-HS1

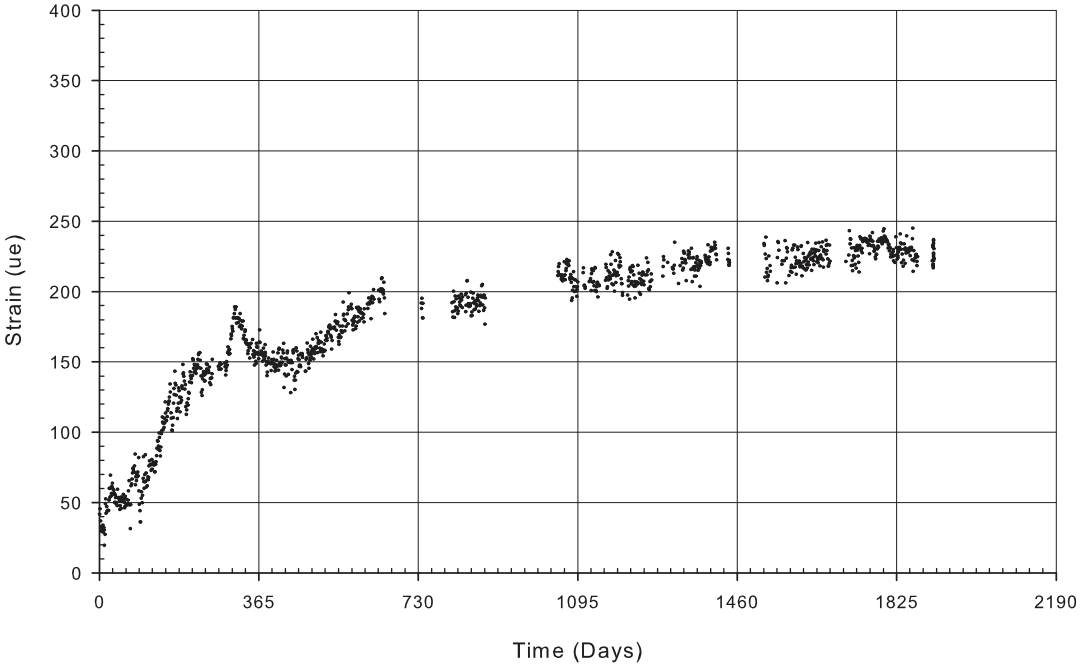
400
350
300
250
200
150
100
50
0
Strain (ue)
0
365
730
1095
1460
1825
2190
Time (Days)

C-HS2

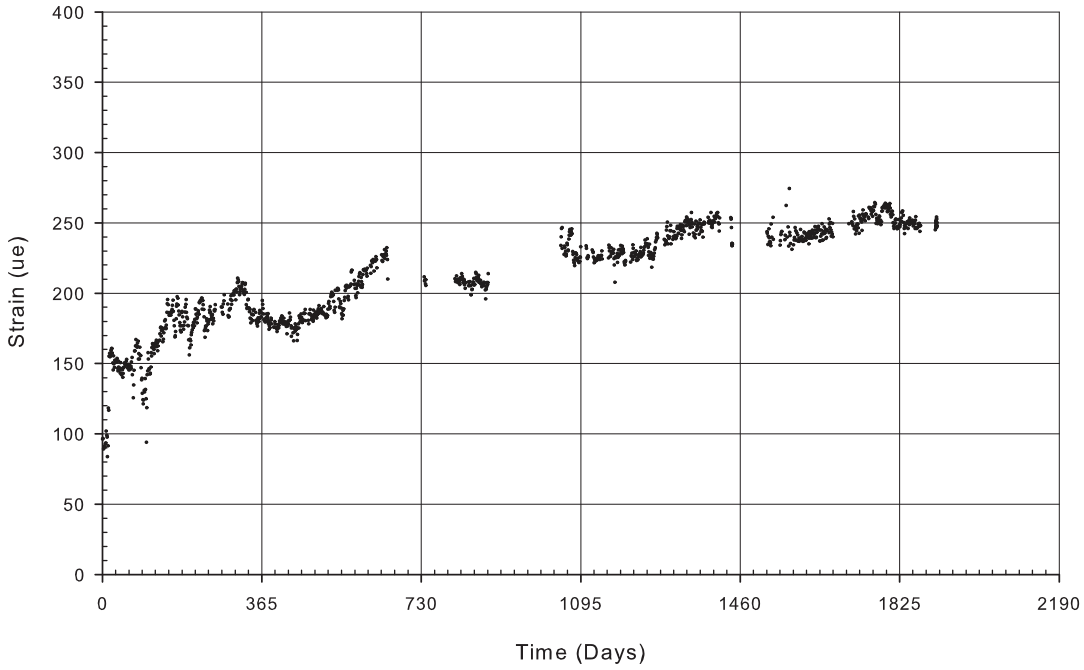
400
350
300
250
200
150
100
50
0
Strain (ue)
0
365
730
1095
1460
1825
2190
Time (Days)

C-HS3

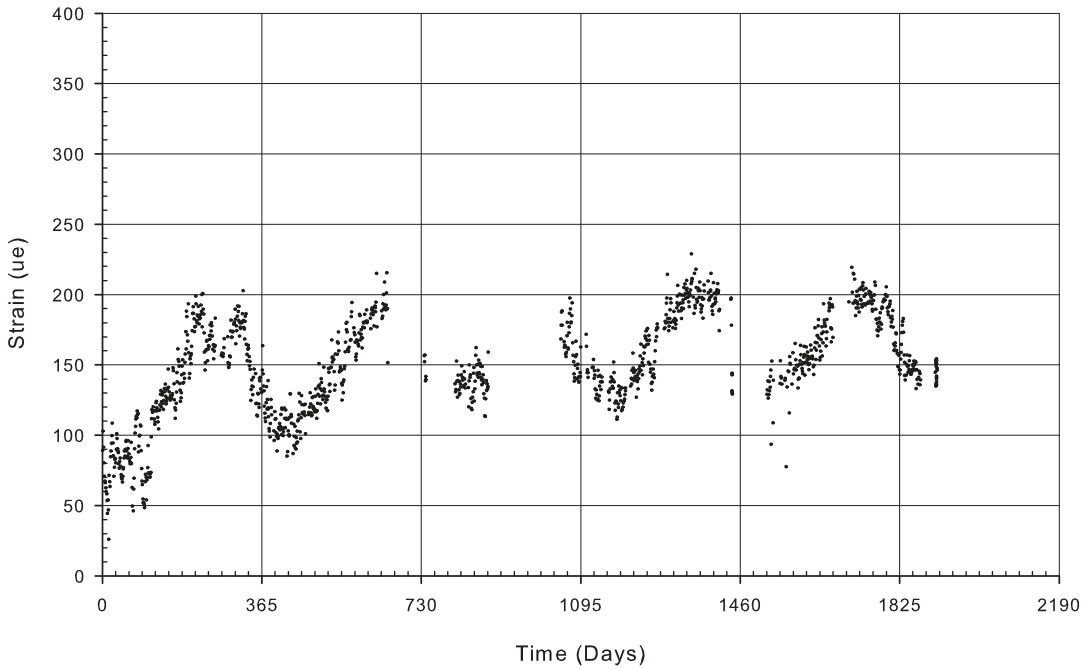
400
350
300
250
200
150
100
50
0
Strain (ue)
0
365
730
1095
1460
1825
2190
Time (Days)

B-CS1

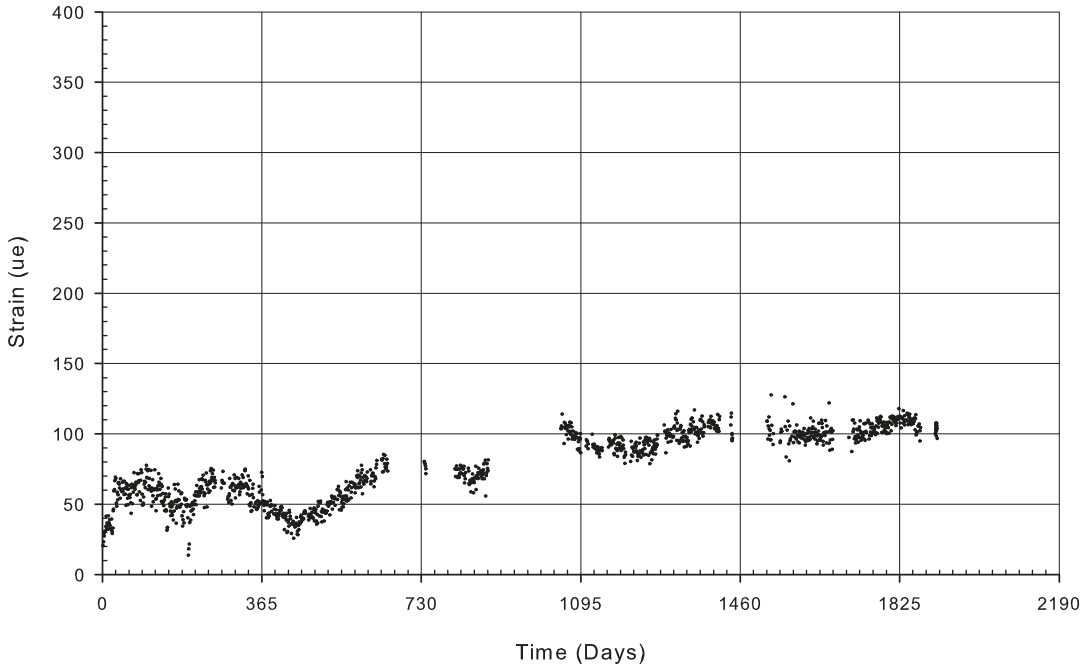
Strain (ue)
400
350
300
250
200
150
100
50
0
0
365
730
1095
1460
1825
2190
Time (Days)

B-CS2

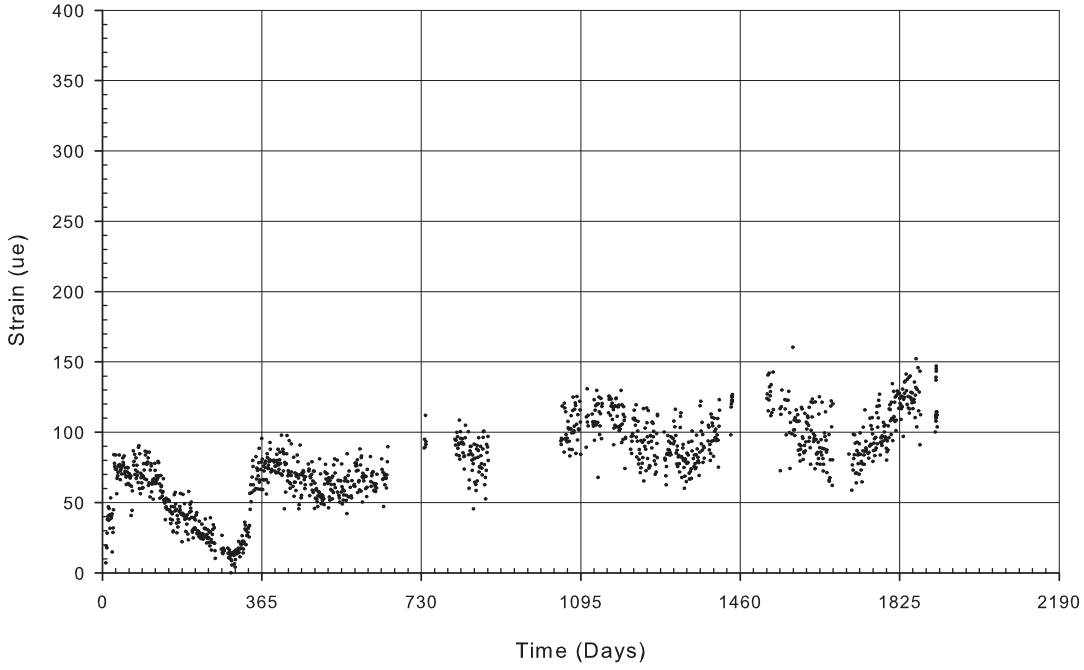
Strain (ue)
400
350
300
250
200
150
100
50
0
0
365
730
1095
1460
1825
2190
Time (Days)

B-CS3

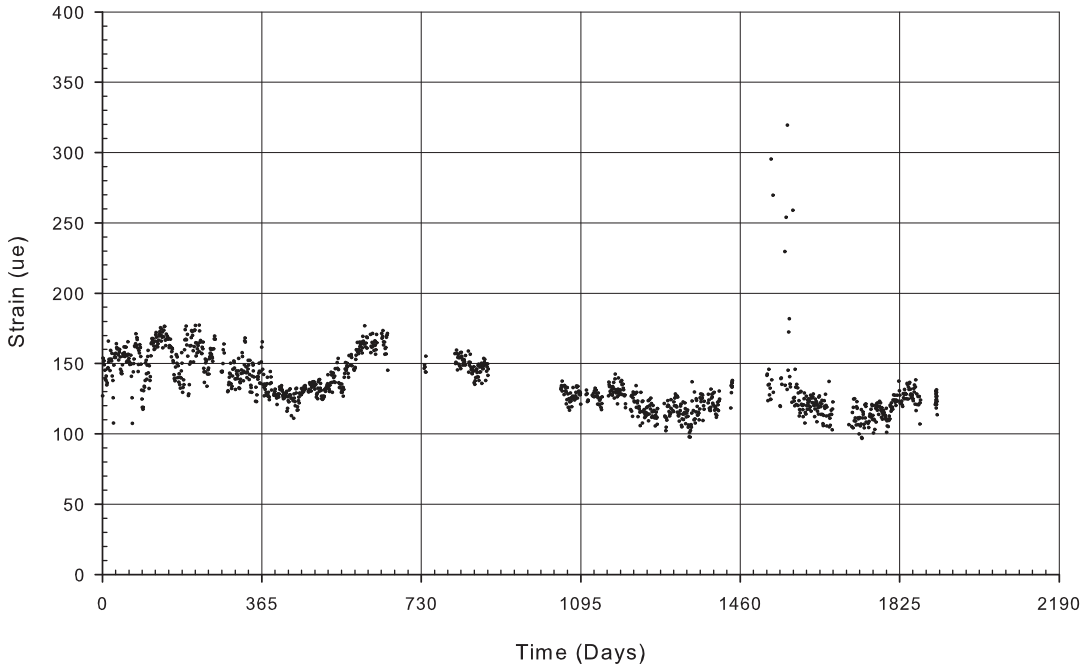
Strain (ue)
400
350
300
250
200
150
100
50
0
0
365
730
1095
1460
1825
2190
Time (Days)

B-HS1

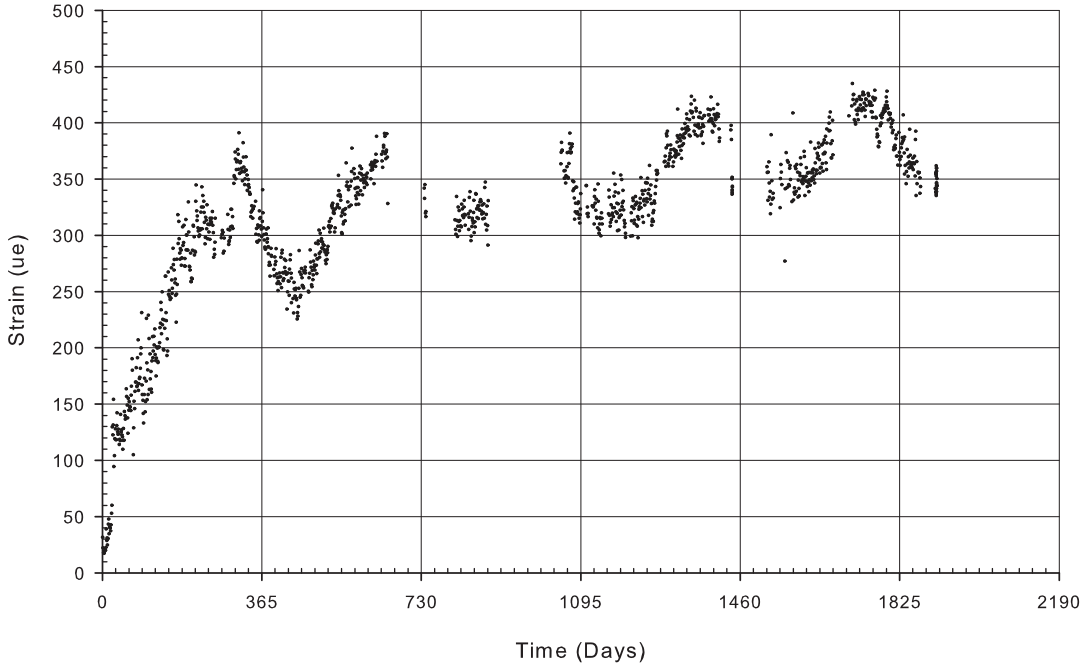
Strain (ue)
500
450
400
350
300
250
200
150
100
50
0
0
365
730
1095
1460
1825
2190
Time (Days)

B-HS2

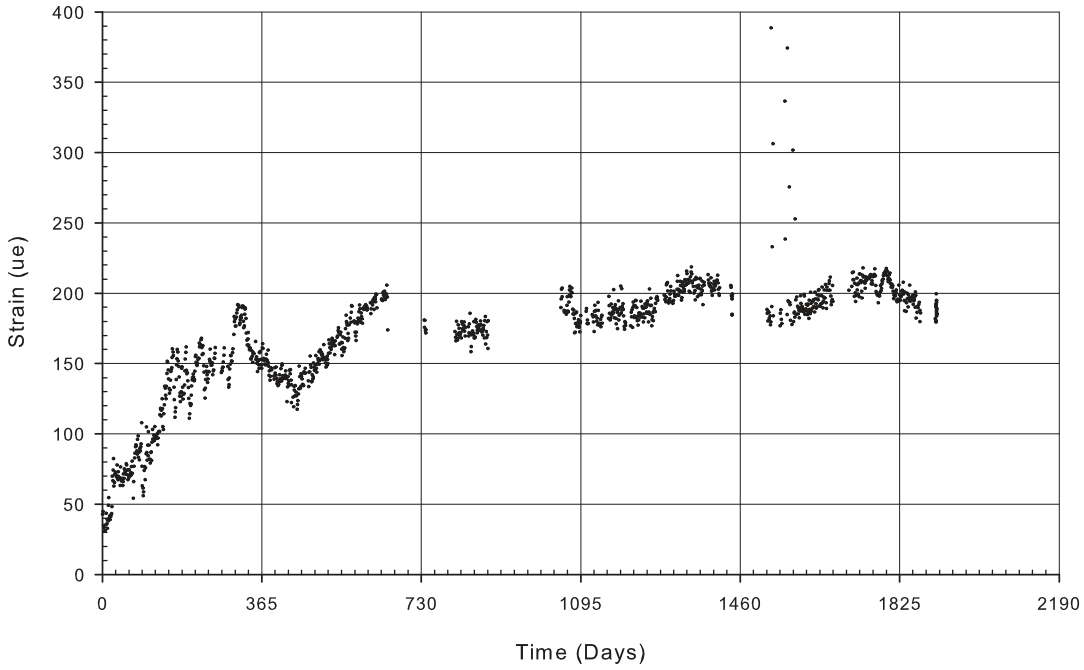
400
350
300
250
200
150
100
50
0
Strain (ue)
0
365
730
1095
1460
1825
2190
Time (Days)

B-HS3

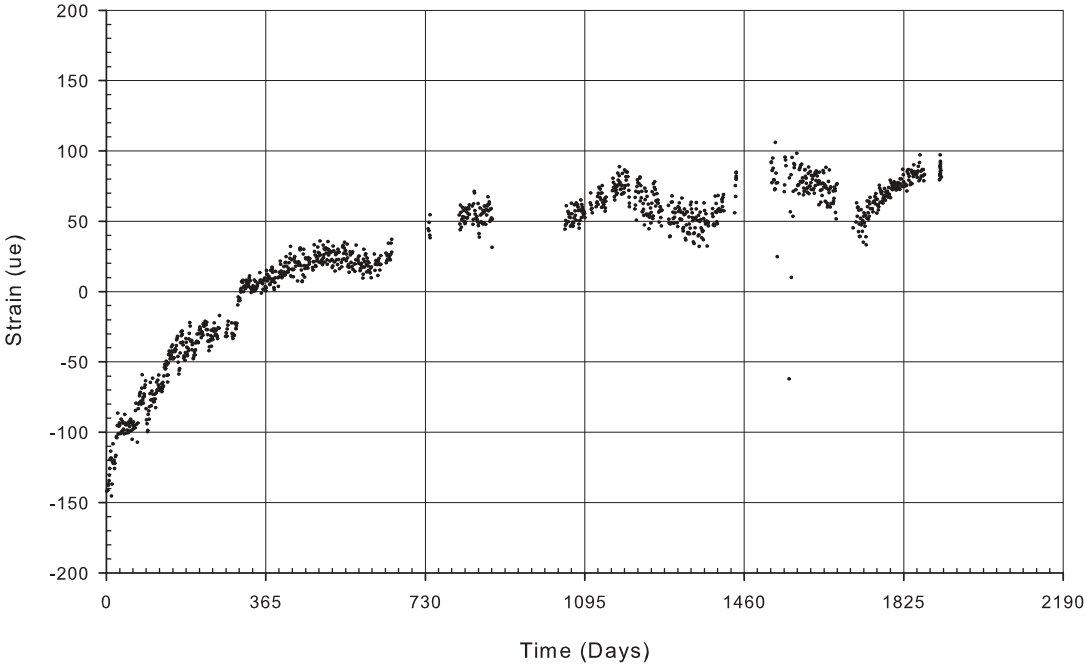
200
150
100
50
0
-50
-100
-150
-200
Strain (ue)
0
365
730
1095
1460
1825
2190
Time (Days)

B-HS4

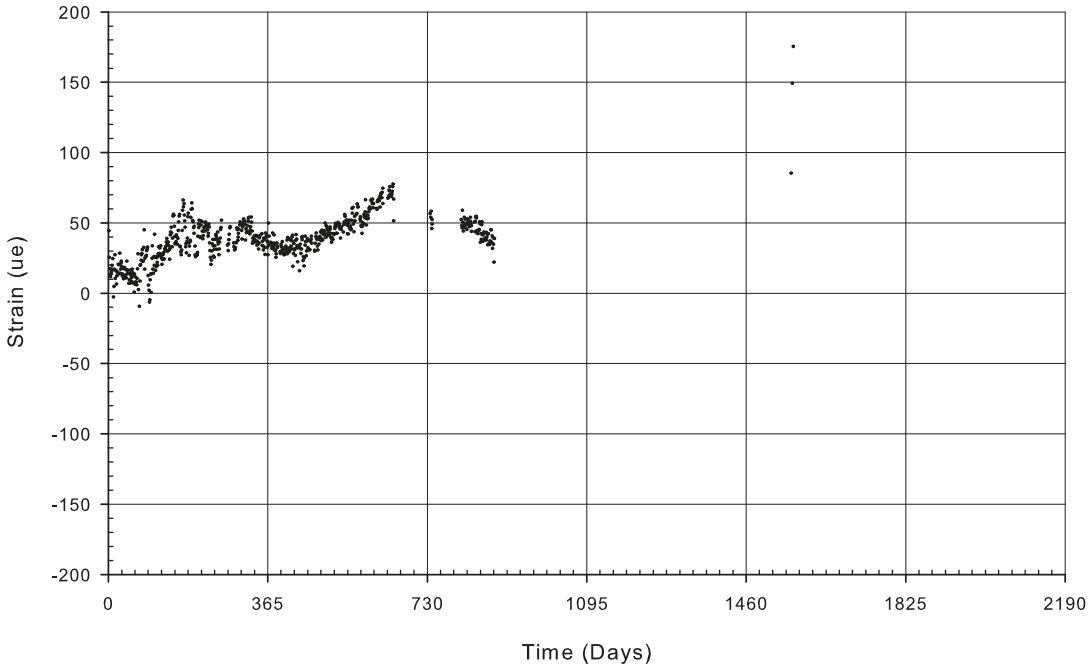
200
150
100
50
0
-50
-100
-150
-200
Strain (ue)
0
365
730
1095
1460
1825
2190
Time (Days)

B-HP1

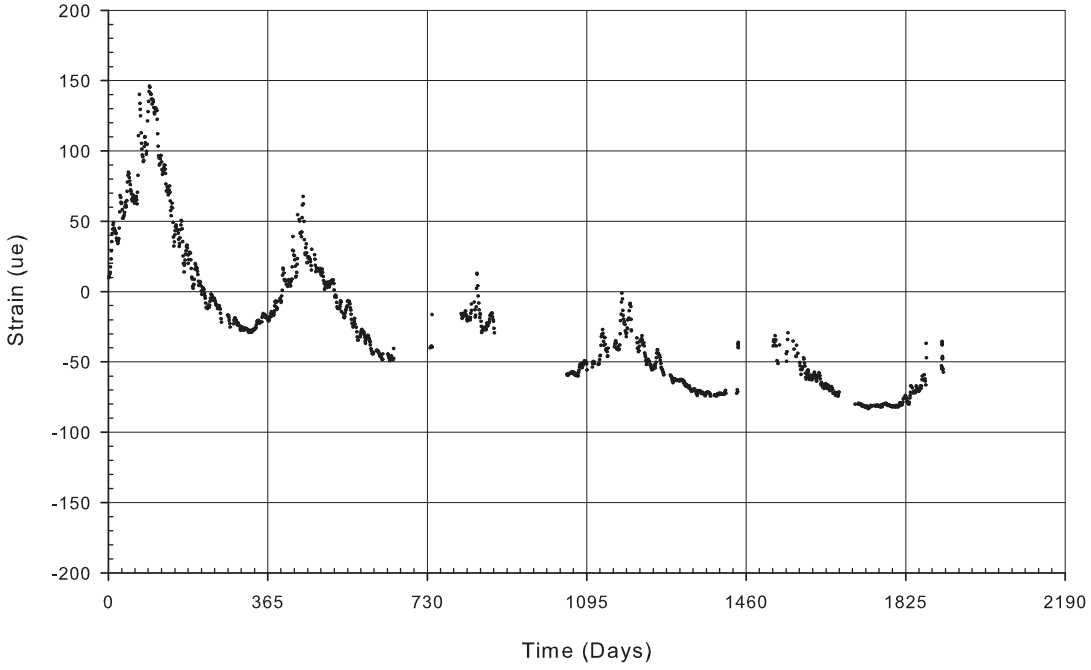
200
150
100
50
0
-50
-100
-150
-200
Strain (ue)
0
365
730
1095
1460
1825
2190
Time (Days)

B-HP2

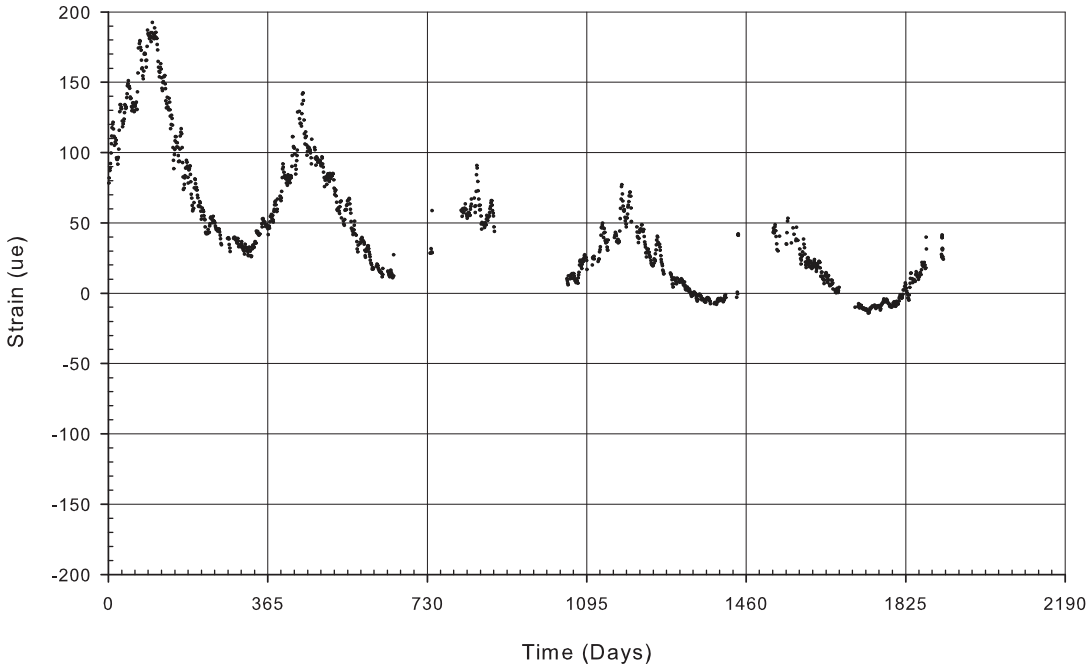
200
150
100
50
0
-50
-100
-150
-200
Strain (ue)
0
365
730
1095
1460
1825
2190
Time (Days)

B-HP3

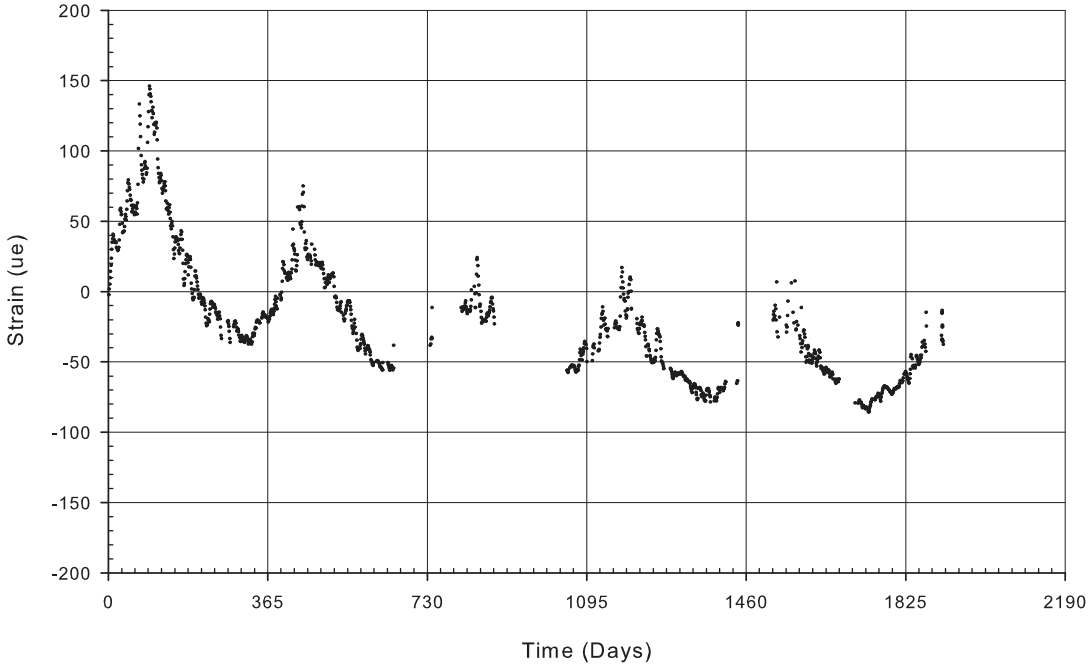
200
150
100
50
0
-50
-100
-150
-200
Strain (ue)
0
365
730
1095
1460
1825
2190
Time (Days)

B-HP4

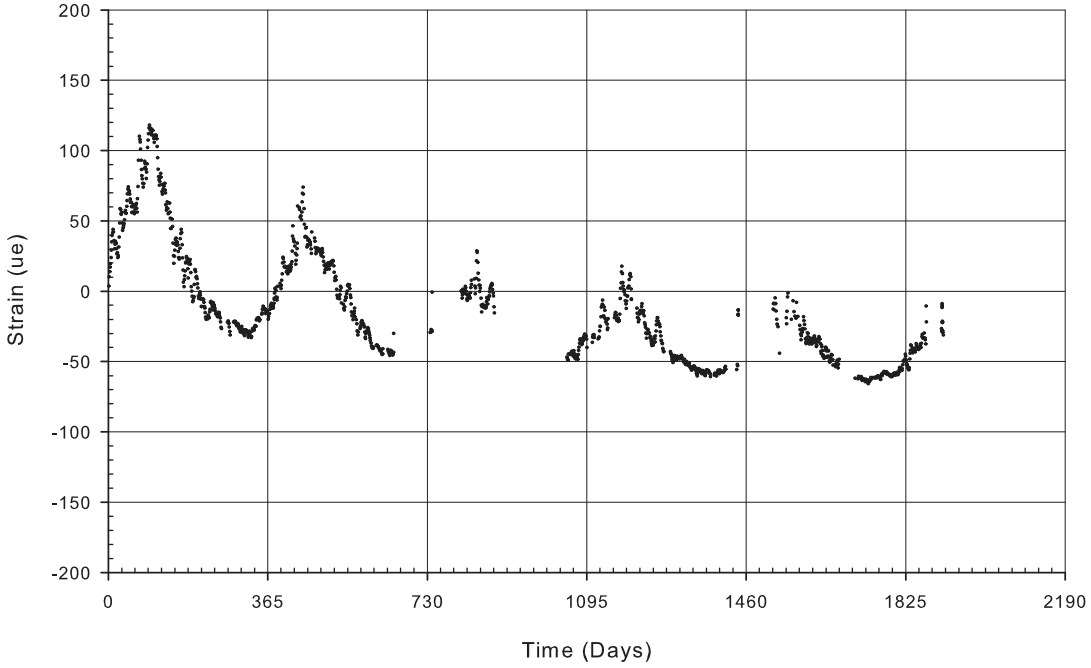
200
150
100
50
0
-50
-100
-150
-200
Strain (ue)
0
365
730
1095
1460
1825
2190
Time (Days)

B-HP5

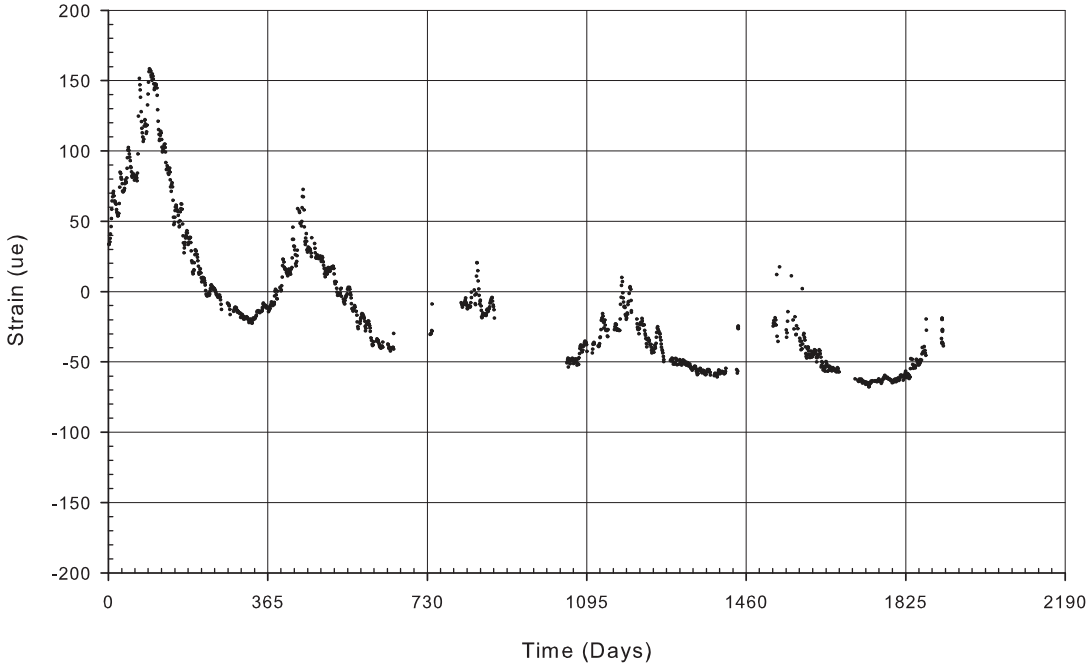
200
150
100
50
0
-50
-100
-150
-200
Strain (ue)
0
365
730
1095
1460
1825
2190
Time (Days)

B-HP6

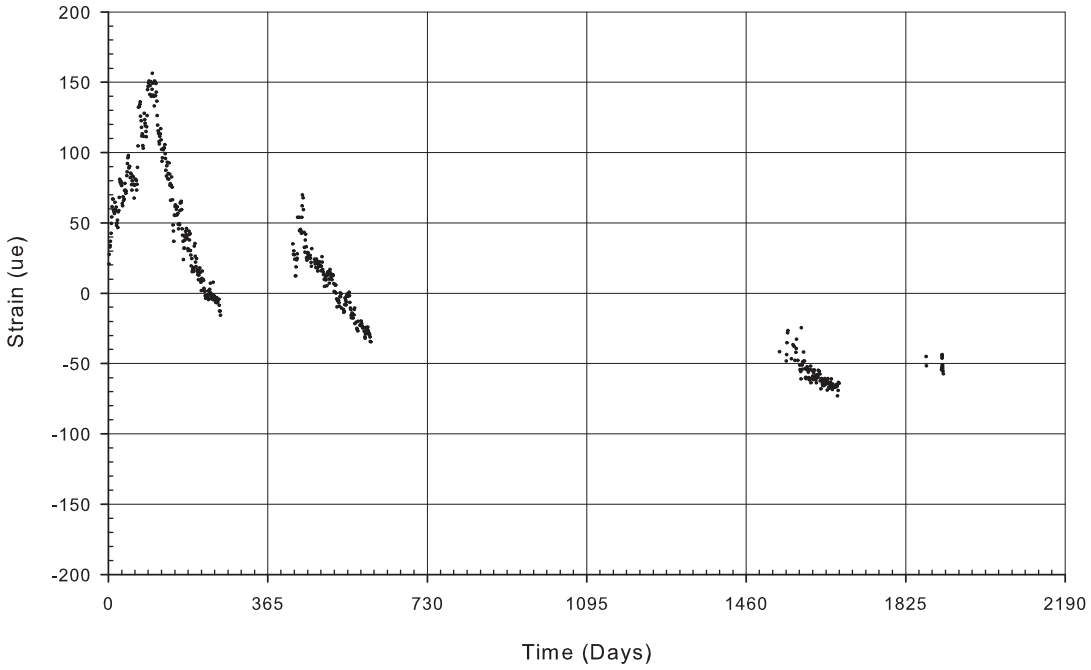
200
150
100
50
0
-50
-100
-150
-200
Strain (ue)
0
365
730
1095
1460
1825
2190
Time (Days)

C-HS1

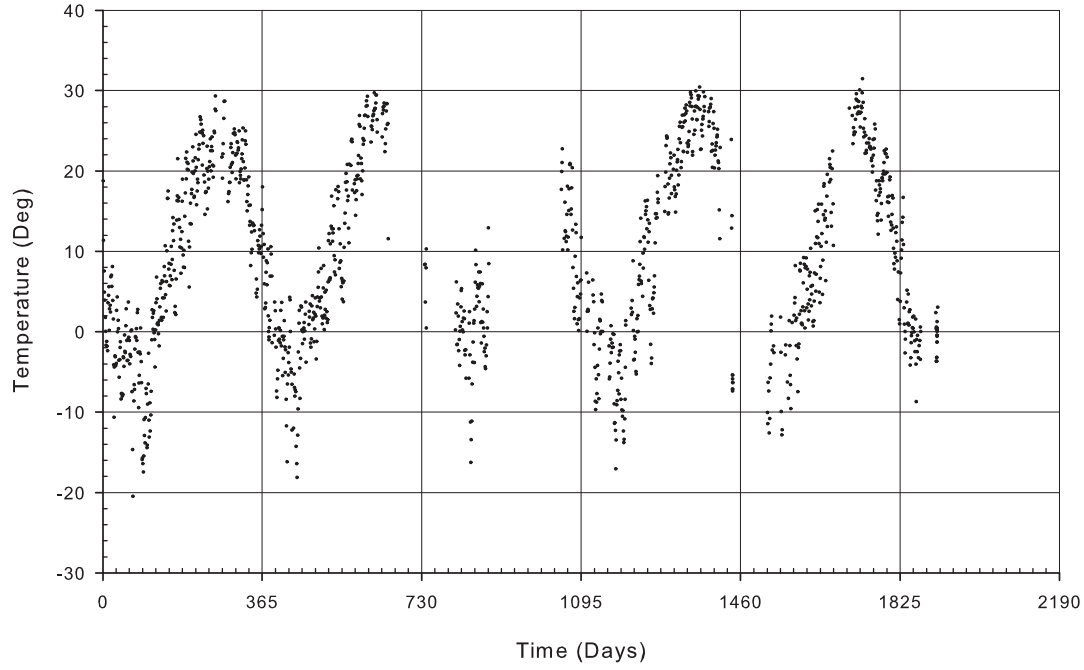
40
30
20
10
0
-10
-20
-30
Temperature (Deg)
0
365
730
1095
1460
1825
2190
Time (Days)

C-HS2

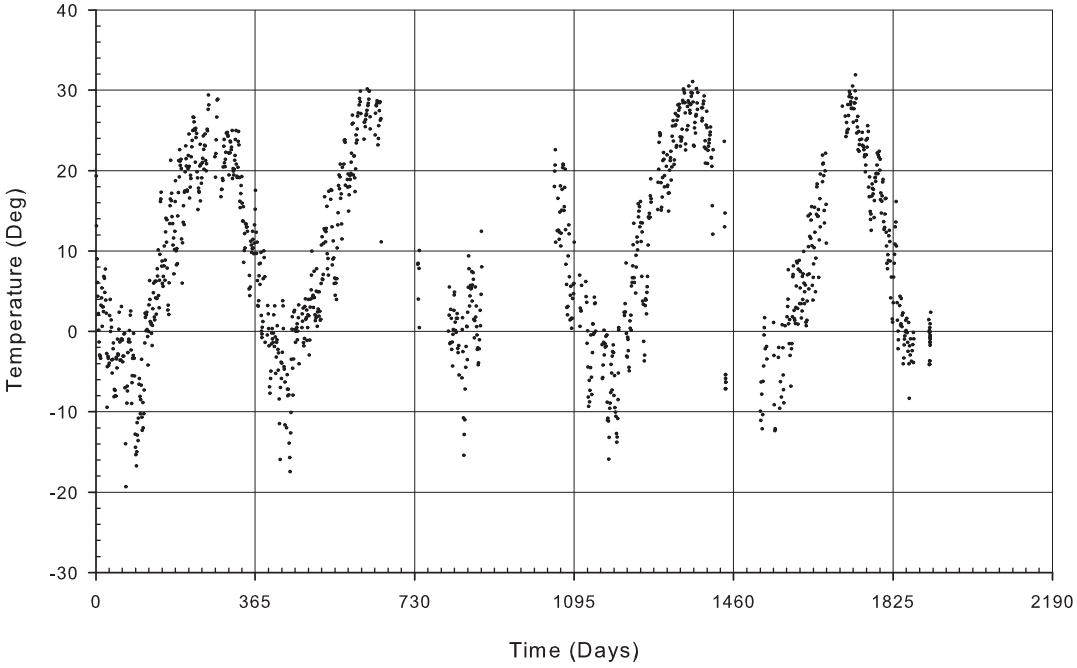
40
30
20
10
0
-10
-20
-30
Temperature (Deg)
0
365
730
1095
1460
1825
2190
Time (Days)

C-HS3

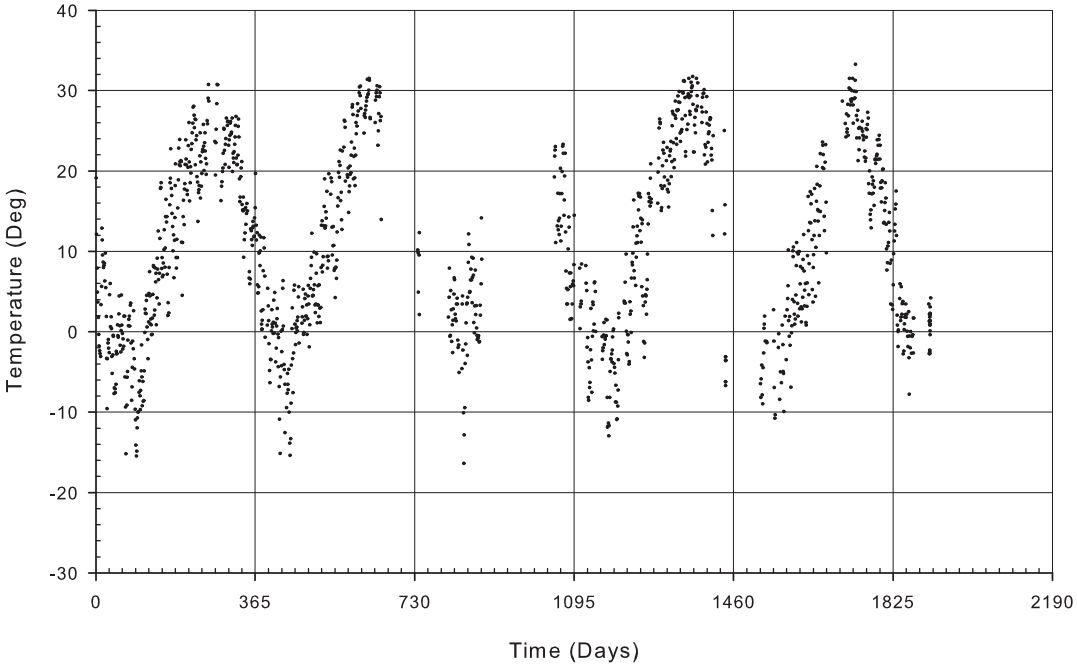
40
30
20
10
0
-10
-20
-30
Temperature (Deg)
0
365
730
1095
1460
1825
2190
Time (Days)

B-CS1

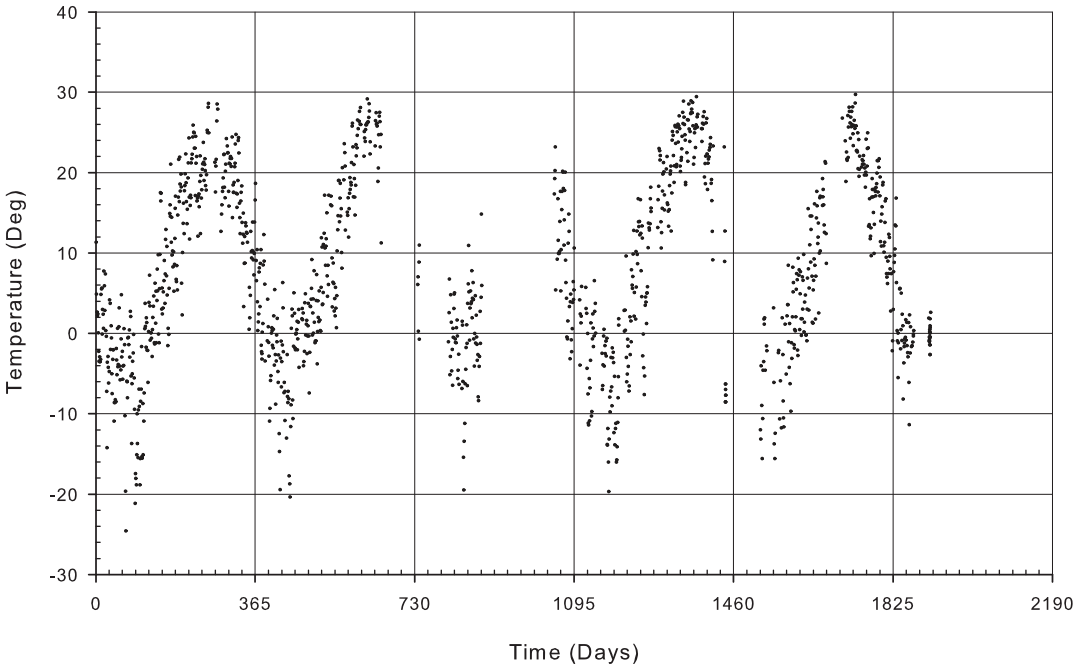
40
30
20
10
0
-10
-20
-30
Temperature (Deg)
0
365
730
1095
1460
1825
2190
Time (Days)

B-CS2

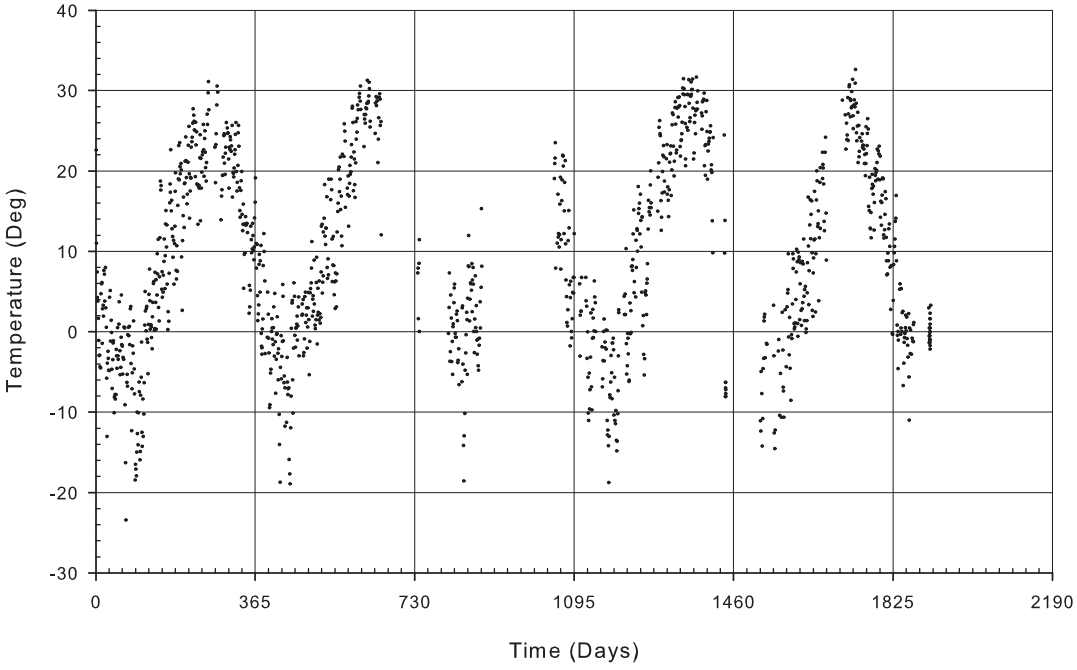
40
30
20
10
0
-10
-20
-30
Temperature (Deg)
0
365
730
1095
1460
1825
2190
Time (Days)

B-CS3

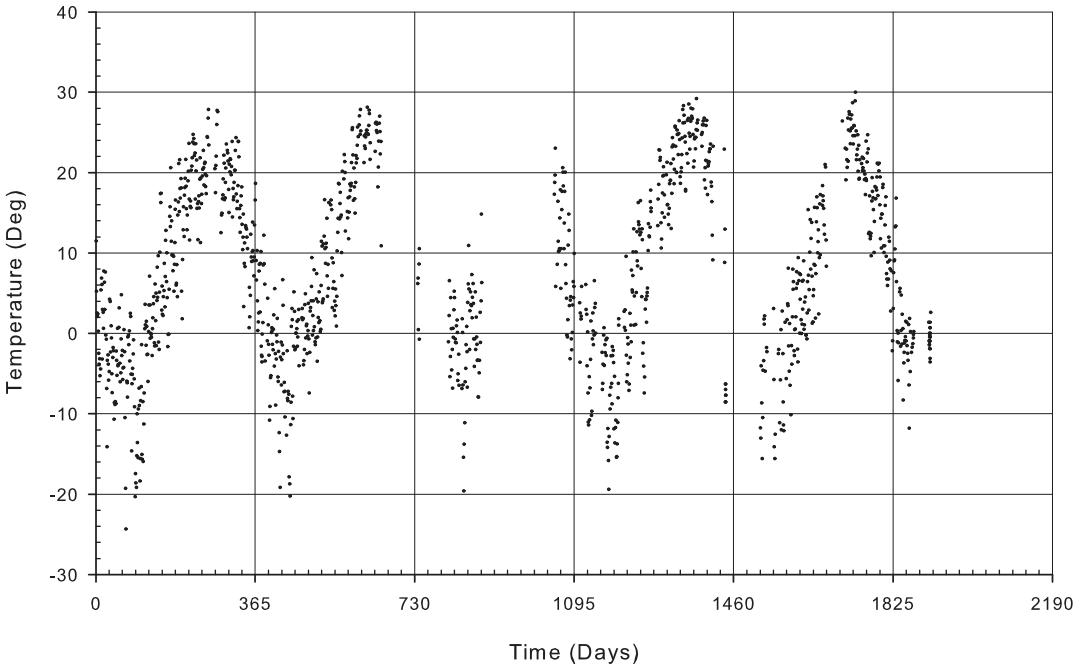
40
30
20
10
0
-10
-20
-30
Temperature (Deg)
0
365
730
1095
1460
1825
2190
Time (Days)

B-HS1

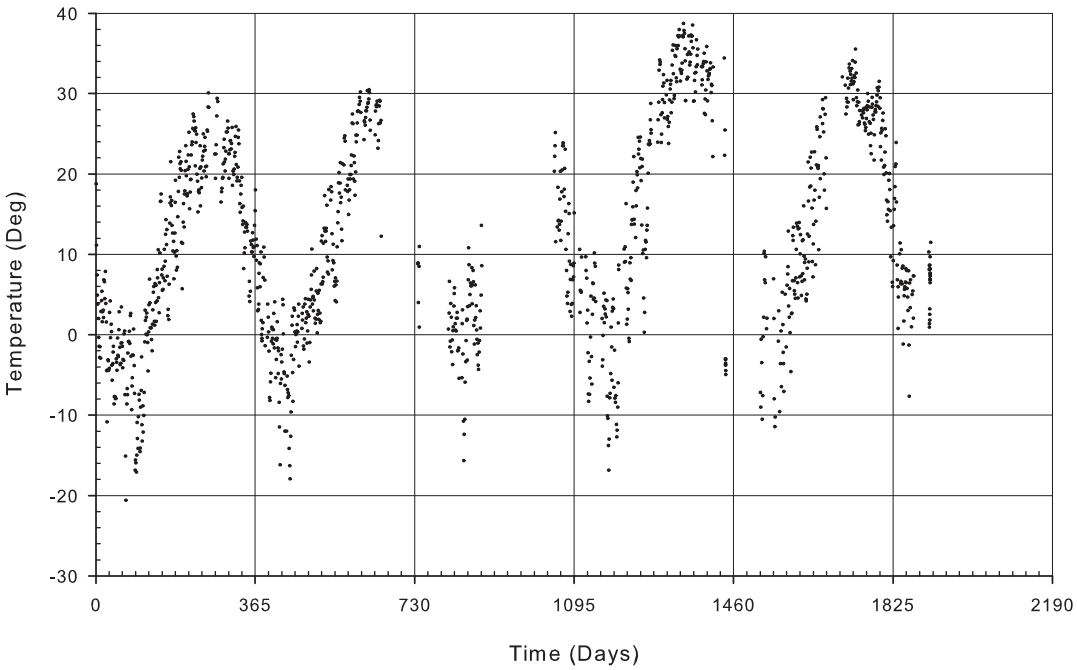
40
30
20
10
0
-10
-20
-30
Temperature (Deg)
0
365
730
1095
1460
1825
2190
Time (Days)

B-HS2

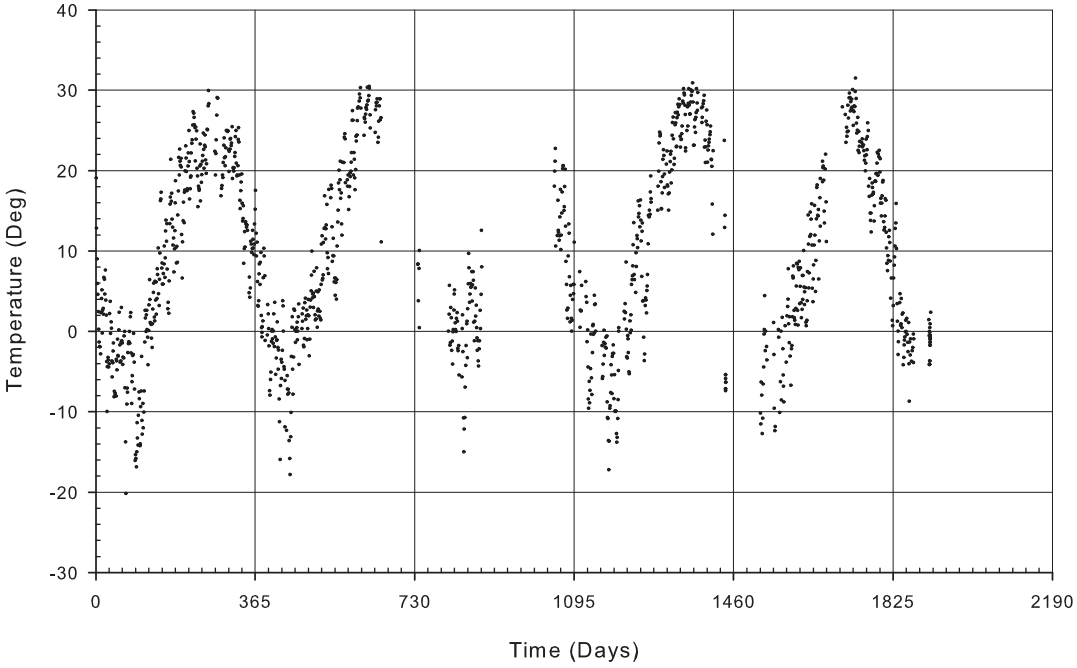
40
30
20
10
0
-10
-20
-30
Temperature (Deg)
0
365
730
1095
1460
1825
2190
Time (Days)

B-HS3

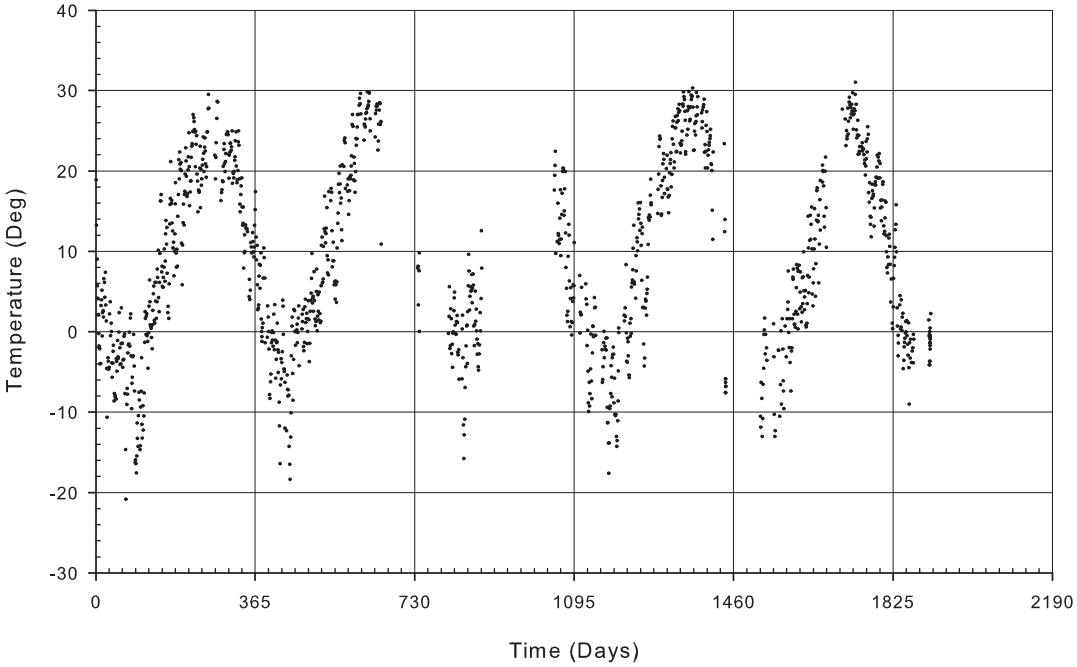
40
30
20
10
0
-10
-20
-30
Temperature (Deg)
0
365
730
1095
1460
1825
2190
Time (Days)

B-HS4

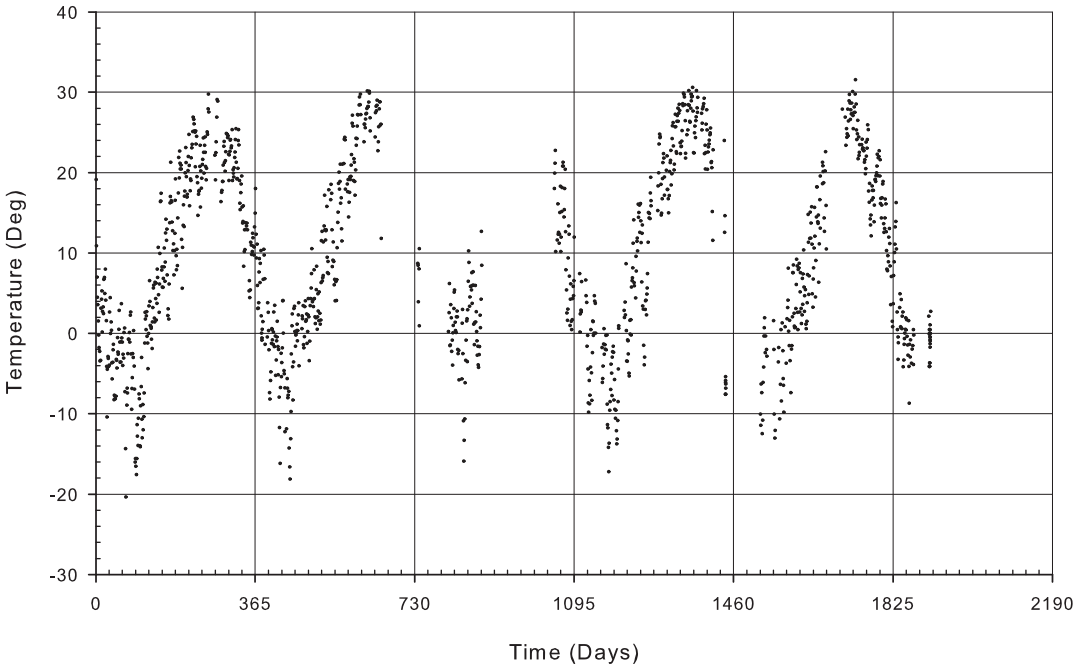
40
30
20
10
0
-10
-20
-30
Temperature (Deg)
0
365
730
1095
1460
1825
2190
Time (Days)

B-HP1

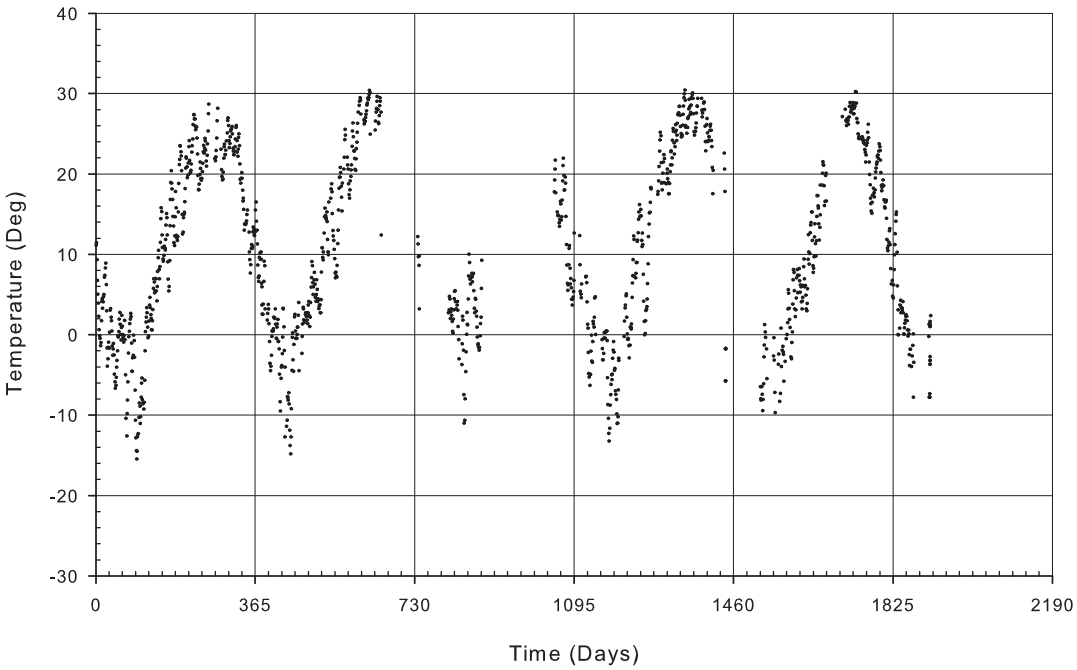
40
30
20
10
0
-10
-20
-30
Temperature (Deg)
0
365
730
1095
1460
1825
2190
Time (Days)

B-HP2

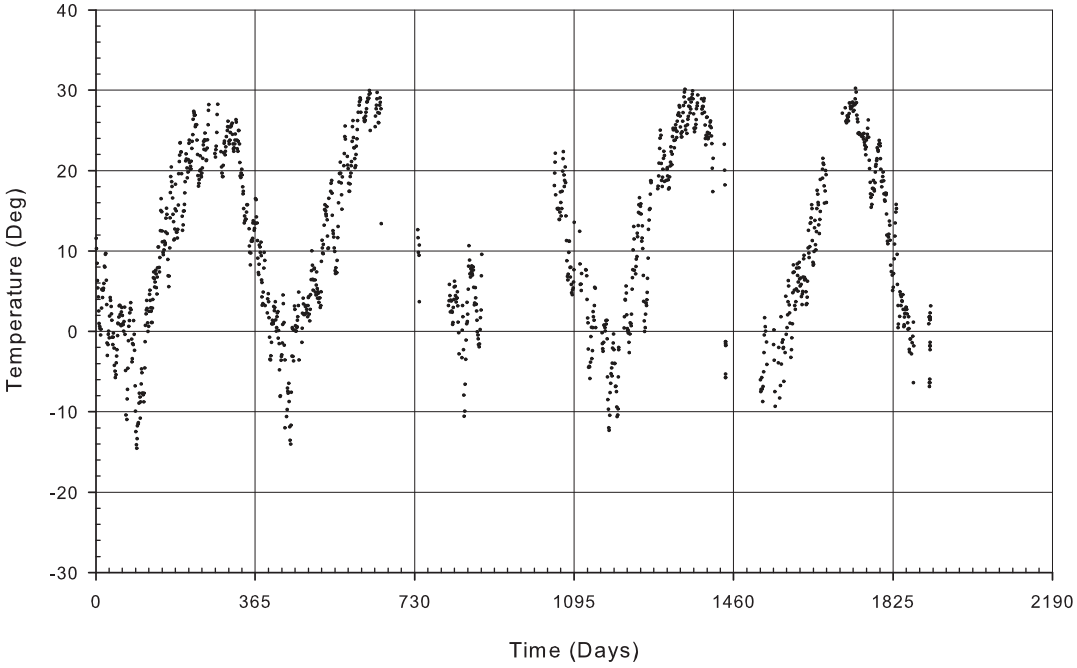
40
30
20
10
0
-10
-20
-30
Temperature (Deg)
0
365
730
1095
1460
1825
2190
Time (Days)

B-HP3

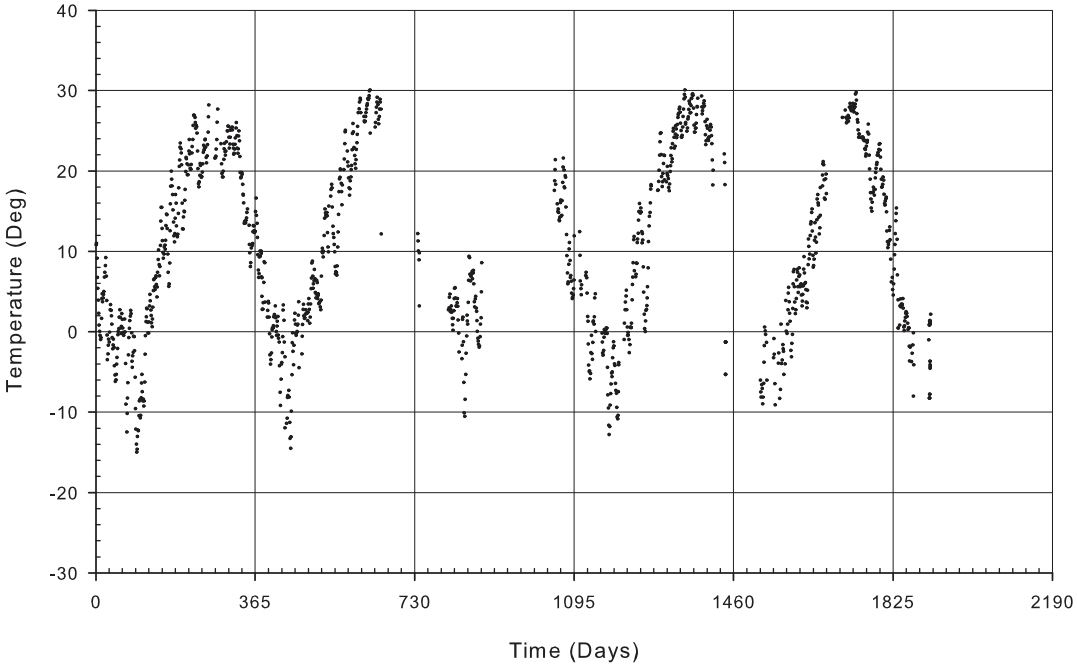
40
30
20
10
0
-10
-20
-30
Temperature (Deg)
0
365
730
1095
1460
1825
2190
Time (Days)

B-HP4

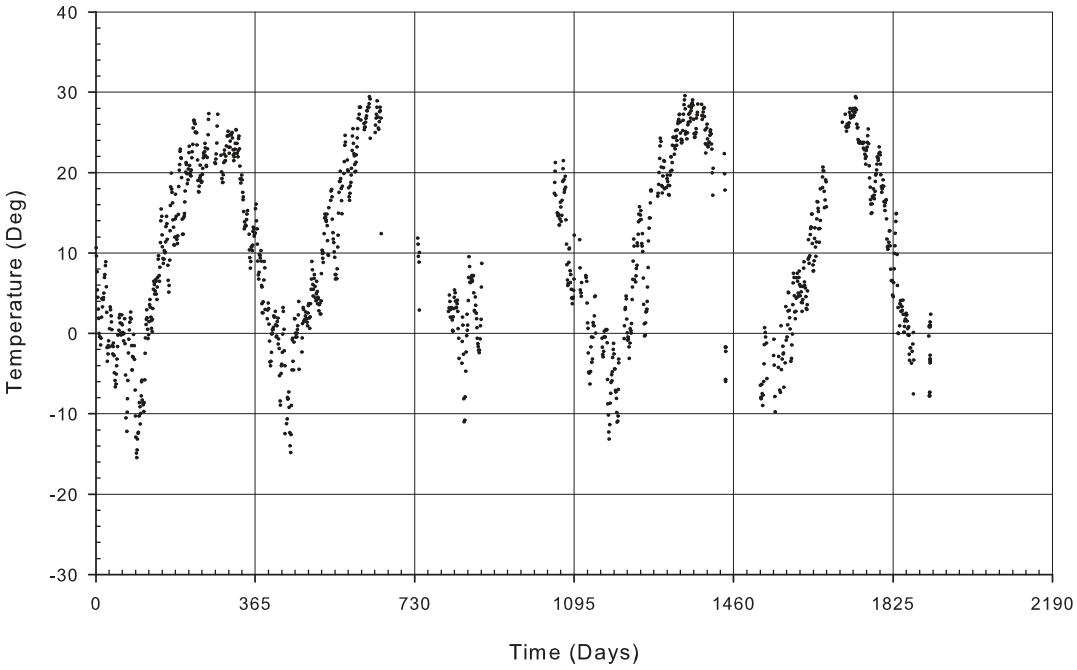
40
30
20
10
0
-10
-20
-30
Temperature (Deg)
0
365
730
1095
1460
1825
2190
Time (Days)

B-HP5

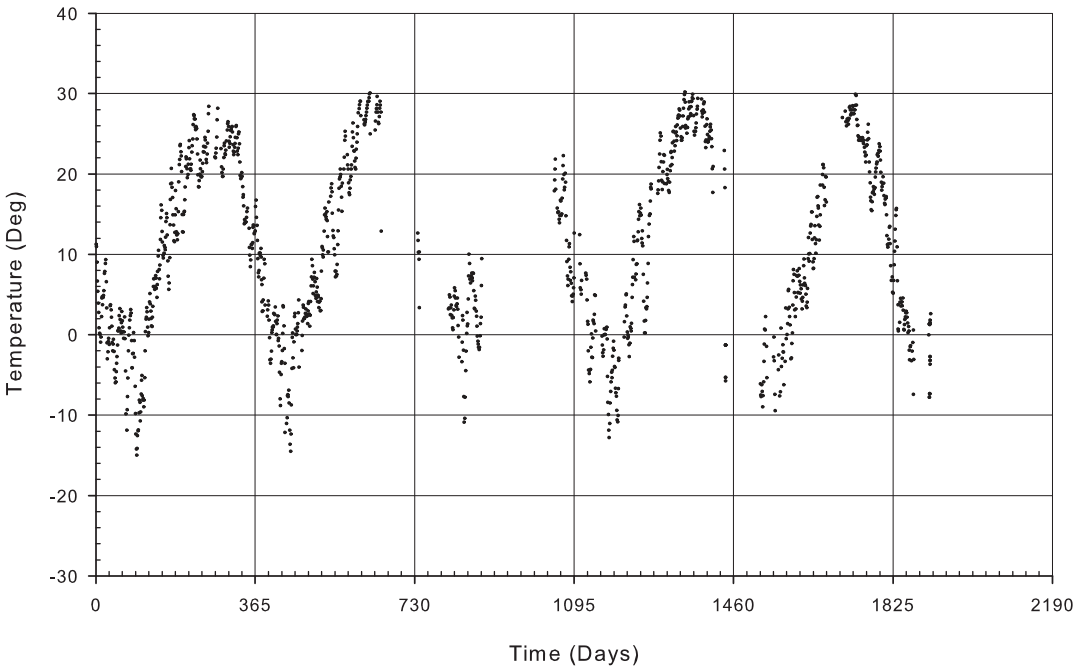
40
30
20
10
0
-10
-20
-30
Temperature (Deg)
0
365
730
1095
1460
1825
2190
Time (Days)

B-HP6

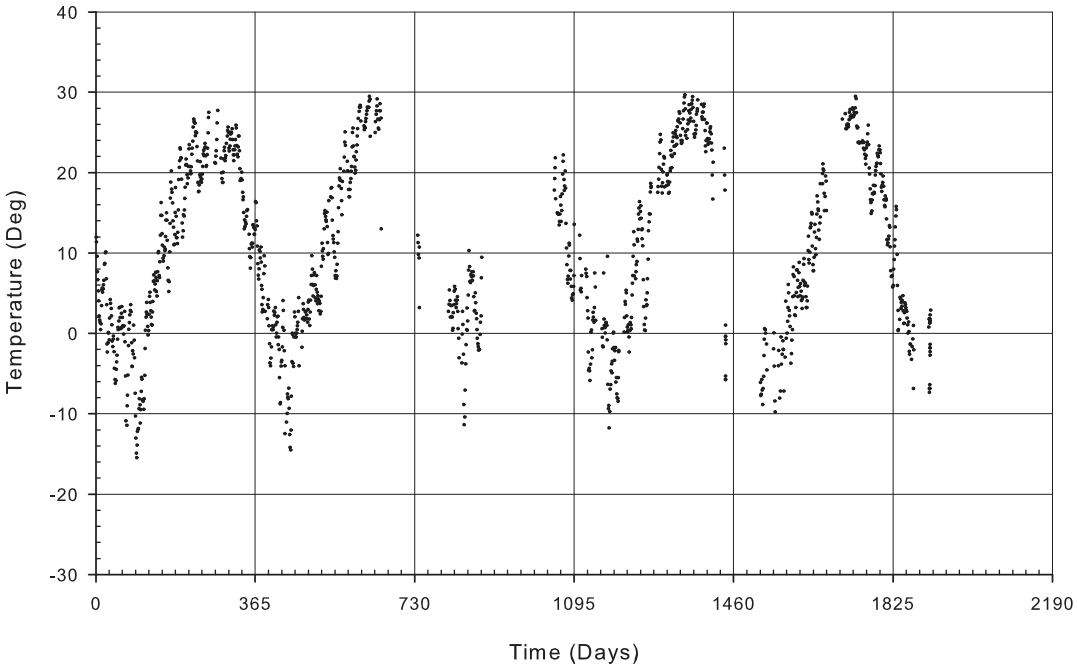
40
30
20
10
0
-10
-20
-30
Temperature (Deg)
0
365
730
1095
1460
1825
2190
Time (Days)

B-VD1

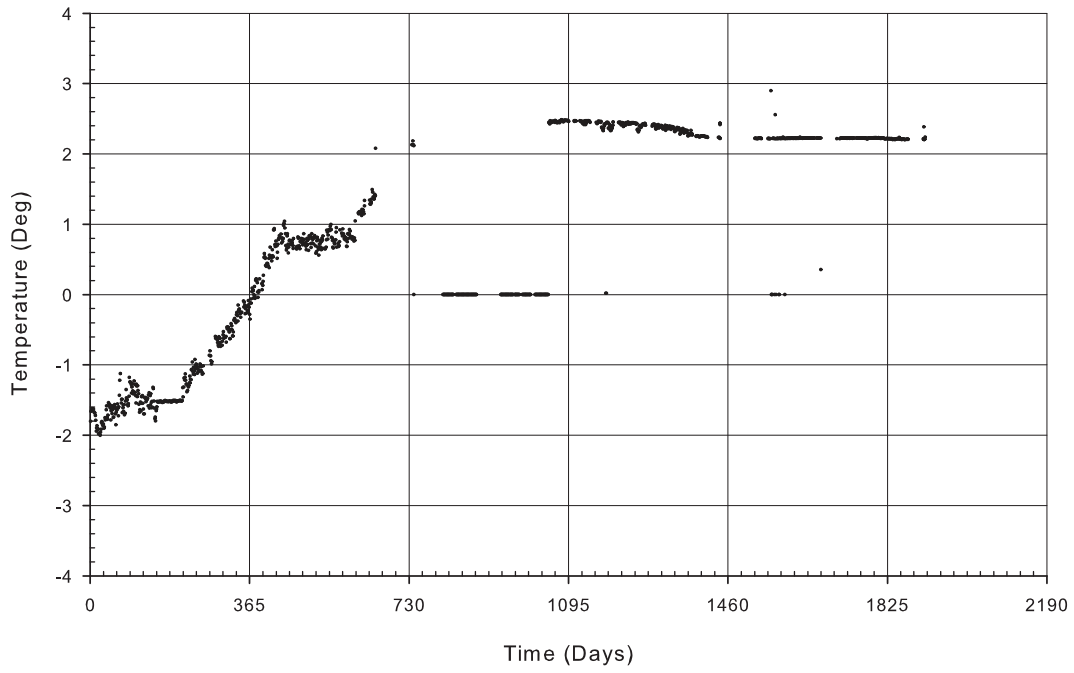
4
3
2
1
0
-1
-2
-3
-4
Temperature (Deg)
0
365
730
1095
1460
1825
2190
Time (Days)

B-VD1

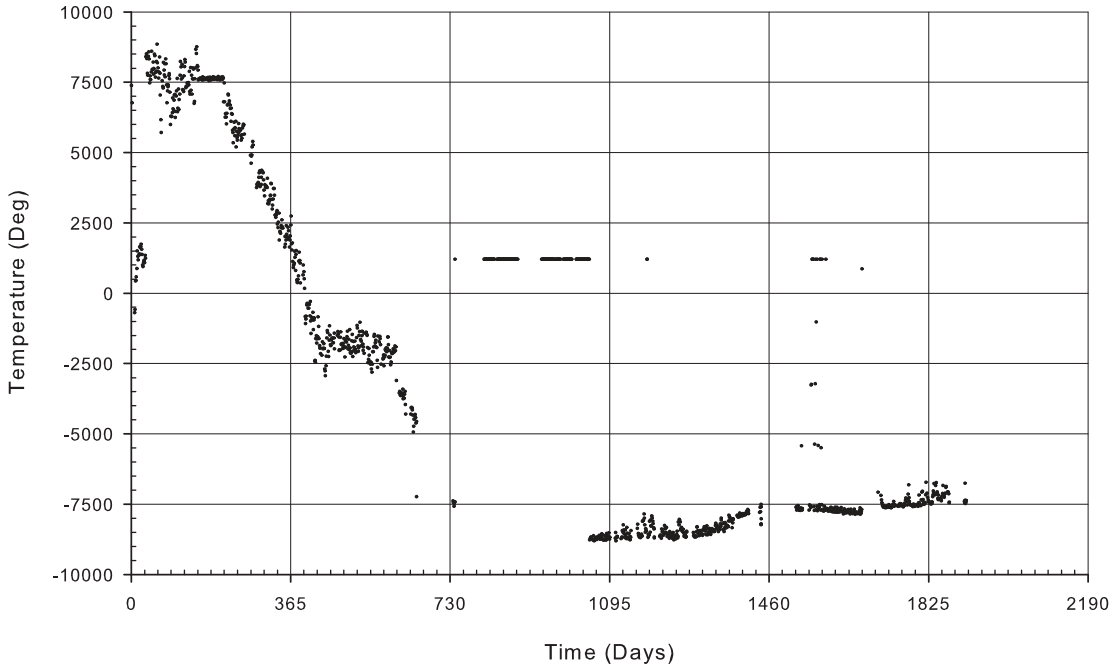
10000
7500
5000
2500
0
-2500
-5000
-7500
-10000
Temperature (Deg)
0
365
730
1095
1460
1825
2190
Time (Days)

B-VD2

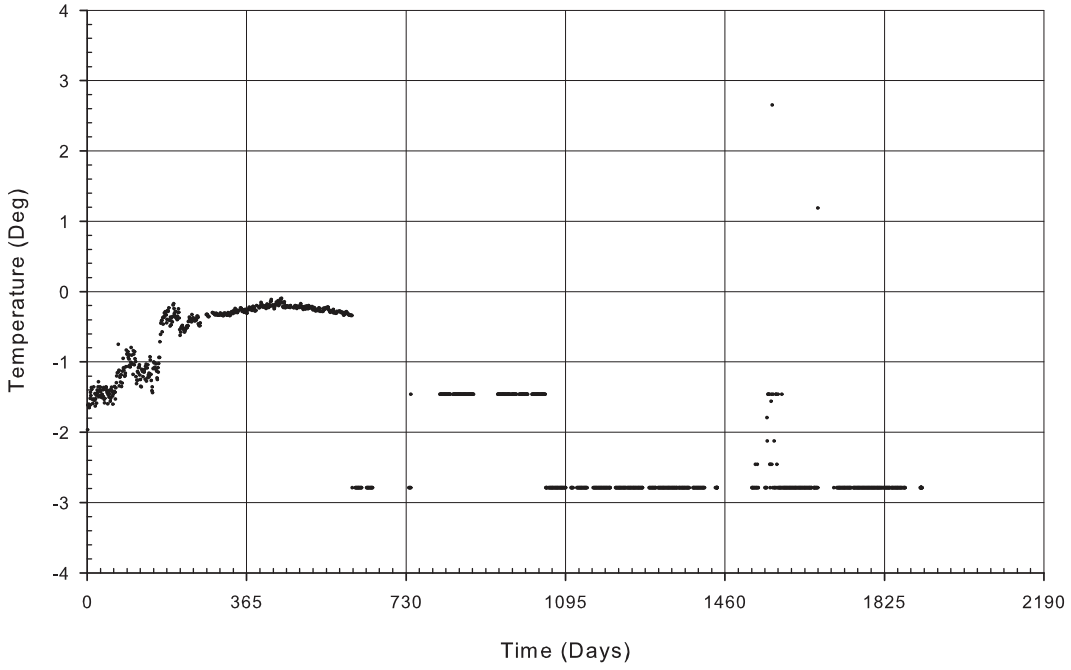
4
3
2
1
0
-1
-2
-3
-4
Temperature (Deg)
0
365
730
1095
1460
1825
2190
Time (Days)

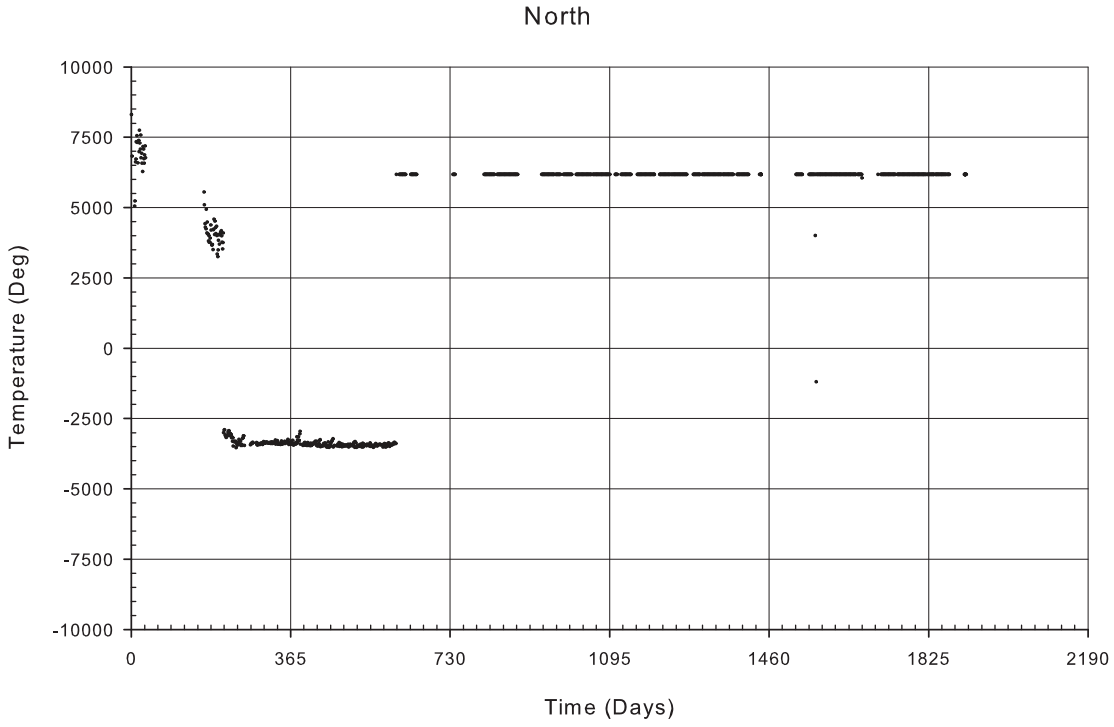
North
10000
7500
5000
2500
0
-2500
-5000
-7500
-10000
Temperature (Deg)
0
365
730
1095
1460
1825
2190
Time (Days)

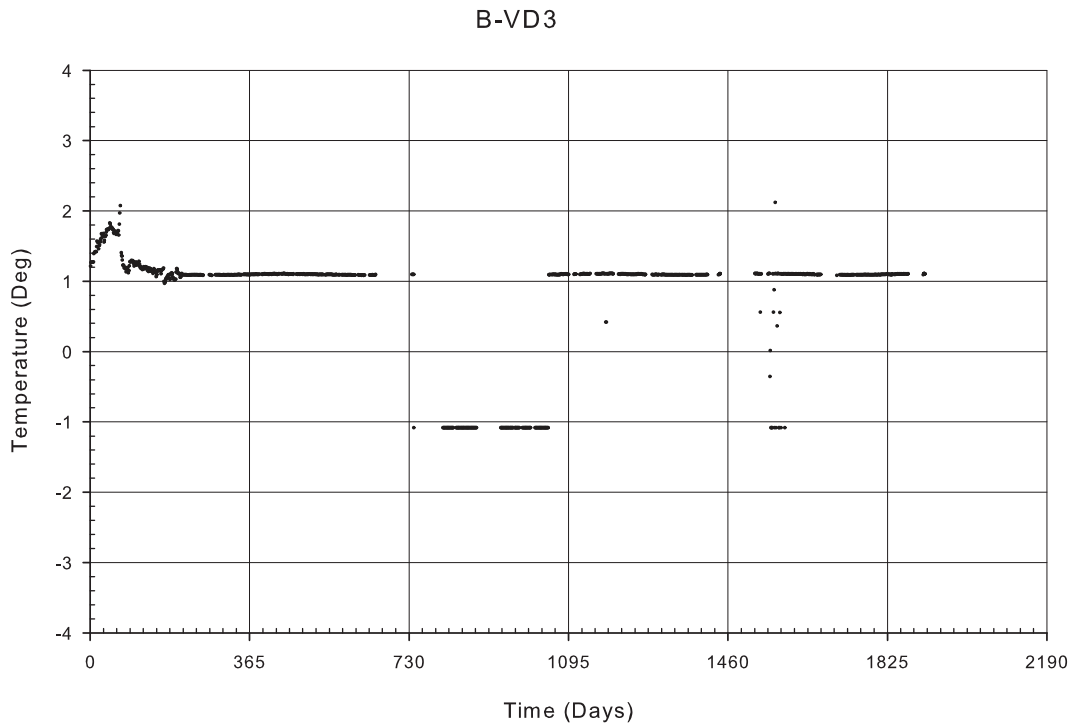
B-VD3
4
3
2
1
0
-1
-2
-3
-4
Temperature (Deg)
0
365
730
1095
1460
1825
2190
Time (Days)

B-VD3

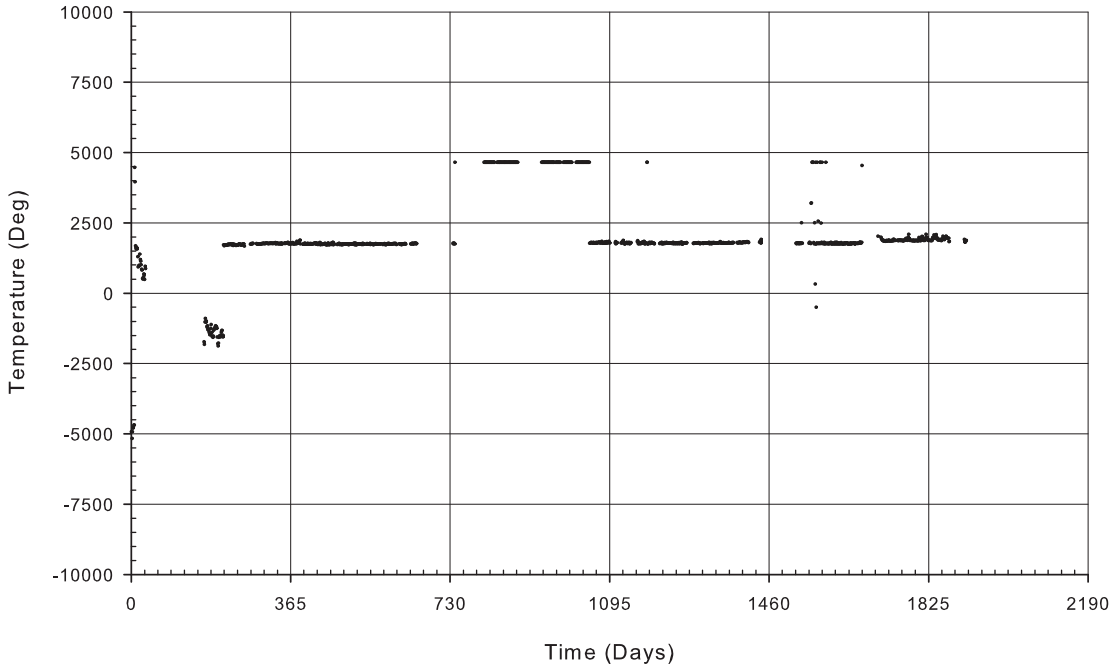
10000
7500
5000
2500
0
-2500
-5000
-7500
-10000
Temperature (Deg)
0
365
730
1095
1460
1825
2190
Time (Days)

B-VD4

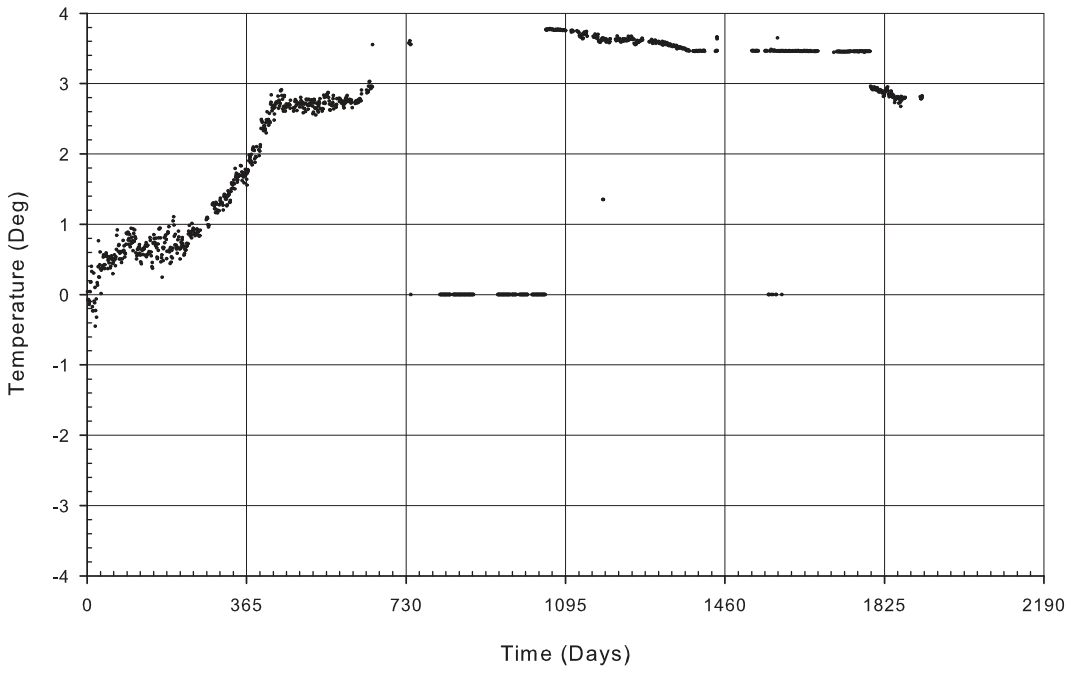
4
3
2
1
0
-1
-2
-3
-4
Temperature (Deg)
0
365
730
1095
1460
1825
2190
Time (Days)

South

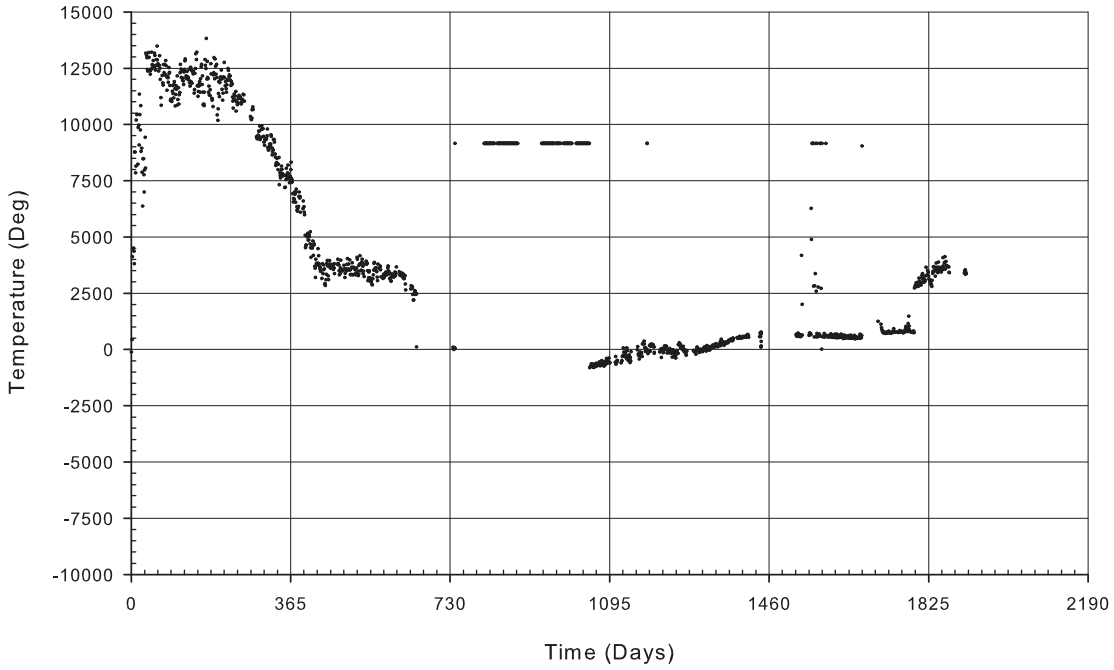
15000
12500
10000
7500
5000
2500
0
-2500
-5000
-7500
-10000
Temperature (Deg)
0
365
730
1095
1460
1825
2190
Time (Days)

ODD_9

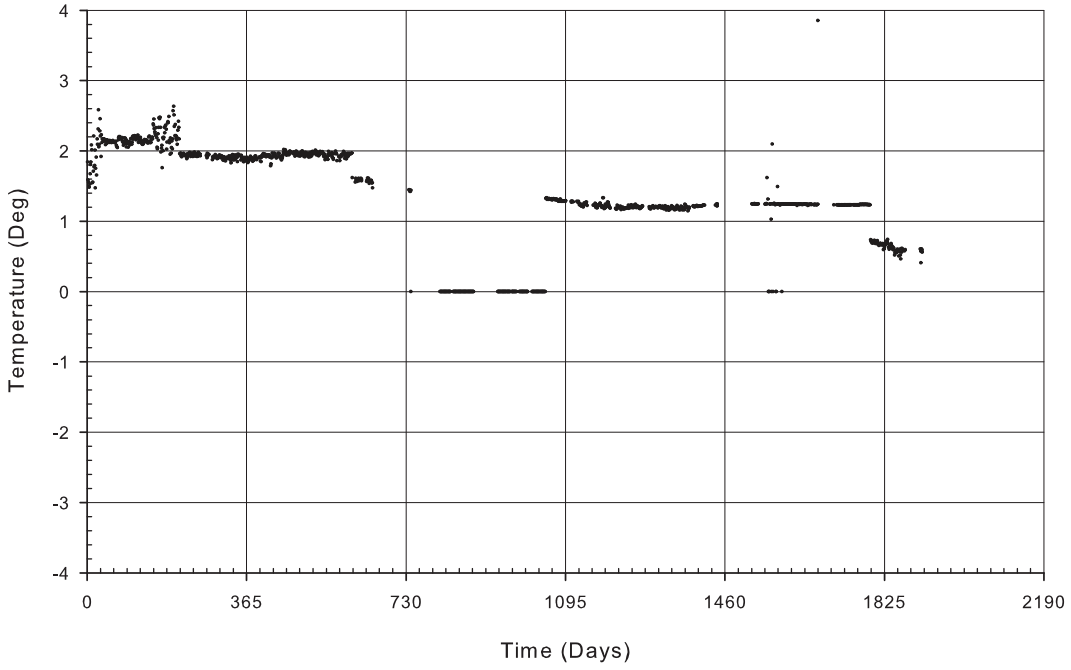
4
3
2
1
0
-1
-2
-3
-4
Temperature (Deg)
0
365
730
1095
1460
1825
2190
Time (Days)

ODD_10

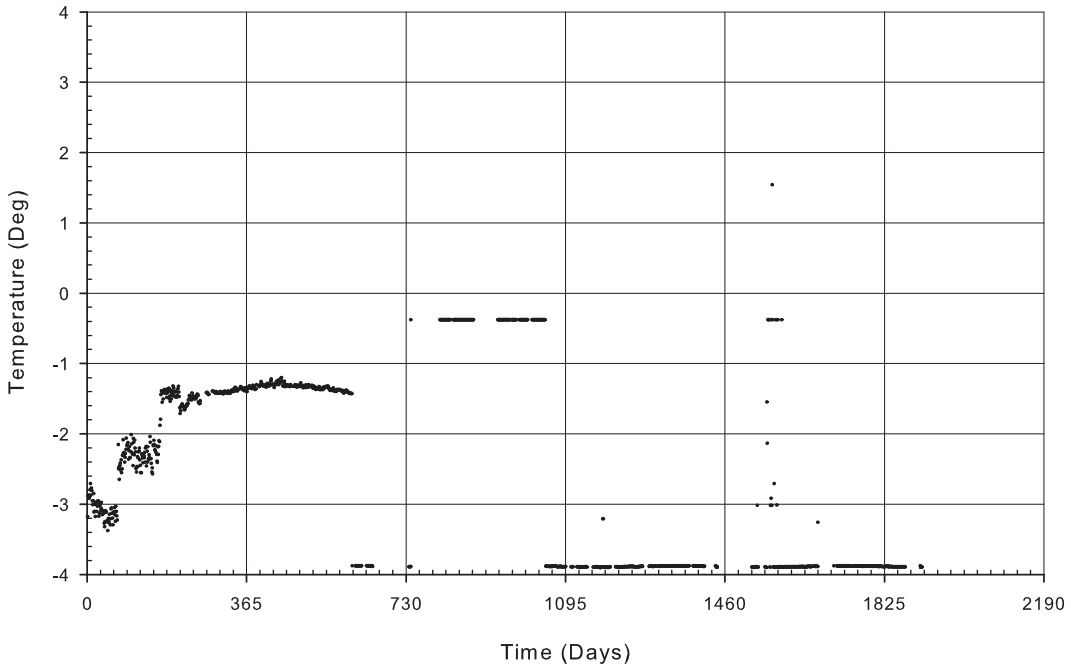
Temperature (Deg)
4
3
2
1
0
-1
-2
-3
-4
0
365
730
1095
1460
1825
2190
Time (Days)

ODD_11

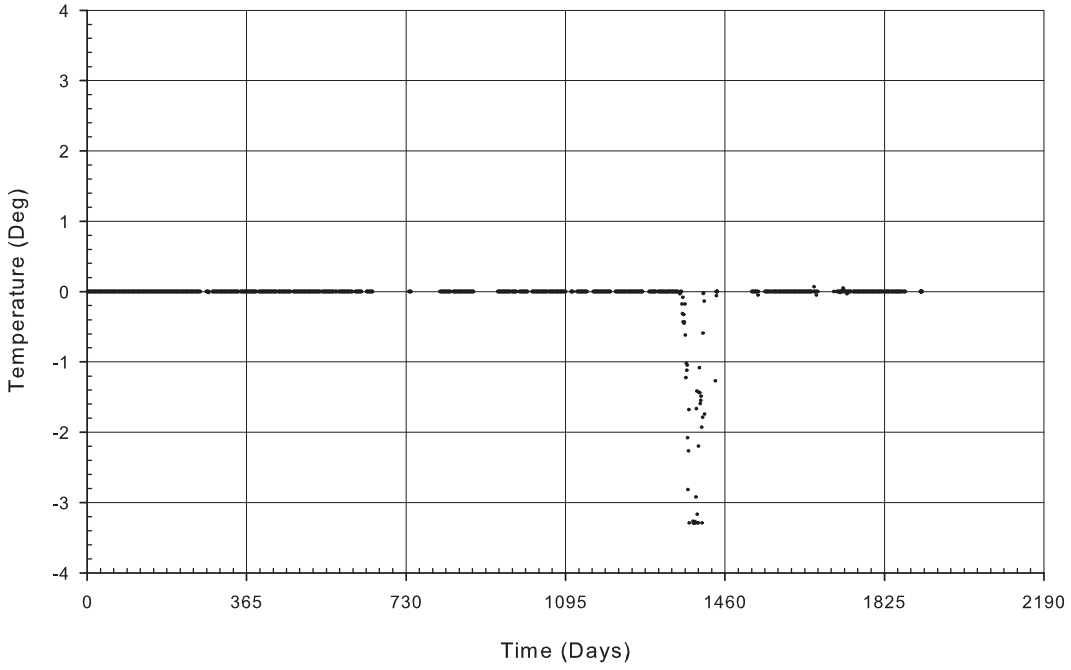
Temperature (Deg)
4
3
2
1
0
-1
-2
-3
-4
0
365
730
1095
1460
1825
2190
Time (Days)

ODD_12

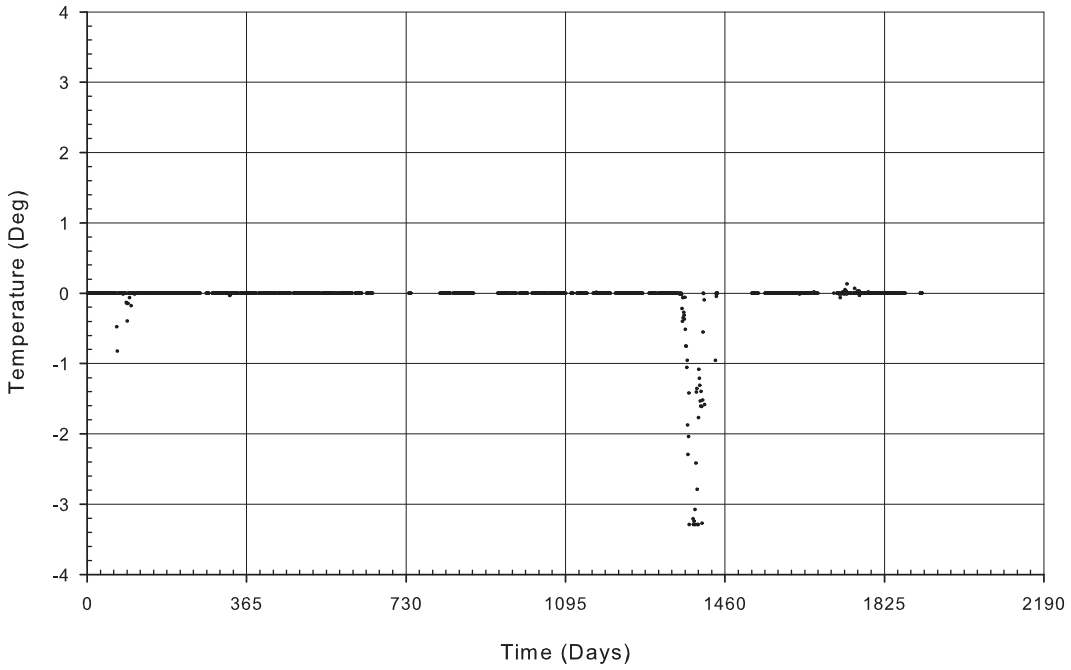
4
3
2
1
0
-1
-2
-3
-4
Temperature (Deg)
0
365
730
1095
1460
1825
2190
Time (Days)

ODD_13

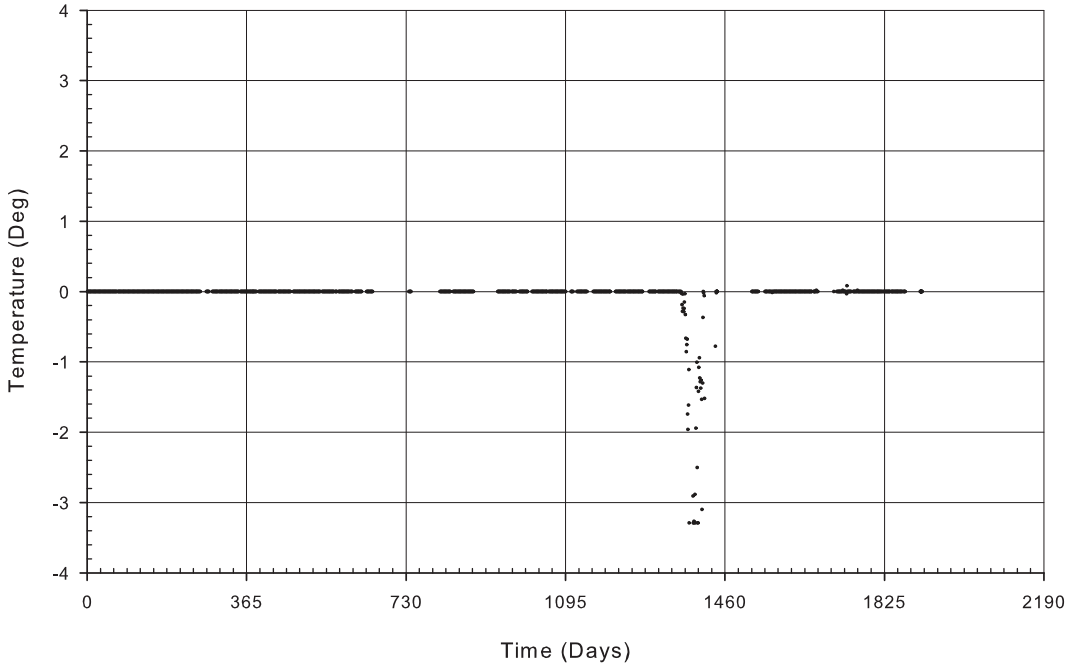
4
3
2
1
0
-1
-2
-3
-4
Temperature (Deg)
0
365
730
1095
1460
1825
2190
Time (Days)

ODD_14

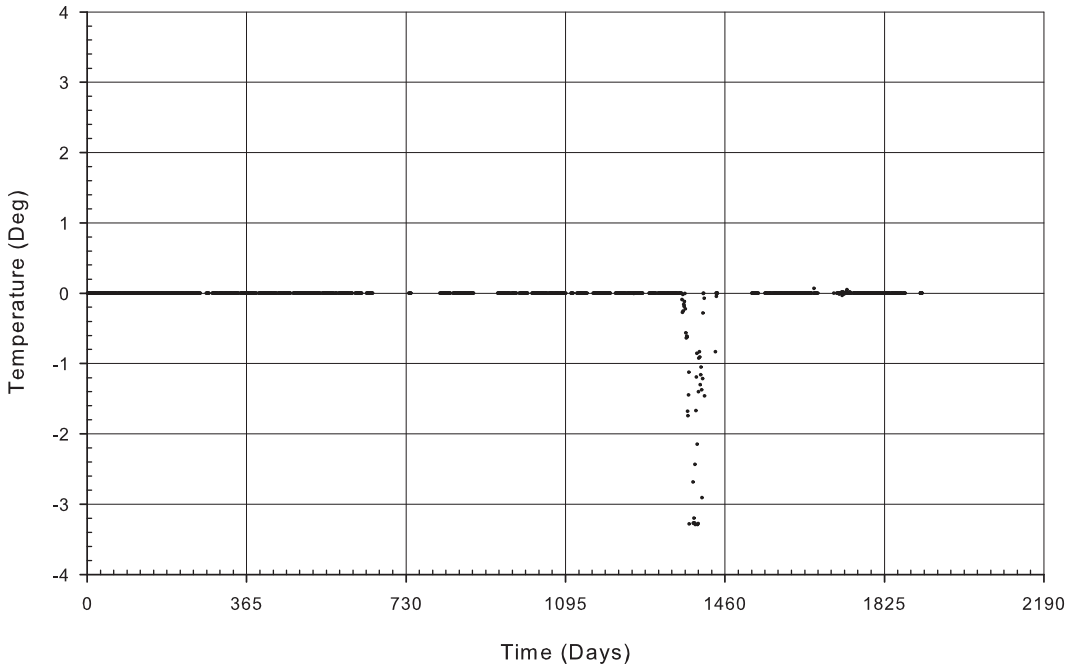
Temperature (Deg)
4
3
2
1
0
-1
-2
-3
-4
0
365
730
1095
1460
1825
2190
Time (Days)

ODD_15

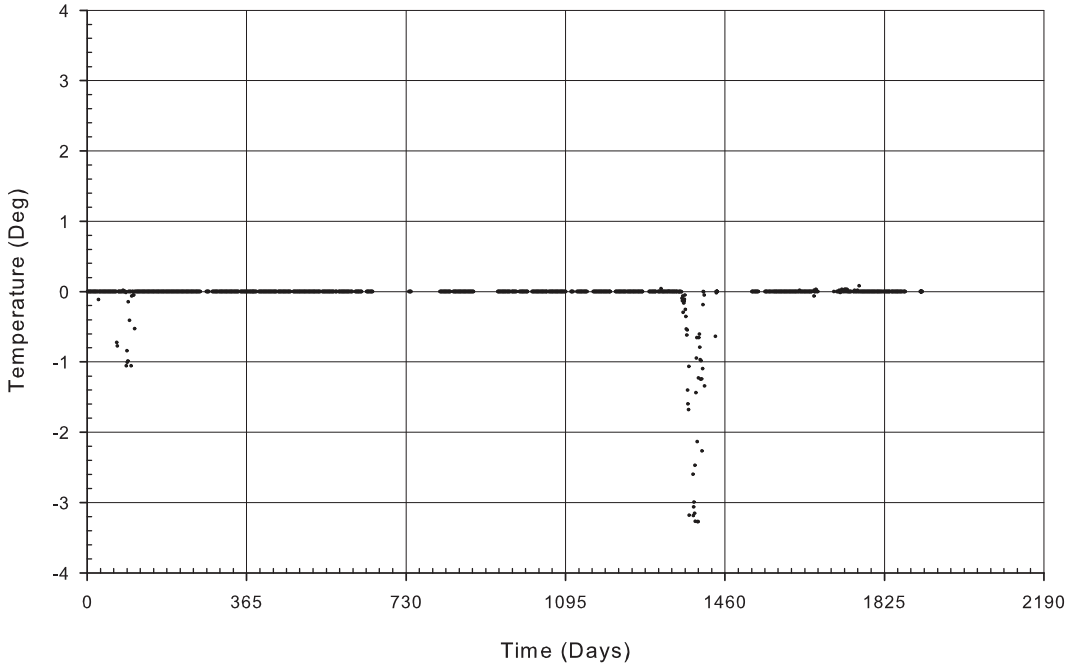
Temperature (Deg)
4
3
2
1
0
-1
-2
-3
-4
0
365
730
1095
1460
1825
2190
Time (Days)

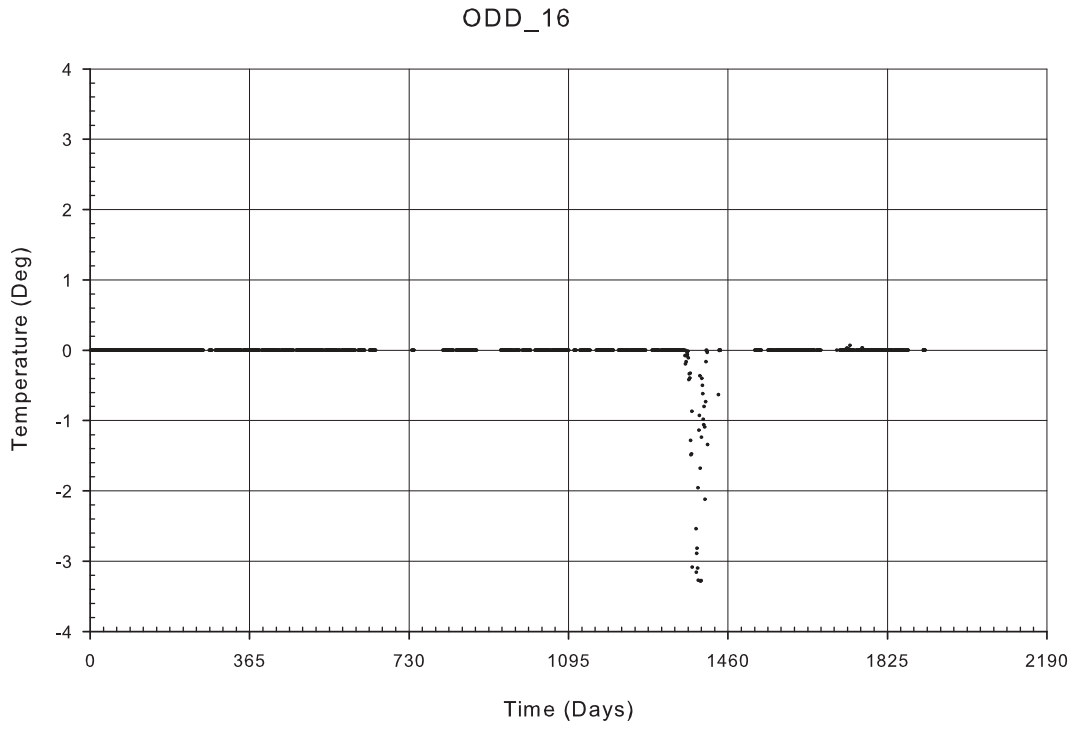
ODD_16
Temperature (Deg)
4
3
2
1
0
-1
-2
-3
-4
0
365
730
1095
1460
1825
2190
Time (Days)

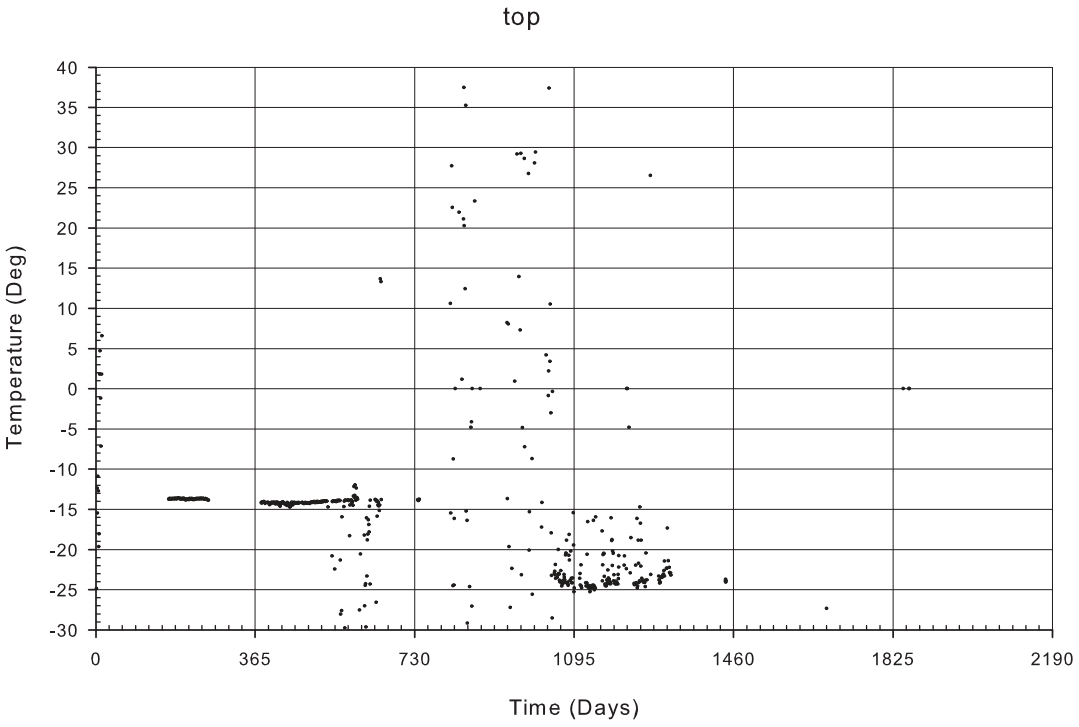
top
Temperature (Deg)
40
35
30
25
20
15
10
5
0
-5
-10
-15
-20
-25
-30
0
365
730
1095
1460
1825
2190
Time (Days)

t1

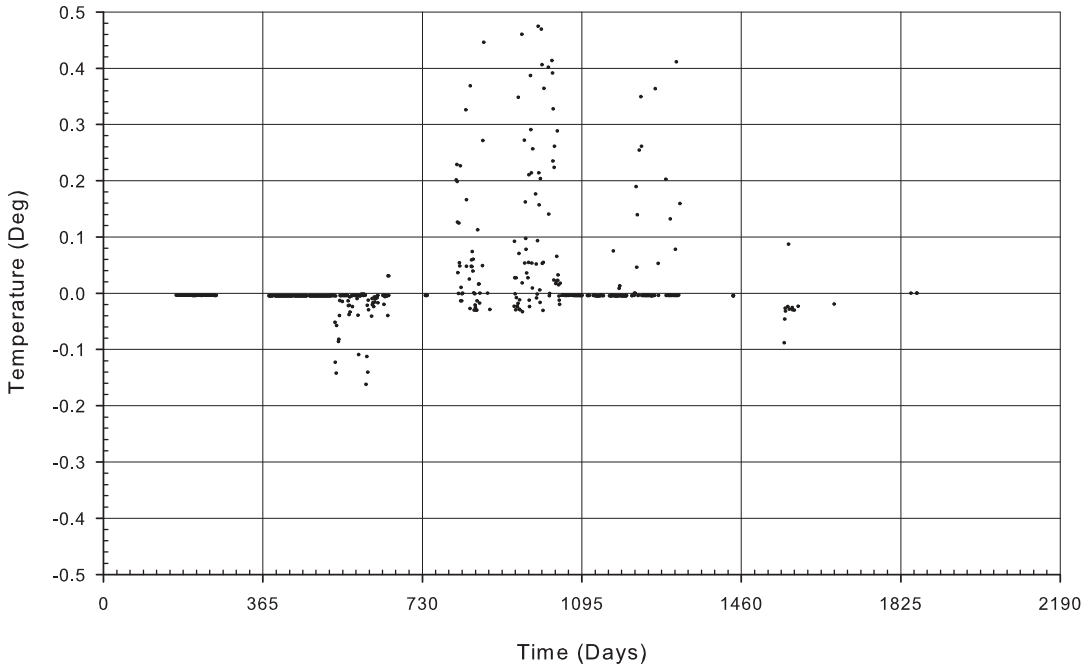
0.5
0.4
0.3
0.2
0.1
0.0
-0.1
-0.2
-0.3
-0.4
-0.5
Temperature (Deg)
0
365
730
1095
1460
1825
2190
Time (Days)

t2

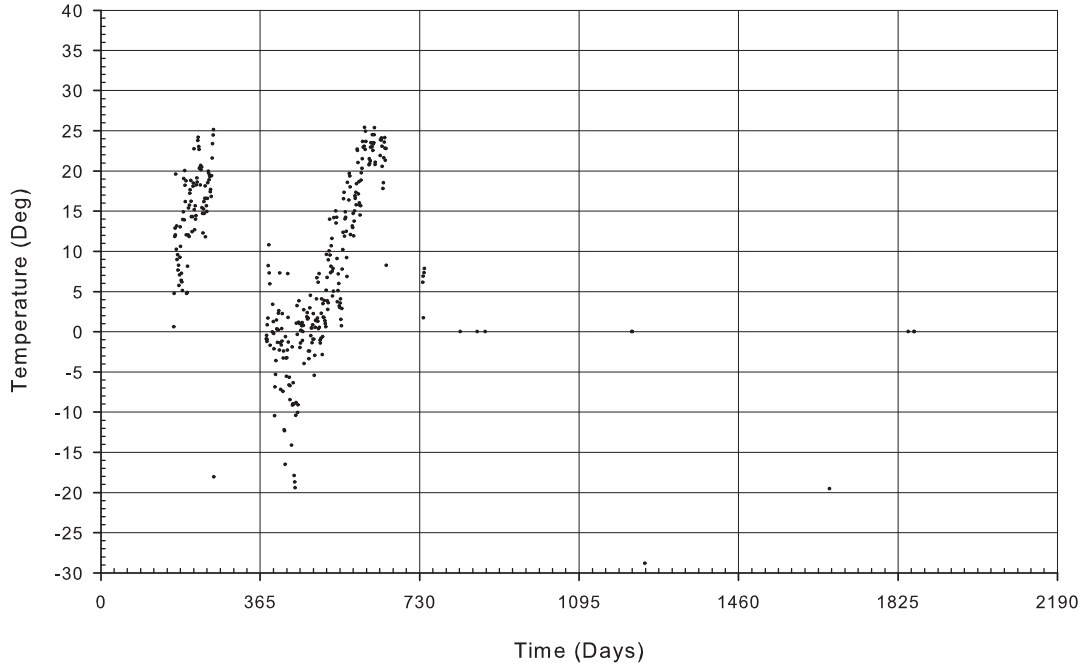
40
35
30
25
20
15
10
5
0
-5
-10
-15
-20
-25
-30
Temperature (Deg)
0
365
730
1095
1460
1825
2190
Time (Days)

middle

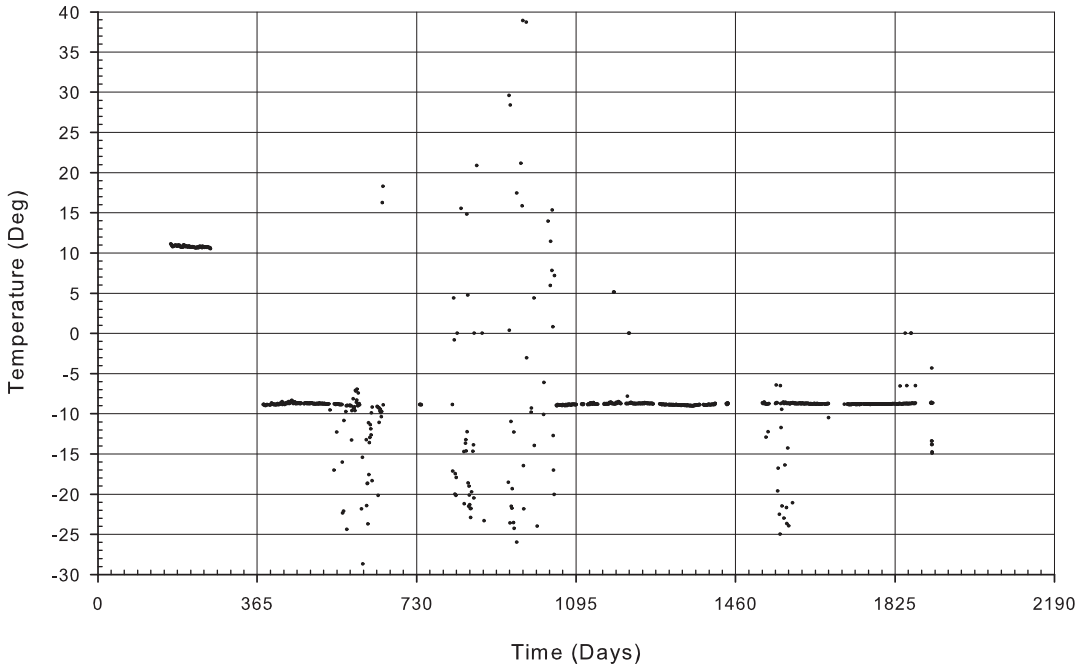
40
35
30
25
20
15
10
5
0
-5
-10
-15
-20
-25
-30
Temperature (Deg)
0
365
730
1095
1460
1825
2190
Time (Days)

m1

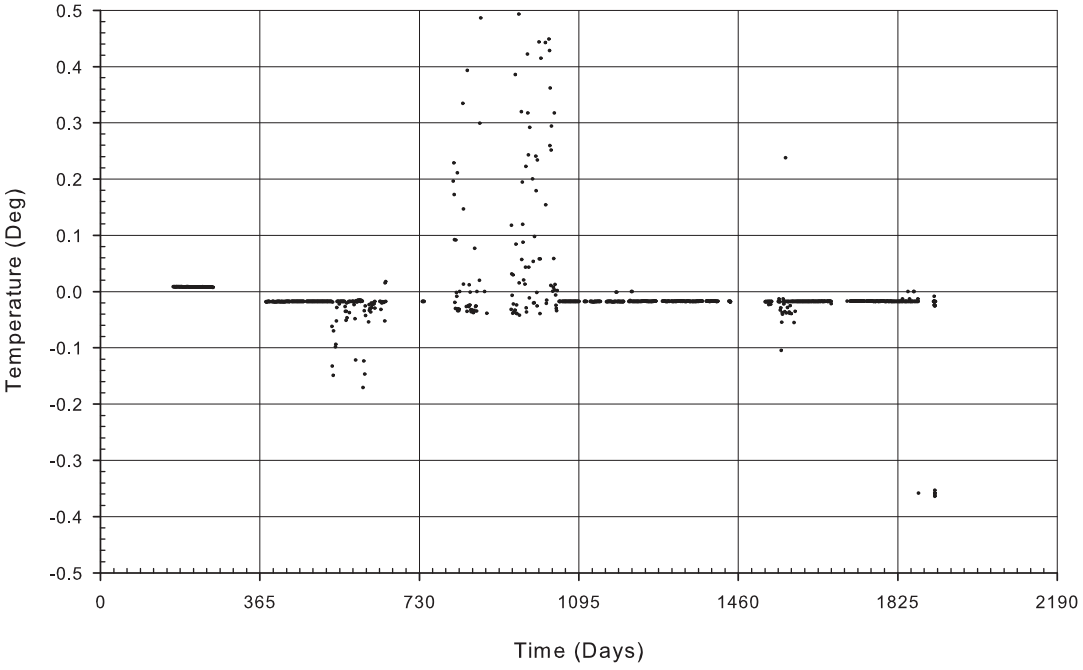
0.5
0.4
0.3
0.2
0.1
0.0
-0.1
-0.2
-0.3
-0.4
-0.5
Temperature (Deg)
0
365
730
1095
1460
1825
2190
Time (Days)

m2

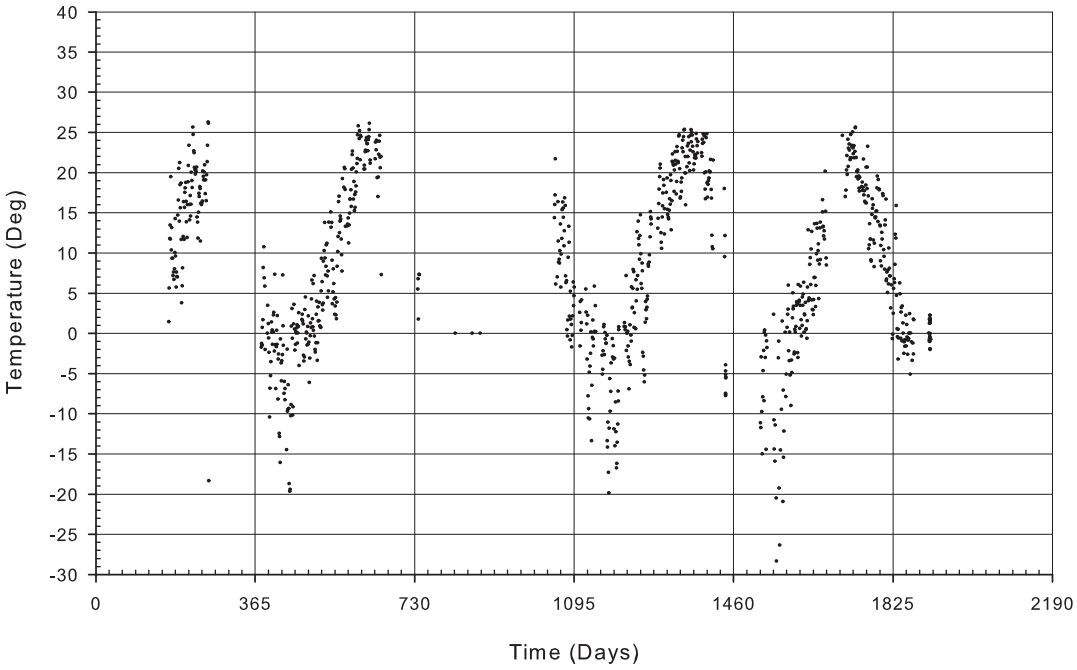
40
35
30
25
20
15
10
5
0
-5
-10
-15
-20
-25
-30
Temperature (Deg)
0
365
730
1095
1460
1825
2190
Time (Days)

bottom

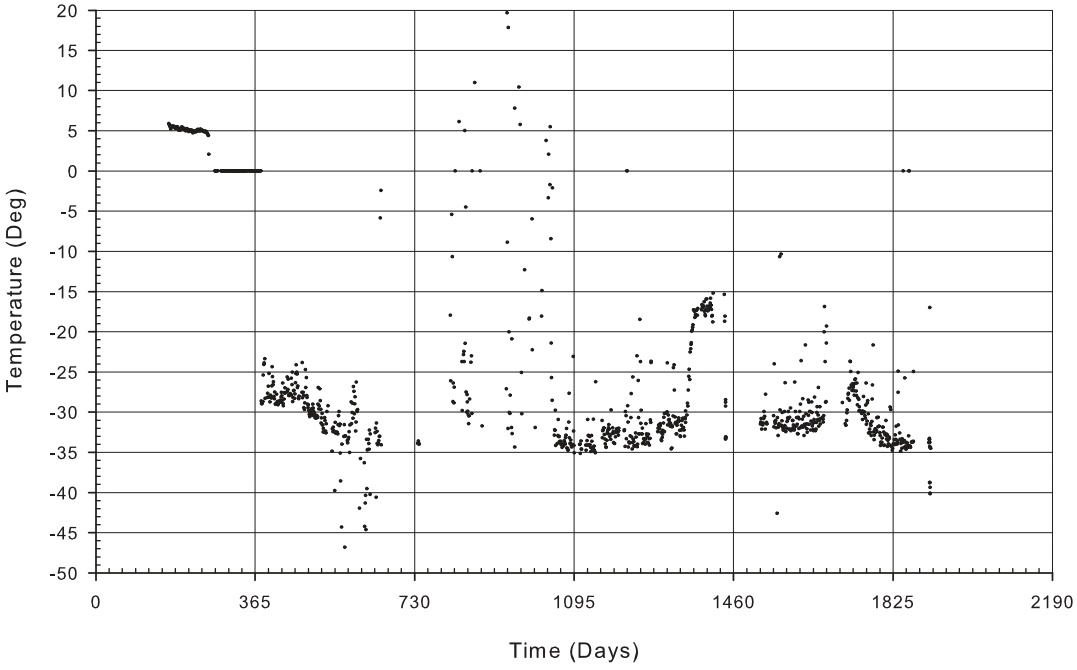
20
15
10
5
0
-5
-10
-15
-20
-25
-30
-35
-40
-45
-50
Temperature (Deg)
0
365
730
1095
1460
1825
2190
Time (Days)

b1

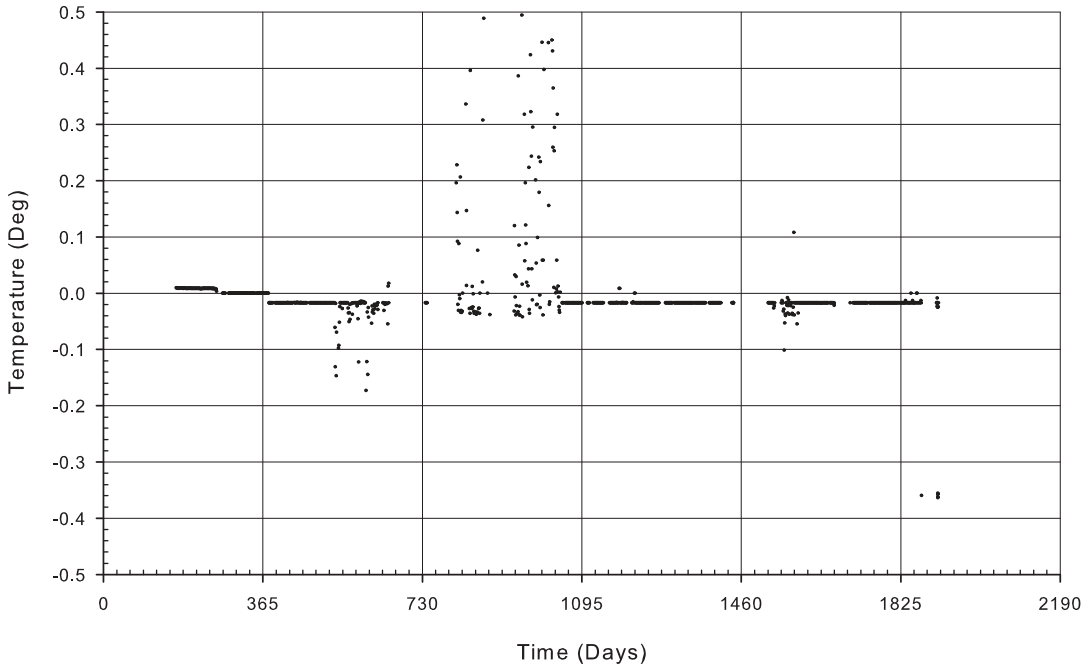
0.5
0.4
0.3
0.2
0.1
0.0
-0.1
-0.2
-0.3
-0.4
-0.5
Temperature (Deg)
0
365
730
1095
1460
1825
2190
Time (Days)

b2

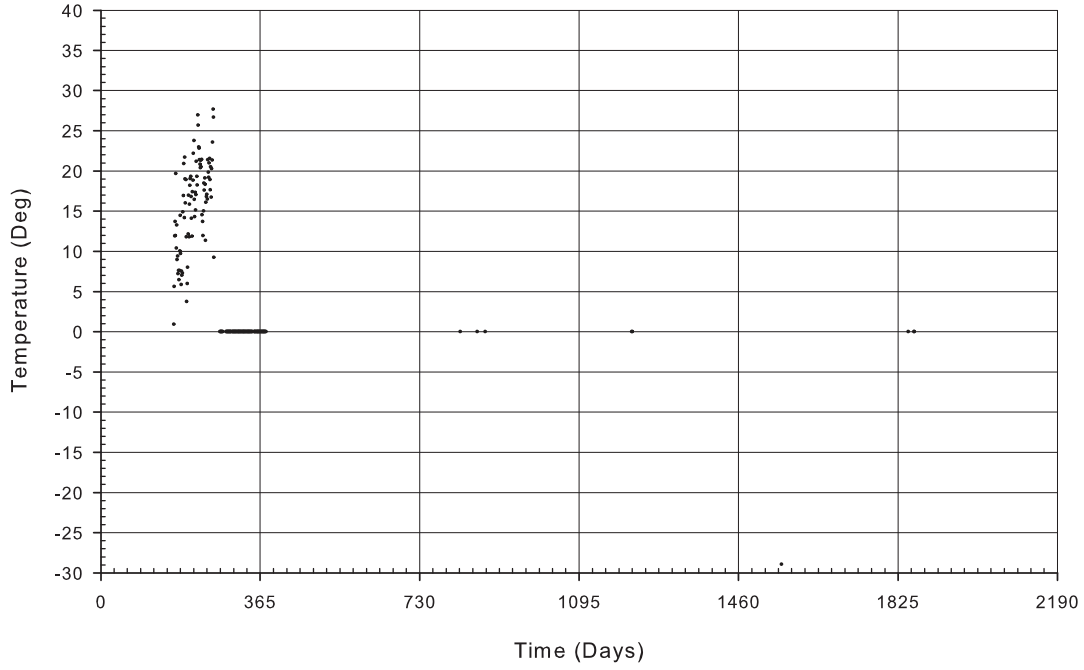
40
35
30
25
20
15
10
5
0
-5
-10
-15
-20
-25
-30
Temperature (Deg)
0
365
730
1095
1460
1825
2190
Time (Days)

b3

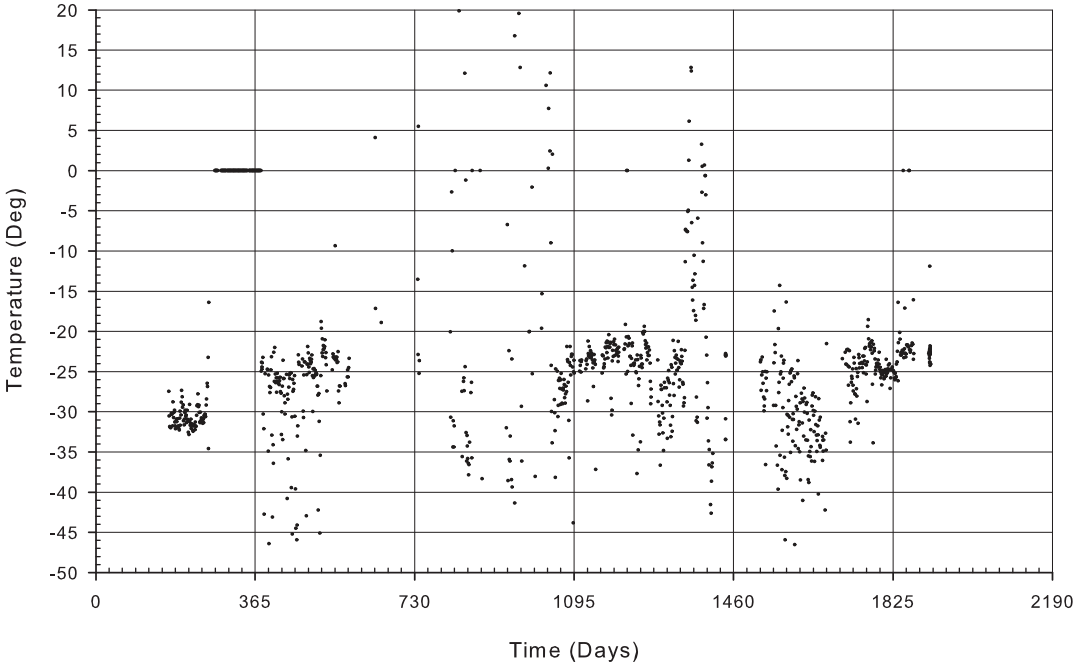
20
15
10
5
0
-5
-10
-15
-20
-25
-30
-35
-40
-45
-50
Temperature (Deg)
0
365
730
1095
1460
1825
2190
Time (Days)

north

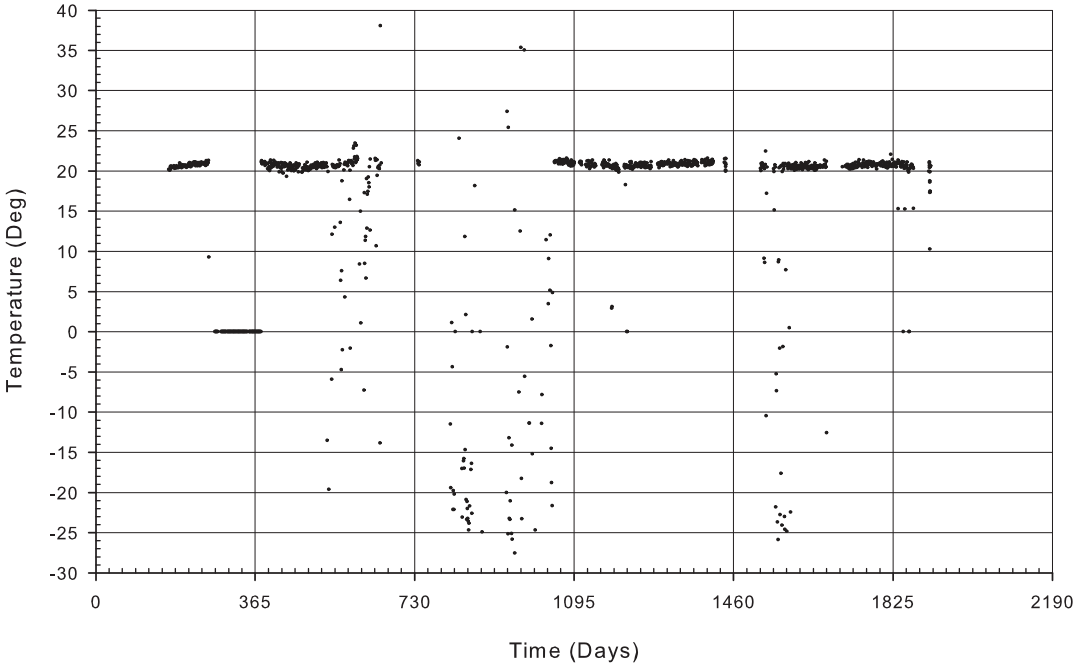
40
35
30
25
20
15
10
5
0
-5
-10
-15
-20
-25
-30
Temperature (Deg)
0
365
730
1095
1460
1825
2190
Time (Days)

n1

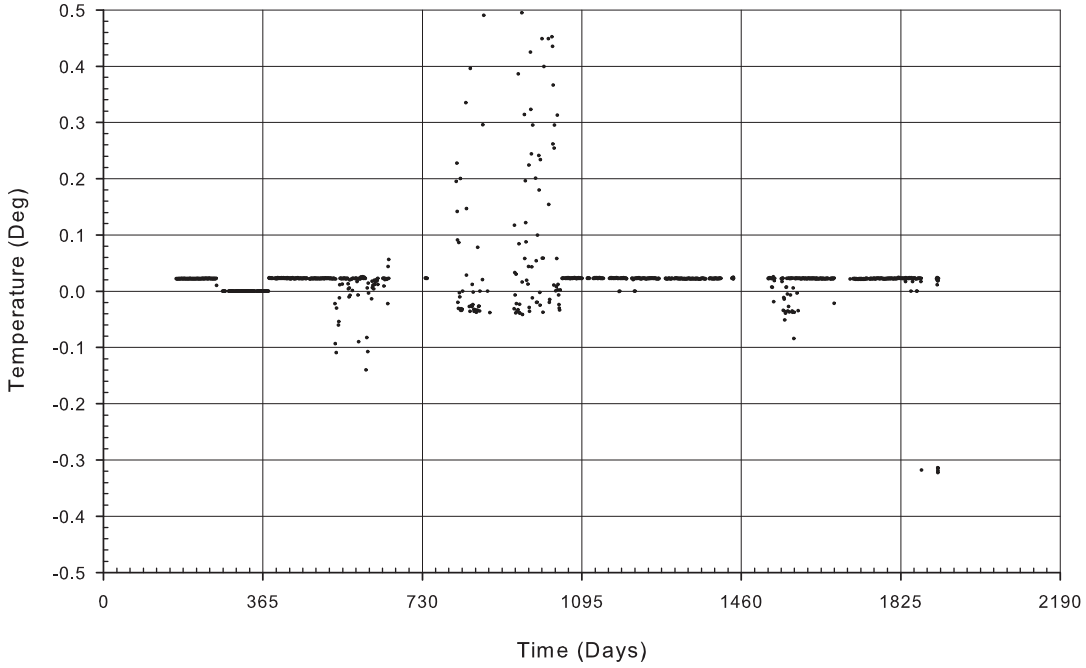
0.5
0.4
0.3
0.2
0.1
0.0
-0.1
-0.2
-0.3
-0.4
-0.5
Temperature (Deg)
0
365
730
1095
1460
1825
2190
Time (Days)

n2

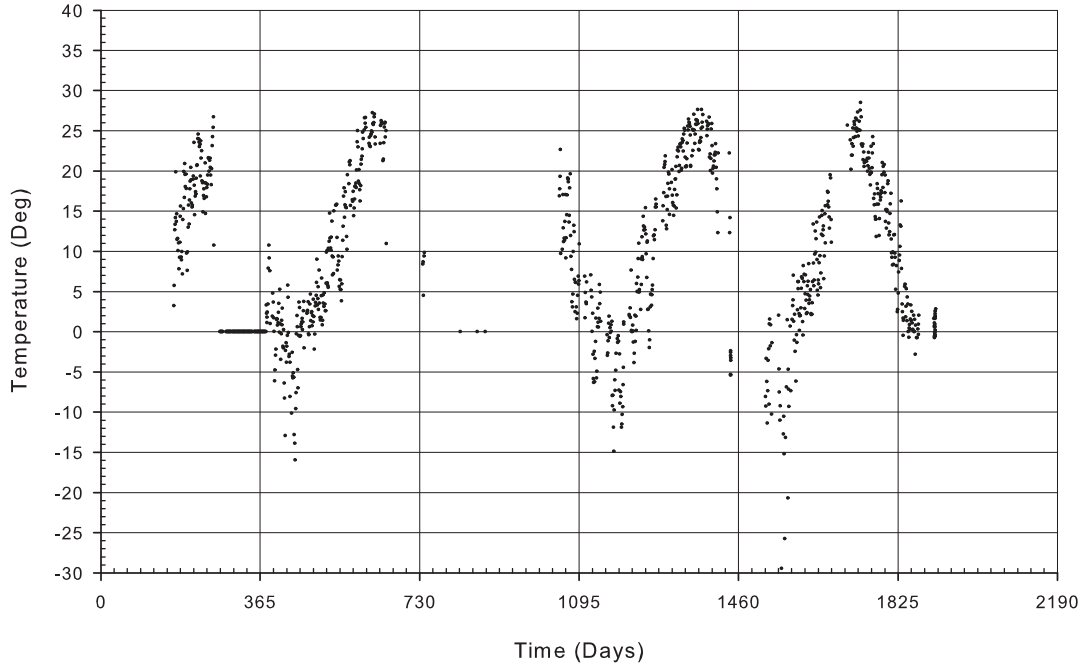
40
35
30
25
20
15
10
5
0
-5
-10
-15
-20
-25
-30
Temperature (Deg)
0
365
730
1095
1460
1825
2190
Time (Days)

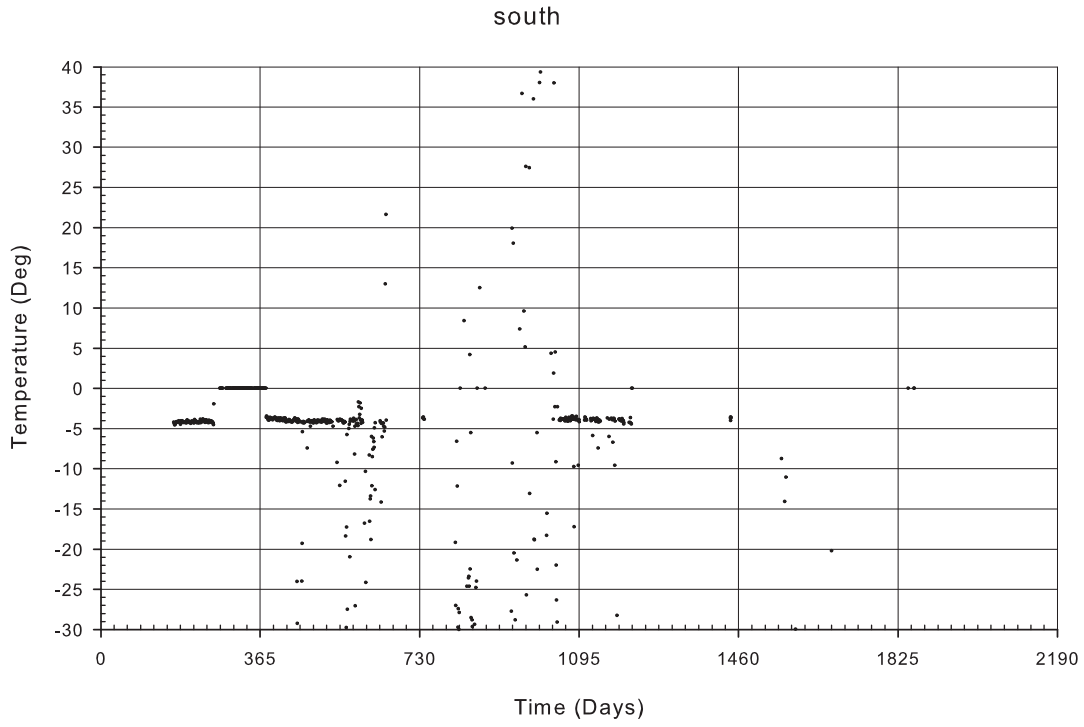
south
Temperature (Deg)
40
35
30
25
20
15
10
5
0
-5
-10
-15
-20
-25
-30
0
365
730
1095
1460
1825
2190
Time (Days)

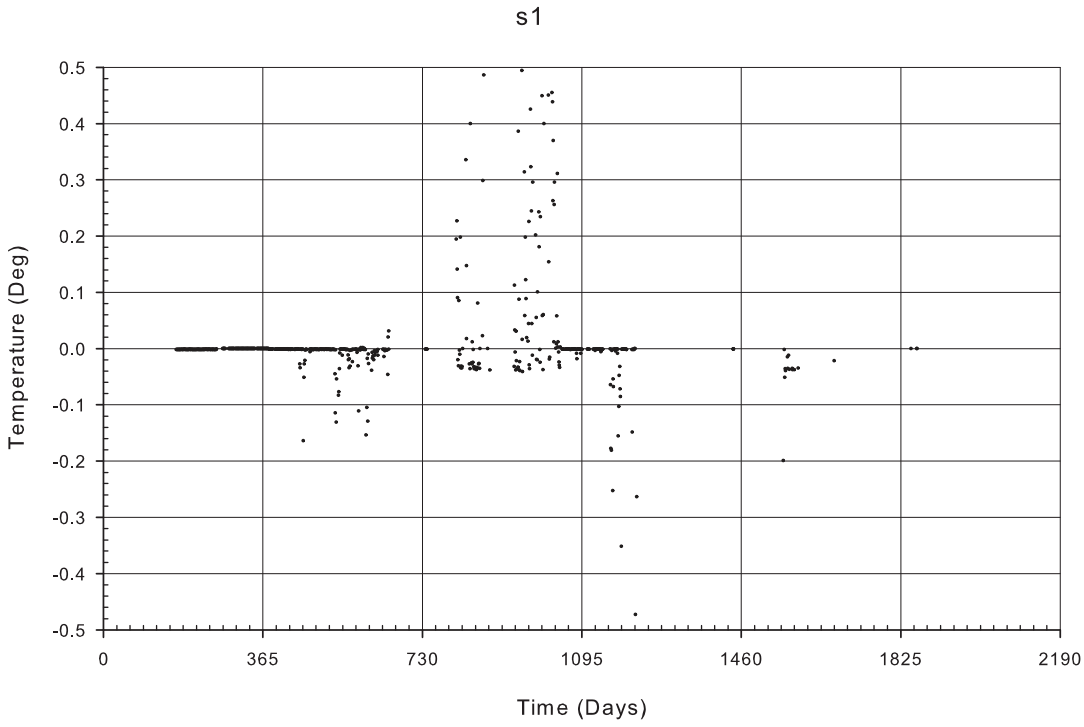
s1
Temperature (Deg)
0.5
0.4
0.3
0.2
0.1
0.0
-0.1
-0.2
-0.3
-0.4
-0.5
0
365
730
1095
1460
1825
2190
Time (Days)

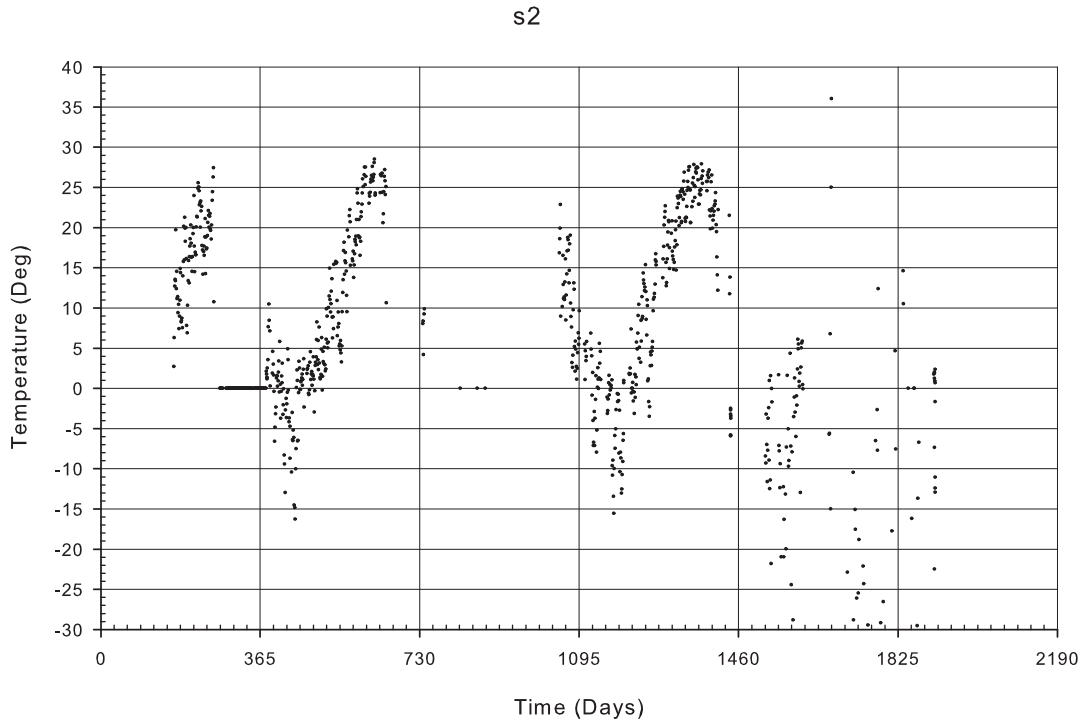
s2
Temperature (Deg)
40
35
30
25
20
15
10
5
0
-5
-10
-15
-20
-25
-30
0
365
730
1095
1460
1825
2190
Time (Days)

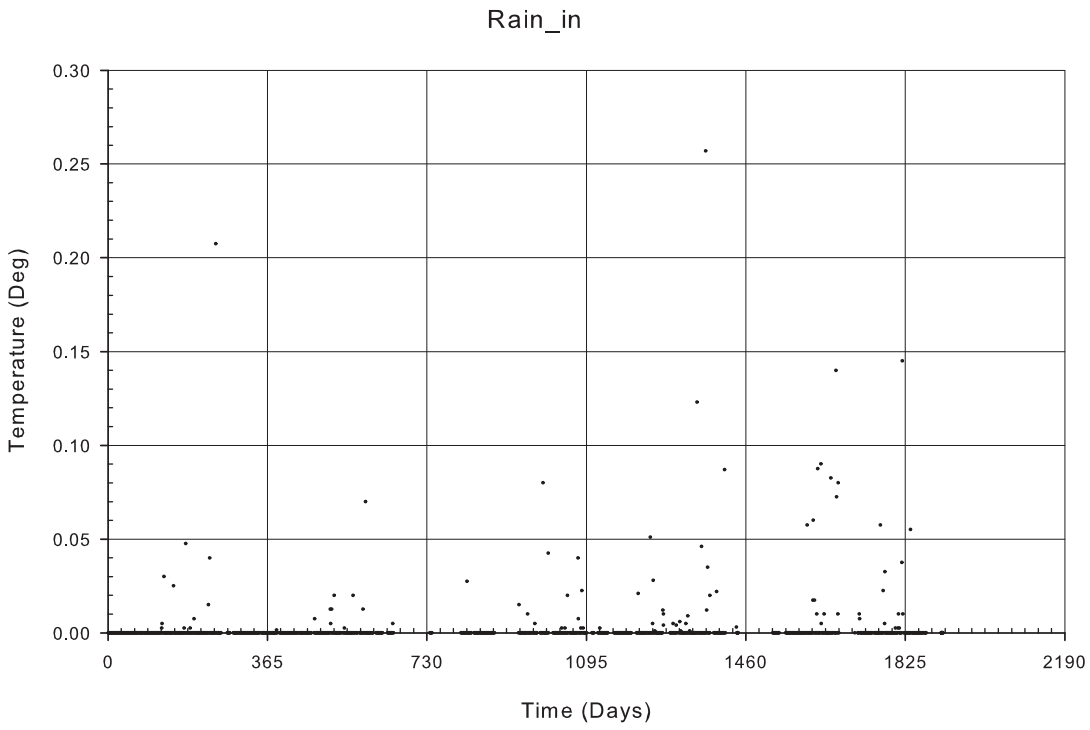
Rain_in
Temperature (Deg)
0.30
0.25
0.20
0.15
0.10
0.05
0.00
0
365
730
1095
1460
1825
2190
Time (Days)

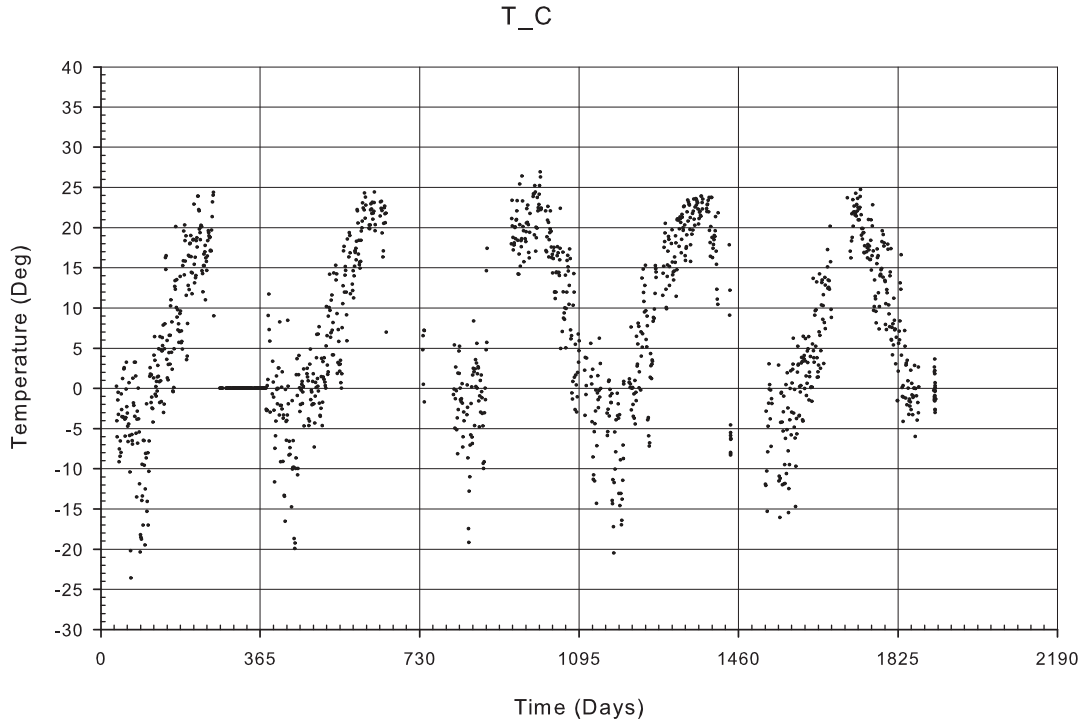
T_C
Temperature (Deg)
40
35
30
25
20
15
10
5
0
-5
-10
-15
-20
-25
-30
0
365
730
1095
1460
1825
2190
Time (Days)

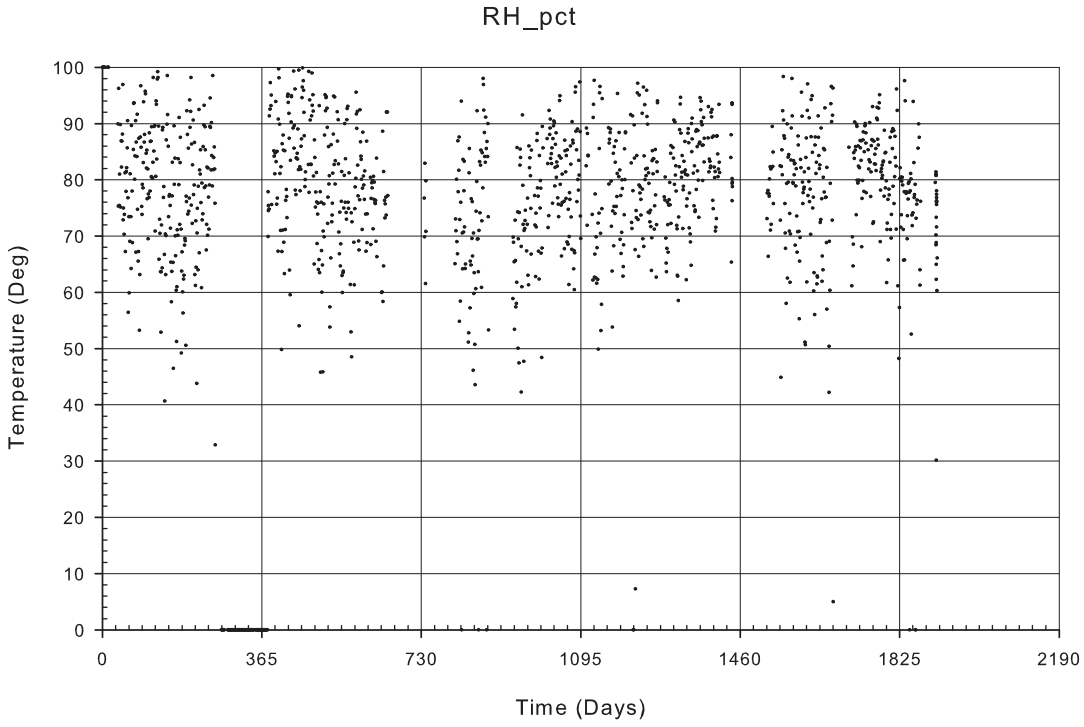
RH_pct
Temperature (Deg)
100
90
80
70
60
50
40
30
20
10
0
0
365
730
1095
1460
1825
2190
Time (Days)

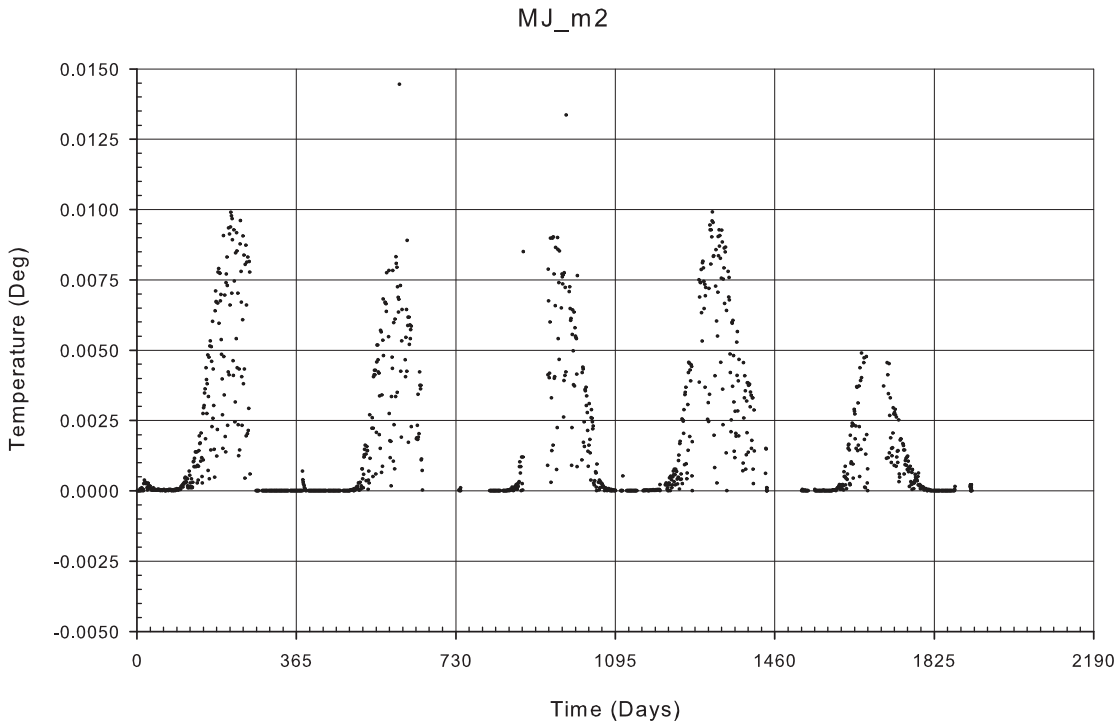
MJ_m2
0.0150
0.0125
0.0100
0.0075
0.0050
0.0025
0.0000
-0.0025
-0.0050
Temperature (Deg)
0
365
730
1095
1460
1825
2190
Time (Days)

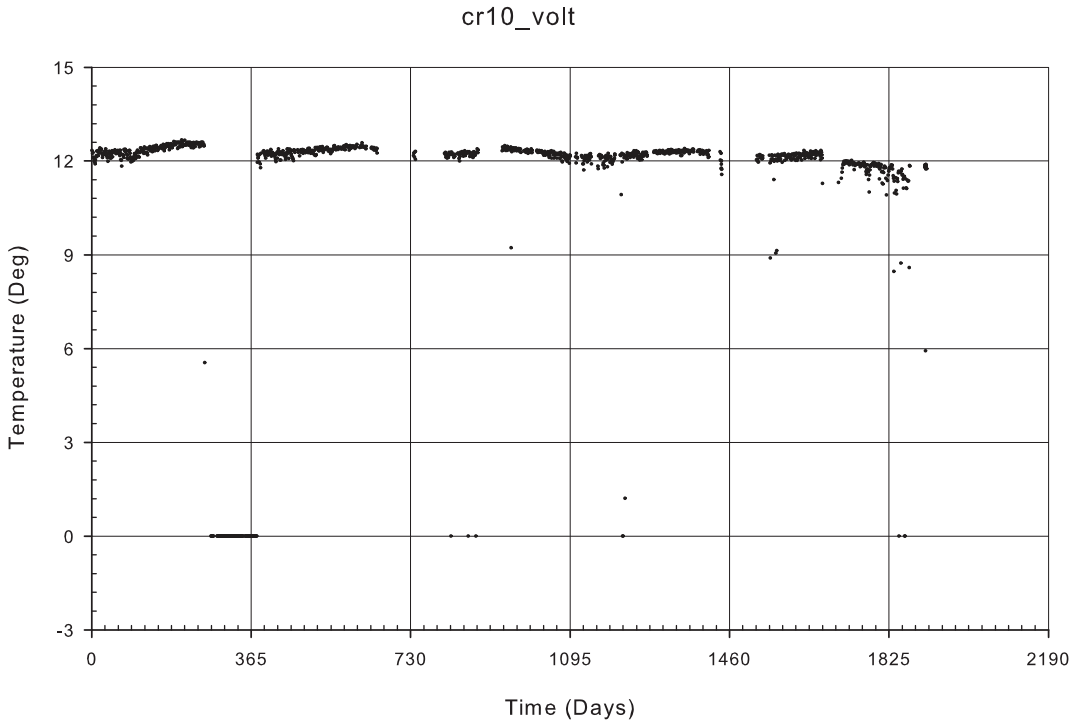
cr10_volt
15
12
9
6
3
0
-3
Temperature (Deg)
0
365
730
1095
1460
1825
2190
Time (Days)

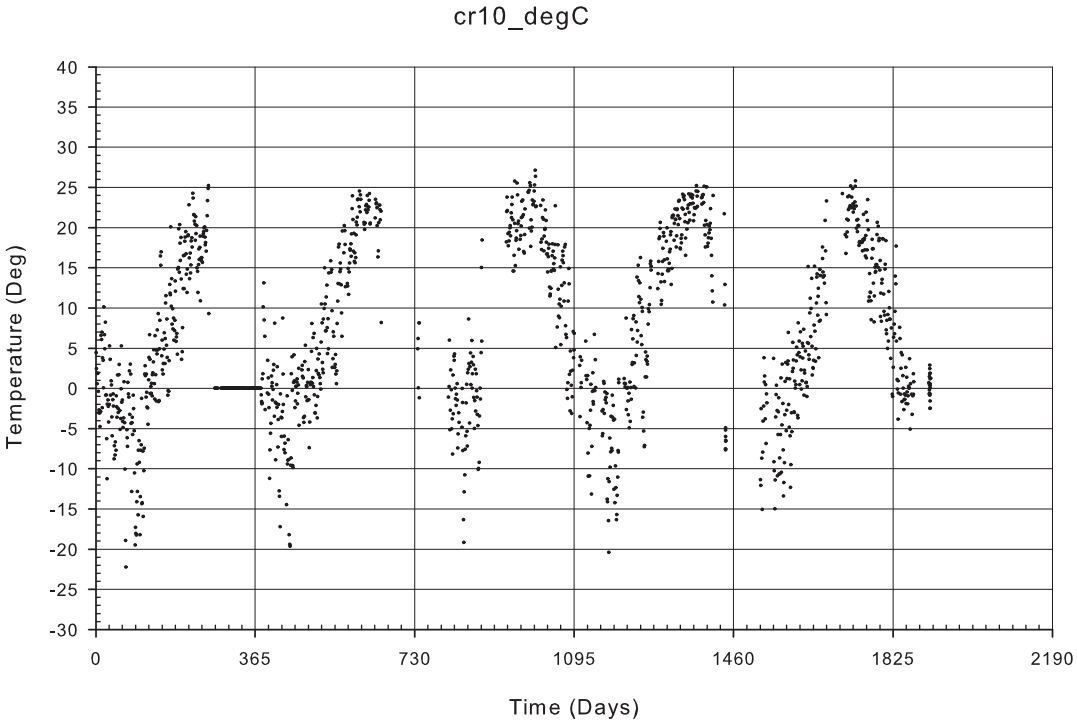
cr10_degC
Temperature (Deg)
40
35
30
25
20
15
10
5
0
-5
-10
-15
-20
-25
-30
0
365
730
1095
1460
1825
2190
Time (Days)